CRANFIELD UNIVERSITY

HENRY ANDRES PORRAS PERUCHO

DEVELOPMENT OF A TOOL TO ANALYSE HELICOPTER PERFORMANCE INCORPORATING NOVEL SYSTEMS

SCHOOL OF ENGINEERING

Msc By Research

MSc by Research Thesis

Academic Year: 2012 - 2013

Supervisor: Dr. Craig Lawson

September 2013

CRANFIELD UNIVERSITY

SCHOOL OF ENGINEERING
Msc By Research

MSc by Research Thesis

Academic Year 2012 - 2013

HENRY ANDRES PORRAS PERUCHO

DEVELOPMENT OF A TOOL TO ANALYSE HELICOPTER PERFORMANCE INCORPORATING NOVEL SYSTEMS

Supervisor: Dr. Craig Lawson
September 2013

ABSTRACT

The aerospace industry has always been looking forward new developments with the aim to create more environmental friendly aircraft, as well as to improve their performance.

Over the last few years, a prominent research topic to achieve these challenging goals has been focussed on the incorporation of more electric Secondary Power Systems (SPS), this concept is known as More Electric Aircraft (MEA) or All Electric Aircraft (AEA) when the internal combustion engine is also replaced. Among others, Airbus is using Electro-hydrostatic Actuators, (EHAs) to combine hydraulic and electric power in A320 and A340 for flight tests since 1993. The company TTTECH applied the same concept by working on the development of an electrical steering system for an aircraft nose landing gear, and power source rationalization and electrical power flexibility in aircraft. Some of the advantages stated when the MEA concept is applied are: reduction in aircraft weight and performance penalties related to conventional SPS.

Although the More/All electric aircraft concept provided satisfactory results for fixed-wing aircraft, research for rotary-wing aircraft is less common. This encourages the assessment of fuel consumption and performance penalties due to conventional and more electric SPS at conceptual level, which could achieve similar outcomes, while finding the best configuration possible.

This project takes into account the previous research focused on fixed-wing aircraft and studies on new technologies for SPS within Cranfield University, this includes electrical Ice Protection System (IPS), Environmental Control System (ECS) and Actuation System (AS). Additionally, Fuel System (FS) and Electrical System (ES) capabilities were added, developing a generic tool able to predict the total power requirements depending on the flight conditions. This generic tool was then integrated with a performance model, where overall fuel consumption is calculated for a flight mission, giving continuity and improvement to the work already done.

Secondary systems configuration and operating characteristics for a representative light single-engine rotary-wing aircraft were tailored, and the systems behaviour is presented. Finally, fuel consumption was calculated for a baseline mission profile, and compared to the fuel consumption when the systems are not included. The baseline mission set the initial flight conditions from which a parametric study was carried out; by varying these conditions the parametric study determined total fuel requirements for the analysed flight segments. An increment of up to %1.9 in the fuel consumption was found by integrating the proposed systems to the performance model, showing the impact produced by the systems, and the importance of studying different technologies to minimise it.

Keywords:

Rotorcraft, Penalties, Fuel Consumption, Mission Profile, More Electric Aircraft

ACKNOWLEDGEMENTS

A single page is far from enough to thank all the people that helped me along the process of this project, and I present my most sincere apologies for not being able to include and/or remember all your names, in my defence I have not slept for the past few days prior to writing this.

First, I would like to thank GOD for the opportunities given to me and the countless times I have asked for help in order to achieve my goals.

My deepest gratitude goes to my parents, Elsy Perucho Gomez and Henry Porras Vargas, without your continuous support and love I would not have been able to carry out this project. Infinite thanks also to my grandmother “nonita Bertha, tus llamadas diarias me hicieron sentir que nunca sali de casa”. To my aunts, uncles and cousins, your words have given me the strength required to overcome the most difficult times, many of which have come to pass. To my sister “Andy” your company and love all this time is unforgettable.

Thanks to my supervisors, Dr. Craig Lawson and Dr. Adrian Clarke for the constant support and dedication throughout these years. Also I would like to thank Professor Alastair Cooke for helping me grasp a better understanding of the aerodynamics of rotorcraft.

I would like to thank COLFUTURO and the Clean Sky Joint Initiative for sponsoring my research.

Thank to my Colombian friends in Cranfield: Julio, Leo, Juan, Harold, Alejandro, Jhonn, Hernan, Carolina, Carlos, Rolando, Rodrigo and more, every time I needed you, you were always present.

Thanks to my roommates and colleges, Francis and Charles, it was a pleasure to spend this time with you.

Thanks to my friends Ramey, Marc, Sam and many others for their technical support. Finally I would like to thank Rowena, Dan, Dan 2, Leckie, Lewis and James for making me feel at home.

TABLE OF CONTENTS

LIST OF FIGURES

LIST OF TABLES

LIST OF EQUATIONS

LIST OF ABBREVIATIONS

A	Ampere
AC	Alternate Current
ACM	Air Cycle Machine
AEA	All Electric Aircraft
AH	Ampere Hour
APU	Auxiliary Power Unit
AS	Actuation System
BEMT	Blade Element and Momentum Theory
BET	Blade Element Theory
CSD	Constant Speed Drive
DC	Direct Current
DCM	Direction Cosine Matrix
DTI	Department of Trade Industry
ECS	Environmental Control System
EHA	Electro-hydrostatic Actuator
EHA	Electro-hydrostatic Actuation
ELA	Electrical Load Analysis
EMA	Electromechanical Actuator
ES	Electrical System
ESHA	Electro-Servo Hydraulic Actuator
EU	European Union
FS	Fuel System
GRC	Green RotorCraft
HPM	Helicopter Performance Model
Hz	Hertz
IDG	Integrated Drive Generator
IPS	Ice Protection System
JTI	Joint Technology Initiative
KVA	Kilovolt Ampere
KW	Kilowatt
LRU	Line Replaceable Unit
MEA	More Electric Aircraft
MEE	More Electric Engine
MESEMA	Magnetoelastic Energy Systems for Even More Electric Aircraft
M-file	Matlab file
MOET	More Open Electrical Technologies
MT	Momentum Theory
NASA	National Astronautics and Space Administration
NiCd	Nickel Cadmium
OCV	Open Circuit Voltage
PBW	Power-By-Wire
PMG	Permanent Magnet Generator

POA	Power Optimization Aircraft
RAT	Ram Air Turbine
RMEM	Rotorcraft Mission Energy Management
RPM	Revolutions Per Minute
RSim	Rapid simulation target
SOC	State Of Charge
SPS	Secondary Power Systems
SSPC	Solid State Power Controller
TIMES	Totally Integrated More Electric Systems
V	Volts
VAC	Volts Alternate Current
VCM	Vapor Cycle Machine
VDC	Volts Direct Current
VSCF	Variable-Speed/Constant-Frequency

LIST OF SYMBOLS

Ar	Rotor area [m^2] [ft^2]
B_l	Torque-speed curve slope [N m s/rad]
B_m	Damping coefficient [Nms]
B	Blade tip-loss factor
BR	Blade root
$\overrightarrow{Cpl}$	Pitch link distance [ft]
C_T	Thrust coefficient
C_l	Section lift coefficient
C_{l_α}	Aerofoil lift-curve-slope [1/rad]
C_{m_0}	Aerofoil moment coefficient
C	Battery charging factor
CO_2	carbon dioxide [kg]
c	Blade chord [m] [ft]
dC_T	Incremental thrust coefficient
dL	Incremental lift [lbf]
dTr	Incremental thrust [Lbf]
$\{E_1\ E_2\ E_3\}$	Helicopter coordinate system
E_0	Battery constant voltage [V]
$Exp(t)$	Exponential zone
e_a	Back emf [V]
e	error function
$\overrightarrow{F_{pl}}$	Pitch link force vector [Lbf]
I	Current [A]
I_b	Blade mass moment of inertia

$I_{f_{section}}$	Blade section angular moment of inertia about the feathering axis
I_θ	Section mass moment of inertia about the feathering axis
i^*	Filtered current [A]
i_a	Armature current [A]
i_f	Field current [Amp]
i_{fs}	Series-field current [Amp]
i_r	Current required [A]
i_t	Terminal current [A]
i	Battery current [A]
it	Actual battery charge [Ah]
J	Inertia [kg m^2]
K	Polarisation constant [V/Ah]
k_r	Spring constant for the blade root in pitch
L_{AA}	Armature self-inductance [H]
L_{AF}	Field-Armature mutual inductance [H]
L_{AFs}	Series field-Armature mutual inductance [H]
L_{FF}	Field self-inductance [H]
L_{FFs}	Series-field self-inductance [H]
NOx	Oxides of nitrogen [g]
Nb	Number of blades or Blade azimuthal position
P	Power [Watt]
Q	Battery capacity [Ah]
R_a	Armature resistance [Ohm]
R_f	Field resistance [Ohm]
R	Resistance [Ohm] or Rotor radius [m] [ft]
$\overrightarrow{rb}$	Distance between the origin and the blade-pitch horn connection [ft]
$\overrightarrow{rh}$	Distance between the centre of the blade-pitch horn connection and the horn-pitch link connection [ft]
$\overrightarrow{rh'}$	$\overrightarrow{rh}$ rotated around E_3 [ft]
$\overrightarrow{rp}$	Distance between the origin and the swashplate-pitch link connection [ft]
r_{fs}	Series-field resistance [Ohm]
r	Blade non-dimensional radial position
T_E	Electromagnetic torque [Nm]
T_L	Load torque [Nm]
Tr	Rotor thrust [N] [Lbf]
T_S	Source torque [Nm]
U_P	Out-of-plane velocity component [m/s] [ft/s]
U_T	In-plane velocity component [m/s] [ft/s]
U	Resultant velocity [m/s] [ft/s]
V_∞	Forward flight velocity [m/s] [ft/s]
V_{batt}	Battery Voltage [V]

V_c	Climb velocity [m/s] [ft/s]
V_{tip}	Blade tip speed [m/s] [ft/s]
v_a	Armature voltage [V]
v_f	Field voltage [V]
v_{fs}	Series-field voltage [V]
v_h	Induced velocity in hover [m/s] [ft/s]
v_i	Induced velocity [m/s] [ft/s]
v_t	Terminal voltage [V]
W	Weight [N] [lbf]
w_r	Rotor speed [rad/s]
$\overrightarrow{Z_{col}}$	Swashplate translation along E_3 [ft]
α_0	zero-lift angle of attack [rad]
α_{rh}	Angle between $\overrightarrow{rh}$ and E_2 [rad]
α	Effective angle of attack [rad]
β_0	Blade conning angle [rad]
β_{1c}	Blade lateral flapping angle [rad]
β_{1s}	Blade longitudinal flapping angle [rad]
β_{rh}	Angle between $E_2$and $\overrightarrow{rh}$ [rad]
γ	Lock number
η	Swashplate tilt angle [rad]
$\ddot{\theta}$	Blade angular acceleration
$\hat{\theta}$	Pitch direction
θ_0	Blade collective pitch [rad]
θ_{1c}	Lateral blade pitch [rad]
θ_{1s}	Longitudinal blade pitch [rad]
θ_{tw}	Blade twist rate
$\theta_{(r)}$	Blade pitch radial position [rad]
θ	Blade pitch [rad]
λ_h	Induced inflow ratio in hover
λ_i	Induced inflow ratio
μ	Advance ratio
ρ	Density [slug/ft^3]
σ	Blade solidity
τ_a	Armature circuit time constant
τ_f	Field circuit time constant
τ_{fa}	Series-machine time constant
ϕ	Induced angle of attack [rad]
ψ	Azimuthal blade position
Ω	Rotor angular velocity [rad/s]

1 Introduction

One of the most important objectives pursued by the Aerospace industry is related to performance improvements, two of the main areas taken into account to accomplish it are fuel consumption and pollutant emissions reduction, as well as decreasing aircraft weight and engine performance penalties due to secondary systems operation.

In order to comply with these requirements, electric energy for aircraft systems power generation or even as a primary propulsion system is been under investigation since 1980s. Electric energy technology is already implemented in automotive and rail transport segments, showing a promising future.

While numerous studies on airplanes have been based on performance penalties due to conventional secondary systems, and the benefits gained by powering them using electrical energy, analysis for helicopters are focussed on trajectory optimization [1,2,3] without taking into account the impact generated from SPS. The Clean Sky JTI (Joint Technology Initiative), under the Green RotorCraft (GRC3) has pointed out that weight and energy savings could be gained by looking into electrical systems solutions [4].

1.1 Objectives

This project main objective is to create a tool to analyse helicopter fuel consumption incorporating secondary systems power requirements in Matlab/Simulink®.

In order to achieve the project main objective, specific objectives were defined as:

- *Development of conventional Electrical System (ES).*
- *Development of helicopter actuator forces calculation algorithm.*
- *Integration of Actuation System (AS).*

- *Integration of Fuel system (FS).*
- *Integration of electrical Environmental Control System (ECS).*
- *Integration of electrical Ice Protection System (IPS).*
- *Secondary Systems tool integration with a helicopter performance model.*

1.2 Methodology

A literature review was carried out, focussed on the SPS architectures on the Bell 206L-4 helicopter, which is the baseline helicopter for this project, the proposed systems to be included were studied, as well. Special focus was done in the helicopter ES components and requirements.

After the literature review was finished, a model of the conventional ES was developed, based on load requirements and DC machine dynamic characteristics, adding this capability to the proposed secondary systems tool. For this reason, a survey taking into account the ES loads and an Electrical Load Analysis (ELA) were included. The behaviour of the DC machine with respect to flight phase, and therefore load requirement, will be presented.

When the ES was finished, integration of the AS was addressed. As the AS was modelled for an A320 Aircraft, the actuator forces calculation model had to be replaced. This was done by developing a generic algorithm able to calculate the force produced by the main rotor actuators.

The algorithm was based on the combination of two different approaches:

- A blade aerodynamic approach, proposed by Tobon[5], was developed for calculation of the blade aerodynamic forces.
- A swashplate kinematic and dynamic approach, proposed by Corl[6], was included to account for the swashplate components position and torsional forces due to pitch settings.

Both approaches developed by the authors were defined only for the hover condition, while the algorithm presented in this project covers hover, axial climb and forward flight conditions.

To complete the development of the proposed tool, the next stage was integration of FS, IPS and ECS, special care was put on eliminating common inputs within the individual models, without altering their behaviour.

When the systems were added to the tool, model dependencies on Matlab/Simulink had to be eliminated if integration with a Helicopter Performance Model (HPM) written in other language was intended. For this reason, a model executable that communicates using text files was presented as a solution. In order to reduce the number of inputs required by the executable to run, it was decided that specific parameters related to characteristics of individual systems were fixed, allowing only parameters related to flight conditions to be user defined.

Finally, fuel consumption derived from the use of SPS was calculated, to accomplished this objective, a HPM developed within the Aerospace Department of Cranfield University was used as a platform [1]. The HPM is employed for trajectory optimization of light single-engine helicopters, and so, a well-defined mission profile was provided and used to compare results in terms of fuel burn. Additionally, a parametric study was developed by changing the operating conditions of the flight segments included, showing the impact produced by the proposed systems on the helicopter fuel consumption under different flight conditions.

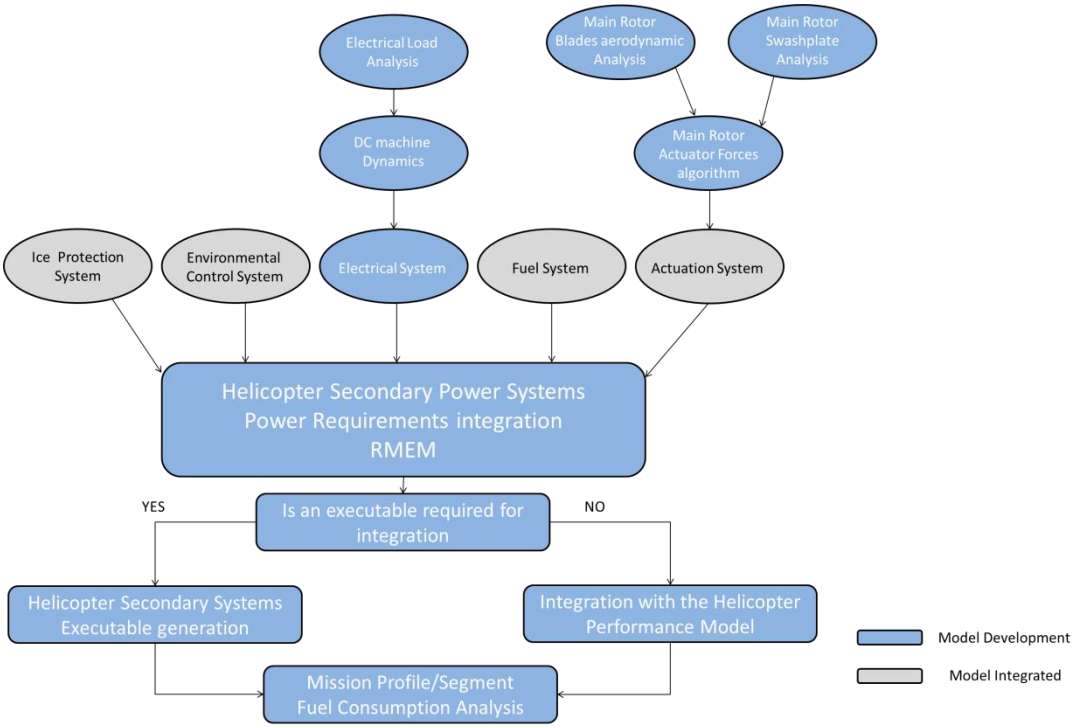

Figure 1-1 Process Flow Chart

1.3 Thesis structure

This document will present the literature review in Chapter 2; it includes an overview of Helicopter SPS, emphasis is put on the systems installed on the Baseline helicopter and ES configurations. MEA and More Electric Engine (MEE) concepts, as well as principles of operation of the systems to be integrated are also studied in this chapter.

Chapter 3 provides a description of the tool created, the processes used to develop and/or integrate the models into the tool, and the generation of the model executable.

Results of the individual models developed, and fuel consumption analysis for the proposed mission are presented in Chapter 4.

Conclusions and recommendations of future work are given in chapters 5 and 6 respectively.

2 Literature Review

2.1 Helicopter Secondary Airframe Systems

The secondary power systems of a helicopter are electrical, hydraulic, pneumatic, and fluidic. Figure 2-1 shows conventional applications of SPS, which includes engine starting by means of the electrical system, ice protection from fluidic or pneumatic systems, and flight controls and landing gear from the hydraulic system. In some cases, such as avionics and lights, the power must be electrical. But, for other subsystems, as shown in Table 2-1, a study must be made to select the most appropriate power source [7].

Table 2-1 Power sources and capabilities

Requiremet / Power Source	Communications Lighting	Flight control	Low power functions (low accuracy)	Starters
Electrical	x	x	x	x
Hydraulic		x		x
Pneumatic				x
Fluidic		x	x	

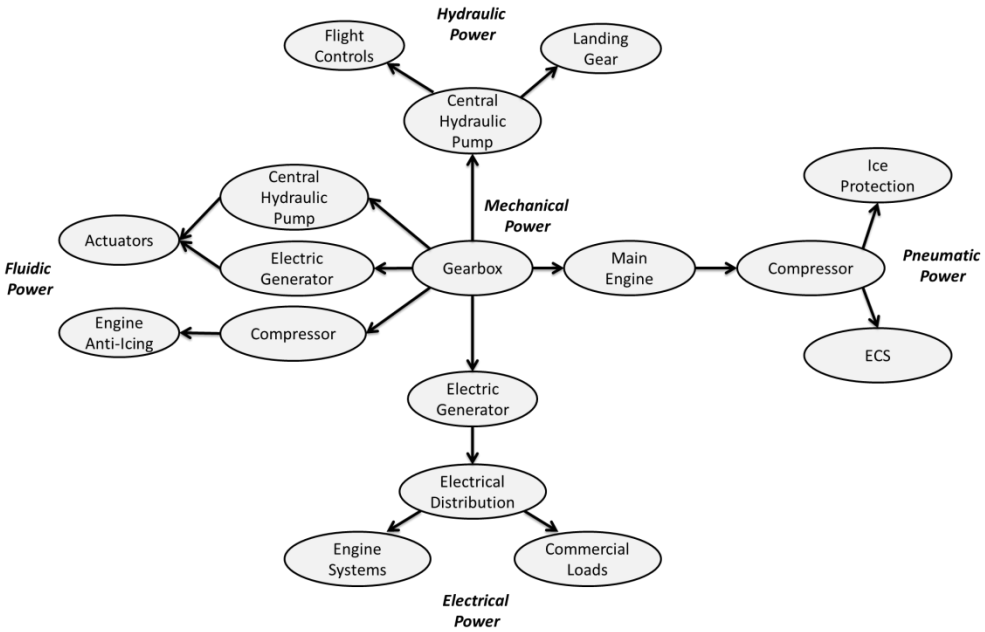

Figure 2-1 Aircraft Power Systems

Additionally, due to improvement in electrical power components, and reduction in weight, fuel consumption and performance penalties, efforts have been made to replace all secondary power systems by an electrical system.

2.1.1 Hydraulic System

Due to advantages in power density, size, and high response, hydraulic power is extensively used on aircraft, mostly for flight control functions, landing gears, and braking. Hydraulic systems main applications are: stability augmentation, full power capabilities, appropriate flight characteristics at low control system force levels, and engine starting by means of a hand pump and an accumulator. The flight functions required for helicopters are cyclic pitch, collective pitch, and directional control [7].

Depending on the all-up mass and rotor concepts, hydraulic boosters are used to reduce pilot's workload, or a complete hydraulic system to operate the flight controls with control loads beyond the pilot's handling capability, and retractable landing gears [8].

A common helicopter hydraulic system is compound by a hydraulic pump, fluid reservoir, filters, accumulators, servo valves, and 3 hydraulically powered actuators situated on the main rotor, two for cyclic control, and one for collective control, in some cases a fourth actuator is placed on the tail rotor.

In the Bell 206 L-series helicopters, the hydraulic system has three actuators, a reservoir, and a solenoid valve as primary elements. Control of the tail rotor is accomplished by means of mechanical linkages.

2.1.2 Environmental Control System

Appropriate levels of comfort must be provided to crew and passengers along a flight mission, including ground operation. Temperature, air and pressure are key factors to control in order to maintain comfortable conditions [9].

Apart from controlling the cabin temperature, air humidity and oxygen concentration, modern ECS are used for avionics, fuel and hydraulic subsystems, as heat loads transfer are allowed between different mediums [9].

For helicopters, the ECS operation is reduced to airframe, propulsion units and other secondary power systems integration, as when maximum operating conditions are encountered, levels of oxygen and pressure are still acceptable for the occupants [7].

Common ECS configurations for helicopters involve heating and ventilating systems used for occupants and avionics environmental control [7].

For the Bell 206 L-series helicopter, the ECS installed is a cabin heater by means of a bleed air heating system. As the bleed air heater is not able to provide cooling, a Vapor Cycle Machine (VCM) is used for air conditioning purposes as additional equipment [10].

The bleed air heating system consists of bleed air plumbing, shut-off valve, heater control valve and heater ejectors [11].

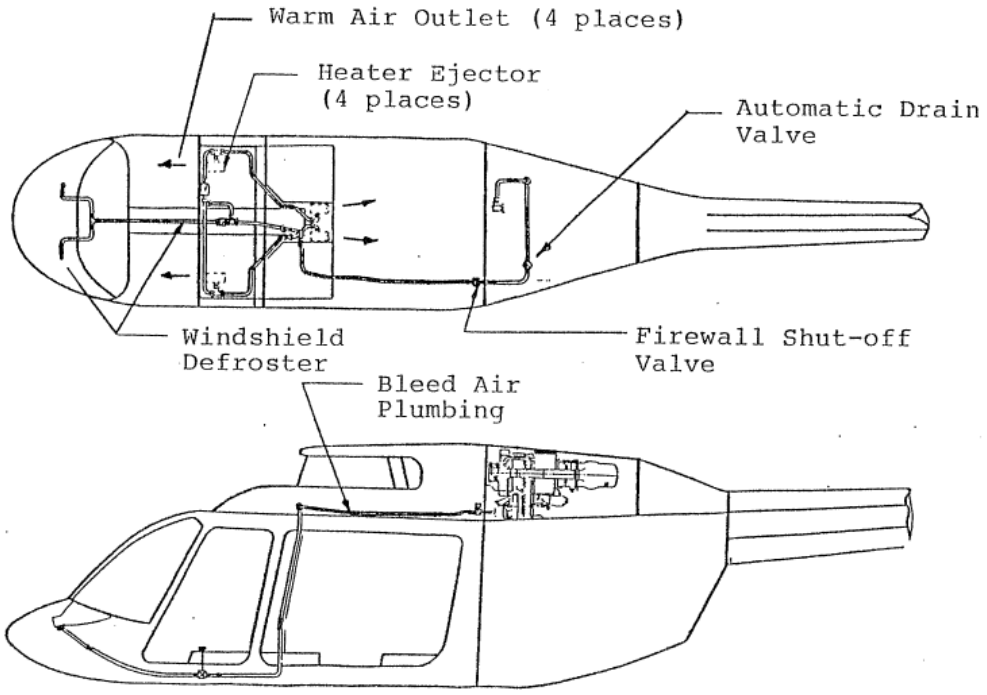

Figure 2-2 cabin bleed air heating [11]

The vapor cycle air conditioning system major components are the compressor, condenser – blower assembly, and evaporator/cabin blower units [11].

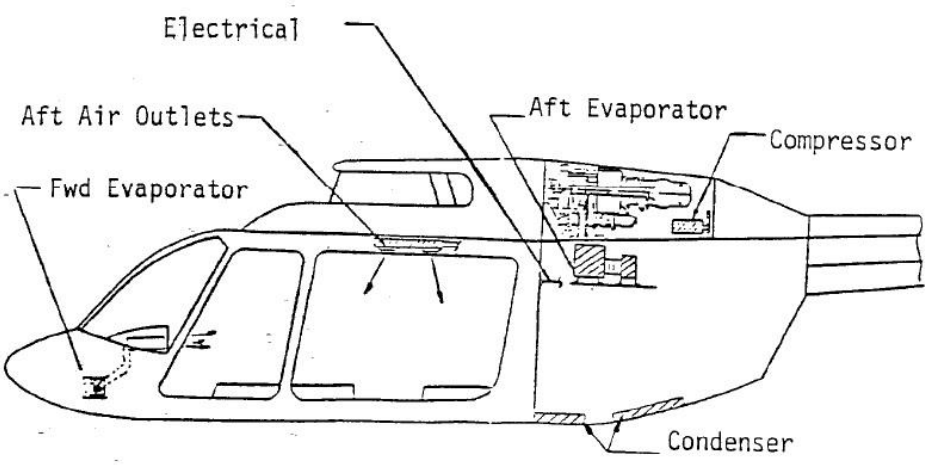

Figure 2-3 Bell 206 Air conditioning system [10]

Power consumption studies demonstrated that conventional ECSs power consumption is one of the highest among non-propulsive systems, and that an electric ECS will benefit engine performance and fuel consumption [12].

2.1.3 Fuel System

Tanks, devices for refuelling and defueling, lines for fuel transportation between engines and tanks, pumps and valves are the main components of a FS. Additionally, instrumentation is provided along the system to maintain constant supervision of the system. If multiple engines are installed, the FS must ensure operation of any engine from any tank installed while maintaining normal operation of remaining engines [7].

The bell 206L-4 fuel system comprises three fuel cells, two boost pumps, an engine driven fuel pump, an electric sump drain, check and thermal relieve valves, a pressure transducer, and three fuel filters.

2.1.4 Ice Protection System

Ice accretion is a critical factor that must be avoided for safe operation of the aircraft. Aircraft most vulnerable parts related to ice formation are wing leading edges and engine intakes. If ice formation is allowed on the wing leading edges,

loss of aerodynamic properties is detected, leading to reduction in aircraft control. Damages on the engine occur when ice in the intake breaks and enters the engine, producing the same effects as for the wings.

Additionally, windscreens and air data sensors are protected from ice formation to ensure clear view from the crewmembers, and to avoid loss of air data information, which is critical for safe operation of the aircraft. Control of ice formation in the windscreens and air data sensors is achieved by means of electrically heated elements. Wings and engines are protected by using hot bleed air from the engine until the IPS is activated [9].

2.1.5 Electrical System

Several advances have been made in electrical systems as aircraft are becoming more dependent on electrically powered components. The vast majority of aircraft equipment is powered at 115 VAC, 400Hz constant frequency. A Constant Speed Drive (CSD) is used to generate 115 VAC at constant frequency and counteract the engine speed variation typically a 2:1 speed range (full power speed/flight idle speed). The combination between the generator and CSD is called Integrated Drive Generator (IDG). The possibility of replacing the complex hydro-mechanical CSD systems, by more reliable Variable-Speed/Constant-Frequency (VSCF) systems is under investigation [9].

At the same time, the US Military Forces are working in the generation of 270 VDC electrical systems, transformed to 115 VAC 400Hz or 28 VDC depending on the equipment power requirements, as this could lead to reductions in weight and amount of power conversion, creating a more efficient system. Together with these improvements, advances in high power contactors, solid-state power switches, and microelectronics is enabling the implementation of concepts for electrical power management distribution, protection and load switching [9].

Aircraft Electrical Systems Characteristics

Table 2-2 Aircraft Electrical System Generic Characteristics and Components

Power Generation					
AC Generator		DC Generator		Battery	
Power Generation Control					
Voltage Regulator	Pre-Amplifier	Power Amplifier	Equalising Coils	Current Transformer	Mutual Reactor
Primary Power Distribution					
Generator Control Braker (GCB)		Bus Tie Breaker (BTB)	APU (GCB)	External Power Contactor (EPC)	
Power Conversion					
Inverters	Transformer Rectifier Unit (TRU)		Auto-Transformer		Battery Charger
Secondary Power Distribution					
Relay		Circuit-breaker		Solid-state Power Controller	

- **Power Generation**

  Aircraft Electrical System power generation is based on AC or DC generators and batteries.

  - ***AC Power Generation***

    For AC power generation, the main components are a Permanent Magnet Generator (PMG), an excitation stator which surrounds an excitation rotor containing diodes, and a power rotor encompassed by a power stator [9].

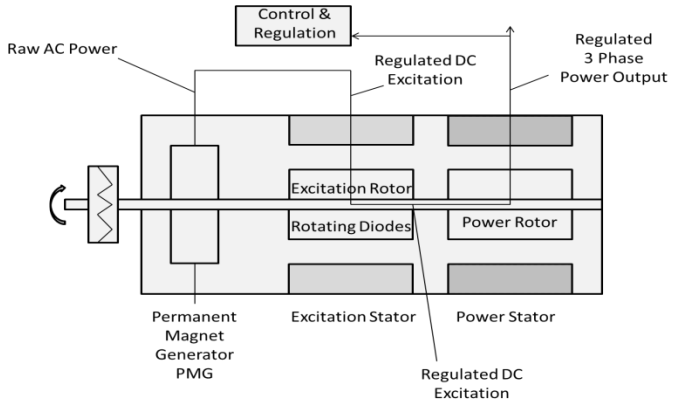

Figure 2-4 Principle of operation of modern AC generator [9]

The power generated by the PMG is variable frequency and voltage, this power is sensed by the control and regulation, where the current

flow into the excitation stator windings is modulated, the excitation stator controls the generated voltage in the excitation rotor. The rotation of the rotor is then rectified by the diodes, supplying regulated and controlled DC voltage to the windings located on the power rotor. Finally, AC voltage in the power stator is induced by the power rotor rotating field; this voltage is the delivered to the loads.

Three different systems of AC power generation can be designed, Variable-Frequency, Constant-Frequency and Constant-Frequency with onboard APU AC electrical system [7].

- Variable-frequency AC electrical system compounds a rectifier plus an inverter to deliver constant frequency, and a DC generator for starting. This system is used when the constant frequency power requirement is less than 10% of the total power requirement. A variable-frequency AC system requires a DC starter-generator or a transformer-rectifier if electrical engine starting is required.

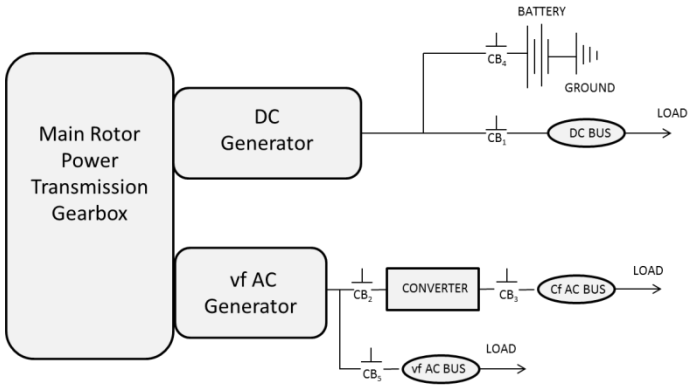

Figure 2-5 Variable Frequency AC system [7]

- Constant-frequency AC system, in this system a hydraulic CSD is used to power the AC generator and a DC generator for starting.

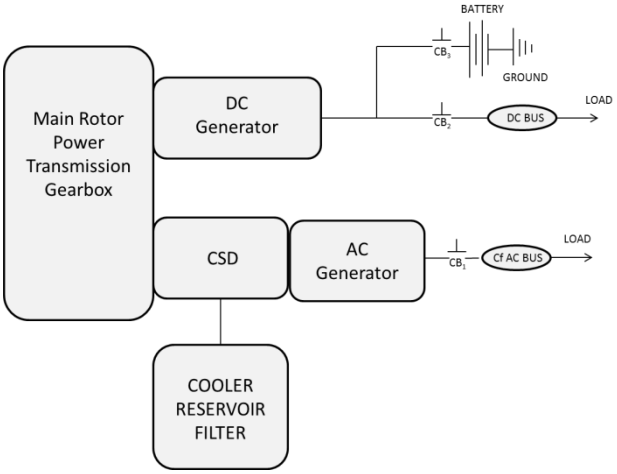

Figure 2-6 Constant-Frequency AC system [7]

- Constant-frequency AC electrical system with on-board APU. The DC starter-generator is replaced by an APU, improving the electrical system performance. In this configuration, bleed air is provided to a pneumatic starter, to start the main helicopter engines, by means of the APU.

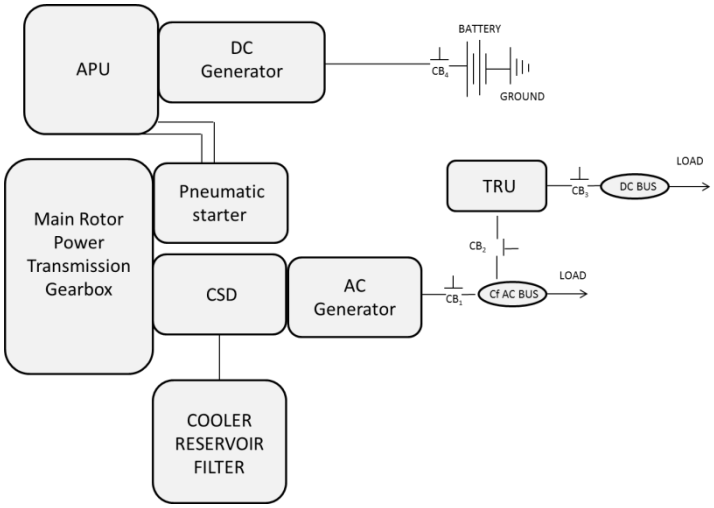

Figure 2-7 Constant-Frequency AC system with on-board APU [7]

- ***DC Power Generation***

A generator is used to supply the aircraft loads with a DC voltage. This voltage is 28 VDC, but 270 VDC systems are under investigation. To eliminate voltage fluctuations, the generator terminal voltage is regulated. A DC generator is called a self-exciting machine

because it incorporates electro-magnets for electrical power generation. This electrical power is then converted by a commutator to steady DC voltage [7].

A vast majority of DC generators in service includes brushes and a commutator, but recent studies prove the success of brushless DC generators, which increases the generator service life [7].

The usual DC generator configuration for aircraft applications is shunt-connected, where the field coils are connected in parallel with the armature. A characteristic of shunt generators is the voltage to reduce when the load current increases, as it is desired to maintain the voltage to a constant value (usually 28 VDC); a voltage regulator is added to modify the field current, maintaining constant terminal voltage when the load varies [9].

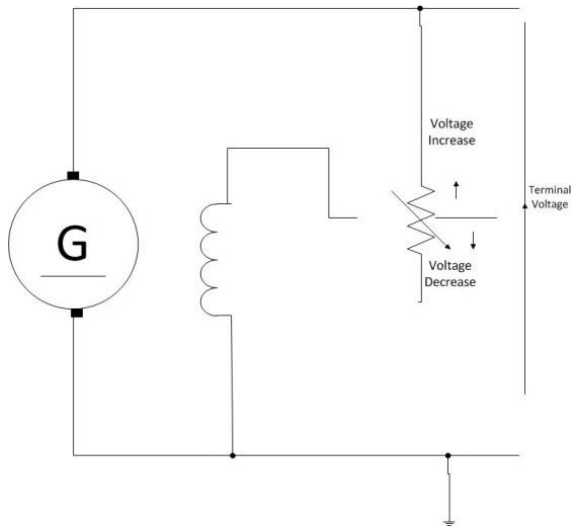

Figure 2-8 Shunt-wound DC generator with voltage regulation [9]

The most common electrical system in current helicopters is the DC system. Primary power is generated by the main rotor power transmission. An inverter, operating from the DC bus, provides constant frequency AC for avionics. Switches or circuit breakers are required to isolate components when failures occur, to apply power to the proper load buses, and to switch on standby components when necessary.

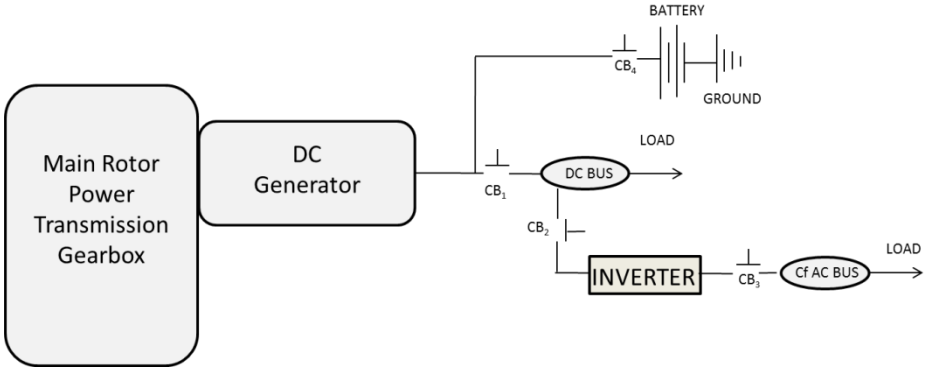

Figure 2-9 Typical DC system [7]

A DC electrical system is an optimal solution for helicopters with electrical engine starting, as the DC starter-generator, if sized for starting, will produce excess power when acting as a generator. This avoids the use of inverters within the system [7].

The drawbacks of a DC generation power are the requirement of heavy wires and cables due to low voltage transmission, inefficiency of inverters, increase in weight as more components use AC current, and even the inclusion of direct-driven variable frequency AC generators which would result in a more complex distribution system.

- **Power Generation Control**

The primary elements of the power system control are voltage regulation, parallel operation, protection functions, under/overfrequency protection, and differential current protection [7].

Voltage regulation is achieved by a voltage regulator which modifies the field current to ensure that terminal voltage is maintained in DC power generation. Control loops with error detectors, preamplifiers and power amplifiers for AC voltage regulation are used.

Parallel operation: is used for both AC Constant-Frequency and DC power generation. The generators, regulated by voltage regulators, are paralleled to carry an equal proportion of electrical load avoiding unequal

loading. For Variable-Frequency AC generation, parallel operation is not possible; in this case, the control is obtained by current transformers, error detection circuitry, and pre amplifiers/power amplifiers.

Protection functions: reverse circuit breakers or relays are used to prevent reverse current in DC generation. Overvoltage senses the faults in the field excitation circuit in AC and DC generation. Undervoltage protection for AC and DC generation is similar to reverse current in a single generator. In a multi-generator configuration, undervoltage is part of parallel operation.

Under/over-frequency protection, in AC generation only, is controlled by the load sharing function.

Differential current protection. Differential current transformers sense the phase current along the system, when a large difference between individual phase current is sensed the generator is disconnected.

- **Primary Power Distribution**

  The main aircraft generator, alternate aircraft generator, APU, ground power, back-up converter and Ram Air Turbine (RAT), through power contactors, are capable of generate the primary power distribution.

- **Power conversion**

  To power some aircraft equipment, it is necessary to transform from different power forms: From DC to AC, in this case static inverters are used to convert from 28 VDC to 115 VAC.

  From AC to DC, Transformer Rectifier Units are employed to deliver 28 VDC, and to charge the batteries.

  From AC to AC, to provide a power step-up or step-down autotransformers are considered.

- **Batteries**

  Batteries are used to provide power in system start-up and alternative power generation while back-up sources enter in operation after a power failure.

- **Secondary Power Distribution**

  To achieve an adequate secondary power distribution, contactors and circuit breakers are used for power switching capabilities and system protection in case of an overload respectively. Solid State Power Controllers (SSPCs), which can perform both tasks, can also be implemented.

- **Electrical Loads**

  After the electrical power is generated, it is delivered to the aircraft systems as:

  - Motors and actuation used for linear and rotary actuation, in engine control, flight controls and flap/slat operation.
  - Hydraulic and fuel valves, pumps and control valves for ancillary equipment.
  - Starter, gyroscope and fan motors to provide starting for engines, APUs, gyroscopes and air to passengers or equipment.
  - Lighting used for external and internal lighting systems.
  - Heating for electrically IPS and windscreen heating.
  - Avionics to power Line Replaceable Units (LRUs).

Engine maximum starting torque is a key factor when designing an ES, if the torque is less than 90 lb-ft, a 400-A, 28 VDC starter-generator powered by nickel-cadmium batteries is sufficient to start the system. A 90 lb-ft limit characterises small engines [7].

In a helicopter electrical system, 28 VDC are used to power engine fuel pumps, lights, and weapons (if installed), Constant-Frequency 400Hz AC or 28 VDC for

avionics, and Variable-Frequency AC is used for de-icing and to power loads not affected by frequency fluctuation [7].

A survey realised in over 25 helicopters, as listed in **Error! Reference source ot found.**, shows that DC is used in 15 of them as primary power generation and static inverters are used to provide AC electrical current.

Table 2-3 Helicopter Electrical Systems Main Components [13]

HELICOPTER ELECTRICAL SYSTEM	
Helicopter	MAIN COMPONENTS
Aerospatiale SA 330 PUMA	three-phase 200 VAC electrical power supplied by two 15 KVA 400Hz alternators 28.5 V 10 KW DC power provided from the AC system by two transformer-rectifiers Main aircraft battery for self-starting and emergency power
Aerospatiale SA 341/342 Gazelle	28 VDC electrical system supplied by 4 KW engine driven generator and 40 AH battery optional 26 V system supplied by 0.5 KVA alternator at 115/200 V 400 Hz
Augusta A 109	28 VDC electrical system, using two 30 V 150 A engine-driven starter/generators, and one 24 V 13 AH Ni/Cd battery single phase AC power at 400 Hz supplied by two 115/26 V 250 VA solid-state static inverters third inverter as emergency back-up
A 109KM	Two 160 A 28 VDC self-cooled starter/generators and 27 Ah 28 V Ni/Cd battery optional two 250 VA or two high load 600 VA 115/26 VAC 400 Hz static inverters for optional electric system one 6 KVA alternator and one standby 250 VA solid-state inverter
Augusta Bell AB 212 ASW	28 VDC and three phase 200/115 V or single phase 26 VAC at 400 HZ two standard generators are integrated with a 20 KVA alternator
Augusta-Bell 412 EP and Griffon	28 VDC and three phase 200/115 V or single phase 26 V AC at 400 HZ two standard generators are integrated with a 20 KVA alternator

Table 2-3 Helicopter Electrical Systems Main Components cont. [13]

Augusta-Sikorsky AS-61 A	two 20 KVA 200 V three-phase 400 Hz engine driven generators 260 single-phase AC supply fed from the AC's 22 AH Ni/Cd battery through an inverter DC power provided as a secondary system from two 200 A transformer rectifier units
Augusta-Sikorsky AS-61-R (HH-3F) Pelican	24 V 22 AH battery two 20 KVA 115 VAC generators one 300 A DC generator APU standard
American Sportscopter Ultrasport	dual carburettor two-stroke engine with electric starter 12 V battery 14 V alternator
Bell 47	28 V 50 A generator electric starter heavy-duty battery
Bell 205	30 V 300 A DC starter/generator
Bell 206 JetRanger/SeaRanger	150 A starter/generator one 28 V 13 AH Ni/Cd battery optional 28 V 17 AH Ni/Cd battery
Bell 206 Kiowa	150 A starter/generator one 24 V 13 AH Ni/Cd battery
Bell 206 LongRanger	28 VDC electrical power from 150 A starter/generator 17 AH battery
206LT	two 150 A starter/generators 28 AH Ni/Col Battery
Bell 209 HueyCobra and SeaCobra	10kVA 400 Hz AC alternator with emergency bus battery driven standby pump
Bell 209 SuperCobra	two 28 V 400 A DC generators two 24 V 34.5 AH batteries and three inverters main 115 V AC, 1 kVA single-phase at 400 HZ standby 115 V AC three-phase at 400 Hz 750 VA, three phase at 400 Hz and a dedicated 115 V AC 365 VA single-phase for missile system
Bell 212	28 VDC electrical system supplied by two completely independent 30 V 200 A (de-rated to 150 A) starter/generators secondary AC power supplied by two independent 250 VA single-phase solid-state inverters third inverter for protection 40 AH Ni/Cd battery

Table 2-3 Helicopter Electrical Systems Main Components cont. [13]

Bell 222	model 222B supplied by dual 150 A DC generators dual 250 VA AC inverters 17 AH Ni/Cd storage battery dual inverters deleted in 222UT and 34 AH battery
Bell 230	Dual 28 VDC electrical system two 30 V 200 A engine-mounted starter/generators de-rated to 180 A 24 V 28 AH Ni/Cd battery
Bell 406 (AHIP)	Primary electrical power provided by 10 KVA 400Hzthree phase 120/208 VAC alternator secondary power by 200 A 28 VDC transformer-rectifier unit backup power by 500 VA 400 Hz single phase 155 VAC solid-state inverters and 200 A 28 VDC starter generator
Bell 407	28 VDC powered by 180 A starter/generator 17 AH Ni/Cd battery
Bell 412	as Bell 212 except inverters are 450 VA
Bell 427	28 VDC power from 17 AH Ni/Cd battery and two engine mounted 17 AH starter/generators 28 AH battery and 200 A starter/generator optional
Bell 430	Dual 28 VDC electrical system powered by two 30 V 200 A engine-mounted starter/generators de-rated to 180 A 24 V 28 AH NiCd battery
BOEING 114 and 414 Chinook	two 40 kVA air-cooled alternators driven by transmission drive system Solar T62-T-2B APU drives a 20 kVa generator and hydraulic motor pump, providing electrical and hydraulic power to main engine start and system operation on the ground
Boeing 234 Commercial Chinook	two 40 kVA air-cooled alternators driven by transmission drive system Solar T62-T-2B APU rated at 71 KW (95 SHP), drive auxiliar gearbox on rear transmission to start engines and provide power for to flying control system hydraulic pumps and two alternators
Boeing AH-64 Apache	two 35 kVA fully redundant engine-driven AC generators two transformer-rectifiers and URDC standby battery AlliedSignal GTP 36-55 (H) 93 KW (125 SHP) APU (36-155(BH) in AH-64D) for engine starting

Bell 206 Electrical System

The ES is 28 VDC. It includes a 24 volt, 17AH Nickel Cadmium (NiCd) battery, a 28 V 150 A starter/generator, a voltage regulator, relays, switches and circuit breakers. A 28 V, 400 A External Power Unit provides direct current for starting and servicing by means of an external power receptacle.

2.2 More/All Electric Aircraft

The idea of an electric aircraft is not new. In 1884, brothers Albert and Gaston Tissandier designed ‘La France’, a dirigible which was the first airship to be powered by electricity, it flew for 25 minutes. In 1973, Fred Militky flew a motor glider type HB-3 airframe powered by a bank of VARTA NiCd batteries for 25 minutes In both cases, weight and duration of the batteries where the major drawbacks.

In World War II, some military aircraft like the British Vulcan, and Vickers Valiant ‘V’ bombers, used electrical power for primary flight controls and other functions. But, research for other secondary power sources started due to insufficient power generation capability, volume necessity for the required power conditioning system, and advance control requirements for the electrical power system.

Since then, pneumatic power, powers the ECS and IPS. Mechanical power is used on hydraulic pumps, engine pumps, and the generator. Hydraulic power, powers the actuation system for primary and secondary flight control, engine actuation and some ancillary equipment. Electrical power is used for avionics and lights among others.

The main drawbacks of pneumatic and hydraulic powers are low efficiency and difficulty in detecting leaks for the first one, and heavy and inflexible infrastructure and the potential leakage of dangerous and corrosive fluids for the second one [14].

Although, secondary power generation by these four main forms is still in use on aircraft, the aim of reducing or eliminating hydraulic, pneumatic and

mechanic power systems, and replacing them with electrical power has risen since end of 1970's.

United States Air Force and NASA started two programs: a development and demonstration program called More Electric Aircraft (MEA), with the target to reduce or eliminate the need of centralized aircraft hydraulic, mechanical, and pneumatic power systems, replacing them with an electrically-based power system. And Power Optimization Aircraft (POA), in 2002, which tries to optimize the management of electrical power on aircraft in order to reduce non-propulsive power and reduce fuel consumption [15].

In 2001, the Totally Integrated More electric Systems (TIMES) program supported by the Department of Trade Industry (DTI), started with the objective of integration of previously developed systems into an electrical network to determine the viability of using such a network in a future MEA [14].

In 2004, the European Union EU, launched the Magnetoelastic Energy Systems for Even More Electric Aircraft (MESEMA) with the aim of designing, producing and testing 'innovative transducer systems based on active materials' to reduce the level of disturbance noise in helicopters, and replacing the helicopter rotor blade pitch angle actuation systems [16].

In 2006, the More Open Electrical Technologies (MOET) project was aimed to establish the new industrial standard for electrical design system of commercial aircraft, usable by the business and regional aircraft and rotorcraft, as well [17].

In 2008, the Clean Sky program funded by the European Commission and the aeronautical Industry began, with the aim of reducing CO_2, fuel consumption, NO_x emissions, and external noise and to create a green product life cycle.

Having an electrical power system for non-propulsive power, hydraulic pumps, engine hydraulic power generation and bleed air off-take, are eliminated and electric engine start-up, ECS, IPS and actuators must be considered.

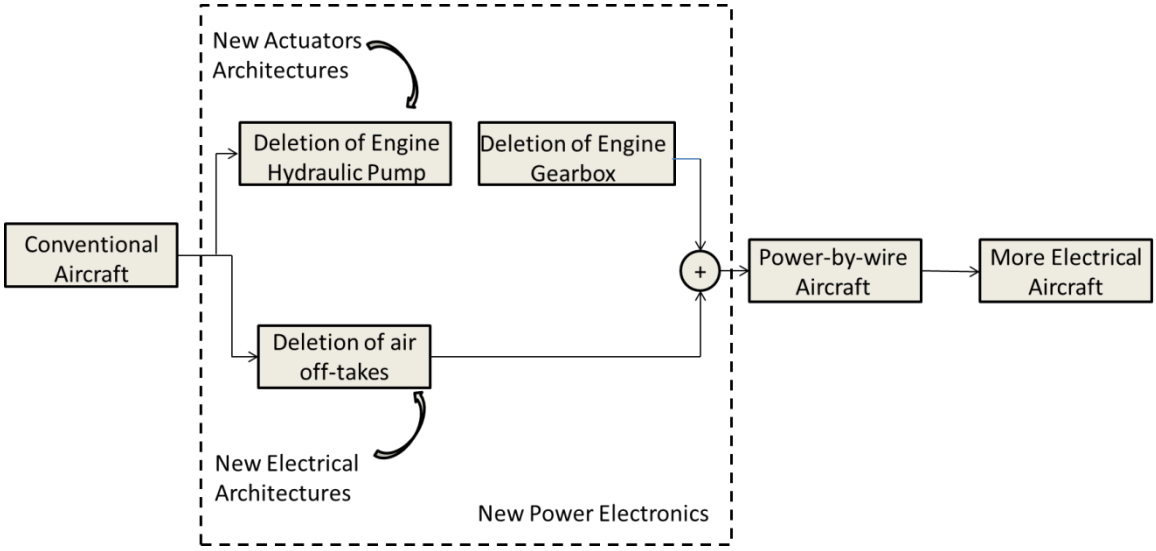

Figure 2-10 Moving towards MEA [14]

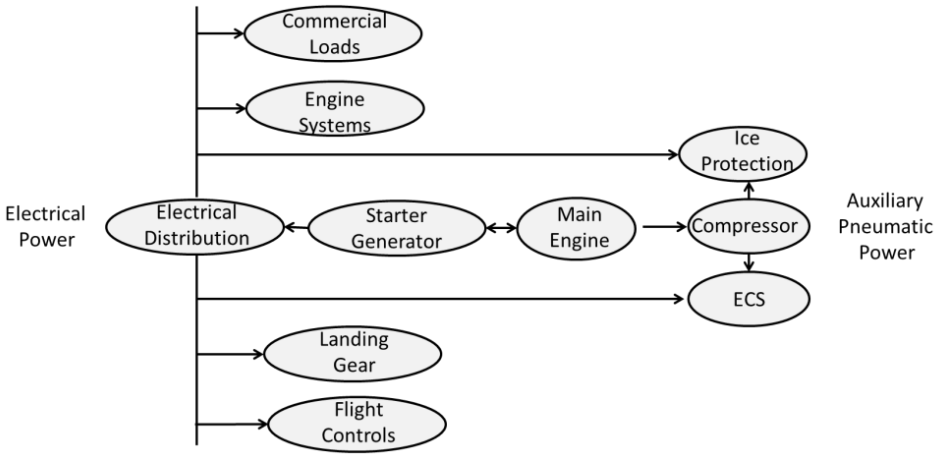

Figure 2-11 Schematic of MEA power distribution [14]

The MEA must assure high standards of power delivery, integration and safety to the aircraft's loads at any flight phase, by means of the ES.

In the MEA architecture a starter/generator, driven by the engine, produces the electrical power, which is transported through wires to a fault-tolerant electrical network to feed all the aircraft subsystems. In this design, electrical power converters could be used, eliminating the gearbox, which would lead to the possibility of using advance magnetic bearings [14].

A conceptual design of an electric helicopter powertrain was presented by [18]. This conceptual design of a one or two-seater helicopter, based on the

Robinson R22 does not include hydraulic assistance, which simplifies the control and AS.

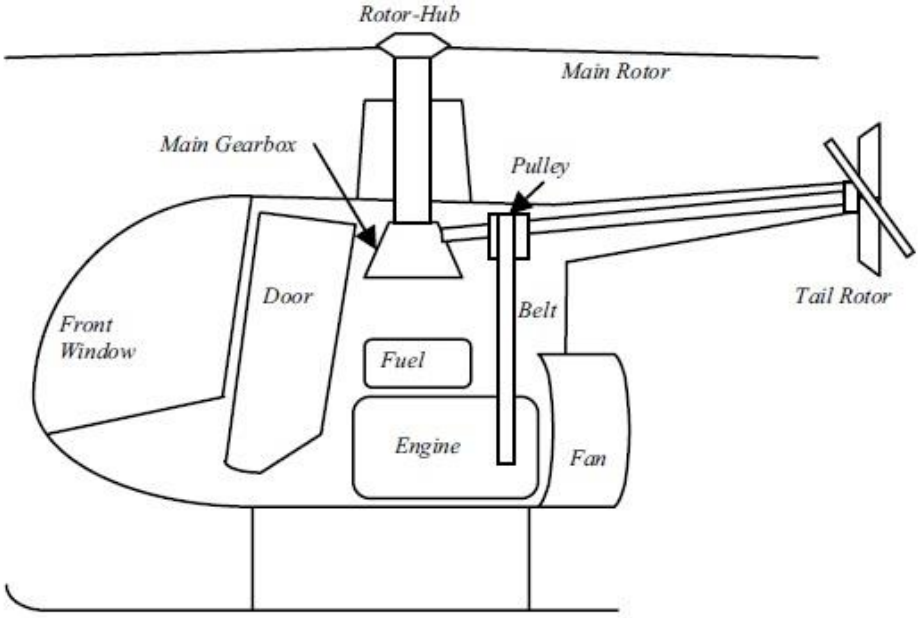

Figure 2-12 conventional helicopter powertrain [18]

The proposed electric powertrain of the helicopter will use an electric drive controlled by the pilot; this component will change from DC voltage generated on the electrical source, to AC voltage required to run the electrical engine, and then distribute the energy to the rotor system.

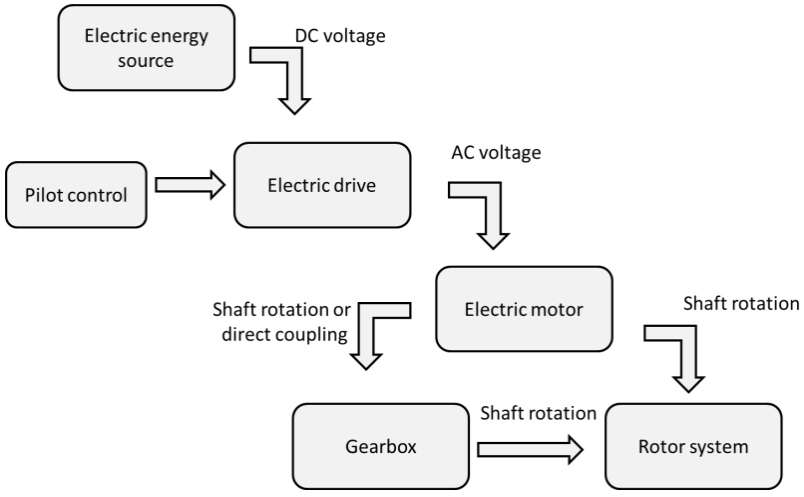

Figure 2-13 Electric powertrain system design [18]

For this design, Lithium-Ion batteries were chosen as primary power generation, showing in the best scenario only 0.5 hours of flight when using the same mass as the conventional power generation, and with an increase of almost 4 times in weight if the endurance requirement is 2 hours [18].

2.2.1 More Electric Engine

The More Electric Engine (MEE) advantages are reduction in losses that can be achieved by eliminating the accessory gearbox, and incorporating an electric motor for the ECS [19].

When the MEE concept is used, the accessory gearbox is replaced by an electric fuel pump, which avoids the use of a bypass system for the excess fuel flow at higher speeds; this configuration improves the fuel system, Fuel-cooled oil cooler, and engine efficiencies, by eliminating of the Air-cooler oil cooler.

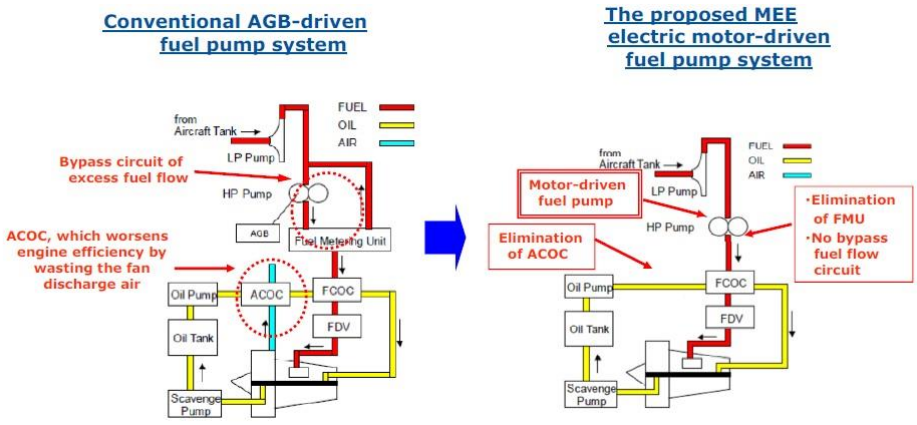

Figure 2-14 MEE [19]

2.2.2 More Electric Actuation System

To reduce hydraulic actuation system, required mostly for flight control systems, a Power-By-Wire (PBW) concept is considered, using electrical actuation systems. These systems can be Electro-hydrostatic Actuation (EHA) system or Electromechanical Actuation (EMA) system. The difference between EHA and

EMA is that for EHA, an electric motor drives a hydraulic pump which is in charge of driving the respective actuator. For EMA, the actuator is driven directly by the electric motor [20].

The advantage of using an electrical actuation system is the capability to control the power requirements along a mission.

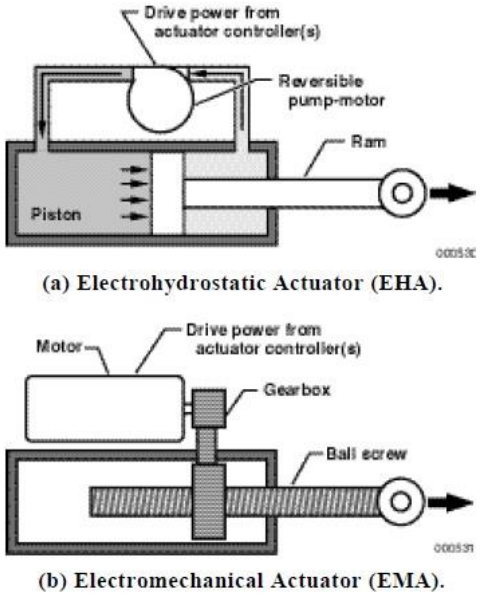

Figure 2-15 Example of power by wire actuators [21]

2.2.3 Electric ECS

For the helicopter electrical ECS, an electric compressor drives the air to the air conditioning pack, eliminating the bleed air from the main compressor. The advantages of using an electrical ECS are improvements in efficiency, and capabilities of regulate the power needed for the system in each flight phase, reducing the excessive extraction of energy [22].

As for the conventional ECS installed as standard equipment in the Bell 206 L-4, does not provide air conditioning, an electrical Air Cycle Machine (ACM) was proposed by [23].

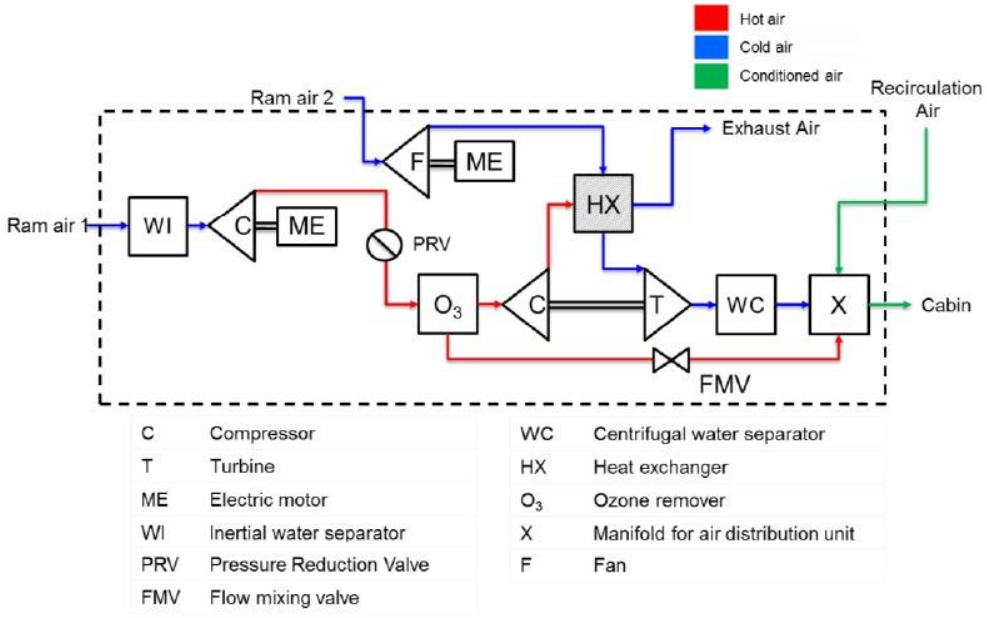

Figure 2-16 Electrical ECS configuration [23]

2.2.4 Electric IPS

For the Electric IPS, a numerical model was developed by calculating the power needed to keep the protected areas free of ice based on the Messinger method [24].

In this method, the protected surfaces are divided into control volumes, to compute a mass and energy balance analysis, so the rate of water catch, water evaporation, heat transfer coefficients and heat flux can be obtained [24].

The mass balance analysis was performed using empirical data, and for the energy balance analysis, convection losses, sensible heating, and latent heat flux were the only parameters taken into account [24].

3 Theoretical Work

3.1 Rotorcraft Mission Energy Management (RMEM) model

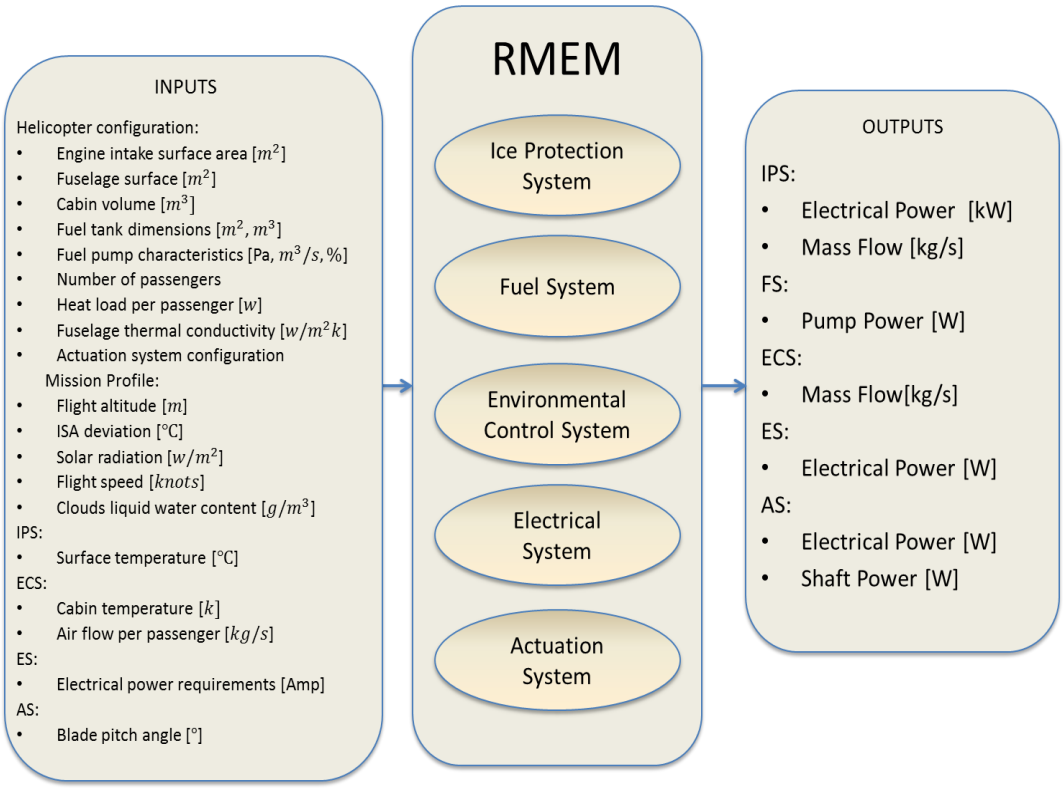

Figure 3-1 RMEM schematic

The RMEM model is a tool created at conceptual level by students within the Aerospace Engineering Department with the purpose of predicting the helicopter secondary airframe systems power requirements during a mission or flight segment. It represents and simulates individual systems onboard the helicopter, and provides a framework to evaluate novel systems' impact on performance at vehicle level.

The RMEM model was developed in Matlab/Simulink®, for this reason the capability of coupling it with helicopter performance models written in different languages was required. In order to achieve this, as a first approach, an executable able to read and write text files was created, eliminating the RMEM dependency from Matlab/Simulink®. Adding this capability, it was possible to run the model with a helicopter performance model written in FORTRAN.

The RMEM comprises five models: Ice Protection System (IPS), Fuel System (FS), Environmental Control System (ECS), Electrical System (ES), and Actuation System (AS).

- **RMEM PRINCIPLES OF OPERATION**

  Due to the capacity of tailoring RMEM to a specific HPM requirement, different alternatives of handling the model are presented in this section.

  The first RMEM version included two systems: IPS and ECS. The systems' parameters were treated as constants within the model, making complicated to update them if different configurations were used.

  For RMEM version 2 (RMEMva2), three systems were added, the ES, the FS, and the AS. Additionally, an M-file was incorporated, the M-file purpose is to handle directly all the parameters, to run an algorithm required for the AS and to execute RMEMva2 along with a HPM.

  The ES system power requirement capability added is based on the ES components required to be powered and the DC generator dynamic response to achieve the requirement.

  The AS calculates the main rotor actuators forces required by means of an actuator forces algorithm that takes into account blade aerodynamic forces and swashplate kinematics and dynamics depending on pitch inputs. It also includes the capability of calculating the power requirement of electromechanical and electro-hydrostatic actuators.

  For the FS, fuel pump characteristics, tank dimensions, characteristics of the fuel feed, losses in the system components and pipe geometries were considered.

  The RMEMva2 has been successfully integrated with two different HPM. The first model, also within the Aerospace Department, created in Matlab/Simulink®, computes the helicopter total power requirements for four individual segments along a flight mission: ground, hover, climb and forward flight. For this case, one set of inputs relating the operating

conditions was required to run both models, it calculates the helicopter power requirement and fuel consumption in each segment. The second HPM developed by the Power and Propulsion Department, is written in FORTRAN, which generated a need of eliminating Matlab® dependencies, to accomplish it, and achieving the models' integration, an executable was chosen as the best solution. Additionally, this HPM was developed to run a complete flight mission, because of this, the RMEMva2 inputs were reduced to the minimum required and coupled with the HPM outputs, generating the SPS power requirement for single points along the different flight segments.

3.1.1 Ice Protection System

The IPS can be hot bleed air or an electrical system, maintaining the surface temperature above freezing point of water and directing it backwards the heated area.

Mostly engine anti-icing and pitot heating equipment are installed on small helicopters due to weight issues. The IPS installed in the bell 206-L4 is an engine bleed air for the engine inlet, and a pitot heat system.

The electrical IPS developed for a medium size helicopter, to keep the engine intake protected, is based on the Messinger control volume method.

The model has three modules: mass and energy conservation, power module, and energy module. The first module calculates local water catch and heat transfer coefficients for every control volume, the second module estimates the power required to maintain the surface free of ice, and finally, the last module calculates the energy consumed according to the mission selected. , for further information please refer to [24].

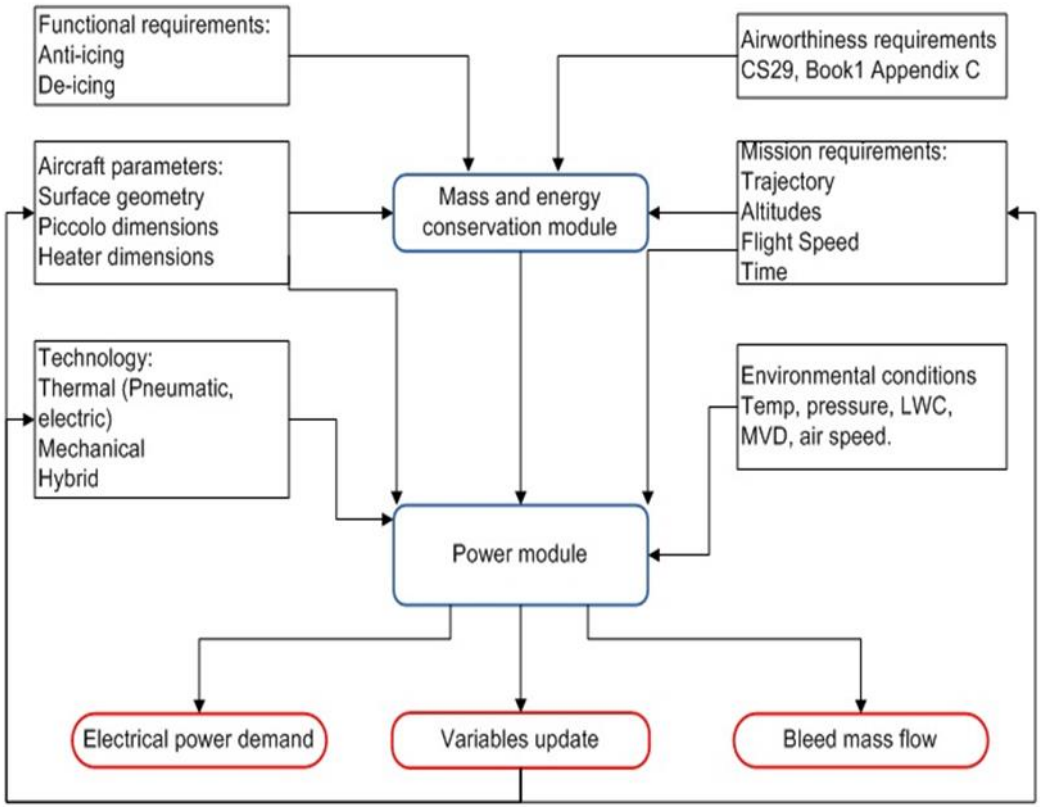

Figure 3-2 IPS model schematic [24]

3.1.2 Environmental Control System

The ECS provides adequate temperature and air quality to crew and passengers regarding the adverse ambient conditions which can be presented during a flight mission, and for avionic cooling purposes.

An Electric ACM was modeled to achieve these objectives. The simulation process first step involves establishing the requirements, which are fixed parameters and cannot be changed like the aircraft geometry, air requirement or number of passengers.

The next step involves the mission parameters which establish ambient conditions, flight altitude and temperature selected by the crew. For further information please refer to [23].

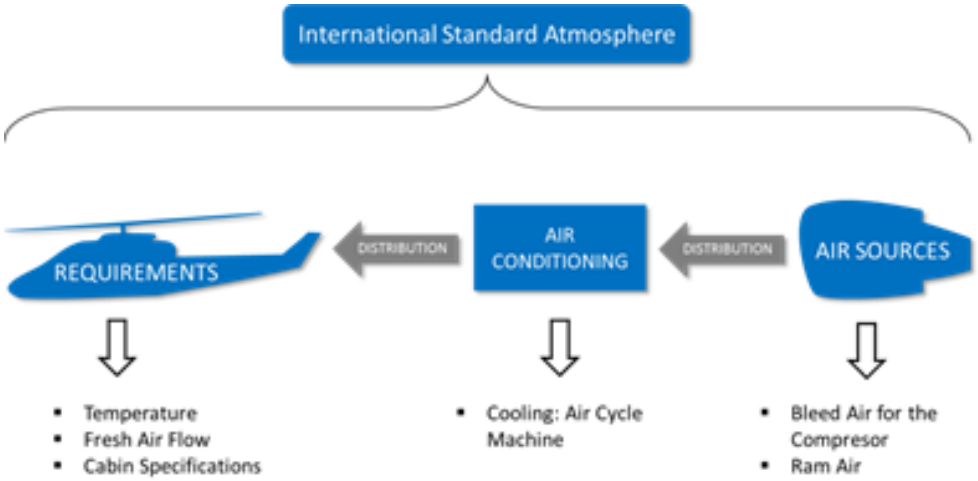

Figure 3-3 ECS model schedule [23]

3.1.3 Fuel System

For the fuel system modelling, only the fuel supply subsystem is taken into account, its main components are the fuel tank, measurement devices, feed lines, valves and fuel pumps.

In this system, the fuel pump is the only component requiring considerable amounts of power, for this reason the model represents the fuel pump characteristics, dimensions of the tank and characteristics of the fuel feed into the system [1].

1. Engine
2. Engine fuel pump and filter
3. Hose (L=0.17)
4. AFT Fuel filter
5. Hose (L=0.2m)
6. Tube (L=0.3m)
7. Fuel shutoff valve
8. Fuel pressure gage
9. Tank
10. Hose (L=1m)
11. Hose (L=0.36m)
12. Check valves
13. Thermal relief valve
14. Hose (L=0.56m)x2
15. Fuel boost pump

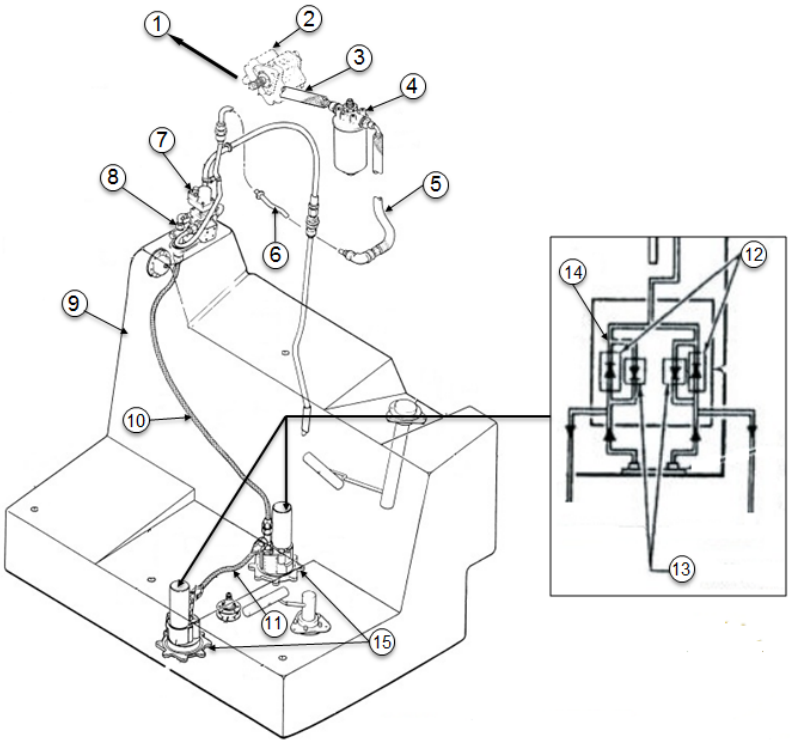

Figure 3-4 Fuel System Components and Dimensions

3.1.4 Electrical System

The bell 206L-4 helicopter electrical system is a single wire DC system, it consists of a 150 A 28 volt starter/generator, a 17AH 24 V NiCd battery, a voltage regulator, and a 400 A 28 V external power receptacle. There are no AC loads installed and after a generator failure, the battery must be capable of operating one fuel boost pump for approximately 3 hours.

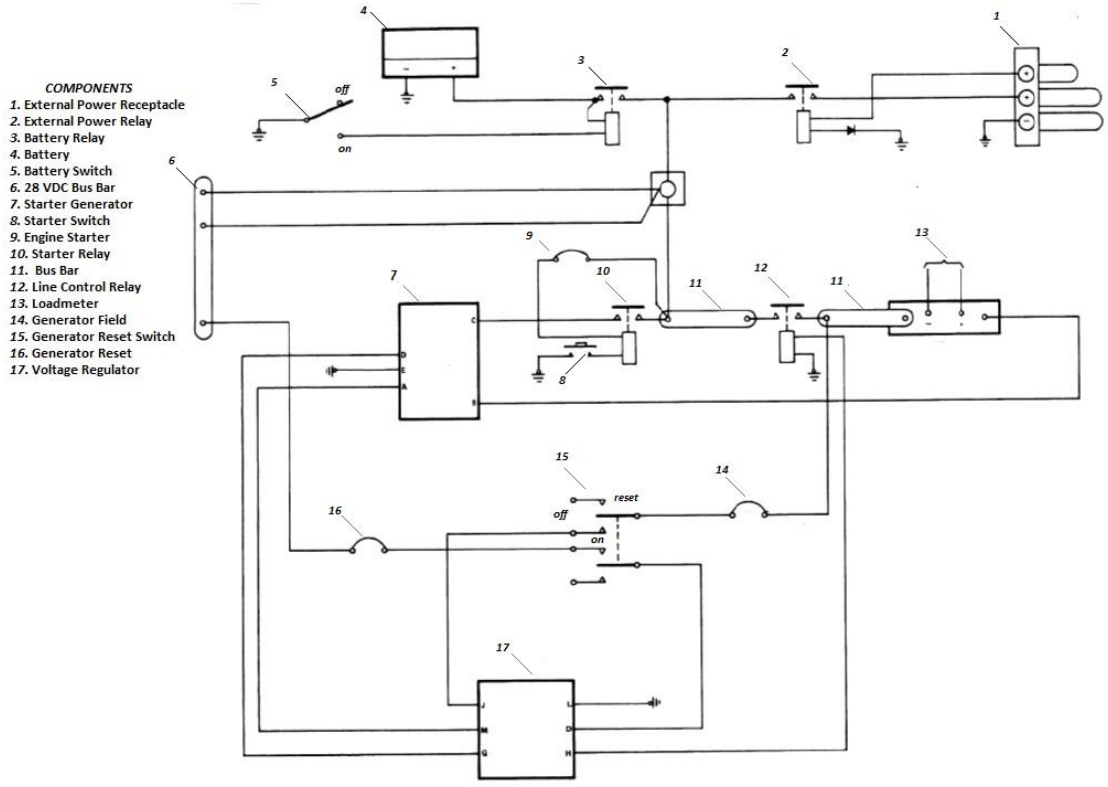

Figure 3-5 Electrical System Diagram

The electrical system proposed for incorporation in the RMEM is modelled based on battery and DC machine dynamic characteristics using Matlab/Simulink®, it comprises a starter/generator, a battery, and the loads; the external power receptacle was not included in this model. The voltage regulator is not included as the generator voltage was assumed to be constant along the DC machine operation.

The model is divided in 4 sections:

- Starter section:

The Starter section is related to the engine starting modelling; to achieve this purpose the battery provides energy to the starter/generator, which transforms this energy into torque, transmitting it to the engine.

- Generator section:

In the generator section, the generator mode is taken into account, where the engine RPM is an input to calculate the generator's voltage and current which are transmitted to the voltage regulator for distribution.

- Power distribution section:

In this section, depending on the flight phase the system delivers power to the appropriate components.

- Power requirement section:

Finally, last block calculates the electrical system power requirement for the specific flight phase or mission.

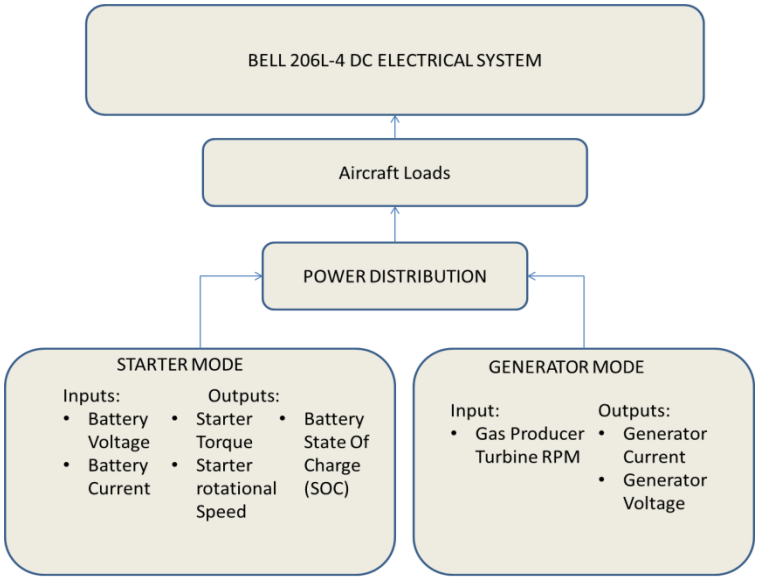

Figure 3-6 Electrical System Schematic

To take into account the load requirement it was necessary to include the components installed on a bell206L-4 helicopter and to develop an electrical load analysis.

Components installed on a bell206L-4

A database was generated to incorporate the components of a Bell 206 L-4. In the cases were information related to the power requirements was not publically available, similar components installed on Bell 206 L-series helicopters, also information from MD helicopters was used [25] [26].

Table 3-1 Bell 206L-4 Electrical Components Database

EQUIPMENT	NO. OF UNITS OR SYS.	AMPS PER UNIT OR SYS.	OPER. TIME IN MIN
ENG OIL PRES TEMP.	1	0.36	CON.
XMSN OIL PRES TEMP.	1	0.03	CON.
GAS PRODUCER RPM	1	0.36	CON.
TORQUE	1	0.36	CON.
TOT	1	0.03	CON.
AIRSPEED	1	0.36	CON.
FUEL QUANTITY	1	0.08	CON.
POWER TURBINE RPM / ROTOR RPM	1	0.08	CON.
WARNING UNIT	1	0.05	CON.
ENGINE OUT HORN	1	0.02	INTR.
INSTRUMENT LAMPS	11	0.44	CON.
EDGE LIGHT PANELS	SYS.	0.10	CON.
ENG OUT	4	0.10	INTR.
BATTERY HOT	4	0.10	INTR.
BATTERY RLY	4	0.10	INTR.
R/FUEL PUMP	4	0.10	INTR.
L/FUEL PUMP	4	0.10	INTR.
ROTOR LOW RPM	4	0.10	INTR.
TRANS OIL PRESSURE	4	0.10	INTR.
TRANS OIL TEMP	4	0.10	INTR.
FUEL LOW	4	0.10	INTR.
ENG CHIP	4	0.10	INTR.
TRANS CHIP	4	0.10	INTR.
FUEL FILTER	4	0.10	INTR.
T/R CHIP	4	0.10	INTR.
GEN FAIL	4	0.10	INTR.
FADEC	1	5.00	INTR.
IGNITER	1	0.75	INTR.
POSITION LIGHTS	4	3.00	CON.
ANTI-COLLISION LIGHTS	SYS.	3.50	CON.
LANDING LIGHTS	2	17.86	INTR.
MAP LIGHT	1	0.50	INTR.
VOLTAGE REGULATOR	1	0.30	CON.
BATTERY RELAY	1	0.60	CON.
EXTERNAL RELAY	1	0.50	CON.
STARTER RELAY	1	0.50	CON.
LINE CONTROL RELAY	1	0.50	CON.
TRANSCIEVER KY196	1	0.40	INTR.
TRANSCIEVER KY196		6.50	CON.
ICS KMA 24K	1	0.44	CON.
FUEL BOOST PUMP	2	11.33	CON.
CABIN HEATER BLEED AIR	SYS.	46.00	INTR.
PITOT TUBE	1	6.50	CON.
KT-76A transponder	1	1.80	CON.
Garmin GNS 530W GPS/COMM/NAV	1	3.00	CON.
KR-87 ADF	1	0.43	CON.
KDM-706A WITH KDI 572 INDICATOR	1	8.93	CON.
KR-21 marker beacon receiver	1	0.25	CON.
Autopilot KAP 150H	SYS.	4.10	INTR.
KRA-405B radio altimeter	1	0.85	CON.
SKY 497 Skywatch System	1	2.50	CON.
Vapor cycle air conditioner	SYS.	17.32	INTR.

Electrical Load Analysis (ELA)

The Electrical Load Analysis (ELA) and Power Source Capacity analysis determine individual systems capacity, by evaluation of average and maximum demands for all operating conditions [27] [28]. The Electrical Load Analysis was performed in accordance to [25] [26] [27] and [28].

A list of electrically operated components and its requirement must be included on the ELA [27]. If the power requirement of a component varies with flight segment, the higher value must be used first [27] [28].

Calculation of total power requirements is done by means of an Electrical Load Analysis chart, taking into account the operating conditions.

The ELA includes:

- Electric Bus Wiring Diagram.
- System Operation.
- Primary and Secondary Power Sources Description.
- Connected Load Chart.
- ELA chart:
    - Equipment electrically powered.
    - The load equipment plus control device requirement.
    - Operating Time: 5 seconds if the load lasts more than 0.3 seconds, 2 minutes if it is more than 5 seconds, and continuous if lasts more than 2 minutes according to [28].
    - Helicopter operating conditions [25] [26] [27] and [28]:
        - Engine Pre-start
        - Engine Start
        - Take-off and Climb (day/night)
        - Hover (day/night)
        - Cruise (day/night)
        - Landing (day/night)
        - Emergency – Generator out (day/night)
    - Conditions of Power Sources:

        - Normal Electrical Power Operation, the power generation systems are available.
        - Emergency Electrical Power Operation, if loss or malfunction of normal electrical power generation systems leads to operation of standby power generation.
    - Calculations:
        - Total Current (A-Min) is calculated by adding the number of units operating simultaneously multiplied by the current per unit multiplied by the operating time.
        - Maximum Demand (A) is calculated by adding the number of units operating simultaneously multiplied by the current per unit.
        - Average Demand (A) is calculated dividing the Total Current by the Duration of flight phase.
        - System Regulation
        - Load Shedding:

          After a loss of the power source occurs, a 5 minute period should be taken into account prior manual load shedding is applied.
    - Emergency or Standby Power Operation:

      As the battery is used to provide a time limited emergency supply period, an analysis of the battery capacity must be undertaken by either a practical test, or calculation.
- Battery Analysis
    - Battery Capacity:

      For the ELA, the battery capacity is calculated in ampere-minutes, taking into consideration that a heavier discharge current will reduce the operating time. High discharge battery currents will be encountered until load shedding is applied when a generator failure takes place, to include this behaviour, the power consumed must be factored by an additional 20% if the average discharge current is more than twice the battery one-hour rating [28].
    - Battery-Charging Current Analysis:

The charging current for any aircraft battery is based on the total elapsed time from the beginning of the charge, and is calculated by:

$$I = A\ x\ C \tag{3-1}$$

where,

I is the average charging current (A)

A is the ampere-hour capacity of the battery, based on the one-hour discharge rate.

C is the battery charging factor, taken from the battery charging curve.

- Engine Starting Electrical Requirements.

Electrical System Model

As it was stated before the model consists of 4 different sections:

In the starter section, a 24 volt 17AH battery was modelled to calculate the battery output current and voltage, as well as its State Of Charge (SOC) based on the battery discharge rate, and the time required for engine starting.

The values related to battery current and voltage are used as inputs for the starter mode, which calculates the motor field and armature currents required to achieve the typical starter output power based on the Starter/Generator specifications for a Bell 206L series helicopter [29].

In the generator section, the gas producer turbine RPM is the input and the load current is the output.

If a different helicopter is to be used, the starter and generator sections include the capability of modelling four different types of DC motors: separately excited, shunt-connected, series-connected, and compound-connected.

In the power distribution section, depending on the flight segment and operating components, a feedback signal is sent to the generator section, which varies a rheostat connected in series with the field resistance in order to match generated and required load currents.

In the last section the overall electric system power requirement is calculated. The power requirement is then added to RMEM output power and integrated with the helicopter performance model to account for the performance penalties of SPS.

- **Starter Block**

  To model the battery power transmission to the starter, a battery block from the Simulink SimPowerSystems library was used as reference for a Nickel-Cadmium battery. Provided that battery characteristics become available, the model can be easily updated to achieve more accurate results.

  To reduce computational time and dependencies from the SimPowerSystems library, the battery characteristics were mapped over a wide range of operating currents, without degrading the battery voltage and SOC results.

  - **Battery Discharge model**

    The discharge model based on [30] calculates the output voltage depending on current consumption and elapsed time as shown in Figure 3-7. It incorporates the relationship between the open circuit voltage (OCV) and SOC

    $$V_{batt} = E_0 - K\frac{Q}{Q - it}it - Ri + Exp\dot{(}t) - K\frac{Q}{Q - it}i^* \quad (3\text{-}2)$$

    where

    V_{batt} = Battery voltage (V)

    E_0 = Battery constant voltage (V)

    K = Polarisation constant (V/Ah) or polarisation resistance (Ω)

    Q = Battery capacity (Ah)

    it = Actual battery charge (Ah)

    R = Internal resistance (Ω)

    i = Battery current (A)

    i^* = Filtered current (A)

    $Exp\dot{(}t)$ = Exponential zone

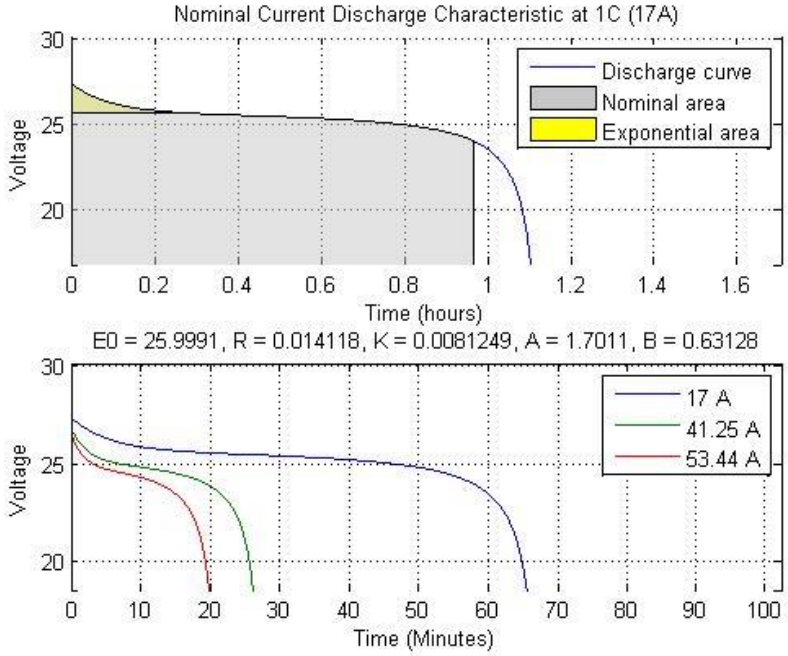

Figure 3-7 Battery discharge curves

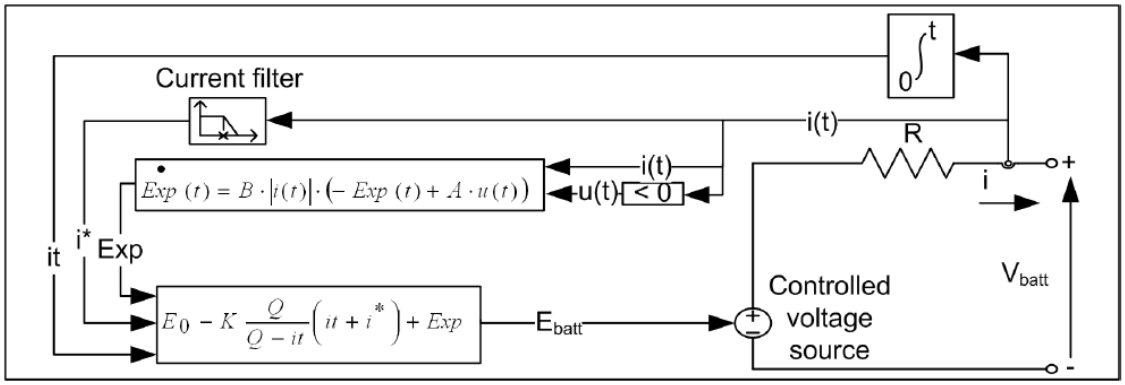

Figure 3-8 Discharge battery model [30]

- **DC Motor model**

  The motor model includes four different configurations depending on the field and armature windings connection: Separately excited, Shunt connected, Series Connected and a Compound DC motor.

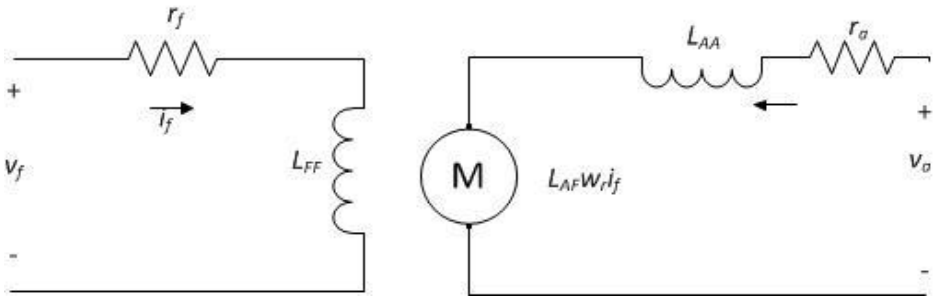

Figure 3-9 DC machine equivalent circuit

The equations required to model the electrical and mechanical characteristics of the different DC motors, based on [31] [32] [33] [34] and [35] will be presented in this section.

- Shunt-connected DC machine

  For a shunt-connected DC machine, the field flux is derived by connecting the field circuit directly across the armature terminals.

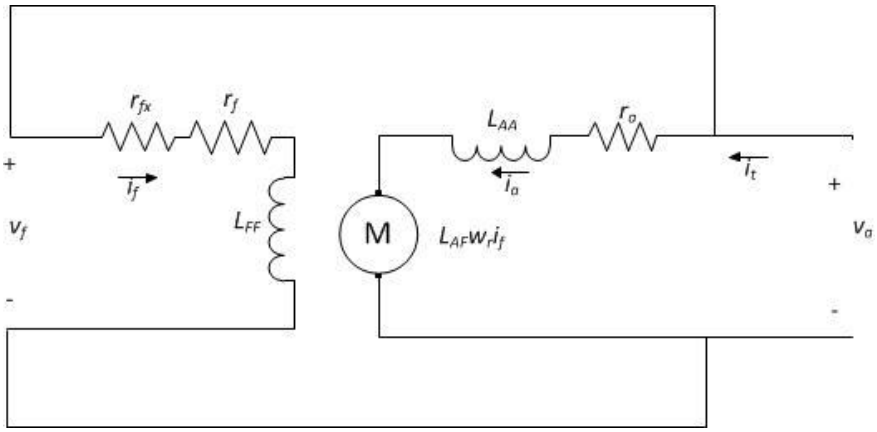

Figure 3-10 Shunt-connected DC machine

Field and armature voltages for a shunt-connected DC machine:

$$\begin{bmatrix} v_f \\ v_a \end{bmatrix} = \begin{bmatrix} R_f + pL_{FF} & 0 \\ w_r L_{AF} & r_a + pL_{AA} \end{bmatrix} \begin{bmatrix} i_f \\ i_a \end{bmatrix} \tag{3-3}$$

where

$R_f = r_f + r_{fx}$ is the field resistance plus any resistance connected in series with the field winding

p represents the operator $\frac{d}{dt}$

w_r is the rotor speed

R_a is the armature resistance

i_a and i_f are the armature and field currents

L_{AA} and L_{FF} are the armature and field windings self-inductances

L_{AF} is the mutual inductance between the field and the rotating armature coils

Solving field and armature voltage equations for i_f and i_a gives:

$$\frac{di_f}{dt} = \left(\frac{v_f}{R_f} - i_f\right)\frac{1}{\tau_f} \tag{3-4}$$

$$\frac{di_a}{dt} = \frac{\frac{v_a - e_a}{R_a} - i_a}{\tau_a} \tag{3-5}$$

e_a is the back EMF

$$e_a = L_{AF} w_m i_f \tag{3-6}$$

τ_f and τ_a are field and armature circuits time constants

$$\tau_f = \frac{L_{FF}}{R_f} \tag{3-7}$$

$$\tau_a = \frac{L_{AA}}{R_a} \tag{3-8}$$

The electromagnetic torque and speed equations for a shunt-connected DC machine are:

$$T_E = L_{AF} i_f i_a = J\frac{dw_m}{dt} + B_m w_m + T_L \tag{3-9}$$

Solving for speed

$$\frac{dw_m}{dt} = \frac{L_{AF} i_f i_a - T_L - B_m w_m}{J} \tag{3-10}$$

where

J is the moment of inertia of the rotor and mechanical system

B_m is the damping coefficient of the machine and the load

T_L is the load torque, positive for a torque on the shaft of the machine and can be related to the rotational speed by

$$T_L = B_l w_m \tag{3-11}$$

B_l is the slope of the torque-speed curve at the operating point.

- Series-connected DC machine

  For a series machine, field and armature circuit are connected in series. A reduction in voltage drop across the field winding is achieved with this connection.

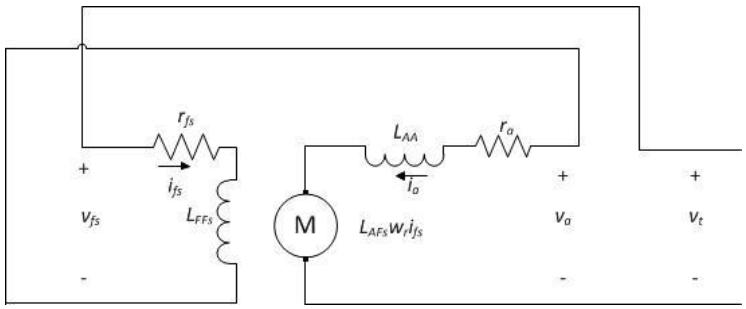

Figure 3-11 Series-connected DC machine

The series field, armature and terminal voltage equations for a series machine are:

$$\begin{bmatrix} v_{fs} \\ v_a \end{bmatrix} = \begin{bmatrix} R_{fs} + pL_{FFs} & 0 \\ w_r L_{AFs} & r_a + pL_{AA} \end{bmatrix} \begin{bmatrix} i_{fs} \\ i_a \end{bmatrix} \tag{3-12}$$

where

$$v_t = v_{fs+} v_a \tag{3-13}$$

Solving for the armature and series field currents

$$\frac{di_a}{dt} = \frac{v_t - [(r_{fs} + r_a + w_m L_{AFs}) i_a]}{\tau_{fa}(r_{fs} + r_a)} = \frac{di_f}{dt} \tag{3-14}$$

where

$$\tau_{fa} = \frac{L_{FFs} + L_{AA}}{r_{fs} + r_a} \tag{3-15}$$

The electromagnetic torque equation for a series-connected machine becomes

$$T_e = L_{AFs} i_a^2 \ = J\frac{dw_m}{dt} + B_m w_m + T_L \tag{3-16}$$

The subscript s is used to denote parameters associated with the series field.

- Compound-connected DC machine

  In compound machine, both shunt and series field winding are incorporated. It is common that the machine characteristics are controlled mostly by the shunt field, while a secondary influence is produced by the series field.

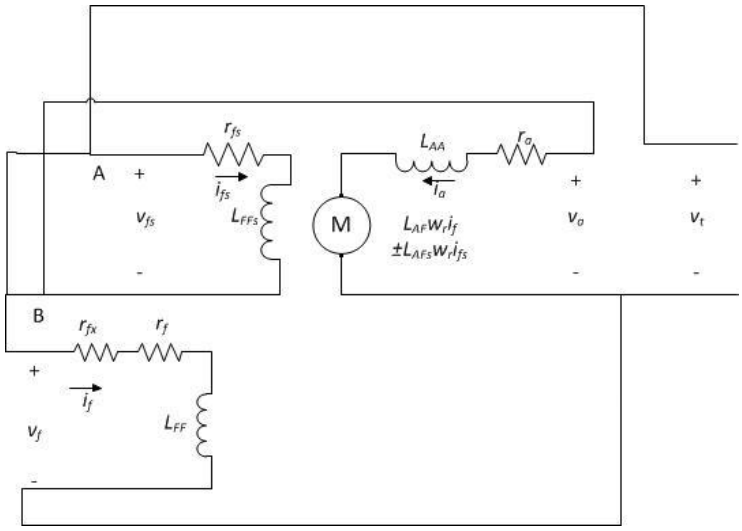

Figure 3-12 Compound-connected DC machine

A compound machine is called cumulative compounding when it is connected in a configuration to aid the flux produced by the shunt field. If the connection is done so as the series field opposes the flux produced by the shunt field, it is called differentially compounding.

The voltage equations for a compound machine are:

$$\begin{bmatrix} v_f \\ v_t \end{bmatrix} = \begin{bmatrix} R_f + pL_{FF} & \pm pL_{FS} & 0 \\ w_r L_{AF} \pm pL_{FS} & \pm w_r L_{AFS} + r_{fs} + pL_{FFs} & r_a + pL_{AA} \end{bmatrix} \begin{bmatrix} i_f \\ i_{fs} \\ i_a \end{bmatrix} \quad (3\text{-}17)$$

The signs in are used to represent either a cumulative or a differential connection.

Additionally, depending on the shunt field connection, the compound machine is called long-shunt when the shunt field is ahead of the series field, or short-shunt when it is behind the series field, as shown in Figure 3-12 by A and B respectively.

The most common configuration is a long-shunt connection and it will be used for this analysis, where the relationship between voltages and currents are given by:

$$v_t = v_f = v_{fs} + v_a \quad (3\text{-}18)$$

$$i_t = i_f + i_{fs} \quad (3\text{-}19)$$

where $i_a = i_{fs}$

Solving for field and armature currents gives:

$$\frac{di_f}{dt} = \frac{\frac{1}{R_f}\left(v_f \mp L_{FS}\frac{di_a}{dt}\right) - i_f}{\tau_{ff}} \quad (3\text{-}20)$$

$$\frac{di_a}{dt} = \frac{1/\left(r_{fs} + r_a\right)\left(v_t \mp w_r L_{AFs} i_a - L_{AF} i_f w_r \mp L_{FS} p i_f\right) - i_a}{\tau_{fa}} \quad (3\text{-}21)$$

$$T_e = L_{AF} i_f i_a \pm L_{AFs} i_a^2 = J\frac{dw_m}{dt} + B_m w_m + T_L \quad (3\text{-}22)$$

where L_{FS} is the mutual inductance between the shunt and the series fields.

- **Generator Section**

  To model the generator section, the rotational speed is the input, and the generated current is the output. To accomplish this, a relationship between the source torque T_s and rotational speed w_m transmitted from the gas producer turbine is used:

$$T_s = B_l w_m \tag{3-23}$$

  - **DC Generator model**

    A DC generator is a DC machine used as a generator, the direction of the power flowing through a DC machine determines if it is operating as a motor or as a generator.

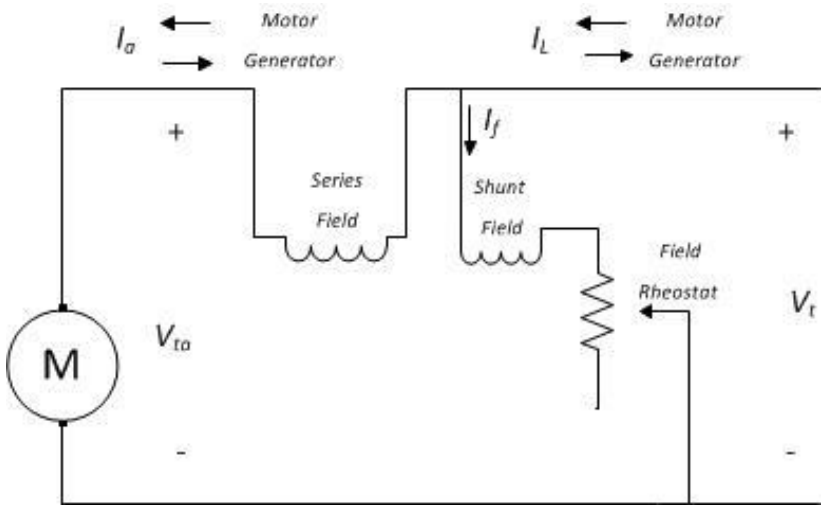

Figure 3-13 DC machine power flow

As for the case of the DC motor model, four different configurations are included in the DC generator model:

- Shunt-connected DC generator

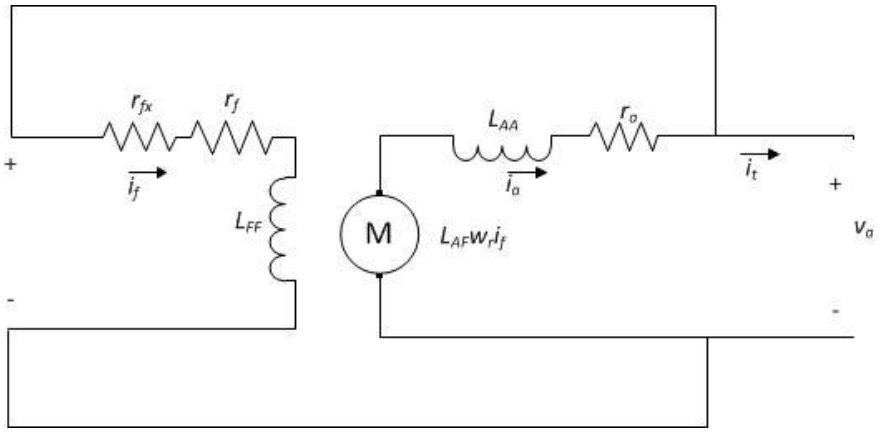

Figure 3-14 Shunt-connected DC machine

Field and armature voltages for a shunt-connected DC generator:

$$\begin{bmatrix} v_f \\ v_a \end{bmatrix} = \begin{bmatrix} R_f + pL_{FF} & 0 \\ w_r L_{AF} & -r_a - pL_{AA} \end{bmatrix} \begin{bmatrix} i_f \\ i_a \end{bmatrix} \tag{3-24}$$

Solving the field and armature voltage equations for i_f and i_a

$$\frac{di_f}{dt} = \left(\frac{v_f}{R_f} - i_f\right)\frac{1}{\tau_f} \tag{3-25}$$

$$\frac{di_a}{dt} = \frac{\frac{e_a - v_{ta}}{R_a} - i_a}{\tau_a} \tag{3-26}$$

The source torque and speed equations for a shunt-connected DC generator are:

$$T_S = J\frac{dw_m}{dt} + B_m w_m + T_E \tag{3-27}$$

Solving for speed

$$\frac{dw_m}{dt} = \frac{T_S - L_{AF} i_f i_a - B_m w_m}{J} \tag{3-28}$$

- Series-connected DC machine

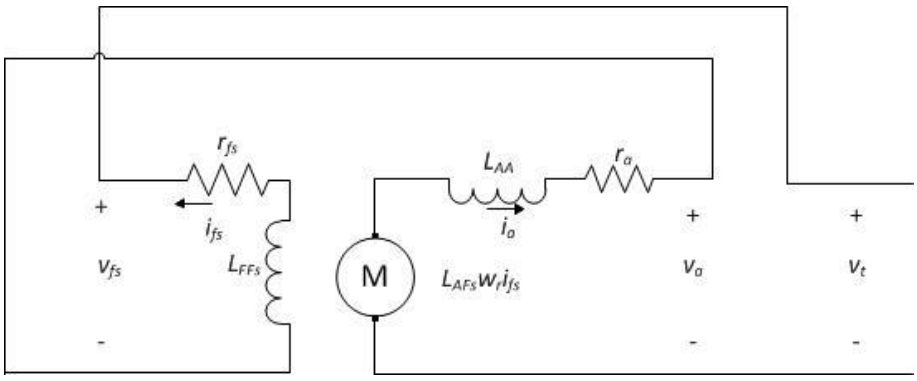

Figure 3-15 Series-connected DC generator

The series field, armature and terminal voltage equations for a series generator are:

$$\begin{bmatrix} v_{fs} \\ v_a \end{bmatrix} = \begin{bmatrix} -R_{fs} - pL_{FFs} & 0 \\ w_r L_{AFs} & -r_a - pL_{AA} \end{bmatrix} \begin{bmatrix} i_{fs} \\ i_a \end{bmatrix} \tag{3-29}$$

where,

$$v_t = v_{fs} + v_a \tag{3-30}$$

Solving for the armature and series field current

$$\frac{di_a}{dt} = \frac{w_m L_{AFs} i_a - (r_{fs} + r_a) i_a - v_t}{\tau_{fa}(r_{fs} + r_a)} = \frac{di_f}{dt} \tag{3-31}$$

The rotational speed equation is:

$$\frac{dw_m}{dt} = \frac{T_S - L_{AFs} i_a^2 - B_m w_m}{J} \tag{3-32}$$

- Compound-connected DC generator

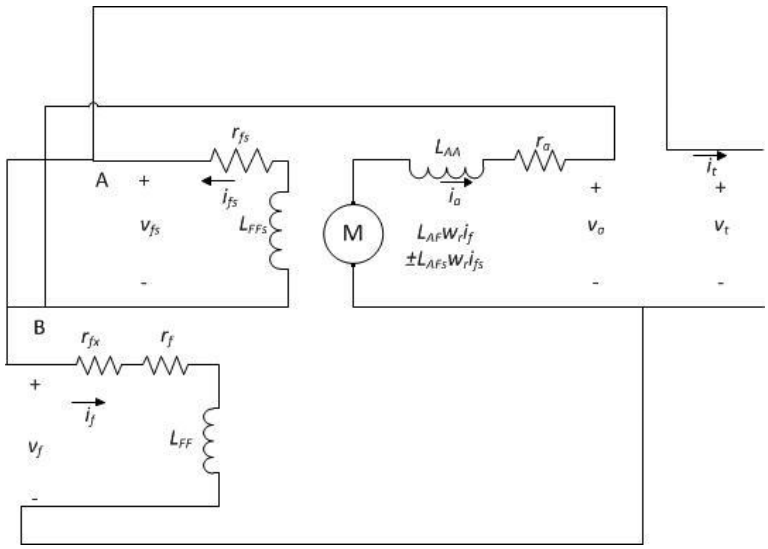

Figure 3-16 Compound-connected DC generator

The voltage equations for a compound generator are:

$$\begin{bmatrix} v_f \\ v_t \end{bmatrix} = \begin{bmatrix} R_f + pL_{FF} & \pm pL_{FS} & 0 \\ w_r L_{AF} \pm pL_{FS} & \pm w_r L_{AFS} - r_{fs} - pL_{FFs} & -r_a - pL_{AA} \end{bmatrix} \begin{bmatrix} i_f \\ i_{fs} \\ i_a \end{bmatrix} \tag{3-33}$$

For a long-shunt connection, the relationship between voltages and currents are given by:

$$v_t = v_f = v_{fs} + v_a \tag{3-34}$$

$$i_t = i_{fs} - i_f \tag{3-35}$$

where

$$i_a = i_{fs}$$

The equation used for the field current is the same as for a compound DC motor, and the armature current equation is:

$$\frac{di_a}{dt} = \frac{1/\left(r_{fs} + r_a\right)\left(L_{AF} i_f w_r \pm w_r L_{AFs} i_a \pm L_{FS} p i_f - v_t\right) - i_a}{\tau_{fa}} \tag{3-36}$$

The rotational speed equation for a compound generator is:

$$\frac{dw_m}{dt} = \frac{T_S - (L_{AF} i_f i_a \pm L_{AFs} i_a^2) - B_m w_m}{J} \quad (3\text{-}37)$$

- **Power distribution section**

Based on the analysis done in the ELA section it is possible to predict the load requirements i_r in the different flight segments. This load requirement will be then compared to the current generated i_t by the generator section. If load produced and required are not within a difference of ±1 A, an iterative process takes place, in order to increase or decrease the field resistance until the target is accomplished.

$$e_n = -i_t - i_r \quad (3\text{-}38)$$

If $e_n > 0$

while $e_n > 1$

$$R_{fn+1} = R_{fn} - 1 \quad (3\text{-}39)$$

If $e_n < 0$

while $e_n < -1$

$$R_{fn+1} = R_{fn} + 1 \quad (3\text{-}40)$$

- **Power Consumption section**

The relationship between torque and speed is used to compute the power required by the ES and added to the overall RMEM power requirements in the different flight segments.

$$P = w_m T_e \quad (3\text{-}41)$$

3.1.5 Actuation System

Different configurations for the AS were integrated with RMEM. The AS model purpose is to calculate the system's power consumption when using hydraulic,

electromechanical, or electro-hydrostatic actuators to assess the helicopter performance penalties in terms of fuel consumption due to these technologies.

The AS was intended for calculating the power requirements of fixed-wing actuators, and so, it included an aero load estimator for fixed-wing control surfaces [36]. This aero load estimator had to be replaced by a rotary-wing main rotor actuators forces algorithm as an initial approach.

In a helicopter main rotor, the blade pitch angle changes according to the swashplate orientation, which is controlled by the actuators. The connection between swashplate and blades is achieved by means of pitch links [37].

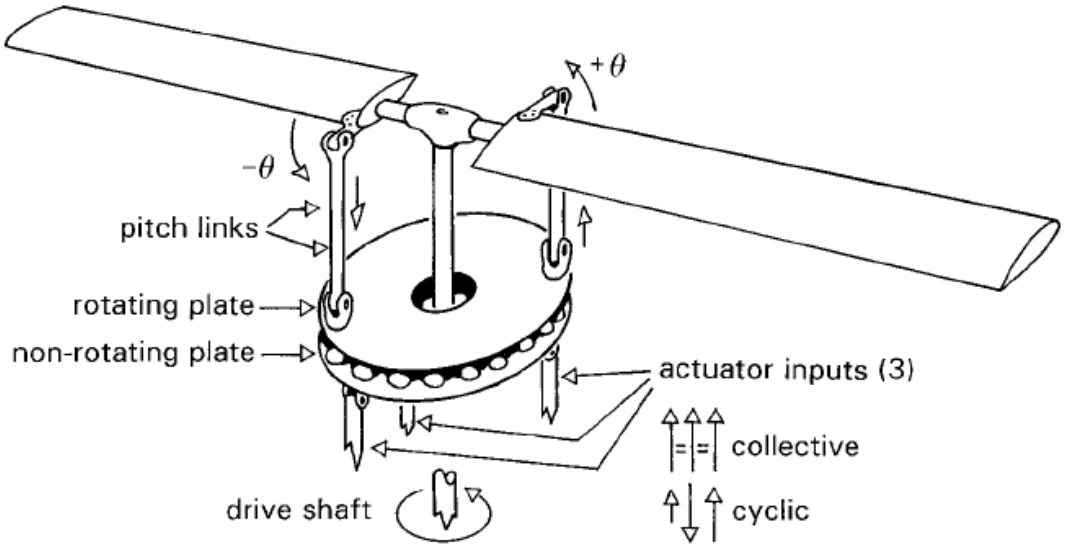

Figure 3-17 Rotor control through a swashplate [38]

According to [5], the torque produced by the blades must be counteracted by the main rotor actuators' forces. This torque is generated from the blade pitching moment and the moment generated by the lift at the flexural axis.

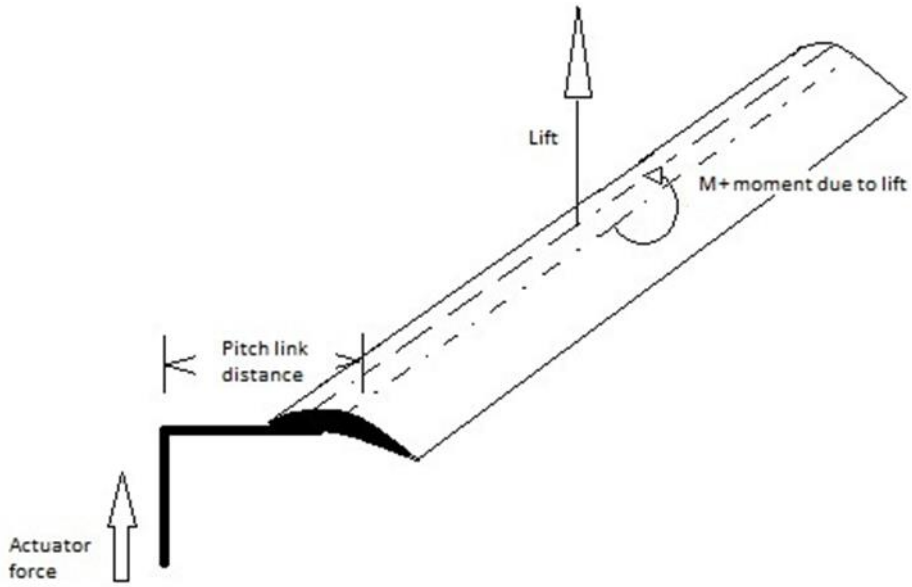

Figure 3-18 Actuator force analysis [5]

Additionally to the torque produced from aerodynamic forces, [6] takes into consideration swashplate kinematics and blade torsional moments. Flap motion is neglected in the analysis as the blade centre of gravity is located at the feathering axis, and the kinematic pitch-flap coupling does not alter the torsional loads.

The proposed algorithm incorporates both approaches, developed for the hover condition, and extents the analysis to axial climb and forward flight conditions. This algorithm was generated and added to the AS model, with the aim of calculating the actuators' force requirement to achieve a specific blade pitch angle.

The algorithm was divided in three different sections:

- Rotor blade aerodynamic analysis.
- Blade-Swashplate kinematic analysis.
- Blade - Swashplate dynamic analysis.

The rotor blade aerodynamic analysis was developed using: the Momentum Theory (MT), the Blade Element Theory (BET) and the Blade Element and Momentum Theory (BEMT) for each flight segment, blade lift due to cyclic and

collective pitch commands is calculated. The equations used for the different theories are based on [37] [38] [39] [40] and [41].

The Blade-Swashplate kinematic analysis takes into account the geometry, initial and final position of the components involved in changing the main rotor blades' pitch, as proposed by [6].

Finally, in the Blade - Swashplate dynamic analysis, pitch link forces required to counteract a combination of blade aerodynamic and inertial forces are estimated.

The pitch link forces are then treated as inputs for the AS to predict overall system power requirements in a complete mission, or individual flight segment, depending on the HPM requirements. The power requirements are calculated for three different system configurations:

- Hydraulic AS.
- Electromechanical AS.
- Electro-hydrostatic AS.

The equations used for blade lift, rotor thrust, and pitching moment calculations based on: linear inflow models, constant chord blades, no hinge offset, linearly twisted blades, no compressibility effects, and constant aerofoil moment coefficient will be presented in the following sections. Blade feathering and flapping are modelled using the first harmonics of the Fourier series, as from the second harmonics, the values can be considered negligible in the analysis.

- ***Rotor blade aerodynamic analysis working principles***

  The blade aerodynamic block computes the lift distribution of each blade along a rotation taking into account collective and cyclic inputs, as well as the blade conning motion in hover, climb and forward flight. As part of the code generation process, the first lift calculation was accomplished under several assumptions, starting with untwisted blades and no losses

in the blade root and tip, until a complete incorporation of each parameter was achieved.

- Hover
  - Momentum Theory

    The theory makes the following assumptions: air is an inviscid an incompressible fluid, the rotor acts as a uniformly loaded or actuator disk with an infinity number of blades so that there is no periodicity in the wake, the flow both upstream and downstream of the disk is uniform, occurs at constant energy and is contained within a streamtube, and no rotation is imparted on the fluid by the action of the rotor.

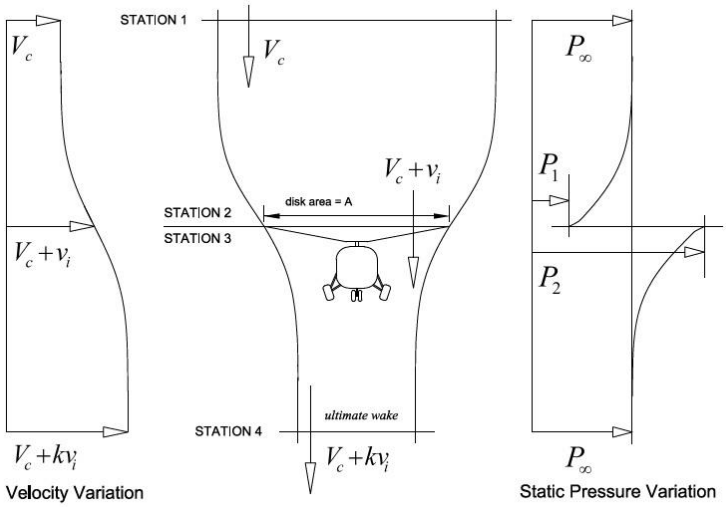

Figure 3-19 Flow through the Actuator Disk [41]

The MT defines a relationship between the rotor thrust coefficient and the rotorcraft weight in hover, this is given by:

$$C_T = \frac{Tr}{\rho Ar(\Omega R)^2} = \frac{W}{\rho Ar(\Omega R)^2} \tag{3-42}$$

where Tr is the rotor thrust.

W is the helicopter weight.

ρ is the air density.

Ar is the rotor area.

Ω is the rotor angular velocity.

and R is the rotor radius.

The velocity imparted to the mass of air contained in the control volume at the rotor disk or induced velocity at the rotor disk is:

$$v_i = -\frac{V_c}{2} + \sqrt{\left(\frac{V_c}{2}\right)^2 + \frac{Tr}{2\rho Ar}} \tag{3-43}$$

In hover the climb velocity $V_c = 0$ and the induced velocity $v_i = v_h$ is the induced velocity in hover.

For helicopters it is the convention to nondimensionalise all velocities by the blade tip speed in hover, V_{tip} because it is a useful quantity when comparing results from different rotors, this is called the induced inflow ratio

In hover: $\lambda_i = \lambda_h$

$$\lambda_h = \frac{v_i}{V_{tip}} = \frac{v_i}{\Omega R} \tag{3-44}$$

- Blade Element Theory

  If a rotor consisting of Nb blades of chord $c(r)$ and radius R, and with a rotational speed Ω is considered, it is possible to gain insight into how the rotor generates thrust by examining the forces generated on a small blade element of span, δr, located at r distance from the hub.

  To calculate the incremental lift per unit span in hover it was necessary to divide the blade into elements, and determine the in-plane velocity component and lift at each element.

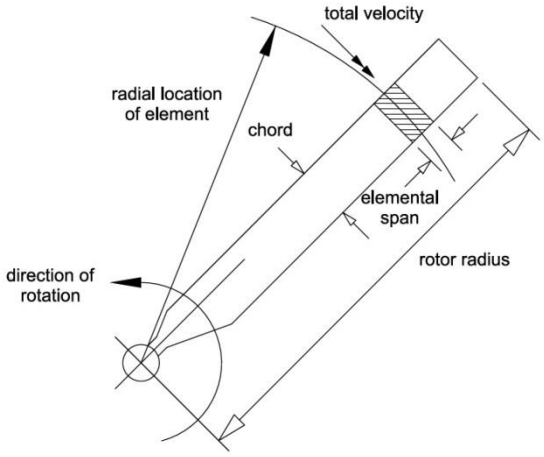

Figure 3-20 Rotor blade element [41]

The magnitude and direction of the airflow relative to the blade element is given by

$$U = \sqrt{(V_c + v_i)^2 + (\Omega r)^2} \tag{3-45}$$

The $V_c + v_i$ term is called the out-of-plane velocity component U_P, and Ωr represents the in-plane component U_T.

Usually U_P is much smaller than U_T and $U \cong U_T$

The inflow angle or induced angle of attack, the effective angle of attack, and the local blade lift coefficient are related to U_T and U_P by:

$$\phi = \tan^{-1}\left(\frac{U_p}{U_T}\right) \tag{3-46}$$

$$\alpha = \theta - \phi \tag{3-47}$$

$$C_l = C_{l_\alpha}(\theta - \emptyset - \alpha_0) \tag{3-48}$$

where:

θ is the blade pitch angle

$C_{l_\alpha}$is the two-dimensional lift-curve-slope of the aerofoil section comprising the rotor.

and $\alpha_0$is the corresponding zero-lift angle, assuming symmetric aerofoils $\alpha_0 = 0$.

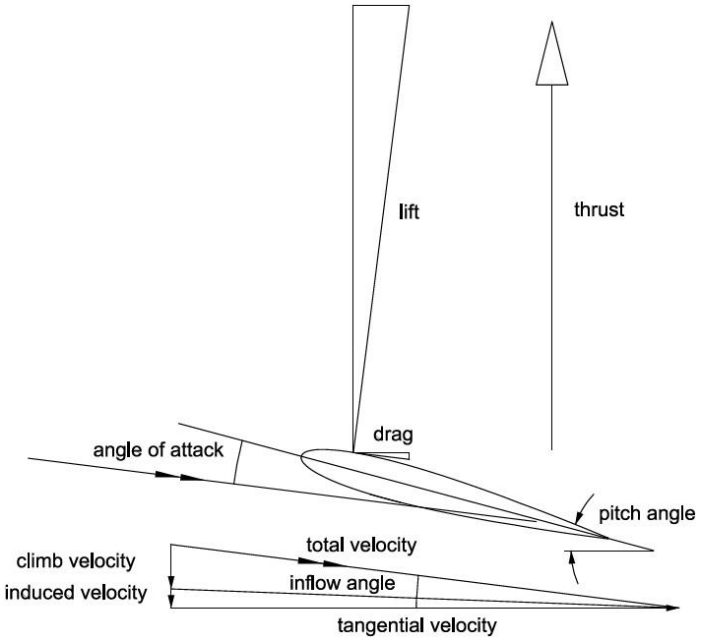

Figure 3-21 Forces at the blade element [41]

The elemental lift was calculated using four different approaches:

- Constant elemental blade pitch $\theta = \theta_0$:
  A blade with zero twist is assumed.
- Linearly twisted blade $\theta_{(r)} = \theta_0 + r\theta_{tw}$:
  For helicopter rotors is common to design the blades with linear twist, where θ_{tw} is the blade twist rate.
- Blade root $0 \leq BR \leq 0.25R$ and Tip-Loss Factor$0.95 \leq B \leq 0.98$ As the blade is not able of producing lift near the root or blade tip, blade root and Tip-Loss factor are used to represent this phenomenon.
- Cyclic inputs

$$\theta(r,\psi) = \theta_0 + r\theta_{tw} + \theta_{1c}\cos\psi + \theta_{1s}\sin\psi \tag{3-49}$$

where θ_{1c} and θ_{1s} are the lateral and longitudinal pitch inputs respectively, and ψ is the azimuthal blade position.

$$dL = \frac{1}{2}\rho V c C_l dr \tag{3-50}$$

The relationship between the incremental lift and incremental thrust coefficient is:

$$dC_T = \frac{NbdL}{\rho A(\Omega R)^2} = \frac{dTr}{\rho A(\Omega R)^2} \tag{3-51}$$

and

$$dC_T = \sum dC_T \tag{3-52}$$

In order to validate the results given for the thrust coefficient, it was compared for each approach with the results given by a different method [39]:

$$C_T = \frac{1}{2}\sigma \int_0^1 c_{l_\alpha}(\theta_0 r^2 - \lambda r)dr \tag{3-53}$$

$$C_T = \frac{1}{2}\sigma \int_{BR}^{B} c_{l_\alpha}\big((\theta_0 + r\theta_{tw})r^2 - \lambda r\big)dr \tag{3-54}$$

$$= \frac{1}{2}\sigma \int_{0.25}^{0.973} c_{l_\alpha}\big((\theta_0 + r\theta_{tw})r^2 - \lambda r\big)dr$$

where σ, the rotor blade solidity is the ratio of blade area to rotor disk area, its value is between 0.07 and 0.12 for helicopters

$$\sigma = \frac{Nbc}{\pi R} \tag{3-55}$$

and λ is the inflow ratio

$$\lambda = \frac{U_P}{U_T} \tag{3-56}$$

- Blade Element and Momentum Theory

  The BEMT is a hybrid method that combines the basic principles form both the BET and the MT, and allows the local conditions for each blade element to be estimated.

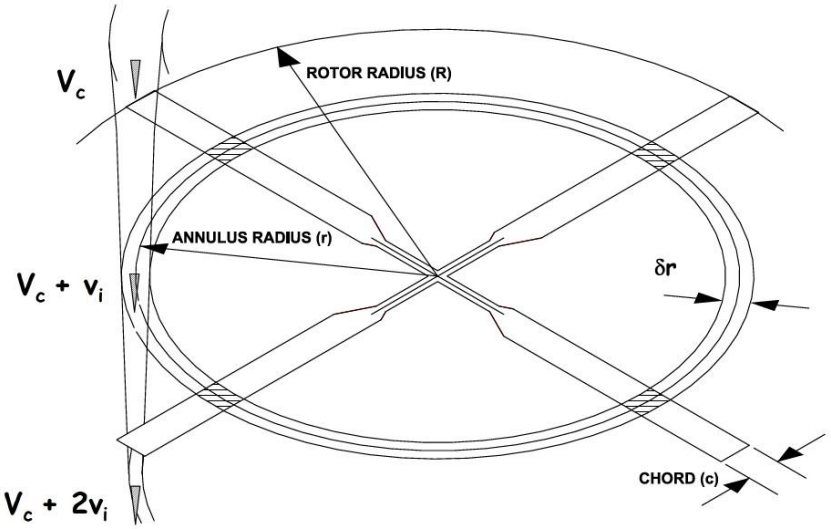

Figure 3-22 Blade Element and Momentum Theory [41]

For the BEMT, the relationship between the induced velocity v_i and the blade tip speed V_{tip} at the blade element is [41]:

$$\frac{v_i}{V_{tip}} = -\frac{1}{2}\left[V_c + \frac{C_{l_\alpha} Nbc\Omega}{8\pi}\right] + \frac{1}{2}\sqrt{\left[V_c + \frac{C_{l_\alpha} Nbc\Omega}{8\pi}\right]^2 - \frac{C_{l_\alpha} Nbc\Omega}{2\pi}\left(V_c - \Omega r\theta_{(r)}\right)} \quad (3\text{-}57)$$

With the induced velocity result given by the BEMT, the incremental lift and drag are estimated again to include the inflow distribution along the blade, and compared to the thrust calculated at the three-quarter radius, which is a representative result of the whole blade

$$T = \frac{1}{2}\rho C_{l_\alpha} NbcV_{tip}R\left[\frac{1}{3}\theta_{0.75} - \frac{\lambda}{2}\right] \quad (3\text{-}58)$$

- Climb

  The incremental lift per unit span and thrust in axial flight was calculated following the same analysis as done by the BEMT in hover to take into account the increment in lift due to collective pitch and climb velocity.

- Forward flight

  For the analysis in forward flight, the rotor angle of attack,α, forward velocity, V_∞, and azimuth angle, ψ, must be taken into account as the

blade position and lift distribution will not be constant along a complete rotation. To reduce computation time, and without compromising the results, constant inflow ratio,λ, is going to be assumed, however it is possible to calculate a linear inflow ratio in order to get more accurate results.

The constant inflow ratio is calculated numerically by means of the MT where the starting value of λ is given from the hover condition, and the iteration finishes when the error $\epsilon < 0.005$. Finally the induced inflow ratio, λ_i , is calculated

$$\lambda_{n=1} = \mu \tan \alpha + \frac{C_T}{2\sqrt{\mu^2 + \lambda_n^2}} \tag{3-59}$$

$$\lambda = \sqrt{\frac{C_T}{2}} \tag{3-60}$$

$$\epsilon = \frac{\lambda_{n+1} - \lambda_n}{\lambda_{n+1}} \tag{3-61}$$

$$\lambda_i = \frac{C_T}{2\sqrt{\mu^2 + \lambda^2}} \tag{3-62}$$

where, μ is the advance ratio given by

$$\mu = \frac{V_\infty}{\Omega R} \tag{3-63}$$

After calculating λ the blade feathering motion is taken into account as a Fourier series, using only the first harmonic terms, knowing that the rest of the harmonic terms can be assumed negligible.

The next step in the forward flight analysis is to calculate the blade flapping motion, $\beta(\psi)$, using:

$$\beta(\psi) = \beta_0 + \beta_{1c} \cos \psi + \beta_{1s} \sin \psi \tag{3-64}$$

where:

$$\beta_0 = \gamma \left[\frac{\theta_0}{8}(1+\mu^2) + \frac{\theta_{tw}}{10}\left(1+\frac{5}{6}\mu^2\right) + \frac{\mu}{6}\theta_{1s} - \frac{\lambda}{6}\right] \tag{3-65}$$

$$\beta_{1c} = \frac{-\frac{8}{3}\mu\left[\theta_0 - \frac{3}{4}\lambda + \frac{3}{4}\mu\theta_{1s} + \frac{3}{4}\theta_{tw}\right]}{1-\frac{1}{2}\mu^2} - \theta_{1s} \tag{3-66}$$

$$\beta_{1s} = \frac{\left(-\frac{4}{3}\mu\beta_0\right)}{\left(1+\frac{1}{2}\mu^2\right)} + \theta_{1c} \tag{3-67}$$

$$\gamma = \frac{\rho C l_\alpha c R^4}{I_b} \tag{3-68}$$

and

$$I_b = \int_0^R m y^2 dy \tag{3-69}$$

Having the feathering and flapping motion, it is possible to calculate the in-plane and out-of-plane velocity components in any azimuth angle using:

$$U_T(y,\psi) = \Omega y + \mu\Omega R sin\,\psi \tag{3-70}$$

$$U_p(y,\psi) = (\lambda_c + \lambda_i)\Omega R + y\dot{\beta}(\psi) + \mu\Omega R\beta cos\,\psi \tag{3-71}$$

Finally the blade incremental lift per unit span in forward flight and thrust coefficient at four different azimuth angles are given by:

$$dL = \frac{1}{2}\rho c C_{l_\alpha}\left(\left(\theta_{(r,\psi)}U_T^2\right) - (U_T U_P)\right)dy \tag{3-72}$$

$$C_T = \frac{1}{2}\sigma C_{l_\alpha}\left[\frac{\theta_0}{3}\left(1+\frac{3}{2}\mu^2\right) + \frac{\theta_{tw}}{4}(1+\mu^2) + \frac{\mu}{2}\theta_{1s} - \frac{\lambda}{2}\right] \tag{3-73}$$

- ***Blade - Swashplate mechanism kinematic analysis***

  The Blade – Swashplate mechanism kinematic analysis takes into account the main rotor geometry, configuration, and blade pitch angles to predict swashplate and pitch links final positions. This analysis is based on [6].

  It is assumed that the force produced by the actuators is the same encountered in the pitch link to maintain the blade position, neglecting the effects of the swashplate; this assumption is valid for a preliminary AS power requirement analysis.

  The analysis predicts the position of the pitch links at the moment when they are situated above the cyclic and collective actuators at each pitch setting. It can be used for a two-bladed or a four-bladed main rotor configuration,

Figure 3-23 Bell206L-4 and MBB Bo105 main rotors

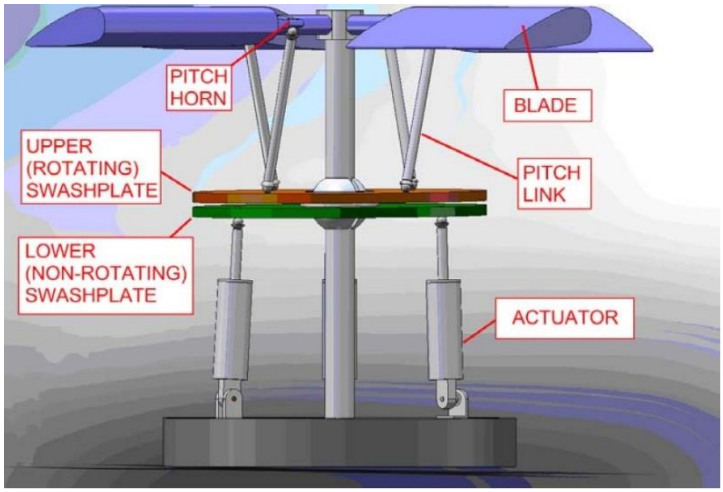

Figure 3-24 Swashplate CAD model [6]

The kinematic analysis requires a coordinate system to be established, and given by $\{E_1, E_3, E_3\}$. The relation between this coordinate system and the conventional system is shown below:

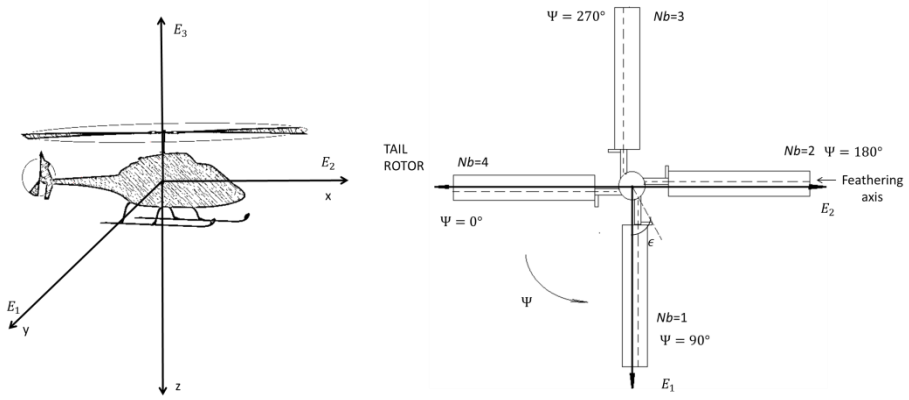

Figure 3-25 Coordinate axis relationship

$$\begin{bmatrix} X \\ Y \\ Z \end{bmatrix} = \begin{bmatrix} 0 & 1 & 0 \\ 1 & 0 & 0 \\ 0 & 0 & -1 \end{bmatrix} \begin{bmatrix} E_1 \\ E_2 \\ E_3 \end{bmatrix} \tag{3-74}$$

If a four-bladed helicopter is to be analysed, Nb is used to represent the blade number. On the other hand, if a two-bladed helicopter is used, Nb represents the blade position according to the azimuthal angle.

After the coordinate system is established, a vectorial approach is used to estimate the swashplate position depending on the blade pitch. The vectorial analysis is done by establishing four vectors, three along the main components of the rotor and a resultant from the system origin.

To initiate the approach, the blade neutral point must be established, this point is given by setting θ_0, θ_{1c} and θ_{1s} equal to zero in the blade pitch equation. The vector analysis origin coincides with the swashplate origin, and the lengths and direction of the vectors are determined by their respective components geometries.

The swashplate is represented by a flat plate, and its dimensions are not taken into account to simplify this analysis.

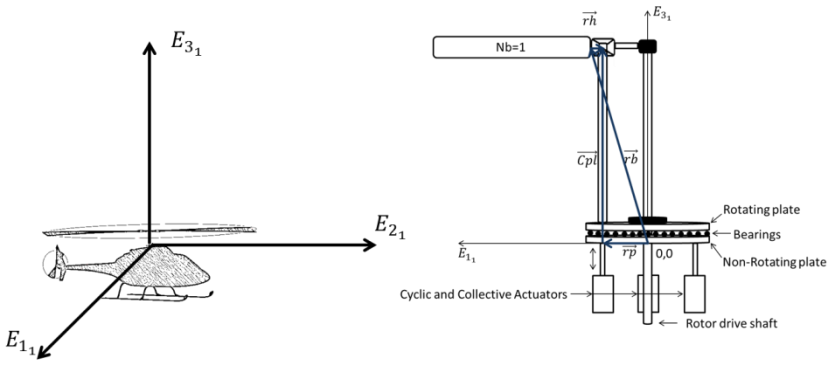

Figure 3-26 Vectorial analysis neutral position

For demonstrative purposes only one blade calculation is shown.

The vectors used are:

$\overrightarrow{rp}$ represents the distance between the origin and the swashplate-pitch link connection.

$\overrightarrow{Cpl}$ represents the pitch link distance.

$\overrightarrow{rh}$ represents the distance between the centre of the blade-pitch horn connection and the horn-pitch link connection.

And $\overrightarrow{rb}$ is the resultant between the origin and the blade-pitch horn connection.

At this point, as a scaling approach was used, $\overrightarrow{rb}$ is unknown, but from figure 48 can be calculated by:

$$\overrightarrow{rb} = \overrightarrow{rp} + \overrightarrow{Cpl} - \overrightarrow{rh} \tag{3-75}$$

To ensure proper calculation of $\overrightarrow{rb}$ it was decided to define a new vector $\vec{k}$, and it must have the same magnitude and direction as $\overrightarrow{Cpl}$.

$$\vec{k} = \overrightarrow{rb} + \overrightarrow{rh} - \overrightarrow{rp} = \overrightarrow{Cpl} \tag{3-76}$$

After $\vec{k}$ is defined, the angles α_{rh} and β_{rh} are estimated.

$$\alpha_{rh} = \sin^{-1}\frac{rhE_1}{|rh|} = -\beta_{rh} \tag{3-77}$$

$$\overrightarrow{rh} = \begin{bmatrix} rhE_1 \\ rhE_2 \\ rhE_3 \end{bmatrix} \tag{3-78}$$

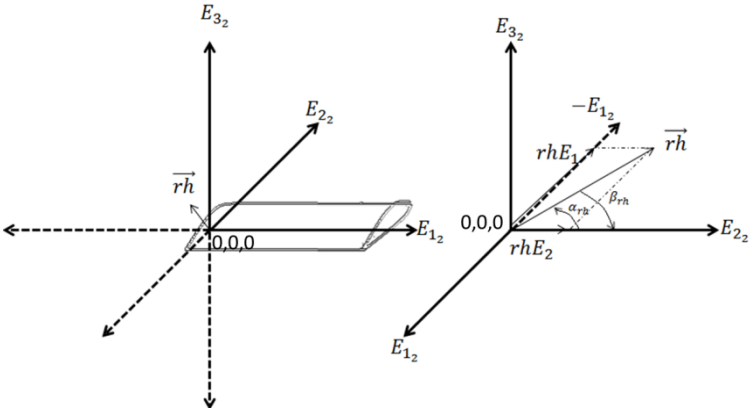

Figure 3-27 rh vector components

β_{rh} is calculated as is the angle required to make a rotation of $\overrightarrow{rh}$ around $E_{3_2}$to place the vector over E_{2_2} using the Direction Cosine Matrix (DCM).

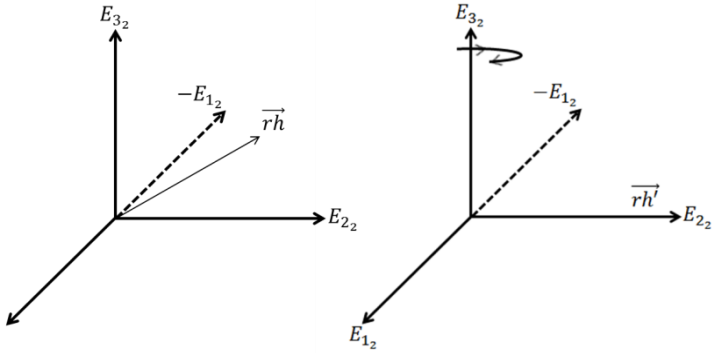

Figure 3-28 rh rotation

$$DCM_{E_{3_2}} = \begin{bmatrix} \cos(\beta_{rh}) & \sin(\beta_{rh}) & 0 \\ -\sin(\beta_{rh}) & \cos(\beta_{rh}) & 0 \\ 0 & 0 & 1 \end{bmatrix} \tag{3-79}$$

The same approach is used for Nb= 2, 3 and 4 locating the vectors along E_{2_2}.

$$\overrightarrow{rh'} = DCM_{E_{3_2}} \overrightarrow{rh} \tag{3-80}$$

Knowing that the direction of $\overrightarrow{rh}$ and $\overrightarrow{rh'}$ will be altered by the same amount as the blade pitch, it is possible to calculate the system new coordinates and swashplate translation represented by $Z_{col}E_{3_1}$ when collective pitch is imparted.

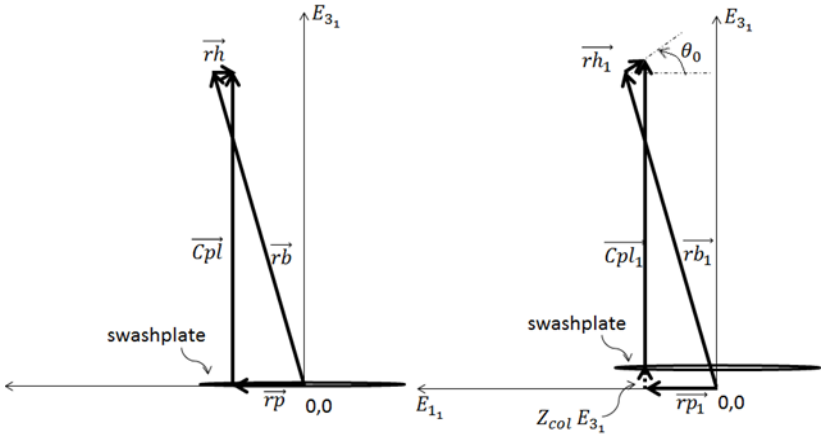

Figure 3-29 Collective pitch imparted

The relationship between $\overrightarrow{rh}$ and $\overrightarrow{rh'}$ is shown in Figure 3-30. The position of $\overrightarrow{rh_1'}$ is calculated using (3-81)

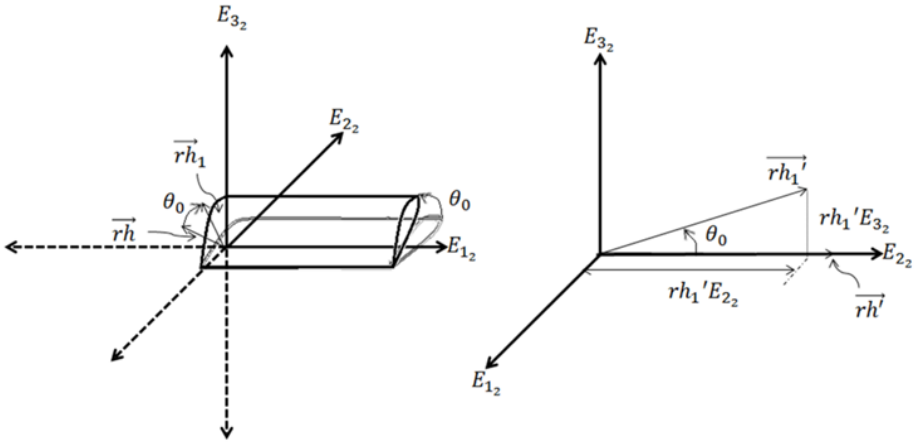

Figure 3-30 Blade and rh direction change relation for collective pitch

$$\overrightarrow{rh_1}' = \begin{bmatrix} 0 \\ |rh|\cos(\theta_0) \\ |rh|\sin(\theta_0) \end{bmatrix} \tag{3-81}$$

Having found $\overrightarrow{rh_1}'$ coordinates, the vector must return to its original points by means of the DCM by

$$\overrightarrow{rh_1} = \begin{bmatrix} \cos(-\beta_{rh}) & \sin(-\beta_{rh}) & 0 \\ -\sin(-\beta_{rh}) & \cos(-\beta_{rh}) & 0 \\ 0 & 0 & 1 \end{bmatrix} \begin{bmatrix} 0 \\ |rh|\cos(\theta) \\ |rh|\sin(\theta) \end{bmatrix} \tag{3-82}$$

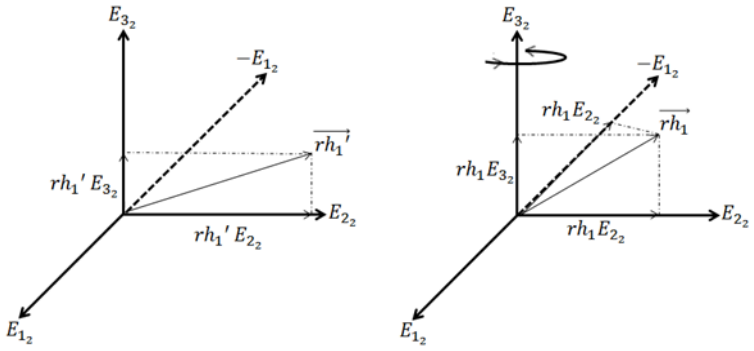

Figure 3-31 rh position after collective pitch is applied

At this point, is convenient to ensure that $|rh| = |rh_1|$ complying with the structural constraint of the components represented by $\overrightarrow{rh}$.

Having the final position of $\overrightarrow{rh_1}$ allows the calculation of the new vector $\overrightarrow{Z_{col}}$. Its coordinate along the E_{3_1} axis is equal to the swashplate final position, and can be found by recalculating $\vec{k}$ using $\overrightarrow{rh_1}$ instead of $\overrightarrow{rh}$ and replacing its component values in:

$$Z_{col}E_{3_1} = kE_{3_1} - \sqrt{|Cpl|^2 - kE_{1_1}{}^2 - kE_{2_1}{}^2} \tag{3-83}$$

A similar analysis is required to include θ_{1c} and θ_{1s}, lateral and longitudinal cyclic pitch inputs respectively, but in this case, as the blade pitch is not constant in a rotation, the swashplate tilt angles must be calculated, and the vector analysis origin is the swashplate centre instead of the swashplate's initial point.

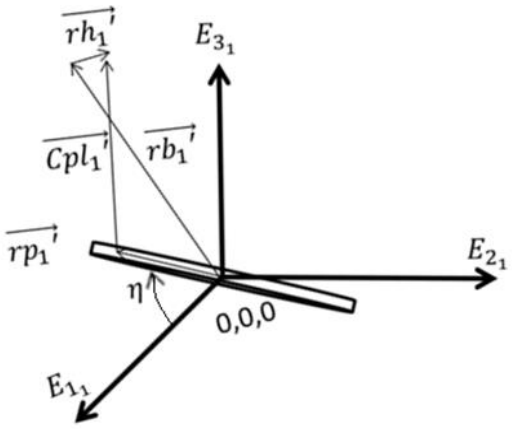

Figure 3-32 Analysis for cyclic inputs

In this case the final position of $\overrightarrow{rh_1}'$ is given by:

$$\overrightarrow{rh_1}' = \begin{bmatrix} 0 \\ |rh|\cos(\theta_{1c}\cos(\psi) + \theta_{1s}\sin(\psi)) \\ |rh|\sin(\theta_{1c}\cos(\psi) + \theta_{1s}\sin(\psi)) \end{bmatrix} \tag{3-84}$$

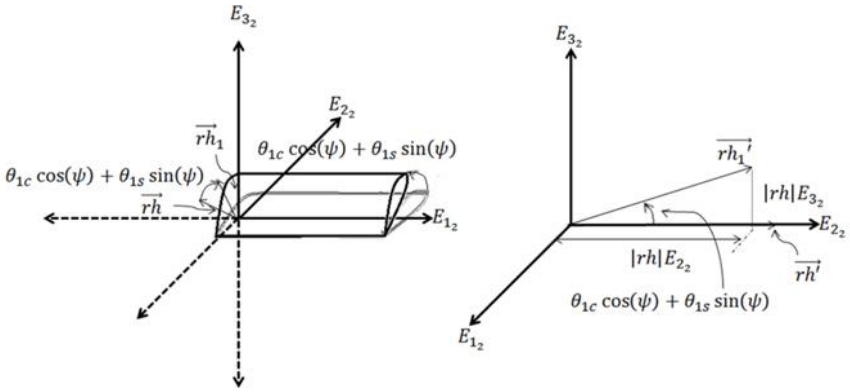

Figure 3-33 Blade and rh direction change relation for cyclic pitch

Rotation from $\overrightarrow{rh_1}'$ to $\overrightarrow{rh_1}$ is accomplished using the same DCM as for the collective pitch.

After having the coordinates of $\overrightarrow{rh_1}$, it is necessary to rotate both $\overrightarrow{rh_1}$ and $\overrightarrow{rb_1}$ to place them in the E_{1_1}- E_{2_1} plane and defining $\vec{k}$ as the resultant of $\overrightarrow{rb_1} + \overrightarrow{rh_1}$

$$DCM = \begin{bmatrix} \sin(\psi) & -\cos(\psi) & 0 \\ \cos(\psi) & \sin(\psi) & 0 \\ 0 & 0 & 1 \end{bmatrix} \tag{3-85}$$

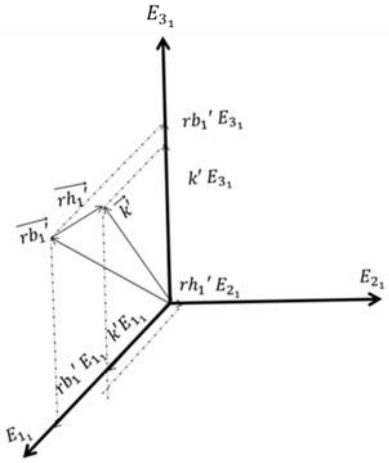

Figure 3-34 K in E1-E2 plane

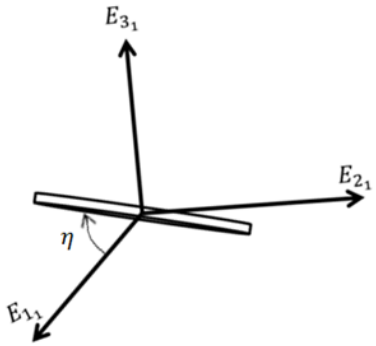

Figure 3-35 swashplate tilt angle

With the definition of $\vec{k}$ it is now possible to calculate the tilt angle η

$$\eta = 2\tan^{-1}\left(\frac{k_3 - \sqrt{k_3^2 - AB}}{A}\right) \tag{3-86}$$

$$A = \left[\frac{(k_1^2 + k_2^2 + k_3^2 + |rp|^2 - |Cpl|^2)}{2rp} + k_1\right] \tag{3-87}$$

$$B = \left[\frac{(k_1^2 + k_2^2 + k_3^2 + |rp|^2 - |Cpl|^2)}{2rp} - k_1\right] \tag{3-88}$$

Knowing the swashplate's tilt angles for each point, the components of $\overrightarrow{rp_1}$ for cyclic inputs are determined.

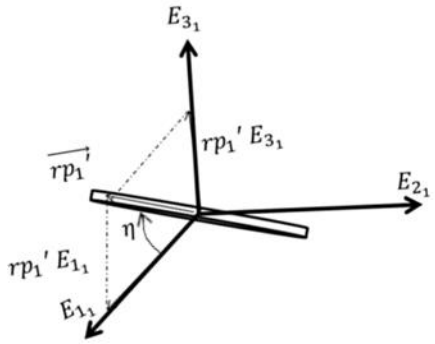

Figure 3-36 rp_1coordinates

$$\overrightarrow{rp_1} = \begin{bmatrix} |rp_1| \cos(\eta) \\ 0 \\ |rp_1| \sin(\eta) \end{bmatrix} \tag{3-89}$$

Having calculated $\overrightarrow{rp_1}$ the only unknown in the cyclic analysis is $\overrightarrow{Cpl_1}$, but from figure 53

$$\overrightarrow{Cpl_1} = \overrightarrow{rb_1} + \overrightarrow{rh_1} - \overrightarrow{rp_1} \tag{3-90}$$

- ***Blade - Swashplate mechanism dynamic analysis***

  After finishing the Blade - Swashplate mechanism kinematic analysis, the forces required by the actuators to maintain a certain blade pitch condition is studied. This is accomplished taking into account aerodynamic and inertial forces transmitted to the blades. The blade torsion-axis moments under consideration are the aerodynamic and propeller moments, and the moment due to inertia. Flap motion is not included in the analysis as it is assumed that it does not affect the blade torsional loads [6].

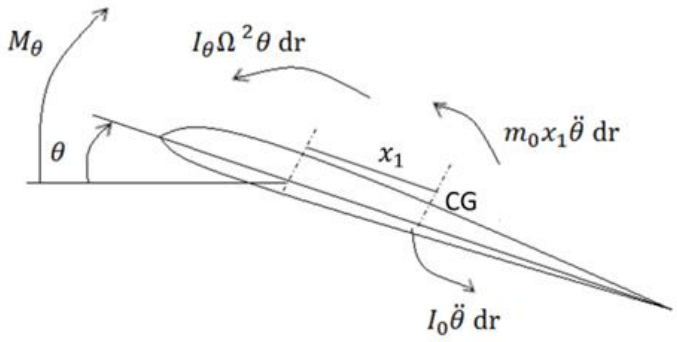

Figure 3-37 Blade segment torsional loads [6]

The moments are integrated along the blade and must be equal to the torque at the blade root produced by the pitch link force.

$$-\int M_\theta dr + \int I_\theta \Omega^2 \theta \, dr + \int I_0 \ddot{\theta} \, dr + \int m_0 x_1 \ddot{\theta} dr + k_r \theta - \left(\overrightarrow{r_h} \times \overrightarrow{F_{pl}}\right) \cdot \hat{\theta} = 0 \quad (3\text{-}91)$$

where

$\hat{\theta}$ is the pitch direction

$\overrightarrow{F_{pl}}$ is the pitch link force vector

I_0 is the mass moment of inertia in pitch about the centre of mass

I_θ is the section mass moment of inertia about the feathering axis

m_0 is the mass per unit of length

k_r is the spring constant for the blade root in pitch

M_θ is the section aerodynamic moment

The blade aerodynamic moment M_a is given by

$$M_a = \int M_\theta dr + Ld = \int \frac{1}{2} \rho U_T^2 c^2 C_{m_0} dr + Ld \quad (3\text{-}92)$$

C_{m_0} is the aerofoil moment coefficient

L is the blade lift calculated in the aerodynamic analysis section

d is the distance from the aerodynamic centre to the blade flexural axis

Using the parallel axis theorem $I_\theta = I_0 + m_0 x_1$ the moment of inertia is

$$\int I_\theta \Omega^2 \theta \, dr + \int I_0 \ddot{\theta} \, dr + \int m_0 x_1 \ddot{\theta} dr = \sum I_{f_{section}} \left(\ddot{\theta} + \Omega^2 \theta_{section} \right) \tag{3-93}$$

$I_{f_{section}}$ is the blade section angular moment of inertia about the feathering axis.

$\ddot{\theta}$ is the blade angular acceleration

$$\ddot{\theta} = \frac{\partial^2 \theta}{\partial t^2} = \Omega^2 \frac{\partial^2 \theta}{\partial \psi^2} \tag{3-94}$$

The pitch link force vector is unknown, but its direction is the same as the pitch link vector, and a relationship can be established by

$$\overrightarrow{F_{pl}} = \widehat{F_{pl}} \left| F_{pl} \right| \tag{3-95}$$

$$\widehat{F_{pl}} = \widehat{Cpl} = \begin{bmatrix} CplE_{1_1} / |Cpl| \\ CplE_{2_1} / |Cpl| \\ CplE_{3_1} / |Cpl| \end{bmatrix} \tag{3-96}$$

The pitch direction is found by means of the direction cosines, for Nb=1:

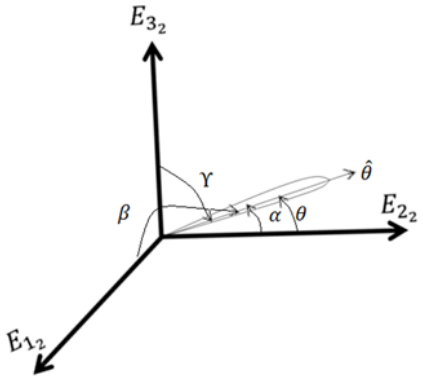

Figure 3-38 Pitch direction

$$\hat{\theta} = \begin{bmatrix} \cos(\alpha) \\ \cos(\Upsilon) \\ \cos(\beta) \end{bmatrix} = \begin{bmatrix} \cos(\theta) \\ \cos(90 - \theta) \\ 0 \end{bmatrix} \tag{3-97}$$

The pitch link force magnitude can be calculated now

$$|F_{pl}| = \frac{-M_a + \sum I_{f_{section}} \left(\ddot{\theta} + \Omega^2 \theta_{section}\right) + k_r \theta}{\left(\overrightarrow{r_h} \times \widehat{F_{pl}}\right) \cdot \hat{\theta}} \tag{3-98}$$

- ***Actuator forces algorithm – Actuation System integration***

  The Actuation system model developed by [36] used in this project is designed to represent the steady-state power consumption demands of a helicopter main rotor actuation system, included are three actuation technologies: a centralised hydraulic system (ESHA), an electromechanical system (EMA), and an electro-hydrostatic (EHA) system.

  The model inputs for the different technologies are the forces required by the actuators to maintain a desired pitch angle by the blades, and the outputs are shaft power for the ESHA and electrical power for EMA and EHA systems.

  As information relating the specific characteristics of the system installed on a Bell 206L-4 helicopter is not available in the public domain, performance specifications of three actuators were used for

each system configuration. For more information related to the model working principles the reader should refer to [36].

3.1.6 RMEM Executable

The process of creating an RMEM executable version starts by defining in the Matlab workspace all the inputs required from the HPM and the aerodynamic algorithm to run the Simulink model. In this case are 7 inputs and the systems parameters are treated as constants within the model.

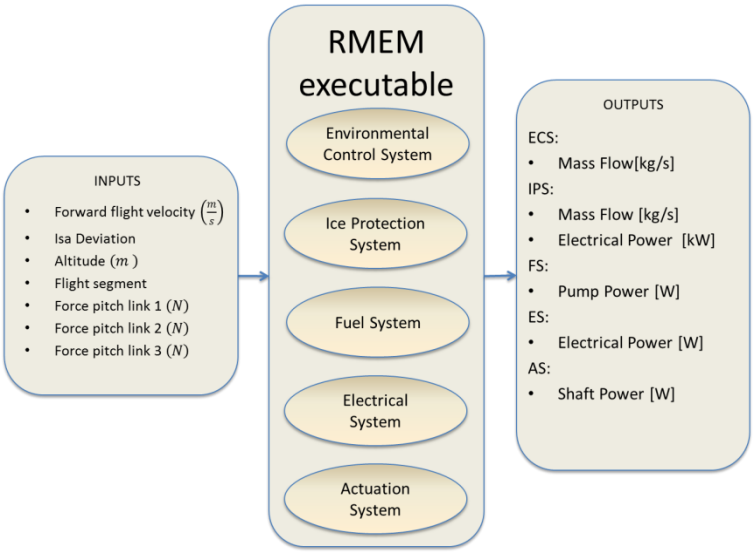

Figure 3-39 RMEM executable inputs

The flight segments are coded from 1 to 5.

Table 3-2 Flight Segment coding

Flight Segment	
Ground	1
Climb	2
Forward Flight	3
Hover	4
Descent	5

After the inputs are defined it is necessary to run the model once, and confirm that there are no warnings generated and that the results were sent to the MATLAB Workspace. The next step is to use the SIMULINK coder rapid

simulation (RSim) target to create the Simulink executable, this coder is used to optimise hybrid dynamic systems executable. The RSim target is found by clicking in configuration parameters, and selecting Code generation from the simulation tab.

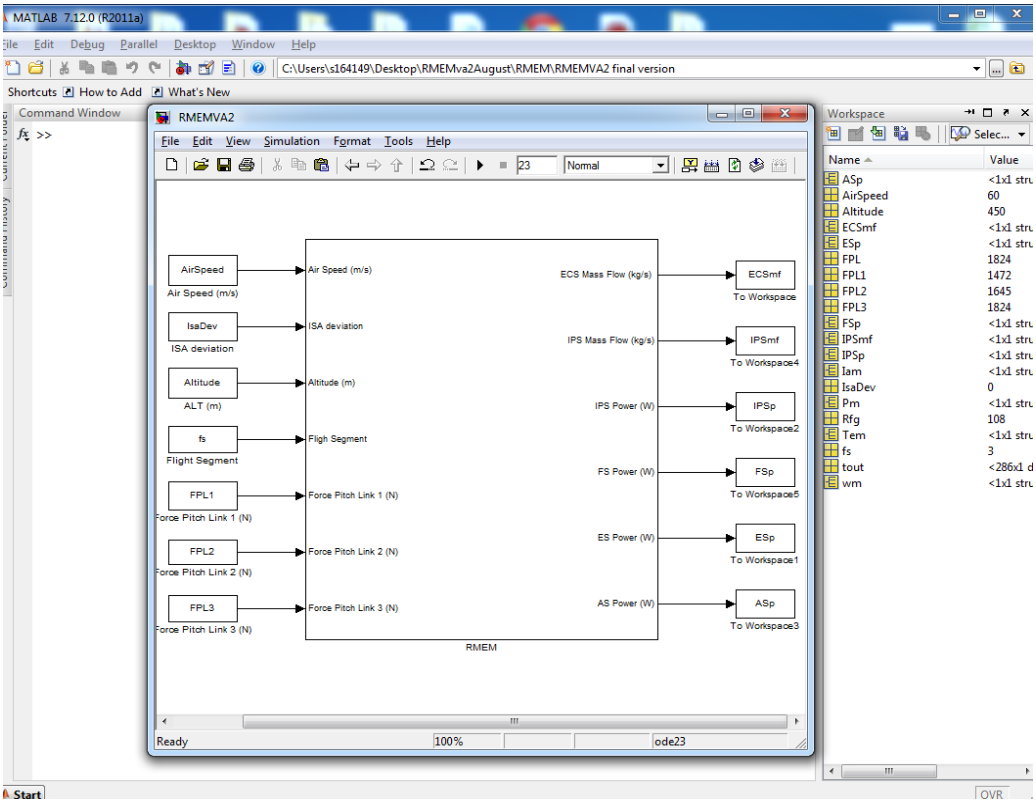

Figure 3-40 Simulink outputs

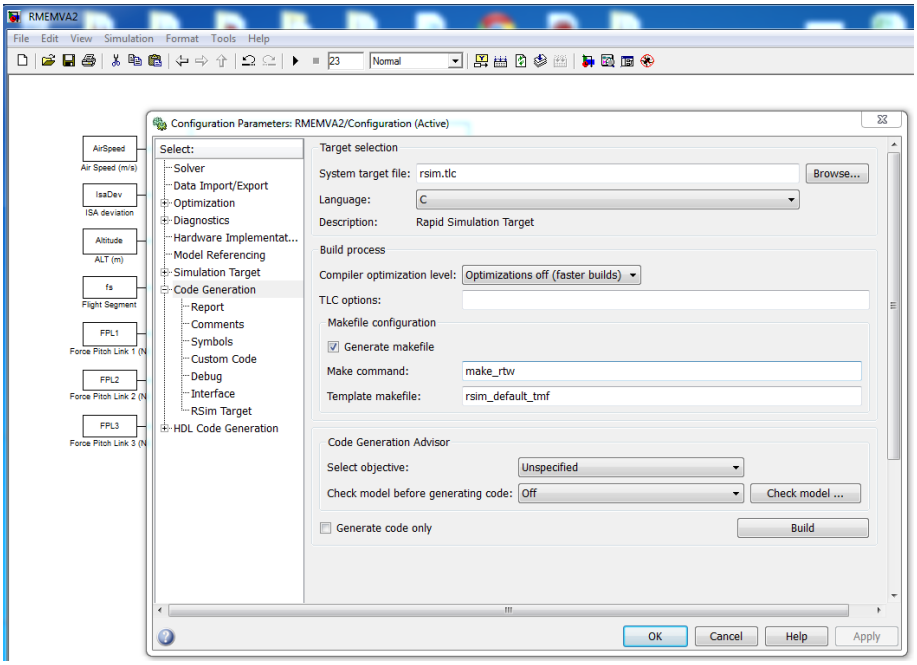

Figure 3-41 Simulink RSim target

When the RSim executable is created is necessary to get the parameter structure of the model, which allows updating the inputs from the HPM. This is done within the command window using the following command:

rtP= rsimgetrtP('model_name') and saving the structure in the workspace.

At this point, the M-file containing the Aerodynamic Algorithm is included, as by using it the inputs can be imported from a .dat file, and updated on the parameter structure with the following comands:

```
file = importdata('inputdata.dat');
for i = 1:size(file.colheaders, 2)
    assignin('base', genvarname(file.colheaders{i}), file.data(:,i));
end

load RMEMVA2rtp.mat;
rtP.parameters(1,1).values(1,1116)=AirSpeed;
rtP.parameters(1,1).values(1,7)=IsaDev;
rtP.parameters(1,1).values(1,12)=Altitude;
rtP.parameters(1,1).values(1,10)=FlightSegment;
rtP.parameters(1,1).values(1,1183)=FPL1;
rtP.parameters(1,1).values(1,1290)=FPL2;
rtP.parameters(1,1).values(1,1397)=FPL3;
save RMEMVA2rtp.mat rtP;
```

Now it is possible to run the RSim executable by using:

```
!RMEMVA2 -p RMEMVA2rtp.mat
```

Finally the new results can be written in a .dat file by loading a .mat file created after the RSim executable was ran:

```
load created.mat
Results(1,1)= rt_results.signals.values(end,1);
header1='Final results';
outf=fopen('outputdata.dat', 'w');
fprintf(outf, ' %s\r\n',header1);
fprintf(outf, '%6.4f\r\n',RESULTS);
fclose(outf);
```

At this point, a MATLAB to C/C++ compiler is used to create an executable of the M-file, eliminating the RMEM MATLAB/SIMULINK dependency:

```
mcc –m mfile_name;
```

Now the model is ready to be integrated to a HPM by means of text files.

4 Results

4.1 Electrical Load Analysis

In order to generate the analysis the following assumptions were taken into consideration:

- The most severe loading condition in which the helicopter will be expected to operate is at night.
- Momentary/intermittent loads, which open and close in a few seconds are not included.
- Communications equipment may have different current consumption depending on operating mode.

4.1.1 Electric Bus Wiring Diagram

The proposed electric bus wiring diagram is based on [25].

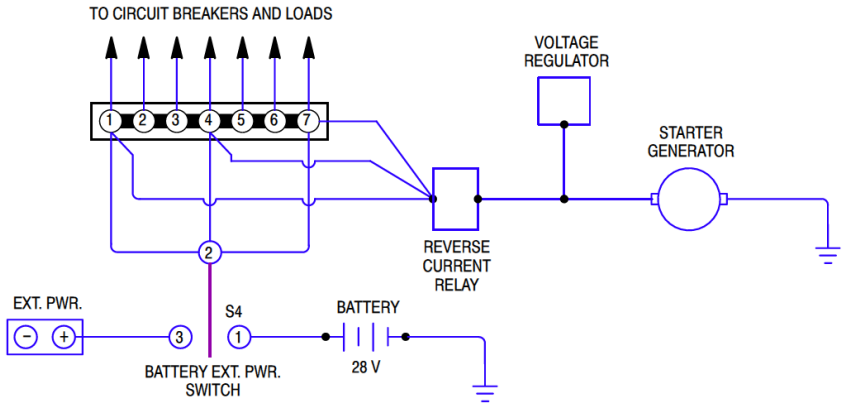

Figure 4-1Electric Bus Wiring Diagram [25]

4.1.2 System Operation:

The Electrical System (ES) consists of all electrical power supply, distribution and control equipment, wiring and miscellaneous associated equipment supplied on the helicopter [25] and [26].

The ES is supplied by a 28 VDC, 150 A engine driven generator, in conjunction with a 24 V nickel-cadmium battery and incorporates an external power

receptacle. The system is a nominal 28 VDC, single wire type installation with helicopter structure used as the ground return [25] and [26].

Control of the Electrical System, exclusive of optional intercom controls, is provided by the switches and circuit breakers on the instrument panel. All circuits of the electrical system are protected by push-to-reset or switch-type circuit breakers. All electrical or electronic units or components that produce electromagnetic energy (rf potential) are bonded to the adjacent structure to ensure a continuous, negligible radio frequency impedance path from the equipment enclosure to the structure [25].

4.1.3 Primary and Secondary Power Sources Description

Starter-generator and battery information is taken from [29] and [42] respectively.

Table 4-1 Power Sources Description

Identification	1	2
Item	DC Starter-Generator	Battery
Number of Units	1	1
Continuous Rating 5 seconds Rating 2 minute Rating	150A	17Ah
Voltage	28.5V	24 VDC
Frequency	-	-
Power Factor	-	-
Manufacturer	Aircraft Parts Corp.	Marathon Power Technologies Company
Model Number	150SG	M^3-1700
Voltage Regulation		-
Frequency Regulation	-	-

Table 4-2 Generator Output Data [29]

GENERATOR OUTPUT					
Speed	Amp Output	Volt	Altitude	Operating Period	Ambient Temp. Max.
7200	120	26	Sea Level	Cont.	121°C
8100	150	28.5	Sea Level	10 Min.	121°C
8100	150	28.5	Sea Level	Cont.	121°C
8100-13000	150	30	Sea Level	Cont.	121°C
14000	0	Over-speed	Sea Level	5 Min.	121°C

4.1.4 Connected Load Chart

As part of the ELA, the connected load chart was generated in accordance to [27] and [28] by including the database of components installed on a bell206L-4 or similar, and based on the number of installed units given by [25] and [26].

Table 4-3 Connected Load Chart

ITEM	EQUIPMENT	NO. OF UNITS OR SYS.	AMPS PER UNIT OR SYS.	OPER. TIME IN MIN
1	ACTUATOR CYCLIC	1		
2	ACTUATOR COLLECTIVE	1		
3	ACTUATOR COLLECTIVE	1		
4	ENG OIL PRES TEMP.	1	0.36	CON.
5	XMSN OIL PRES TEMP.	1	0.03	CON.
6	GAS PRODUCER RPM	1	0.36	CON.
7	TORQUE	1	0.36	CON.
8	TOT	1	0.03	CON.
9	AIRSPEED	1	0.36	CON.
10	FUEL QUANTITY	1	0.08	CON.
12	POWER TURBINE RPM / ROTOR RPM	1	0.08	CON.
13	WARNING UNIT	1	0.05	CON.
14	ENGINE OUT HORN	1	0.02	INTR.
15	INSTRUMENT LAMPS	11	0.44	CON.
16	EDGE LIGHT PANELS	SYS.	0.10	CON.
17	ENG OUT	4	0.10	INTR.
18	BATTERY HOT	4	0.10	INTR.
19	BATTERY RLY	4	0.10	INTR.
20	R/FUEL PUMP	4	0.10	INTR.
21	L/FUEL PUMP	4	0.10	INTR.
22	ROTOR LOW RPM	4	0.10	INTR.
23	TRANS OIL PRESSURE	4	0.10	INTR.
24	TRANS OIL TEMP	4	0.10	INTR.
25	FUEL LOW	4	0.10	INTR.
26	ENG CHIP	4	0.10	INTR.
27	TRANS CHIP	4	0.10	INTR.
28	FUEL FILTER	4	0.10	INTR.
29	T/R CHIP	4	0.10	INTR.
30	GEN FAIL	4	0.10	INTR.
31	FADEC	1	5.00	INTR.
32	IGNITER	1	0.75	INTR.
33	POSITION LIGHTS	4	3.00	CON.
34	ANTI-COLLISION LIGHTS	SYS.	3.50	CON.
35	LANDING LIGHTS	2	17.86	INTR.
36	MAP LIGHT	1	0.50	INTR.
37	VOLTAGE REGULATOR	1	0.30	CON.
38	BATTERY RELAY	1	0.60	CON.
39	EXTERNAL RELAY	1	0.50	CON.
40	STARTER RELAY	1	0.50	CON.
41	LINE CONTROL RELAY	1	0.50	CON.
43	TRANSCIEVER KY196	1	0.40	INTR.
	TRANSCIEVER KY196		6.50	CON.
44	ICS KMA 24K	1	0.44	CON.
45	FUEL BOOST PUMP	2	11.33	CON.
46	CABIN HEATER BLEED AIR	SYS.	46.00	INTR.
47	PITOT TUBE	1	6.50	CON.
48	KT-76A transponder	1	1.80	CON.
49	Garmin GNS 530W GPS/COMM/NAV	1	3.00	CON.
50	KR-87 ADF	1	0.43	CON.
51	KDM-706A WITH KDI 572 INDICATOR	1	8.93	CON.
52	KR-21 marker beacon receiver	1	0.25	CON.
53	Autopilot KAP 150H	SYS.	4.10	INTR.
54	KRA-405B radio altimeter	1	0.85	CON.
55	SKY 497 Skywatch System	1	2.50	CON.
56	Vapor cycle air conditioner	SYS.	17.32	INTR.

4.1.5 Electrical Load Analysis (ELA) Chart

A summary of the ELA chart is presented in this section. It includes the total power requirements of the equipment installed for pre-start and start turbine conditions only [25] [26] [27] and [28]. The completed ELA chart is given in Appendix A

Table 4-4 Electrical Load Analysis chart (Summary)

EQUIPMENT	NO. OF UNITS OR SYS.	AMPS PER UNIT OR SYS.	OPER. TIME IN MIN	TOTAL AMPS	PRE-START		START TURBINE	
					AVERAGE AMPERES		AVERAGE AMPERES	
					5 SEC	2 MIN	5 SEC	2 MIN
INSTRUMENTS								
WARNING LIGHTS								
Total instruments and warning lights	SYS.	3.82	0.00	6.24	2.18	2.18	2.18	2.18
ENGINE CONTROLS								
FADEC	1	5.00	INTR.	5.00	5.00	5.00	5.00	5.00
IGNITER	1	0.75	INTR.	0.75				
LIGHTING								
Total Lighting	SYS.	13.68	0.00	24.86	0.00	0.00	0.00	0.00
ELECTRICAL POWER SYSTEM								
Total electric system	6	2.4	0	2.4	2.4	2.4	0	0
AVIONICS								
Total avionics	2	7.34	0	7.34	7.34	7.34	7.34	7.34
fuel boost pump	2	5.67	CON.	11.33				
cabin heater bleed air	SYS.		INTR.	0.00				
pitot tube	1	6.50	CON.	6.50			6.50	6.50
OPTIONAL EQUIPMENT								
Total optional equipment	SYS.	39.18	0.00	39.18	0.00	0.00	0.00	0.00
BASIC SHIP AMPERES				106.84	30.43	30.43	32.13	32.13
OPTIONAL SHIP AMPERES				39.18	0.00	0.00	0.00	0.00
total				146.02	30.43	30.43	32.13	32.13

4.1.6 System Regulation

To comply with the system regulation requirements, equipment voltage variation under maximum, nominal, minimum, and emergency conditions of 28VDC systems must be ensured [27].

Table 4-5 Equipment Voltage [27]

Operation	Voltage
Maximum	30.3
Nominal	27.5
Minimum	22
Emergency	18

4.1.7 Load Shedding

The load shedding analysis was performed assuming that all electronic equipment is in operation in cruise conditions for 5 minutes [27].

Table 4-6 Load Shedding

EQUIPMENT	NO. OF UNITS OR SYS.	AMPS PER UNIT OR SYS.	OPER. TIME IN MIN	Amp-min in 5-min period	TOTAL AMPS (Day)	TOTAL AMPS (Night)
FLIGHT CONTROLS				0		
ACTUATOR CYCLIC	1			0		
ACTUATOR COLLECTIVE	1			0		
ACTUATOR COLLECTIVE	1			0		
INSTRUMENTS				0		
ENG OIL PRES TEMP.	1	0.36	CON.	1.79	0.36	0.36
XMSN OIL PRES TEMP.	1	0.03	CON.	0.15	0.03	0.03
GAS PRODUCER RPM	1	0.03	CON.	0.15	0.03	0.03
TORQUE	1	0.36	CON.	1.79	0.36	0.36
TOT	1	0.36	CON.	1.79	0.36	0.36
AIRSPEED	1	0.03	CON.	0.15	0.03	0.03
FUEL QUANTITY	1	0.36	CON.	1.79	0.36	0.36
DC LOAD (LOADMETER) / FUEL PRESS	1			0		
POWER TURBINE RPM / ROTOR RPM	1	0.08	CON.	0.375	0.08	0.08
ENGINE OUT				0		
WARNING UNIT	1	0.05	CON.	0.25	0.05	0.05
ENGINE OUT HORN	1	0.02	INTR.	0.1		
INSTRUMENT PANEL & WARNING LIGHTS				0		
INSTRUMENT LAMPS	11	0.04	CON.	0.2		0.44
EDGE LIGHT PANELS	SYS.	0.1	CON.	0.5		0.1
WARNING LIGHTS				0		
ENG OUT	4	0.02	INTR.	0.12		
BATTERY HOT	4	0.02	INTR.	0.12		
BATTERY RLY	4	0.02	INTR.	0.12		
R/FUEL PUMP	4	0.02	INTR.	0.12		

Table 4-6 Load Shedding cont.

EQUIPMENT	NO. OF UNITS OR SYS.	AMPS PER UNIT OR SYS.	OPER. TIME IN MIN	Amp-min in 5-min period	TOTAL AMPS (Day)	TOTAL AMPS (Night)
L/FUEL PUMP	4	0.02	INTR.	0.12		
ROTOR LOW RPM	4	0.02	INTR.	0.12		
TRANS OIL PRESSURE	4	0.02	INTR.	0.12		
TRANS OIL TEMP	4	0.02	INTR.	0.12		
FUEL LOW	4	0.02	INTR.	0.12		
ENG CHIP	4	0.02	INTR.	0.12		
TRANS CHIP	4	0.02	INTR.	0.12		
FUEL FILTER	4	0.02	INTR.	0.12		
T/R CHIP	4	0.02	INTR.	0.12		
GEN FAIL	4	0.02	INTR.	0.12		
PRESS-TO-TEST WARNING LIGHTS	SYS.	1.34	INTR.	6.72		
ENGINE CONTROLS				0		
FADEC	1	5	INTR.	25	5	5
IGNITER	1		INTR.	0		
LIGHTING				0		
POSITION LIGHTS	4	0.75	CON.	3.75		3
ANTI-COLLISION LIGHTS	SYS.	3.5	CON.	17.5	3.5	3.5
LANDING LIGHTS	2	0.00	INTR.	0		0
MAP LIGHT	1		INTR.	0		
ELECTRICAL POWER SYSTEM				0		
VOLTAGE REGULATOR	1	0.3	CON.	1.5	0.3	0.3
BATTERY RELAY	1	0.6	CON.	3	0.6	0.6
EXTERNAL RELAY	1	0.5	CON.	2.5	0.5	0.5
STARTER RELAY	1	0.5	CON.	2.5	0.5	0.5
LINE CONTROL RELAY	1	0.5	CON.	2.5	0.5	0.5
BATTERY CHARGING	1		CON.	0		
AVIONICS				0		
TRANSCIEVER KY196	1	0.4	INTR.	2	6.9	6.9
		6.5	CON.	32.5		
ICS KMA 24K	1	0.44	CON.	2.18	0.44	0.44
fuel boost pump	2	5.67	CON.	56.67	11.33	11.33
cabin heater bleed air	SYS.		INTR.	0		
pitot tube	1	6.5	CON.	32.5	6.5	6.5
OPTIONAL EQUIPMENT				0		
KT-76A transponder	1	1.8	CON.	9	1.8	1.8
Garmin GNS 530W GPS/COMM/NAV	1	3	CON.	15	3	3
KR-87 ADF	1	0.43	CON.	2.14	0.43	0.43
KDM-706A WITH KDI 572 INDICATOR	1	8.93	CON.	44.64	8.93	8.93
KR-21 marker beacon receiver	1	0.25	CON.	1.25	0.25	0.25
Autopilot KAP 150H	SYS.		INTR.	0		
KRA-405B radio altimeter	1	0.85	CON.	4.25	0.85	0.85
SKY 497 Skywatch System	1	2.5	CON.	12.5	2.5	2.5
Vapor cycle air conditioner	SYS.	17.32	INTR.	86.6	17.32	17.32
BASIC SHIP AMPERES				201.52	37.71	41.25
OPTIONAL SHIP AMPERES				175.39	35.08	35.08
TOTAL				376.90	72.79	76.33

4.1.8 Battery Analysis

The battery duration can be calculated assuming worst case scenario which is at night conditions, the following assumptions were used:

- 100% and 80% of the battery capacity in Amp-min is available.
- Pre-load shed at night conditions for 5 minutes.
- Landing load consumption calculated with all optional equipment disconnected, and lasting 5 minutes.
- Minimum Cruise load requirement equal to the ELA chart emergency condition.

With these values, the cruise duration in minutes is given by:

$$\frac{Battery\ Capacity - (Pre\ Load\ Shed + Landing\ Load)}{Cruise\ Load} = Cruise\ Time$$

Finally, the battery duration can be computed by adding the time spent on pre-load, Cruise, and emergency landing conditions:

$$Pre\ Load\ Shed + Cruise + Landing\ Load = Battery\ Time$$

Table 4-7 Total Battery Duration

Battery Duration		
Battery SOC	**100%**	**80%**
Battery Capacity - load shed - landing	516.88	212.26
Cruise Duration minutes	9.67	3.97
Total Battery Time	**19.67**	**13.97**

4.2 Electrical System Model

Validation of the DC machine dynamics was accomplished by comparing the results given by the DC motor block from Matlab/Simulink® SimPowerSystems library against the proposed model based on [32] [33] [34] and [35].

Table 4-8 Motor validation inputs

DC MOTOR VALIDATION INPUTS	
v_f	240 [V]
v_a	240 [V]
R_f	240 [Ω]
R_a	0.6 [Ω]
L_{FF}	120 [H]
L_{AA}	0.012 [H]
L_{AF}	1.8 [H]
J	1 [kg m^2]
B_l	0.2287 [N m s/rad]

Results of field current, armature current, angular velocity, electromagnetic torque and load torque are presented, showing exact match between both models.

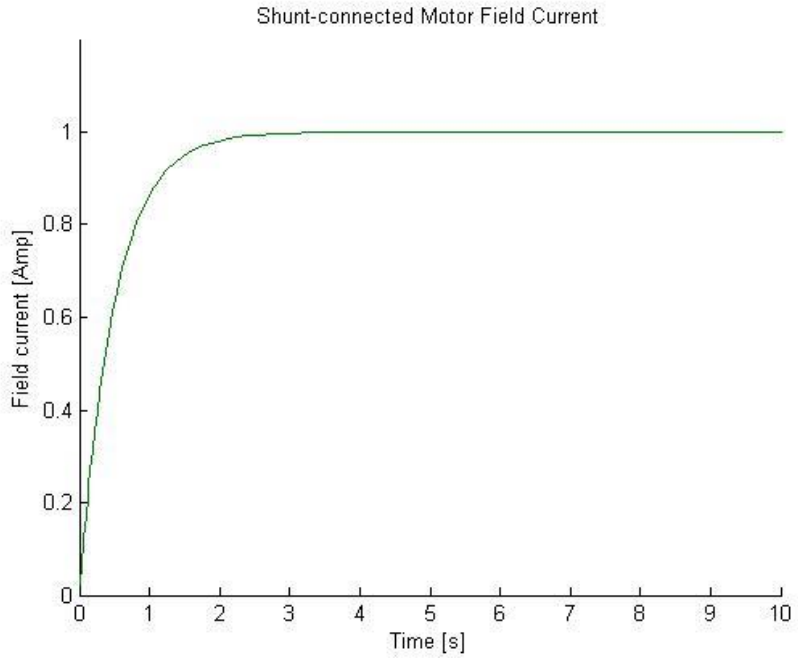

Figure 4-2 Field currents

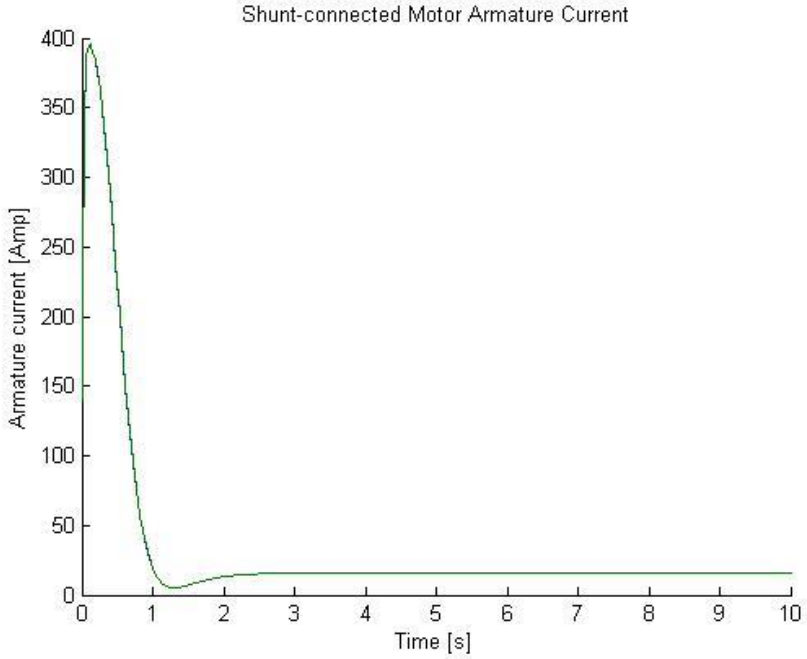

Figure 4-3 Armature currents

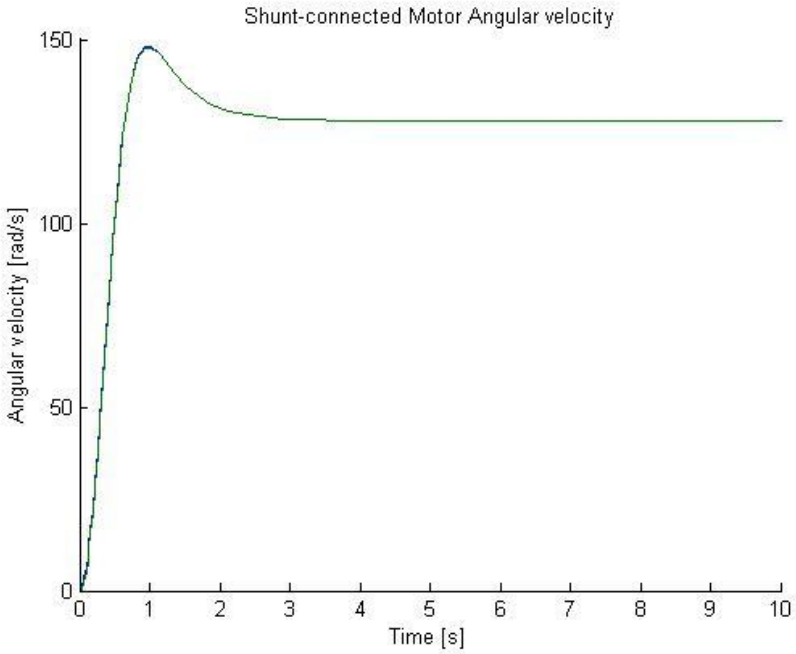

Figure 4-4 Angular velocities

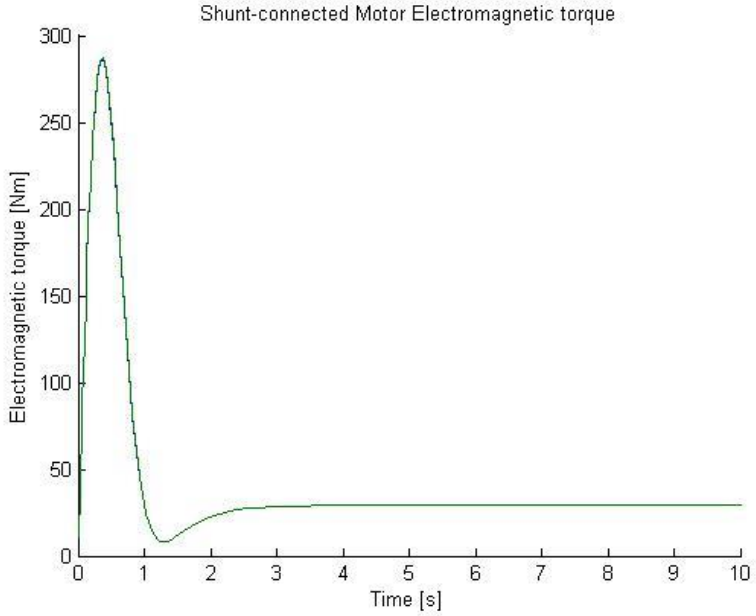

Figure 4-5 Electromagnetic torques

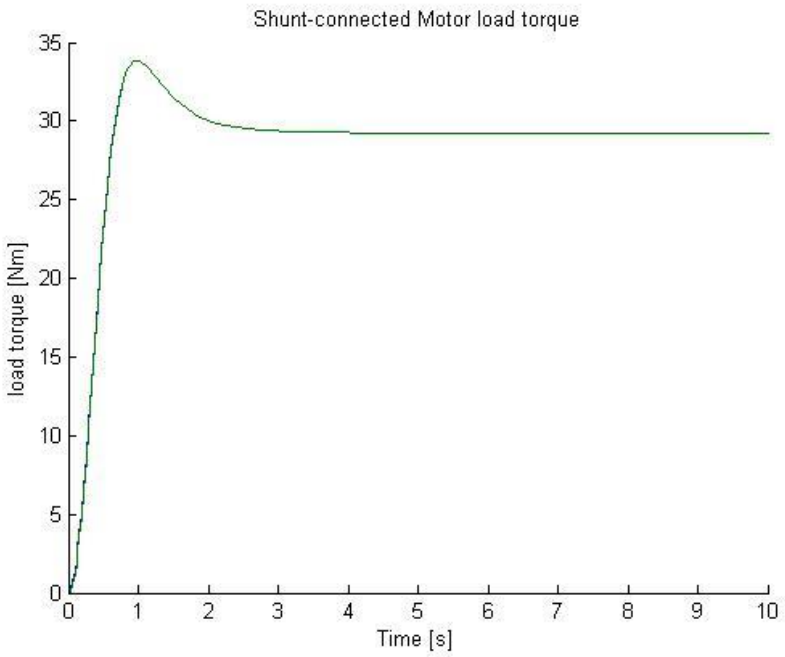

Figure 4-6 Load torques

After validation of the model, the Electrical System was modelled using a shunt-connected DC machine, if characteristics related to series and compound configurations become available, their corresponding results will be presented.

The proposed DC motor Speed-torque curve achieves typical output values presented by the manufacturer [29]. The requirements for engine starting are related to starter typical outputs by using the battery voltage.

Table 4-9 Typical Starter Values

STARTER OUTPUT		
	TYPICAL OUTPUT	MOTOR OUTPUT
Input Voltage [V]	20	21.02
Speed [RPM]	1000	1000
Power [W]	2833	2901

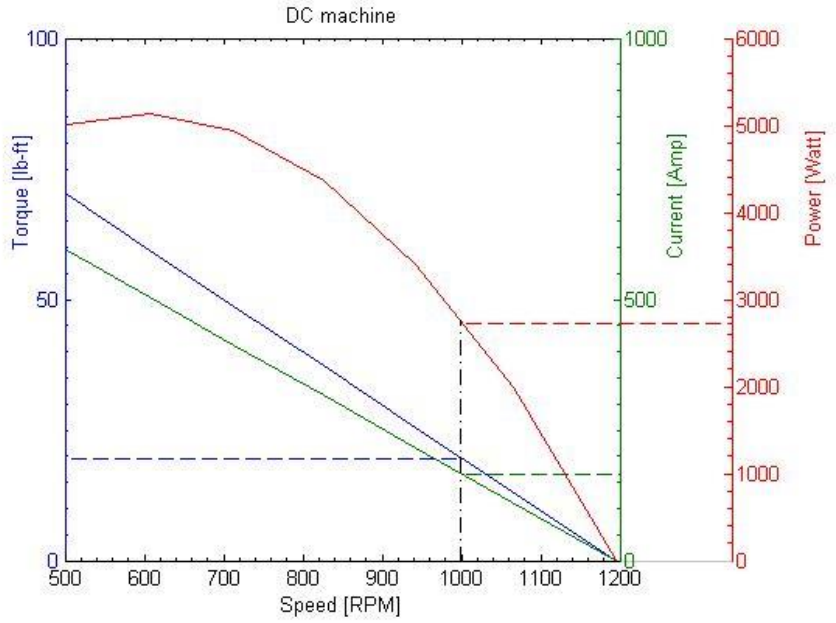

Figure 4-7 DC Motor Speed-Torque curve with constant voltage

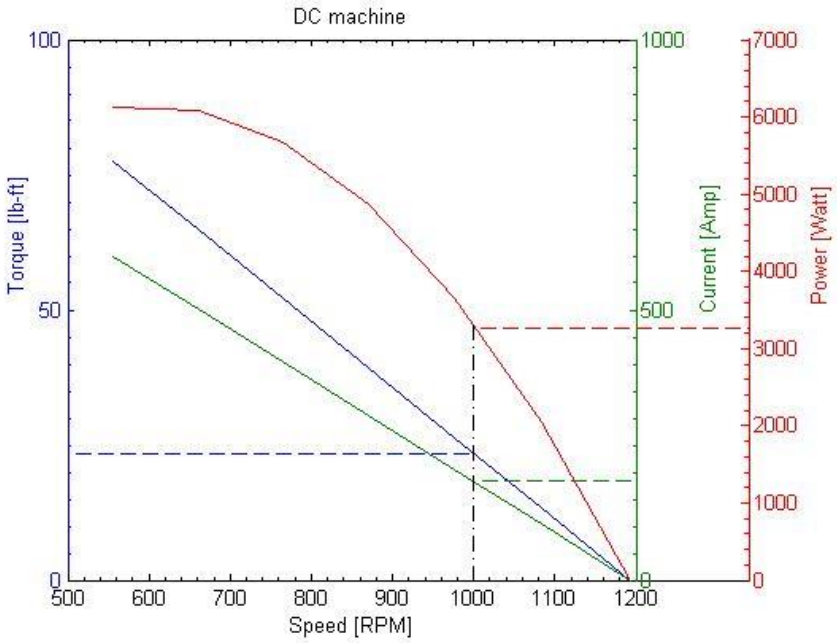

Figure 4-8 DC motor Speed-Torque curve with battery voltage

4.2.1 Starter Block

The motor input current il is equal to the generated armature current plus the field current $ia + if$.

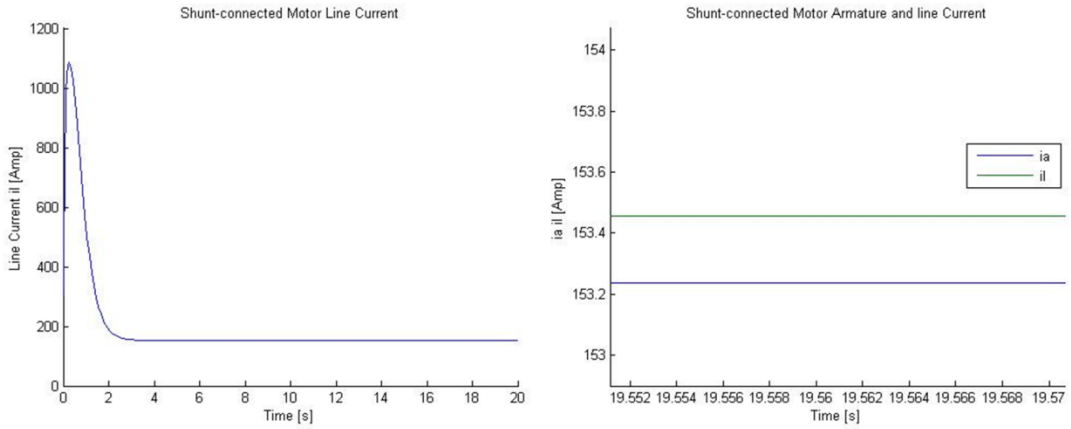

Figure 4-9 Motor line and armature currents

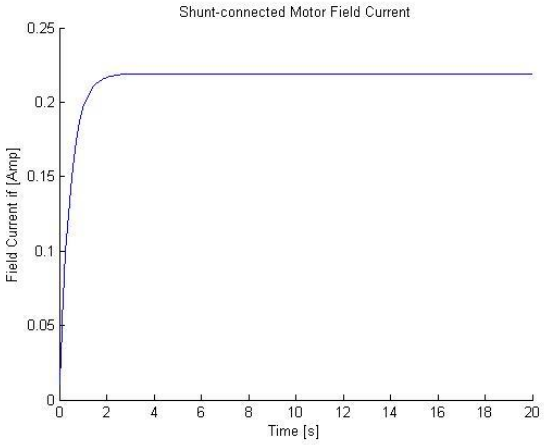

Figure 4-10 Motor field current

Table 4-10 Motor Currents

Motor Input Current il	
Armature Current ia	153.235 [A]
Field Current if	0.219 [A]
Line Current il	153.454 [A]

When steady-state conditions are reached, the electromagnetic torque generated by the motor, must be the same as the load torque applied to the motor by mechanical load (i.e engine).

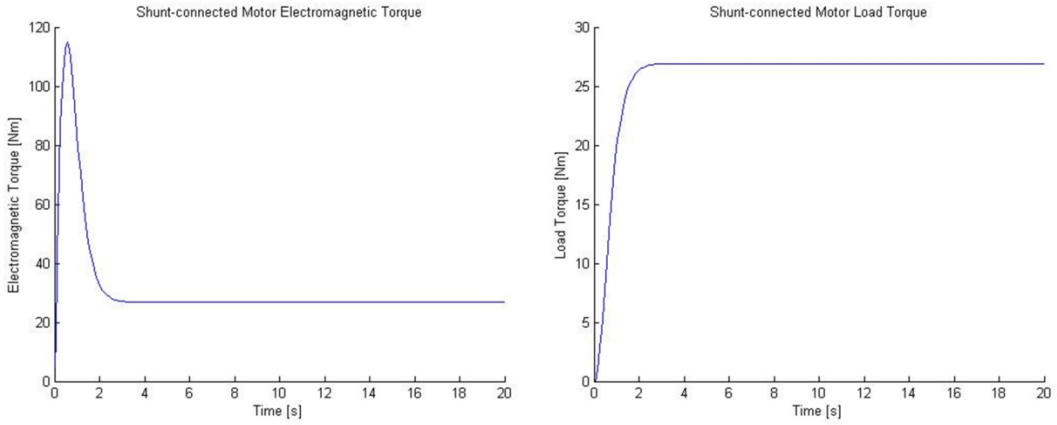

Figure 4-11 DC motor torques

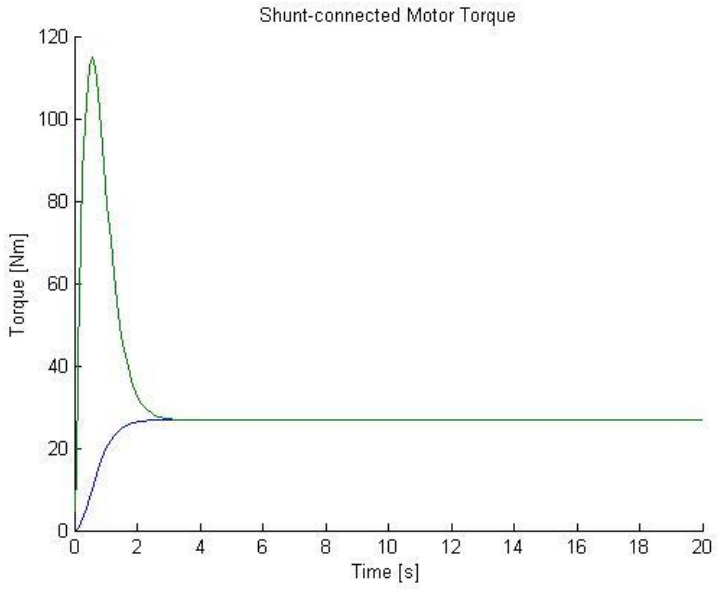

Figure 4-12 electromagnetic and load torque Vs time

Table 4-11 Steady-State motor torque results

Motor Torques in Steady-State conditions	
Electromagnetic torque Te	26.871 [Nm]
Load torque Tl	26.871 [Nm]

The relationship between Te and the angular velocity w is used to calculate the starter output power

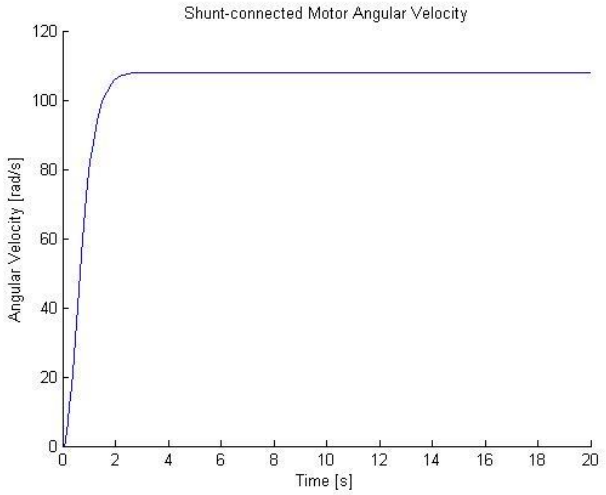

Figure 4-13 Motor angular velocity

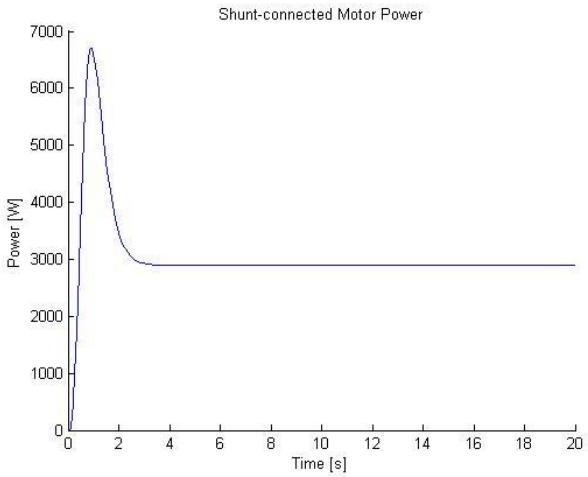

Figure 4-14 Motor power

Table 4-12 Motor output power

Motor Output Power	
Angular velocity w	107.96 [rad/s]
Electromagnetic torque Te	26.871 [Nm]
Output power P	Power 2901 [W]

4.2.2 Generator Block

After the motor steady-state characteristics are met, its final values are used as initial conditions for the generator. At this point the load requirement calculated from the ELA depending on the flight segment is the value to be met by the generator output current il, this is achieved by means of the field rheostat. Again steady-state conditions are met when the generated electromagnetic torque Te and the load torque Ts applied from the engine are equal.

Results of this analysis presented in this section are for the ground condition only, behaviour of the generator in other flight segments can be found in APPENDIX A

- Ground

Table 4-13 Generator results (Ground)

Generator results for ground conditions	
Output voltage [V]	28
Angular velocity [rad/s]	67.68
Required current [Amp]	21.02
Load current [Amp]	21.69
Field resistance [Ω]	55
Power required [W]	612.08

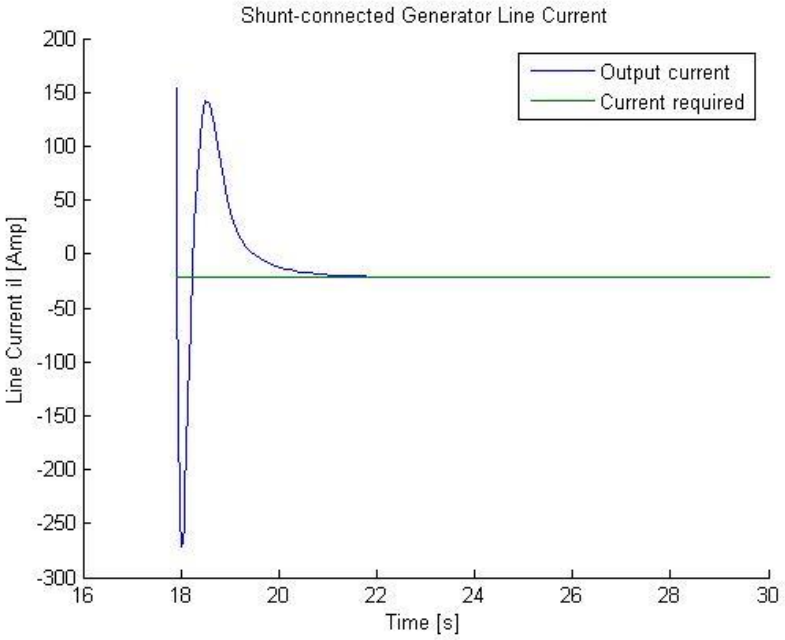

Figure 4-15 Generator current il

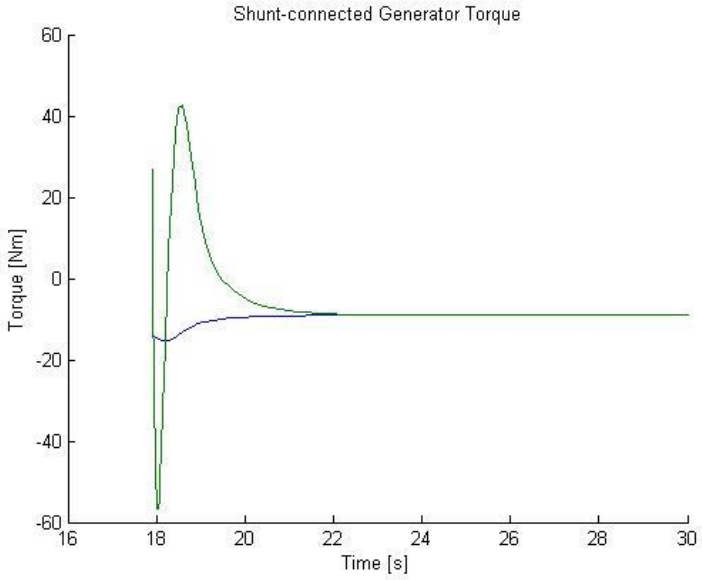

Figure 4-16 Generator steady-state torque

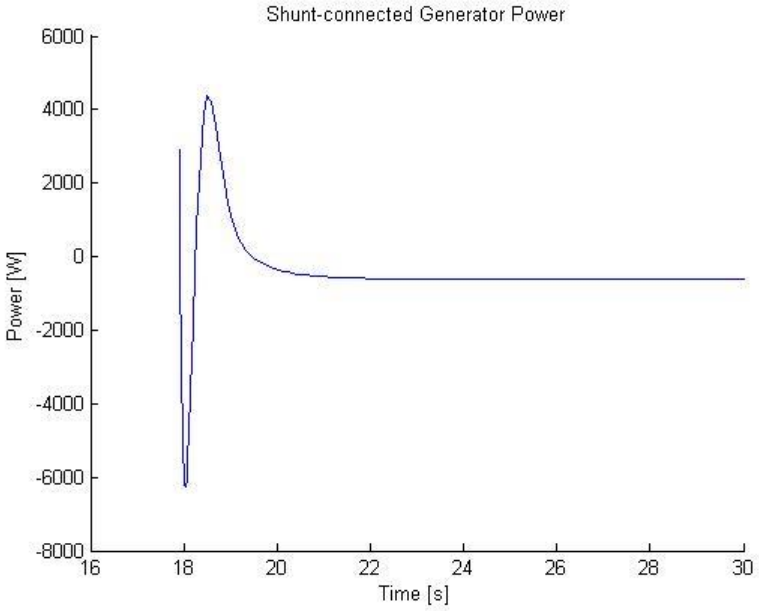

Figure 4-17 Generator power required

4.3 Actuation System

For the actuation system, results of the aerodynamic analysis and swashplate analysis are presented for two helicopters, a Bell 206L-4 and an MBB Bo-105. As information related to the main rotor mechanism of both helicopters was not found on the public domain, approximations related to component dimensions and position of the actuators arms were made based on [40], [41] and [42].

At this point the weight of the helicopters was kept constant and pitch, altitude and velocity were variables for the three different segments.

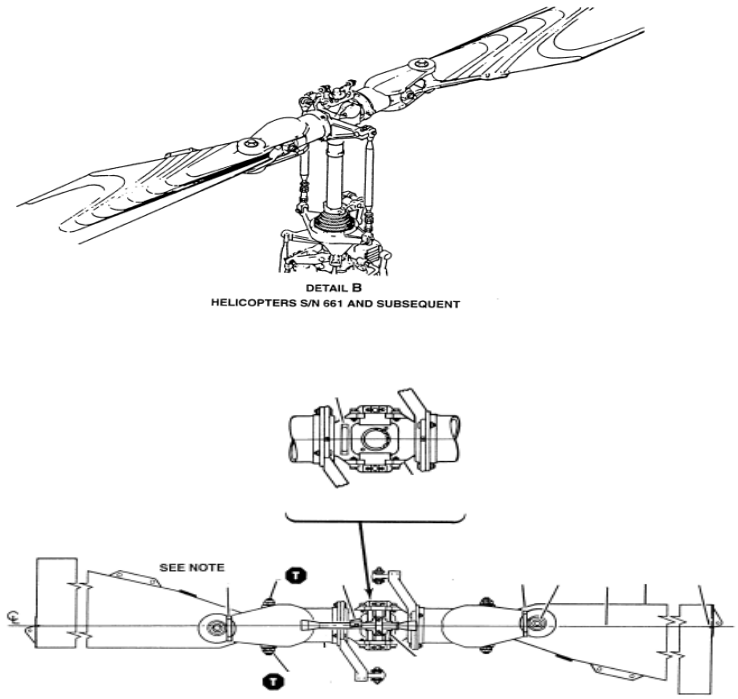

Figure 4-18 Bell 206 A/B series Main Rotor [43] [44]

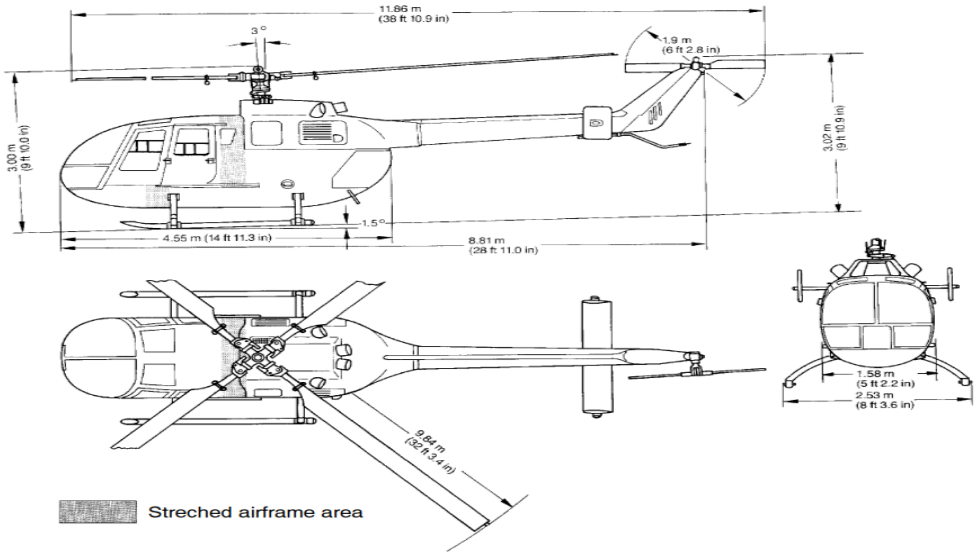

Figure 4-19 MBB Bo 105 Dimensions [45]

4.3.1 Aerodynamic analysis in hover

The aerodynamic analysis presented provides results of lift and thrust distribution from the BET and the BEMT. It shows the effect of the assumptions made by both theories in the outcome when applying the same pitch angle.

Table 4-14 Inputs for Hover

HOVER INPUTS		
	Bell 206L-4	Mbb Bo105
Weight [lb]	4338.7	5000
Altitude [ft]	16.4	16.4
Collective pitch [deg]	15	14.987

- **BET**

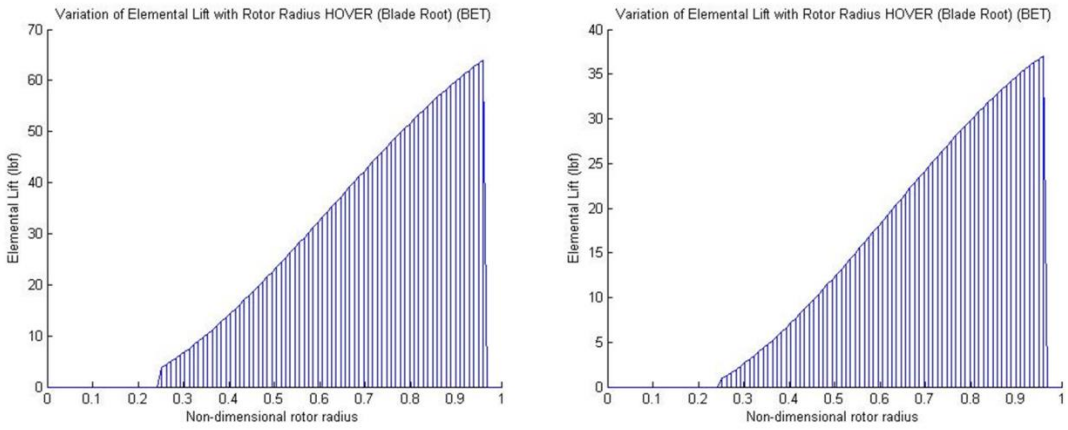

Figure 4-20 Lift distribution BET

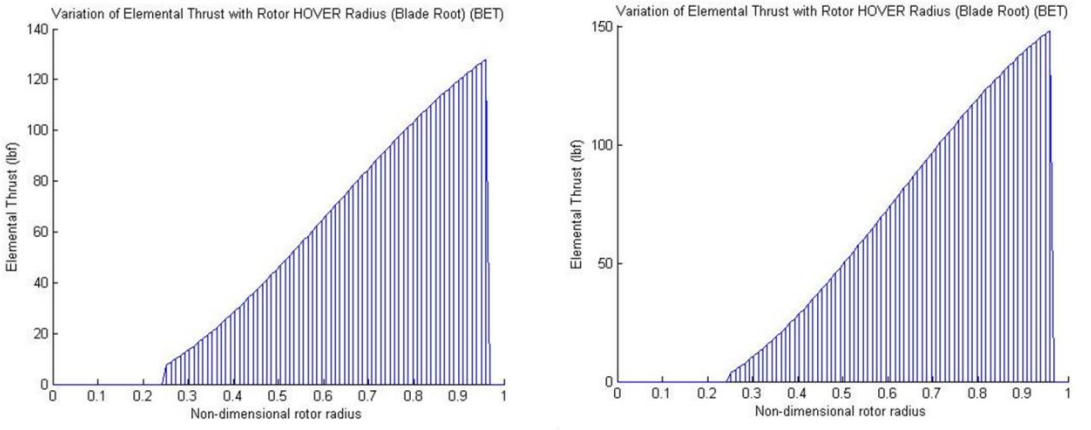

Figure 4-21 Thrust distribution BET

- **BEMT**

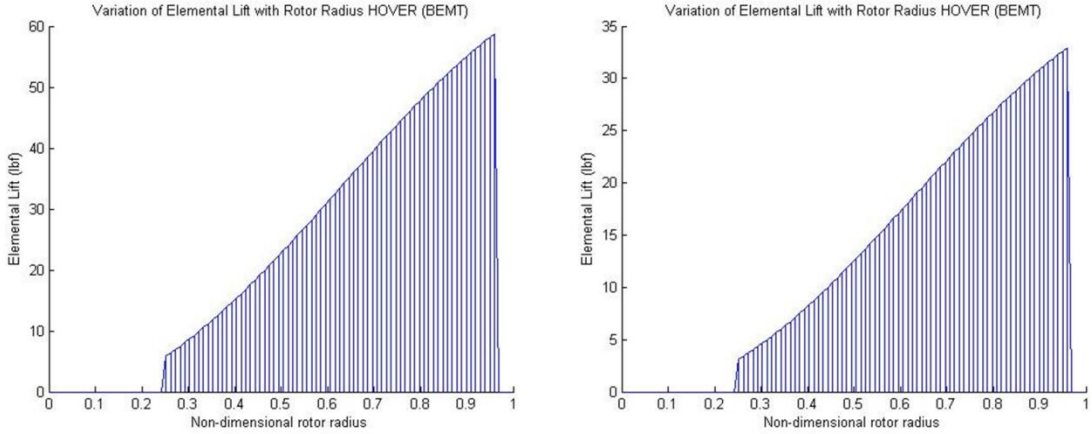

Figure 4-22 Lift distribution BEMT

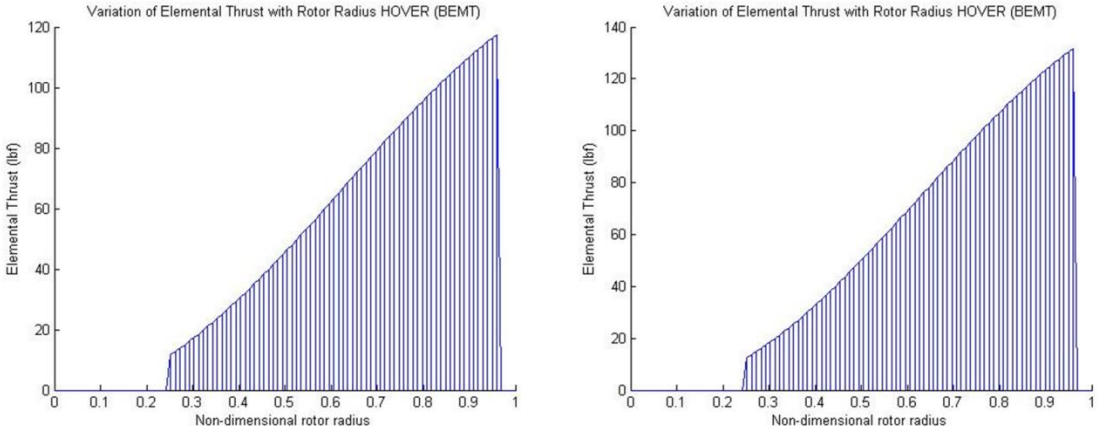

Figure 4-23 Thrust distribution BEMT

Results of lift and thrust related to the approximations for the hover condition are presented in APPENDIX B

4.3.2 Aerodynamic analysis in climb

Table 4-15 Inputs for Climb

CLIMB INPUTS		
	Bell 206L-4	Mbb Bo105
Weight [lb]	4338.7	5000
Altitude [ft]	328.08	328.08
Collective pitch [deg]	15.7103	16.011
Rate of Climb [ft/s]	15.12	15.12

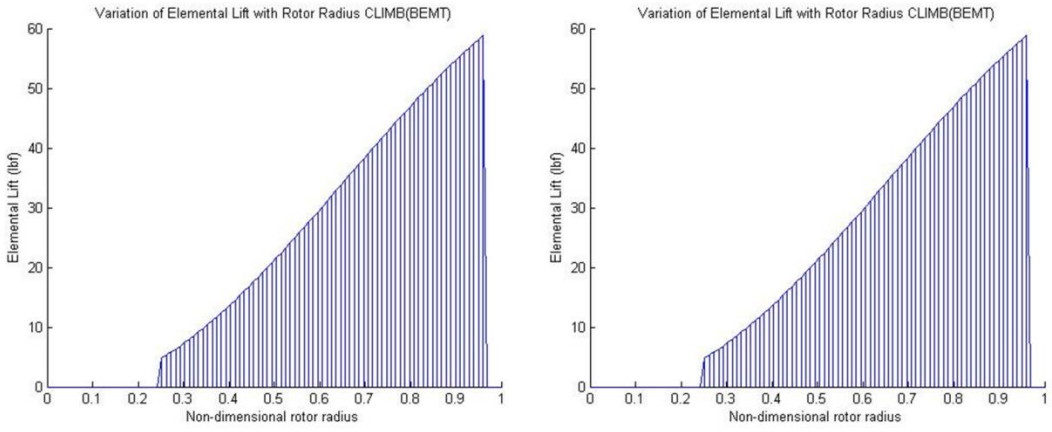

Figure 4-24 Incremental lift per unit span axial flight

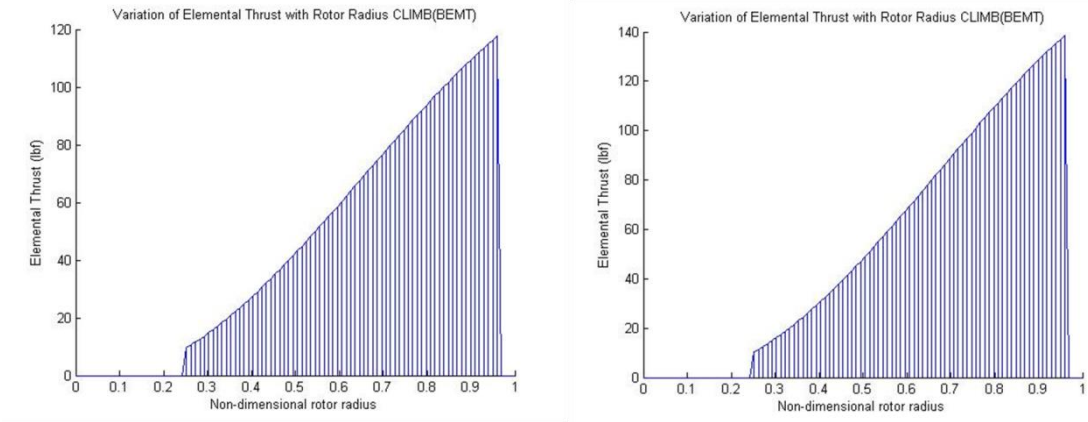

Figure 4-25 Thrust coefficient increment per unit span axial flight

4.3.3 Aerodynamic analysis in forward flight

Table 4-16 Forward Flight Inputs

FORWARD FLIGHT INPUTS		
	Bell 206L-4	Mbb Bo105
Weight [lb]	4338.7	5000
Altitude [ft]	656.16	656.16
Collective pitch [deg]	12.63	12.232
Velocity [ft/s]	118.14	118.14
Rotor tilt angle [deg]	1.45	1.45

Results of the lift distribution for each blade position along a rotation for the Bell 206L-4, and each blade for the Mbb Bo105 are presented as in forward flight the flow is not axisymmetric.

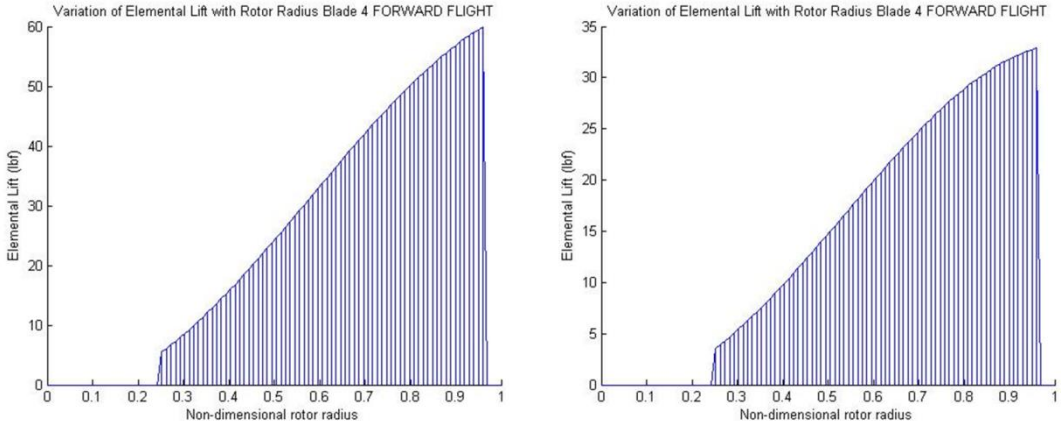

Figure 4-26 Incremental lift per unit span forward flight (azimuth angle=0)

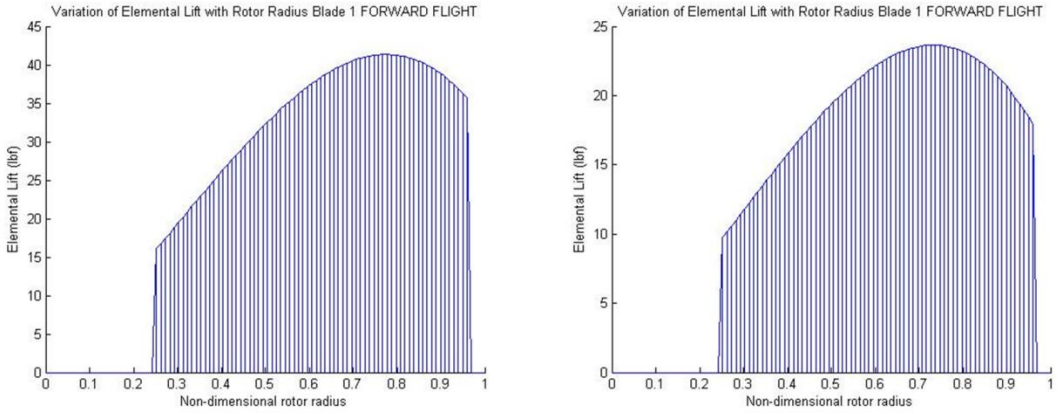

Figure 4-27 Incremental lift per unit span forward flight (azimuth angle=90)

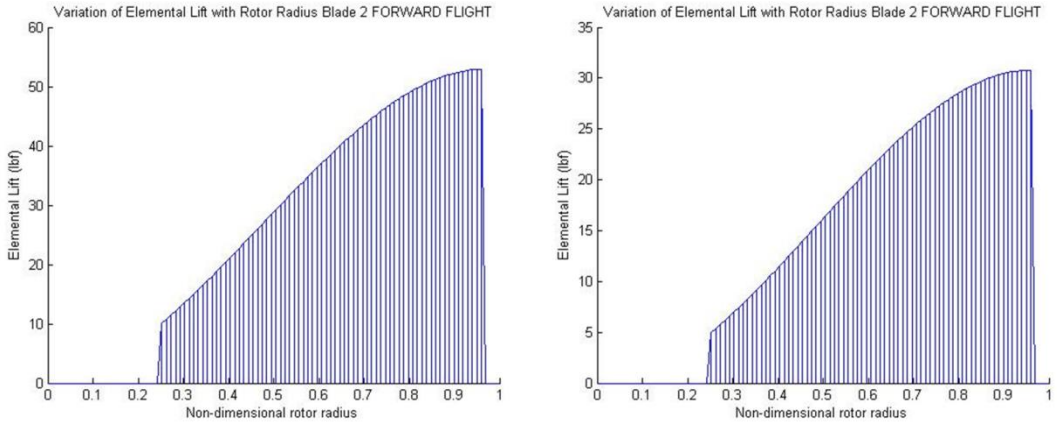

Figure 4-28 Incremental lift per unit span forward flight (azimuth angle=180)

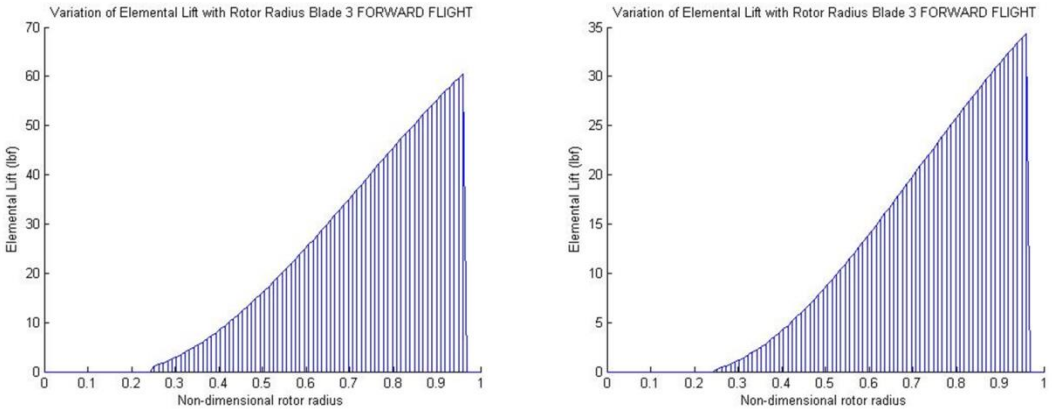

Figure 4-29 Incremental lift per unit span forward flight (azimuth angle=270)

4.3.4 Swashplate analysis

The results given by the swashplate analysis are divided in two sections: the first one is related to dimensions constraints of the mechanism after a new position is acquired when collective and cyclic inputs are applied, and the second section summarises the forces to be generated at the blade pitch to maintain that position. The initial conditions of the mechanism for both helicopters are presented along with results of the dimensions constraints and the pitch link forces, the analysis showing translation of the components is given in APPENDIX B

Table 4-17 Bell 206 L-4 swashplate initial conditions

BELL 206 L-4												
INITIAL CONDITIONS												
Axis	azimuth 0 [rad]			azimuth 1.5708 [rad]			azimuth 3.1416 [rad]			azimuth 4.7124 [rad]		
	rp [ft]	Cpl [ft]	rh [ft]	rp [ft]	Cpl [ft]	rh [ft]	rp [ft]	Cpl [ft]	rh [ft]	rp [ft]	Cpl [ft]	rh [ft]
E1	0.550	0.000	0.550	0.000	0.000	-0.300	-0.550	0.000	-0.550	0.000	0.000	0.300
E2	0.000	0.000	0.300	0.550	0.000	0.550	0.000	0.000	-0.300	-0.550	0.000	-0.550
E3	0.000	2.209	0.000	0.000	2.209	0.000	0.000	2.209	0.000	0.000	2.209	0.000
magnitude	0.550	2.209	0.627	0.550	2.209	0.627	0.550	2.209	0.627	0.550	2.209	0.627

Table 4-18 Bell 206 L-4 force result (hover)

HOVER												
Collective pitch theta 15 [rad]												
magnitude	0.550	2.209	0.627	0.550	2.209	0.627	0.550	2.209	0.627	0.550	2.209	0.627
Cyclic pitch 0 [rad]												
magnitude	0.550	2.209	0.627	0.550	2.209	0.627	0.550	2.209	0.627	0.550	2.209	0.627
swashplate angle [rad]	0.000			0.000			0.000			0.000		
PITCH LINK FORCE RESULT												
Pitch link force [lbf]	2269.000			2269.000			2269.000			2269.000		

Table 4-19 Bell 206 L-4 force result (climb)

CLIMB												
Collective pitch 15.7103 [rad]												
magnitude	0.550	2.209	0.627	0.550	2.209	0.627	0.550	2.209	0.627	0.550	2.209	0.627
Cyclic pitch 0 [rad]												
magnitude	0.550	2.209	0.627	0.550	2.209	0.627	0.550	2.209	0.627	0.550	2.209	0.627
swashplate angle [rad]	0.000			0.000			0.000			0.000		
PITCH LINK FORCE RESULT												
Pitch link force [lbf]	2385.300			2385.300			2385.300			2385.300		

Table 4-20 Bell 206 L-4 force result (forward flight)

FORWARD FLIGHT												
Collective pitch 12.63 [rad]												
magnitude	0.550	2.209	0.627	0.550	2.209	0.627	0.550	2.209	0.627	0.550	2.209	0.627
Cyclic pitch 0 [rad]												
magnitude	0.550	2.209	0.627	0.550	2.209	0.627	0.550	2.209	0.627	0.550	2.209	0.627
swashplate angle [rad]	0.000			0.000			0.000			0.000		
PITCH LINK FORCE RESULT												
Pitch link force [lbf]	1859.500			1859.500			1859.500			1859.500		

Table 4-21 Mbb Bo105 swashplate initial conditions

Mbb Bo105												
INITIAL CONDITIONS												
Axis	azimuth 0 [rad]			azimuth 1.5708 [rad]			azimuth 3.1416 [rad]			azimuth 4.7124 [rad]		
	rp [ft]	Cpl [ft]	rh [ft]	rp [ft]	Cpl [ft]	rh [ft]	rp [ft]	Cpl [ft]	rh [ft]	rp [ft]	Cpl [ft]	rh [ft]
E1	-0.096	-0.067	-0.163	0.096	0.040	-0.217	0.096	0.067	0.163	-0.096	-0.040	0.217
E2	-0.096	-0.040	0.217	-0.096	-0.067	-0.163	0.096	0.040	-0.217	0.096	0.067	0.163
E3	0.000	0.271	0.000	0.000	0.271	0.000	0.000	0.271	0.000	0.000	0.271	0.000
magnitude	0.135	0.282	0.271	0.135	0.282	0.271	0.135	0.282	0.271	0.135	0.282	0.271

Table 4-22 Mbb Bo105 force result (hover)

HOVER												
Collective pitch theta 15 [rad]												
magnitude	0.135	0.282	0.271	0.135	0.282	0.271	0.135	0.282	0.271	0.135	0.282	0.271
Cyclic pitch 0 [rad]												
magnitude	0.135	0.282	0.271	0.135	0.282	0.271	0.135	0.282	0.271	0.135	0.282	0.271
swashplate angle [rad]	0.000			0.000			0.000			0.000		
PITCH LINK FORCE RESULT												
Pitch link force [lbf]	2133.400			2133.400			2133.400			2133.400		

Table 4-23 Mbb Bo105 force result (climb)

CLIMB												
Collective pitch 15.7103 [rad]												
magnitude	0.135	0.282	0.271	0.135	0.282	0.271	0.135	0.282	0.271	0.135	0.282	0.271
Cyclic pitch 0 [rad]												
magnitude	0.135	0.282	0.271	0.135	0.282	0.271	0.135	0.282	0.271	0.135	0.282	0.271
swashplate angle [rad]	0.000			0.000			0.000			0.000		
PITCH LINK FORCE RESULT												
Pitch link force [lbf]	2345.400			2345.400			2345.400			2345.400		

Table 4-24 Mbb Bo105 force result (forward flight)

FORWARD FLIGHT												
Collective pitch 12.63 [rad]												
magnitude	0.550	2.209	0.627	0.550	2.209	0.627	0.550	2.209	0.627	0.550	2.209	0.627
Cyclic pitch 0 [rad]												
magnitude	0.135	0.282	0.271	0.135	0.282	0.271	0.135	0.282	0.271	0.135	0.282	0.271
swashplate angle [rad]	0.000			0.000			0.000			0.000		
PITCH LINK FORCE RESULT												
Pitch link force [lbf]	1580.400			1580.400			1580.400			1580.400		

4.4 RMEM Integration

To predict the fuel consumption penalties derived from the use of secondary power systems, RMEM was integrated to a single light-engine performance model using a Bell206L-4 helicopter as baseline, and a flight mission was defined. Two sets of simulations were run, starting with fuel consumption calculated without RMEM, and the second one taking into account the proposed systems with the aim of predicting the increase in fuel burn do to SPS.

The mission selected for comparison is the same used by [1]:

1. Start the engine and wait for 5 minutes at 60% shaft horsepower.
2. Lift into the hover condition at 5 m during 5 minutes.
3. Climb to 1000 m at 30.867 m/s forward flight
4. Maintain forward flight condition for 180.24 km at 46.3 m/s

Based on the proposed mission, the final fuel consumption without RMEM was 88.386 kg, while 89.503 kg are required if the proposed SPS are to be included in the analysis. This shows an increase in 1.26% of fuel burn, which validates the assumption that the impact due to SPS must be taken into account when predicting the helicopter fuel consumption.

Additionally, if only conventional SPS are used, impact on fuel consumption is expected to be higher, showing the need of analysing more electric SPS

at conceptual level as a mean of developing a more environmental friendly helicopter.

After defining the mission, a single parametric study was applied to estimate the impact of SPS for different flight conditions, and results of fuel consumption increment are presented for four flight segments: ground, hover, climb and forward flight, the reader is referred to APPENDIX C where inputs for the analysis, as well as total fuel burn are included.

4.4.1 Ground

For the ground condition, the parameter chosen for this analysis was the segment time:

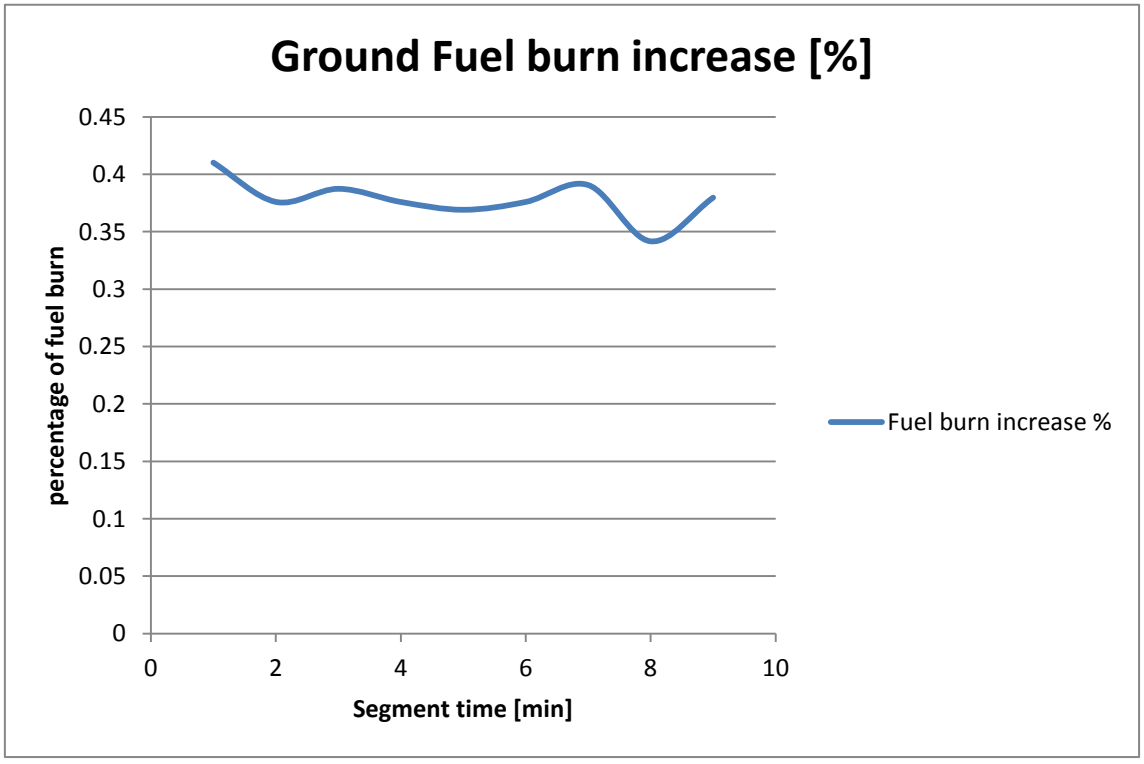

Figure 4-30 Parametric analysis (ground)

A small increase of fuel burn is achieved as for this segment, the AS power requirements are not taken into account, and only ECS, FS and ECS are in operation.

4.4.2 Hover

For the hover segment, the variable taken into account was altitude, varying from 1 to 9 meters, the increase of fuel burn when using different technologies for the AS is presented.

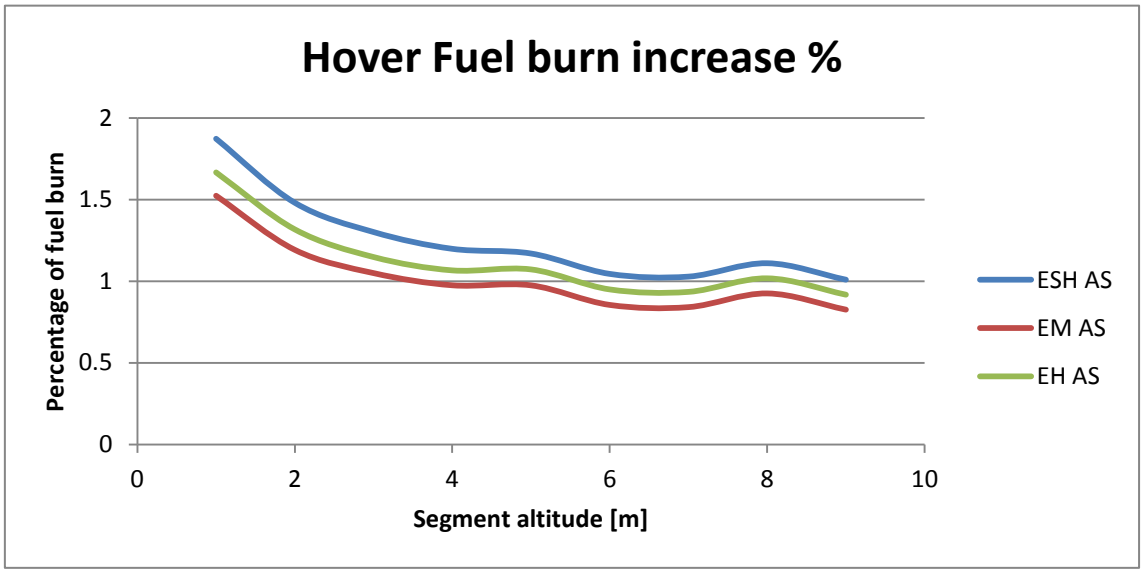

Figure 4-31 Parametric analysis (hover)

Between 1% and 1.87% increase is expected in the hover, depending on the operating conditions, when a conventional AS is used, if a EM AS is used instead, the overall fuel consumption will be between 0.91% and 1.66%, achieving a 0.21% in the highest case only by implementing a more electric AS.

4.4.3 Climb

In the climb segment the forward flight velocity was used for the parametric analysis.

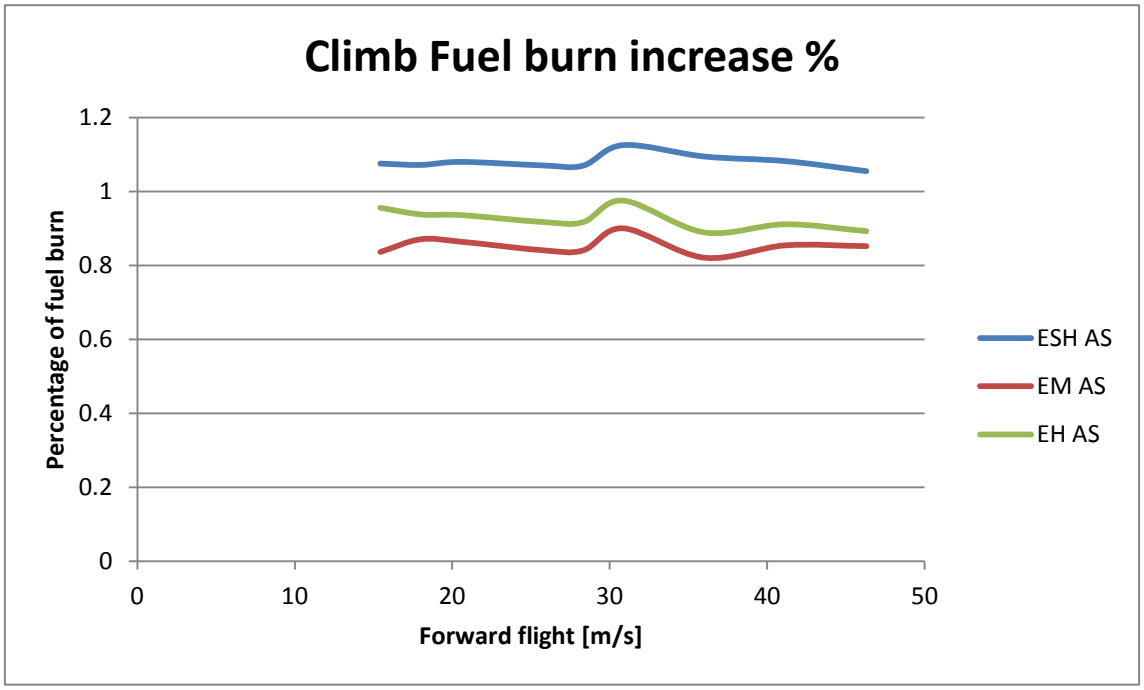

Figure 4-32 Parametric analysis (climb)

For climb a fairly constant fuel burn increase due to SPS is predicted when varying the forward flight speed, however, a reduction of 0.22% in the total fuel consumption will be accomplished if a conventional AS is replaced by an EM AS.

4.4.4 Forward flight

For forward flight, the speed was used again as the variable parameter, while maintaining the same altitude.

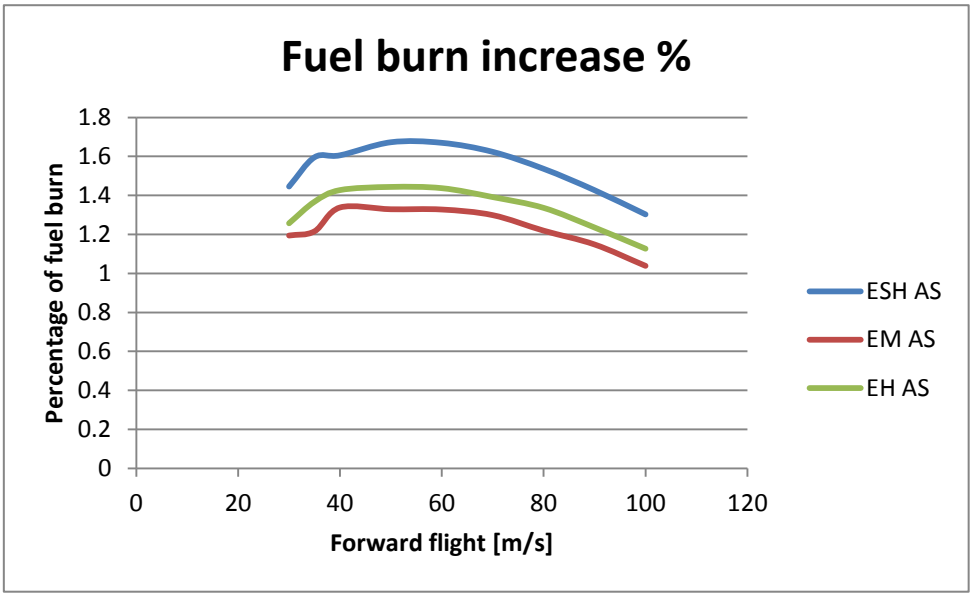

Figure 4-33 Parametric analysis (forward flight)

For forward flight, the predicted increase in fuel consumption when SPS are considered is between 1.3% and 1.67% when the conventional AS is used. As was the case for the other segments, if an EM AS is placed, a 0.3% in total fuel burn can be found. Although the percentage increases between $50\ ^{m}/_{s}$ and $60\ ^{m}/_{s}$, this is due to high reductions in block fuel consumption as the rotorcraft performance increases with forward speed, after $60\ ^{m}/_{s}$ the fuel consumption reduction is negligible.

5 Conclusions

The work presented in this thesis, has highlighted the importance of Secondary Power Systems when analysing the Fuel Consumption of a helicopter throughout a full mission, providing continuity to previous works within the Aerospace Department of Cranfield University. Increments of up to 1.87% in Fuel Consumption were observed under different flight parameters for individual mission segments due to the proposed integration of Secondary Power Systems into a Helicopter performance Model. These results further encourage researchers, and industry, to take into consideration the impact of SPS, along with the possible implementation of novel electric technologies, when designing a more environmental friendly aircraft.

In this project, the Fuel System, an electric Ice Protection System, and an electric Environmental Control system were integrated into a Secondary Power Systems power requirement tool, and further into a high veracity Helicopter Performance Model. Additionally, an Actuation System incorporating three different technologies, namely conventional electro-servohydraulic actuation, electromechanical actuation and electro-hydrostatic actuation, was included in the Secondary Power Systems modelling tool. To complete the proposed tool, a conventional Electrical System was developed based on an Electrical Load Analysis and DC shunt-connected machine dynamics.

Among the tool's capabilities, its dependency on the Matlab/Simulink® software were eliminated, allowing it to be integrated within any Helicopter Performance Model as a stand-alone software, this is expected to encourage future users of Helicopter Performance Models to include Secondary Power Systems impact at mission level in their own models, leading to an increase in the research for more efficient electric configurations.

The considered Fuel System, Ice Protection System and Environmental Control System were tailored to represent the requirements of a Bell 206L-4 helicopter, which is a representative helicopter of the single-light engine category.

For the Actuation System, as it was modelled for a fixed-wing aircraft, a generic Actuator Forces Algorithm for rotary-wing aircraft was developed to replace the fixed-wing aeroload estimator; it considers two different approaches for the calculation of the forces produced by the main rotor actuators. The first approach was based solely on a blade aerodynamics analysis, while the second approach additionally considered swashplate kinematics and blade torsional moments; both analyses were presented only for the hover condition. By coupling both methodologies a more complete analysis was later developed, and calculations of the actuator forces were extended to axial climb and forward flight conditions.

The Electrical System model proposed in this project, has been based solely on the Electrical Load Analysis and DC machine dynamics, it includes four different configurations for DC machines: separately excited DC machine, shunt-connected DC machine, series-connected DC machine and a compound-connected DC machine, all of which are configurations that could be used to model Electrical Systems installed in other helicopters. Within the scope of this project it was decided to use the shunt-connected DC machine, its behaviour was validated against an embedded system of the Matlab/Simulink SimPowerSystems library, showing a 100% agreement in armature current, field current, torque and speed for transient and steady-state conditions.

The integrated Secondary Power Systems tool and Helicopter Performance Model was here controlled by means of an M-file, which simplifies the change of parameters if a different helicopter or individual system configuration is to be considered. In a case where the Secondary Power Systems tool is to be used with a Helicopter Performance Model written in another programming language, it has been proposed to control it by means of text files.

Although an increase in fuel consumption of up to 1.87% was found when integrating the proposed systems into the model, a higher impact is to be expected if only conventional Secondary Power Systems are considered, thus leading to the need for a deeper analysis and modelling of more electric systems for helicopter applications.

The Actuator Forces Algorithm presented in this project neglects the effect of the swashplate on the forces to be produced by the actuators to maintain a certain pitch setting. Calculations of the forces on the actuators produced while the helicopter is still on the ground were not considered in the scope of this project. Additionally for the Electrical System, the voltage regulator, power protection, engine starting requirements and torque were not included either in this project, which opens the field for further improvements to be added to the modelling and understanding of the impact of rotorcraft secondary power systems on the long term fuel consumption of such aircrafts and spawns the possibility for new research topics to investigate alternative ways to fulfil their requirements through the eventual implementation of onboard hybrid power plants dedicated to secondary systems.

6 Recommendations for Future Work

Improvements on the results given by the integrated tools in specific areas, which due to time and availability of information constraints were not presented in this project, can yet lead to a more robust performance model in the near future.

In order to provide continuity to this line of work, and gain insight into the impact of novel technologies for helicopter Secondary Power Systems, it would be important to add the modelling of conventional Power Systems to the tool and compare the fuel consumption when changing the systems configuration.

So far the Ice Protection System model remained unused, as the integrated engine model only works for a condition of ISA +20. By adding more ISA deviations it will be possible to assess the impact of this system on the overall fuel consumption.

Regarding the Electrical System's potential improvement, incorporation of the voltage regulator, specific machine characteristics and engine-generator coupling could be addressed. Additionally, if AC power generation capabilities are added, it should be possible to model an Electrical System that uses AC only or AC and DC power generation.

As some helicopters include an actuator for the tail rotor control, the author would also recommend to include this option in the Actuator Forces Algorithm, as well as to consider the effect of the swashplate on the forces produced by the actuators.

The Helicopter Performance Model descent segment was not included so far in this study, were it to be taken into account a complete mission profile could then be modelled. Additionally, it was developed based on the Momentum Theory, and does not consider blade aerodynamics. Although this issue was addressed within the Actuator Forces Algorithm, the performance model could be updated to include this analysis within, thereby providing a starting point to developing a helicopter trim analysis along a flight mission, providing fuel consumption results for more points in each segment.

As the majority of the models already included in both tools were developed around steady-state conditions, transient behaviours were not taken into account. If dynamic models are to be integrated, a more realistic environment should be created.

Finally, it is recommended to validate the individual models, as well as the integrated tools, against experimental results, thus increasing the level of accuracy and reliability that can be expected of them.

REFERENCES

[1] Linares, C. (2011), *Environmental impact assessment of the operation of conventional helicopters at mission level* (MSc by Research thesis), Cranfield University, Cranfield University.

[2] Goulos, I., Mohseni, M., Pachidis, V., D'Ippolito, R. and Stevens J. (2010), "Simulation Framework Development for Helicopter Mission Analysis", ASME Conference Proceedings (ed.), in: *ASME Turbo Expo 2010: Power for Land, Sea, and Air (GT2010),* Vol. 3, June 14-18, 2010, Glasgow, UK, ASME, United Kingdom, .

[3] Nijland, T., Atyeo, S., and Sinha, A. (2004), "A Simulation Model For Flight Performance Analysis Of Helicopter Mid-Life Upgrade Designs", *30th European Rotorcraft Forum,* 14-16 Sept. 2004, Marseille; France, National Aerospace Laboratory NLR, Amsterdam, .

[4] CleanSky (2012). Integration of innovative electrical systems (GRC3) available in: http://www.cleansky.eu/content/page/integration-innovative-electrical-systems-grc3 (Accessed in May 2012)

[5] Tobon, J. (2011), *V-10 "Sparrowhawk" Rotor Blades, Rotor Hub and Gear-box Design,* Cranfield University, Cranfield University.

[6] Corl, J. (2009), *A COMPARISON OF HELICOPTER ACTIVE ROTOR GUST REJECTION AND VIBRATION ALLEVIATION METHODS*, The Pennsylvania State University, The Pennsylvania State University.

[7] Army Materiel Command, Alexandria, VA (1974), *Engineering design handbook. Helicopter engineering, part 1: Preliminary design (for VFR operation),* AD-A002007; AMCP-706-201-PT-1; Pagination 876P.

[8] Viswasnath, S. and R. Nagarajan., (2002), *"HELICOPTER HYDRAULIC SYSTEM (DESIGN, COMPONENT SELECTION, MODULAR CONSTRUCTION, INTEGRATION & TESTING)"*, in: 23rd Congress of International Council of the Aeronautical Sciences, September 8-13, 2002, Toronto, Canada

[9] Moir, Ian and Seabridge, Allan. (2008). Aircraft Systems: Mechanical, electrical, and avionics subsystems integration, 3rd ed. Wiley, Chichester.

[10] AIR COMM CORPORATION, (2008). BELL 206L-4 CABIN AIR CONDITIONING SYSTEMS (TORQ-LOK PLUMBING), Colorado, USA.
[11] AIR COMM CORPORATION, (1991). BELL 206 L3/L4 CABIN HEATER INSTALLATION INSTRUCTIONS (F/W Shut-off Valve/Temp Sensors), Colorado, USA.
[12] Emerald Group Publishing Limited., (2005). “More-electric aircraft”, Aircraft engineering and Aerospace Technology, Vol 77 Iss: 1,pp.-
[13] *Jane's Helicopter Markets and Systems. s.l. : Janes' Information Group*
[14] Rosero, J. A., Ortega, J. A., Aldabas, E. and Romeral, L. (2007), "Moving towards a more electric aircraft", *Aerospace and Electronic Systems Magazine, IEEE,* vol. 22, no. 3, pp. 3-9
[15] Dipartimento di Ingegneria Elettrica (2011). More Electric Aircraft, available in: http://www.die.unipd.it/~bianchi/didattica/corsi/Azionamenti_Elettrici_Aerospaziale/More_Electric_Aircraft.pdf (Accessed in February)
[16] Community Research and Development Information Service (2007). Final Report – MESEMA (Magnetoelastic Energy Systems For Even More Electric Aircraft), available in: http://cordis.europa.eu/projects/index.cfm?fuseaction=app.details&TXT=mesema&FRM=1&STP=10&SIC=SICAER&PGA=&CCY=&PCY=&SRC=&LNG=en&REF=72824 (Accessed in January)
[17] More Open Electrical Technologies (2009). Final public MOET Technical Report, available in: http://www.eurtd.com/moet/ (Accessed in February)
[18] Durkee, S. R. and Muetze, A. (2010), "Conceptual design of an electric helicopter powertrain", *Power Electronics, Machines and Drives (PEMD 2010), 5th IET International Conference on,* pp. 1.
[19] Morioka, N. and Oyori, H. (2012), “Improved Efficiency via the More electric Engine”, in 50th AIAA Aerospace Sciences Meeting including the New Horizons Forum and Aerospace Exposition, January 9-12, 2012, Nashville, Tenessee.
[20] Xia, X. (2011), *Dynamic Power Distribution Management for All Electric Aircraft* (MSc by Research thesis), Cranfield University, Cranfield University

[21] Stephen C. Jensen, Gavin D. Jenney, Bruce Raymond and David Dawson. (2000), ”Flight Test Experience With an electromechanical Actuator on the F-18 Systems Research Aircraft, presented at the 19th digital Avionics systems Conference, October 7-13, 2000, Philadelphia, Pennsylvania

[22] Tang, C. (2011), environmental Control system for All Electric Flying Crane, Cranfield University, Cranfield University.

[23] Vega, R. (2011), *Analysis of an Electric Environmental Control System to Reduce the Energy Consumption of Fixed-Wing Aircraft and Rotary-Wing Aircraft* (MSc by Research thesis), Cranfield University, Cranfield University.

[24] shinkafi, A. (2011), Electrical Ice Protection Model Specification, unpublished document.

[25] MD helicopters inc. 500 Series – BASIC HMI SECTION 19 ELECTRICAL SYSTEM

[26] MD helicopters inc (2011). HANDBOOK OF MAINTENANCE INSTRUCTIONS INSTRUMENTS-ELECTRICAL-AVIONICS, available in: http://download.mdhelicopters.com/Pubs/Archive%20files/500%20manuals/csp-hmi-3/csp-hmi-3_i0r13p.pdf (accessed in April)

[27] US Department of Defense (1988). MIL-E-7016F Electric Load and Power Source Capacity, Analysis of

[28] Civil Aviation Authority (2004). AIL/0194, aircraft electrical load and power source capacity analysis.

[29] startergenerator.com (2012). Aircraft parts corp. starter-generator technical manual available in: http://www.startergenerator.com/library/media/pdf/apc%20sg%20brochure.pdf (accessed in April)

[30] Tremblay, O., and Dessaint, L.-A., (2009) “Experimental Validation of a Battery Dynamic Model for EV Applications”, World Electric Vehicle Journal. Vol. 3 – ISSN 20325-6653, May 13-16, 2009, Stavanger, Norway

[31] Krause, Paul C. (1986). Analysis of Electric Machinery, 1st ed. McGraw-Hill, New York.

[32] Fitzgerald, A. E., Kingsley, C. and Kusko, A. (1971). Electric Machinery, 3rd ed. McGraw-Hill, New York.

[33] Hindmarsh, J. (1982). Worked Examples in electrical Machines and Drives, 1st ed. PERGAMON PRESS, Oxford.
[34] Chapman, S. J. (2005). ELECTRIC MACHINERY FUNDAMENTALS, 4th ed. McGraw-Hill, Boston.
[35] Wildi, T. (2002). ELECTRICAL MACHINES, DRIVES, AND POWER SYSTEMS, 5th ed. Prentice Hall, New Jersey.
[36] Cooper, M. (2013), *SIMULATING ACTUATOR ENERGY DEMANDS OF AN AIRCRAFT IN FLIGHT* (Ph.D. thesis), Cranfield University, Cranfield University
[37] Leishman, J. (2006), *Principles of Helicopter Aerodynamics,* 2nd ed, Cambridge
University Press, Cambridge.
[38] Padfield, G. D. (1996), *Helicopter Flight Dynamics: The Theory and Application*
of Flying Qualities and Simulation Modelling, 1st ed, Blackwell Science, Cambridge, UK.
[39] Jhonson, W. (1980), HELICOPTER THEORY, 1st ed, Princeton University Press, Guilford.
[40] Shapiro, J. (1955), PRINCIPLES OF HELICOPTER ENGINEERING, 1st ed, Loxley Brothers Limited, Letchworth.
[41] Cooke, A., K. (2012), Rotorcraft Performance, Stability and Control, Lecture notes, Cranfield University, Cranfield University.
[42] MarathonNorco Aerospace. M3-1700L Detailed Data Sheet available in: http://www.mptc.com/batAMH-17.html
[43] Bell helicopter (2009). BHT-206A/B-SERIES-MM-6 CHAPTER 62- MAIN ROTOR.
[44] Bell helicopter (2009). BHT-206A/B-SERIES-MM-8 CHAPTER 67- FLIGHT CONTROLS.
[45] EUROCOPTER (2005). BO 105 Training Manual General.

APPENDICES

Appendix A Electrical System Results

A.1 ELA chart

Table A-1 Electrical Load Analysis

EQUIPMENT	NO. OF UNITS OR SYS.	AMPS PER UNIT OR SYS.	OPER. TIME IN MIN	TOTAL AMPS	PRE-START		START TURBINE	
					AVERAGE AMPERES		AVERAGE AMPERES	
					5 SEC	2 MIN	5 SEC	2 MIN
FLIGHT CONTROLS								
ACTUATOR CYCLIC	1							
ACTUATOR COLLECTIVE	1							
ACTUATOR COLLECTIVE	1							
INSTRUMENTS								
ENG OIL PRES TEMP.	1	0.36	CON.	0.36	0.36	0.36	0.36	0.36
XMSN OIL PRES TEMP.	1	0.03	CON.	0.03	0.03	0.03	0.03	0.03
GAS PRODUCER RPM	1	0.03	CON.	0.03	0.03	0.03	0.03	0.03
TORQUE	1	0.36	CON.	0.36	0.36	0.36	0.36	0.36
TOT	1	0.36	CON.	0.36	0.36	0.36	0.36	0.36
AIRSPEED	1	0.03	CON.	0.03	0.03	0.03	0.03	0.03
FUEL QUANTITY	1	0.36	CON.	0.36	0.36	0.36	0.36	0.36
DC LOAD (LOADMETER) / FUEL PRESS	1							
POWER TURBINE RPM / ROTOR RPM	1	0.08	CON.	0.08	0.08	0.08	0.08	0.08
ENGINE OUT								
WARNING UNIT	1	0.05	CON.	0.05	0.05	0.05	0.05	0.05
ENGINE OUT HORN	1	0.02	INTR.	0.02				
INSTRUMENT PANEL & WARNING LIGHTS								
INSTRUMENT LAMPS	11	0.04	CON.	0.44	0.44	0.44	0.44	0.44
EDGE LIGHT PANELS	SYS.	0.10	CON.	0.1	0.10	0.10	0.10	0.10
WARNING LIGHTS								
ENG OUT	4	0.02	INTR.	0.10				
BATTERY HOT	4	0.02	INTR.	0.10				
BATTERY RLY	4	0.02	INTR.	0.10				
R/FUEL PUMP	4	0.02	INTR.	0.10				
L/FUEL PUMP	4	0.02	INTR.	0.10				
ROTOR LOW RPM	4	0.02	INTR.	0.10				
TRANS OIL PRESSURE	4	0.02	INTR.	0.10				
TRANS OIL TEMP	4	0.02	INTR.	0.10				
FUEL LOW	4	0.02	INTR.	0.10				
ENG CHIP	4	0.02	INTR.	0.10				
TRANS CHIP	4	0.02	INTR.	0.10				
FUEL FILTER	4	0.02	INTR.	0.10				
T/R CHIP	4	0.02	INTR.	0.10				
GEN FAIL	4	0.02	INTR.	0.10				
PRESS-TO-TEST WARNING LIGHTS	SYS.	1.34	INTR.	1.34				
ENGINE CONTROLS								
FADEC	1	5.00	INTR.	5.00	5.00	5.00	5.00	5.00
IGNITER	1	0.75	INTR.	0.75				
LIGHTING								
POSITION LIGHTS	4	0.75	CON.	3.00				
ANTI-COLLISION LIGHTS	SYS.	3.50	CON.	3.50				
LANDING LIGHTS	2	8.93	INTR.	17.86				
MAP LIGHT	1	0.50	INTR.	0.50				
ELECTRICAL POWER SYSTEM								
VOLTAGE REGULATOR	1	0.30	CON.	0.30	0.30	0.30		
BATTERY RELAY	1	0.60	CON.	0.60	0.60	0.60		
EXTERNAL RELAY	1	0.50	CON.	0.50	0.50	0.50		
STARTER RELAY	1	0.50	CON.	0.50	0.50	0.50		
LINE CONTROL RELAY	1	0.50	CON.	0.50	0.50	0.50		
BATTERY CHARGING	1		CON.					
AVIONICS								
TRANSCIEVER KY196	1	0.40	INTR.	6.90	6.90	6.90	6.90	6.90
		6.50	CON.					
ICS KMA 24K	1	0.44	CON.	0.44	0.44	0.44	0.44	0.44
fuel boost pump	2	5.67	CON.	11.33				
cabin heater bleed air	SYS.		INTR.	0.00				
pitot tube	1	6.50	CON.	6.50			6.50	6.50
OPTIONAL EQUIPMENT								
KT-76A transponder	1	1.80	CON.	1.80				
Garmin GNS 530W GPS/COMM/NAV	1	3.00	CON.	3.00				
KR-87 ADF	1	0.43	CON.	0.43				
KDM-706A WITH KDI 572 INDICATOR	1	8.93	CON.	8.93				
KR-21 marker beacon receiver	1	0.25	CON.	0.25				
Autopilot KAP 150H	SYS.	4.10	INTR.	4.10				
KRA-405B radio altimeter	1	0.85	CON.	0.85				
SKY 497 Skywatch System	1	2.50	CON.	2.50				
Vapor cycle air conditioner	SYS.	17.32	INTR.	17.32				
BASIC SHIP AMPERES				63.07	16.92	16.92	21.02	21.02
OPTIONAL SHIP AMPERES				39.18	0.00	0.00	0.00	0.00
total				102.25	16.92	16.92	21.02	21.02

Table A-1 Electrical Load Analysis cont.

EQUIPMENT	TAKEOFF AND CLIMB				HOVER				
	DAY AVERAGE AMPERES		NIGHT AVERAGE AMPERES		DAY AVERAGE AMPERES			NIGHT AVERAGE AMPERES	
	5 SEC	2 MIN	5 SEC	2 MIN	5 SEC	2 MIN	15 MIN	5 SEC	2 MIN
FLIGHT CONTROLS									
ACTUATOR CYCLIC									
ACTUATOR COLLECTIVE									
ACTUATOR COLLECTIVE									
INSTRUMENTS									
ENG OIL PRES TEMP.	0.36	0.36	0.36	0.36	0.36	0.36	0.36	0.36	0.36
XMSN OIL PRES TEMP.	0.03	0.03	0.03	0.03	0.03	0.03	0.03	0.03	0.03
GAS PRODUCER RPM	0.03	0.03	0.03	0.03	0.03	0.03	0.03	0.03	0.03
TORQUE	0.36	0.36	0.36	0.36	0.36	0.36	0.36	0.36	0.36
TOT	0.36	0.36	0.36	0.36	0.36	0.36	0.36	0.36	0.36
AIRSPEED	0.03	0.03	0.03	0.03	0.03	0.03	0.03	0.03	0.03
FUEL QUANTITY	0.36	0.36	0.36	0.36	0.36	0.36	0.36	0.36	0.36
DC LOAD (LOADMETER) / FUEL PRESS									
POWER TURBINE RPM / ROTOR RPM	0.08	0.08	0.08	0.08	0.08	0.08	0.08	0.08	0.08
ENGINE OUT									
WARNING UNIT	0.05	0.05	0.05	0.05	0.05	0.05	0.05	0.05	0.05
ENGINE OUT HORN									
INSTRUMENT PANEL & WARNING LIGHTS									
INSTRUMENT LAMPS			0.44	0.44				0.44	0.44
EDGE LIGHT PANELS			0.10	0.10				0.10	0.10
WARNING LIGHTS									
ENG OUT									
BATTERY HOT									
BATTERY RLY									
R/FUEL PUMP									
L/FUEL PUMP									
ROTOR LOW RPM									
TRANS OIL PRESSURE									
TRANS OIL TEMP									
FUEL LOW									
ENG CHIP									
TRANS CHIP									
FUEL FILTER									
T/R CHIP									
GEN FAIL									
PRESS-TO-TEST WARNING LIGHTS									
ENGINE CONTROLS									
FADEC	5.00	5.00	5.00	5.00	5.00	5.00	5.00	5.00	5.00
IGNITER									
LIGHTING									
POSITION LIGHTS			3.00	3.00				3.00	3.00
ANTI-COLLISION LIGHTS	3.50	3.50	3.50	3.50	3.50	3.50	3.50	3.50	3.50
LANDING LIGHTS									
MAP LIGHT									
ELECTRICAL POWER SYSTEM									
VOLTAGE REGULATOR	0.30	0.30	0.30	0.30	0.30	0.30	0.30	0.30	0.30
BATTERY RELAY	0.60	0.60	0.60	0.60	0.60	0.60	0.60	0.60	0.60
EXTERNAL RELAY	0.50	0.50	0.50	0.50	0.50	0.50	0.50	0.50	0.50
STARTER RELAY	0.50	0.50	0.50	0.50	0.50	0.50	0.50	0.50	0.50
LINE CONTROL RELAY	0.50	0.50	0.50	0.50	0.50	0.50	0.50	0.50	0.50
BATTERY CHARGING	25.50	25.50	25.50	25.50	22.10	22.10	22.10	22.10	22.10
AVIONICS									
TRANSCIEVER KY196	6.90	6.90	6.90	6.90	6.90	6.90	6.90	6.90	6.90
ICS KMA 24K	0.44	0.44	0.44	0.44	0.44	0.44	0.44	0.44	0.44
fuel boost pump	11.33	11.33	11.33	11.33	11.33	11.33	11.33	11.33	11.33
cabin heater bleed air					0.00	0.00	0.00	0.00	0.00
pitot tube	6.50	6.50	6.50	6.50	6.50	6.50	6.50	6.50	6.50
OPTIONAL EQUIPMENT									
KT-76A transponder	1.80	1.80	1.80	1.80	1.80	1.80	1.80	1.80	1.80
Garmin GNS 530W GPS/COMM/NAV	3.00	3.00	3.00	3.00	3.00	3.00	3.00	3.00	3.00
KR-87 ADF	0.43	0.43	0.43	0.43	0.43	0.43	0.43	0.43	0.43
KDM-706A WITH KDI 572 INDICATOR	8.93	8.93	8.93	8.93	8.93	8.93	8.93	8.93	8.93
KR-21 marker beacon receiver	0.25	0.25	0.25	0.25	0.25	0.25	0.25	0.25	0.25
Autopilot KAP 150H	4.10	4.10	4.10	4.10					
KRA-405B radio altimeter	0.85	0.85	0.85	0.85	0.85	0.85	0.85	0.85	0.85
SKY 497 Skywatch System	2.50	2.50	2.50	2.50	2.50	2.50	2.50	2.50	2.50
Vapor cycle air conditioner									
BASIC SHIP AMPERES	63.21	63.21	66.75	66.75	59.81	59.81	59.81	63.35	63.35
OPTIONAL SHIP AMPERES	21.86	21.86	21.86	21.86	17.76	17.76	17.76	17.76	17.76
total	85.07	85.07	88.61	88.61	77.57	77.57	77.57	81.11	81.11

Table A-1 Electrical Load Analysis cont.

EQUIPMENT	CRUISE						LANDING					
	DAY AVERAGE AMPERES			NIGHT AVERAGE AMPERES			DAY AVERAGE AMPERES			NIGHT AVERAGE AMPERES		
	5 SEC	2 MIN	15 MIN	5 SEC	2 MIN	15 MIN	5 SEC	2 MIN	15 MIN	5 SEC	2 MIN	15 MIN
FLIGHT CONTROLS												
ACTUATOR CYCLIC												
ACTUATOR COLLECTIVE												
ACTUATOR COLLECTIVE												
INSTRUMENTS												
ENG OIL PRES TEMP.	0.36	0.36	0.36	0.36	0.36	0.36	0.36	0.36	0.36	0.36	0.36	0.36
XMSN OIL PRES TEMP.	0.03	0.03	0.03	0.03	0.03	0.03	0.03	0.03	0.03	0.03	0.03	0.03
GAS PRODUCER RPM	0.03	0.03	0.03	0.03	0.03	0.03	0.03	0.03	0.03	0.03	0.03	0.03
TORQUE	0.36	0.36	0.36	0.36	0.36	0.36	0.36	0.36	0.36	0.36	0.36	0.36
TOT	0.36	0.36	0.36	0.36	0.36	0.36	0.36	0.36	0.36	0.36	0.36	0.36
AIRSPEED	0.03	0.03	0.03	0.03	0.03	0.03	0.03	0.03	0.03	0.03	0.03	0.03
FUEL QUANTITY	0.36	0.36	0.36	0.36	0.36	0.36	0.36	0.36	0.36	0.36	0.36	0.36
DC LOAD (LOADMETER) / FUEL PRESS												
POWER TURBINE RPM / ROTOR RPM	0.08	0.08	0.08	0.08	0.08	0.08	0.08	0.08	0.08	0.08	0.08	0.08
ENGINE OUT												
WARNING UNIT	0.05	0.05	0.05	0.05	0.05	0.05	0.05	0.05	0.05	0.05	0.05	0.05
ENGINE OUT HORN												
INSTRUMENT PANEL & WARNING LIGHTS												
INSTRUMENT LAMPS				0.44	0.44	0.44				0.44	0.44	0.44
EDGE LIGHT PANELS				0.10	0.10	0.10				0.10	0.10	0.10
WARNING LIGHTS												
ENG OUT												
BATTERY HOT												
BATTERY RLY												
R/FUEL PUMP												
L/FUEL PUMP												
ROTOR LOW RPM												
TRANS OIL PRESSURE												
TRANS OIL TEMP												
FUEL LOW												
ENG CHIP												
TRANS CHIP												
FUEL FILTER												
T/R CHIP												
GEN FAIL												
PRESS-TO-TEST WARNING LIGHTS												
ENGINE CONTROLS												
FADEC	5.00	5.00	5.00	5.00	5.00	5.00	5.00	5.00	5.00	5.00	5.00	5.00
IGNITER												
LIGHTING												
POSITION LIGHTS				3.00	3.00	3.00				3.00	3.00	3.00
ANTI-COLLISION LIGHTS	3.50	3.50	3.50	3.50	3.50	3.50	3.50	3.50	3.50	3.50	3.50	3.50
LANDING LIGHTS										17.86	17.86	17.86
MAP LIGHT												
ELECTRICAL POWER SYSTEM												
VOLTAGE REGULATOR	0.30	0.30	0.30	0.30	0.30	0.30	0.30	0.30	0.30	0.30	0.30	0.30
BATTERY RELAY	0.60	0.60	0.60	0.60	0.60	0.60	0.60	0.60	0.60	0.60	0.60	0.60
EXTERNAL RELAY	0.50	0.50	0.50	0.50	0.50	0.50	0.50	0.50	0.50	0.50	0.50	0.50
STARTER RELAY	0.50	0.50	0.50	0.50	0.50	0.50	0.50	0.50	0.50	0.50	0.50	0.50
LINE CONTROL RELAY	0.50	0.50	0.50	0.50	0.50	0.50	0.50	0.50	0.50	0.50	0.50	0.50
BATTERY CHARGING	10.20	10.20	10.20	10.20	10.20	10.20						
AVIONICS												
TRANSCIEVER KY196	6.90	6.90	6.90	6.90	6.90	6.90	6.90	6.90	6.90	6.90	6.90	6.90
ICS KMA 24K	0.44	0.44	0.44	0.44	0.44	0.44	0.44	0.44	0.44	0.44	0.44	0.44
fuel boost pump	11.33	11.33	11.33	11.33	11.33	11.33	11.33	11.33	11.33	11.33	11.33	11.33
cabin heater bleed air	0.00	0.00	0.00	0.00	0.00	0.00						
pitot tube	6.50	6.50	6.50	6.50	6.50	6.50	6.50	6.50	6.50	6.50	6.50	6.50
OPTIONAL EQUIPMENT												
KT-76A transponder	1.80	1.80	1.80	1.80	1.80	1.80	1.80	1.80	1.80	1.80	1.80	1.80
Garmin GNS 530W GPS/COMM/NAV	3.00	3.00	3.00	3.00	3.00	3.00	3.00	3.00	3.00	3.00	3.00	3.00
KR-87 ADF	0.43	0.43	0.43	0.43	0.43	0.43	0.43	0.43	0.43	0.43	0.43	0.43
KDM-706A WITH KDI 572 INDICATOR	8.93	8.93	8.93	8.93	8.93	8.93	8.93	8.93	8.93	8.93	8.93	8.93
KR-21 marker beacon receiver	0.25	0.25	0.25	0.25	0.25	0.25	0.25	0.25	0.25	0.25	0.25	0.25
Autopilot KAP 150H	4.10	4.10	4.10	4.10	4.10	4.10	4.10	4.10	4.10	4.10	4.10	4.10
KRA-405B radio altimeter	0.85	0.85	0.85	0.85	0.85	0.85	0.85	0.85	0.85	0.85	0.85	0.85
SKY 497 Skywatch System	2.50	2.50	2.50	2.50	2.50	2.50	2.50	2.50	2.50	2.50	2.50	2.50
Vapor cycle air conditioner	17.32	17.32	17.32	17.32	17.32	17.32						
BASIC SHIP AMPERES	47.91	47.91	47.91	51.45	51.45	51.45	37.71	37.71	37.71	59.11	59.11	59.11
OPTIONAL SHIP AMPERES	39.18	39.18	39.18	39.18	39.18	39.18	21.86	21.86	21.86	21.86	21.86	21.86
total	87.09	87.09	87.09	90.63	90.63	90.63	59.57	59.57	59.57	80.97	80.97	80.97

Table A-1 Electrical Load Analysis cont.

EQUIPMENT	EMERGENCY - GENERATOR OUT					
	DAY AVERAGE AMPERES			NIGHT AVERAGE AMPERES		
	5 SEC	2 MIN	15 MIN	5 SEC	2 MIN	15 MIN
FLIGHT CONTROLS						
ACTUATOR CYCLIC						
ACTUATOR COLLECTIVE						
ACTUATOR COLLECTIVE						
INSTRUMENTS						
ENG OIL PRES TEMP.	0.36	0.36	0.36	0.36	0.36	0.36
XMSN OIL PRES TEMP.	0.03	0.03	0.03	0.03	0.03	0.03
GAS PRODUCER RPM	0.03	0.03	0.03	0.03	0.03	0.03
TORQUE	0.36	0.36	0.36	0.36	0.36	0.36
TOT	0.36	0.36	0.36	0.36	0.36	0.36
AIRSPEED	0.03	0.03	0.03	0.03	0.03	0.03
FUEL QUANTITY	0.36	0.36	0.36	0.36	0.36	0.36
DC LOAD (LOADMETER) / FUEL PRESS						
POWER TURBINE RPM / ROTOR RPM	0.08	0.08	0.08	0.08	0.08	0.08
ENGINE OUT						
WARNING UNIT	0.05	0.05	0.05	0.05	0.05	0.05
ENGINE OUT HORN						
INSTRUMENT PANEL & WARNING LIGHTS						
INSTRUMENT LAMPS				0.44	0.44	0.44
EDGE LIGHT PANELS				0.10	0.10	0.10
WARNING LIGHTS						
ENG OUT						
BATTERY HOT						
BATTERY RLY						
R/FUEL PUMP						
L/FUEL PUMP						
ROTOR LOW RPM						
TRANS OIL PRESSURE						
TRANS OIL TEMP						
FUEL LOW						
ENG CHIP						
TRANS CHIP						
FUEL FILTER						
T/R CHIP						
GEN FAIL						
PRESS-TO-TEST WARNING LIGHTS						
ENGINE CONTROLS						
FADEC	5.00	5.00	5.00	5.00	5.00	5.00
IGNITER						
LIGHTING						
POSITION LIGHTS				3.00	3.00	3.00
ANTI-COLLISION LIGHTS	3.50	3.50	3.50	3.50	3.50	3.50
LANDING LIGHTS						
MAP LIGHT						
ELECTRICAL POWER SYSTEM						
VOLTAGE REGULATOR	0.30	0.30	0.30	0.30	0.30	0.30
BATTERY RELAY	0.60	0.60	0.60	0.60	0.60	0.60
EXTERNAL RELAY	0.50	0.50	0.50	0.50	0.50	0.50
STARTER RELAY	0.50	0.50	0.50	0.50	0.50	0.50
LINE CONTROL RELAY	0.50	0.50	0.50	0.50	0.50	0.50
BATTERY CHARGING						
AVIONICS						
TRANSCIEVER KY196	6.90	6.90	6.90	6.90	6.90	6.90
ICS KMA 24K	0.44	0.44	0.44	0.44	0.44	0.44
fuel boost pump	5.67	5.67	5.67	5.67	5.67	5.67
cabin heater bleed air						
pitot tube	6.50	6.50	6.50	6.50	6.50	6.50
OPTIONAL EQUIPMENT						
KT-76A transponder	1.80	1.80	1.80	1.80	1.80	1.80
Garmin GNS 530W GPS/COMM/NAV	3.00	3.00	3.00	3.00	3.00	3.00
KR-87 ADF	0.43	0.43	0.43	0.43	0.43	0.43
KDM-706A WITH KDI 572 INDICATOR	8.93	8.93	8.93	8.93	8.93	8.93
KR-21 marker beacon receiver	0.25	0.25	0.25	0.25	0.25	0.25
Autopilot KAP 150H						
KRA-405B radio altimeter	0.85	0.85	0.85	0.85	0.85	0.85
SKY 497 Skywatch System	2.50	2.50	2.50	2.50	2.50	2.50
Vapor cycle air conditioner						
BASIC SHIP AMPERES	32.05	32.05	32.05	35.59	35.59	35.59
OPTIONAL SHIP AMPERES	17.76	17.76	17.76	17.76	17.76	17.76
total	49.80	49.80	49.80	53.34	53.34	53.34

A.2 Electrical System Model Generator Block

- Climb

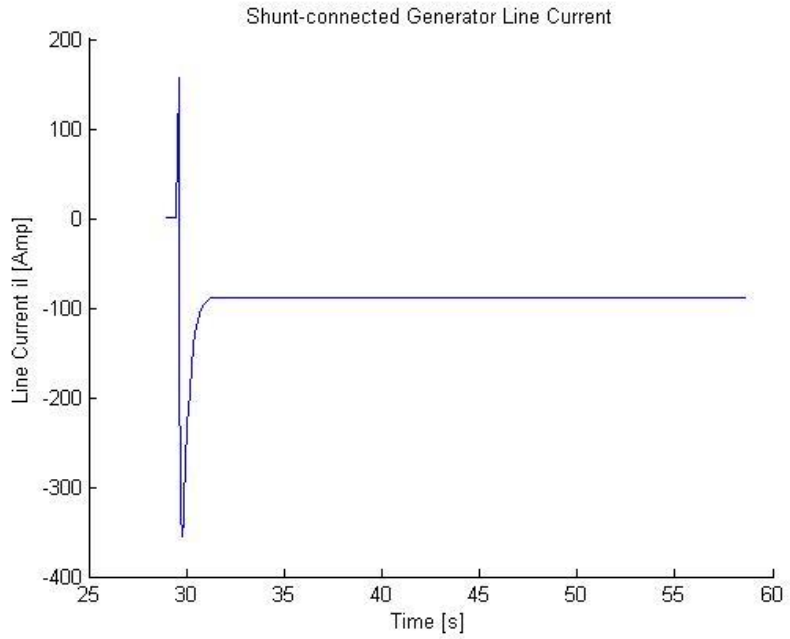

Figure A-1 Generator Line Current

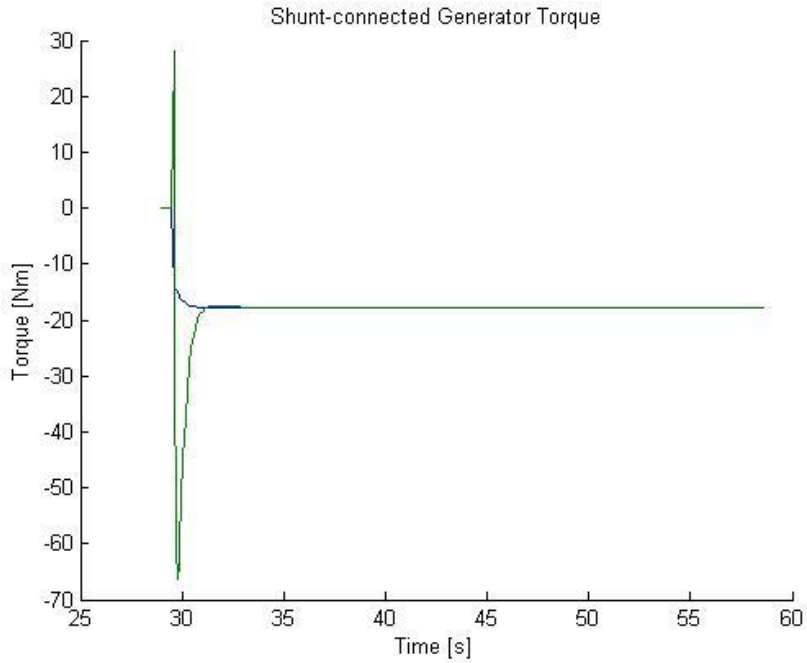

Figure A-2 Generator Torque (Climb)

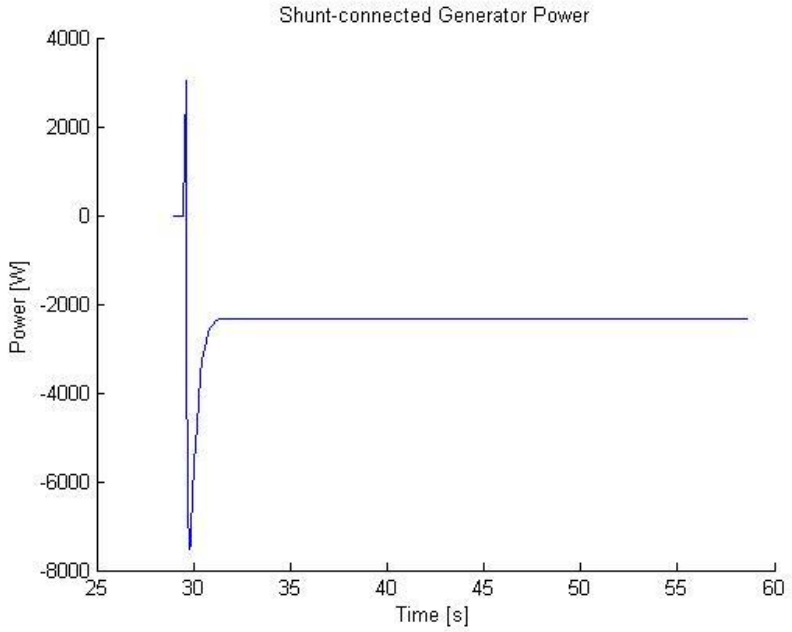

Figure A-3 Generator Power (Climb)

- Hover

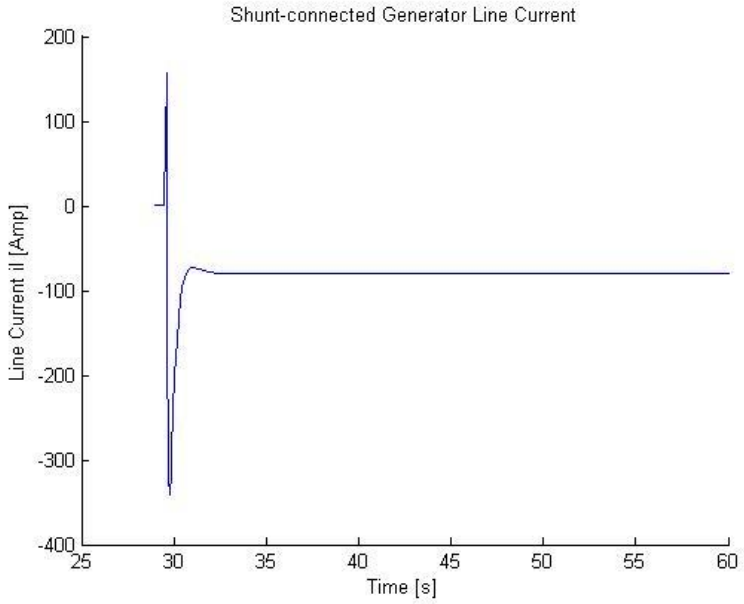

Figure A-4 Generator Line Current (Hover)

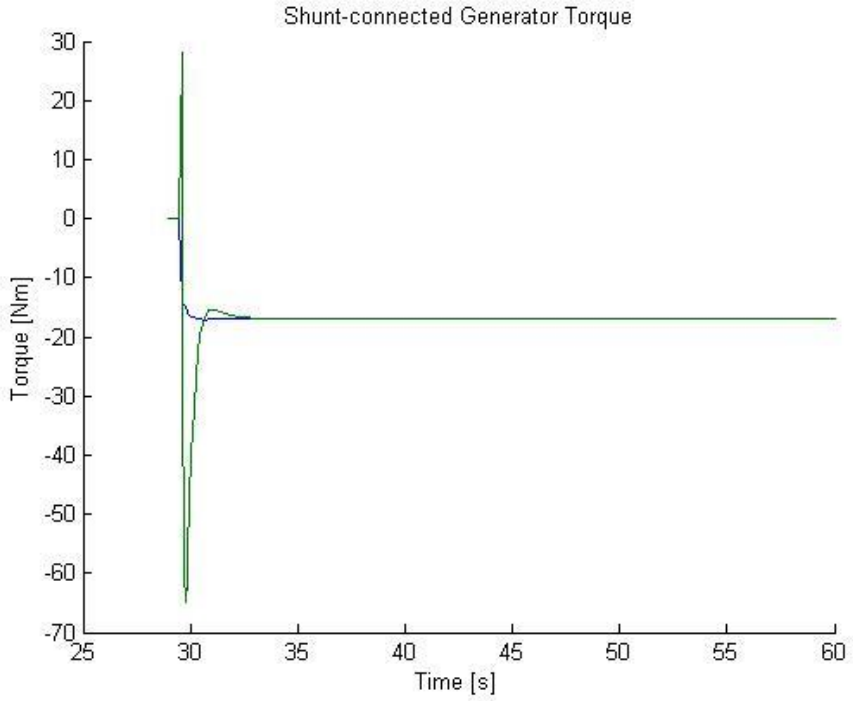

Figure A-5 Generator Torque (Hover)

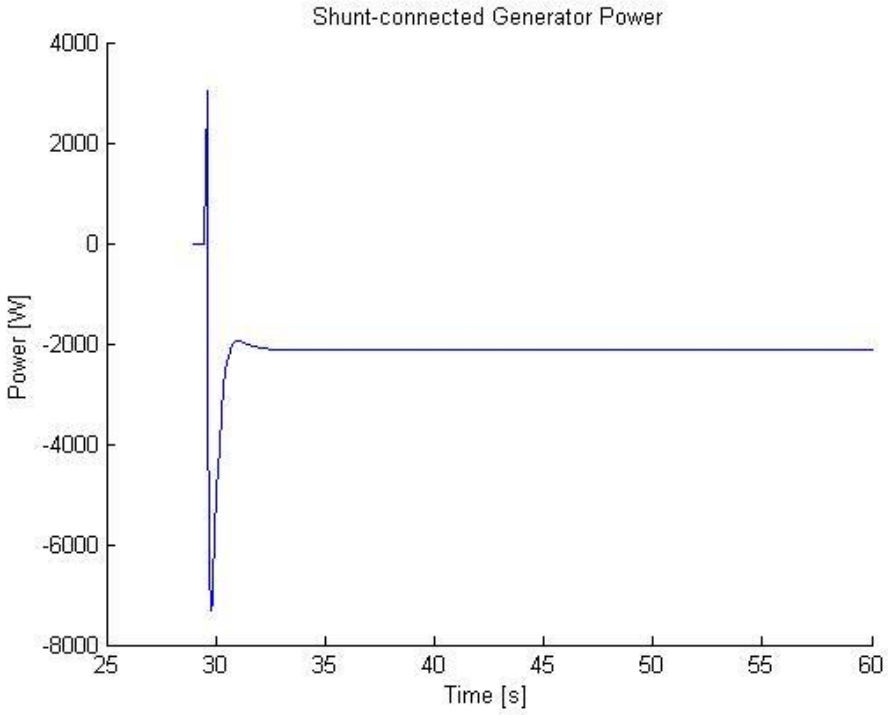

Figure A-6 Generator Power (Hover)

- Cruise

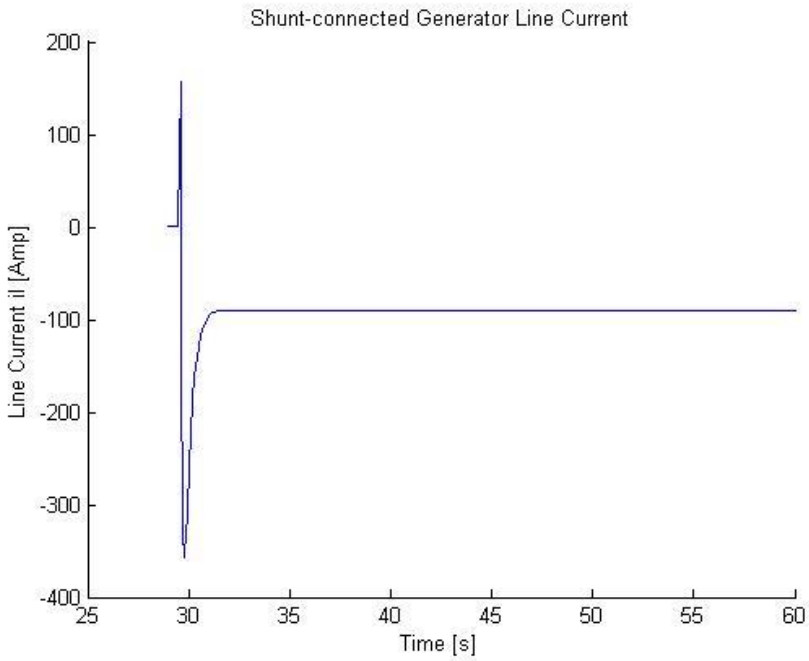

Figure A-7 Generator Line Current (Cruise)

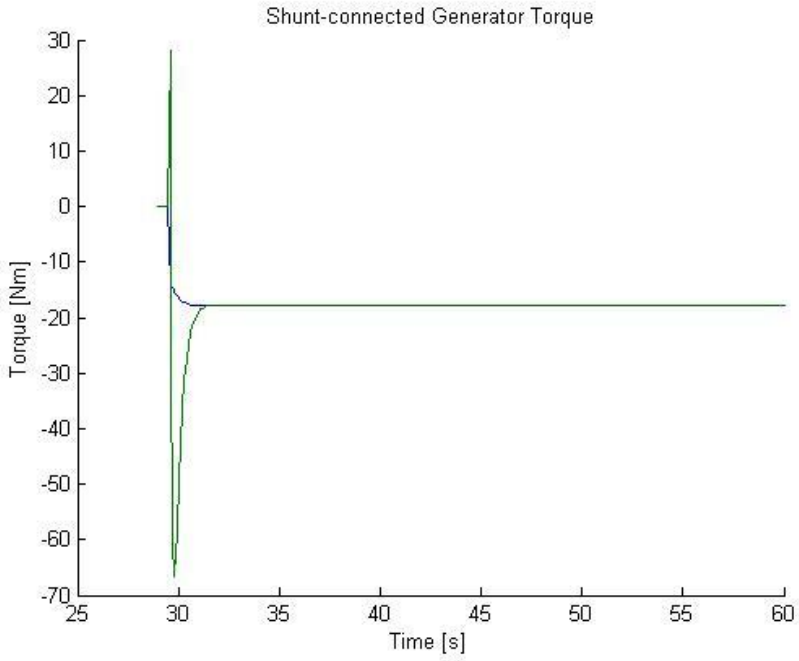

Figure A-8 Generator Torque (Cruise)

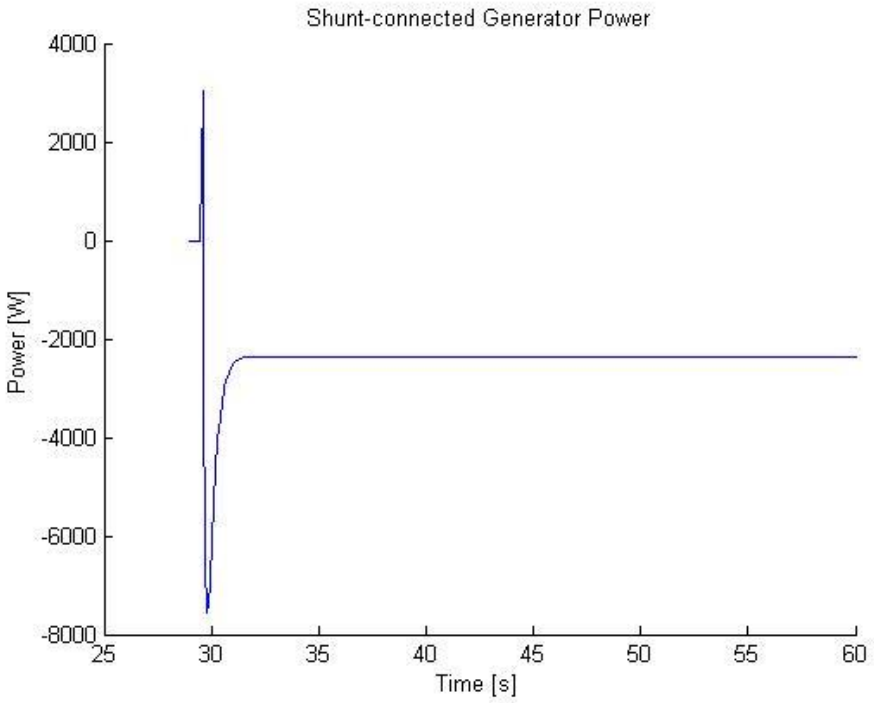

Figure A-9 Generator Power (Cruise)

- Landing

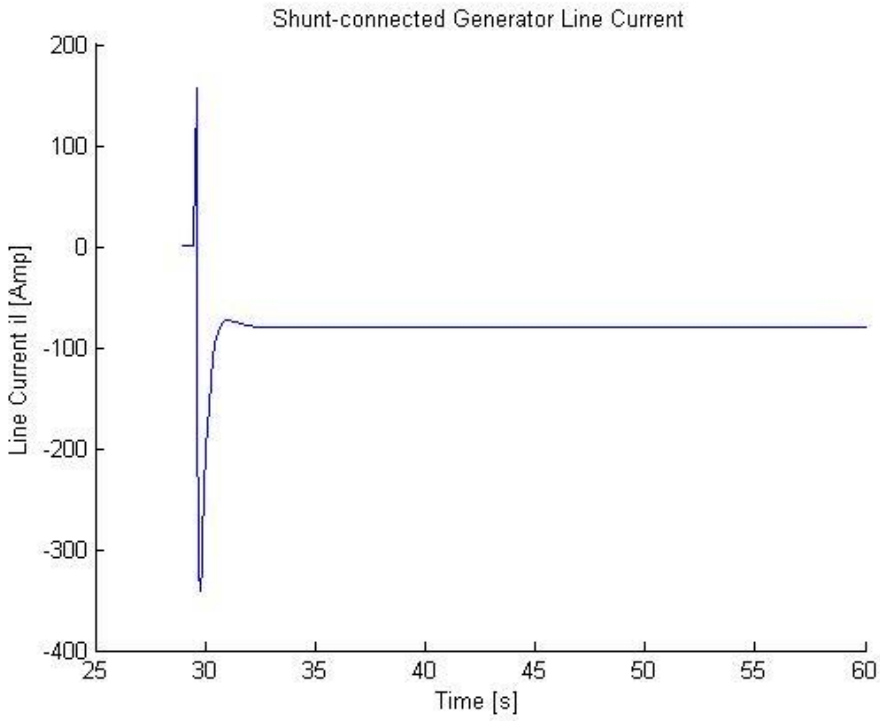

Figure A-10 Generator Line Current (Landing)

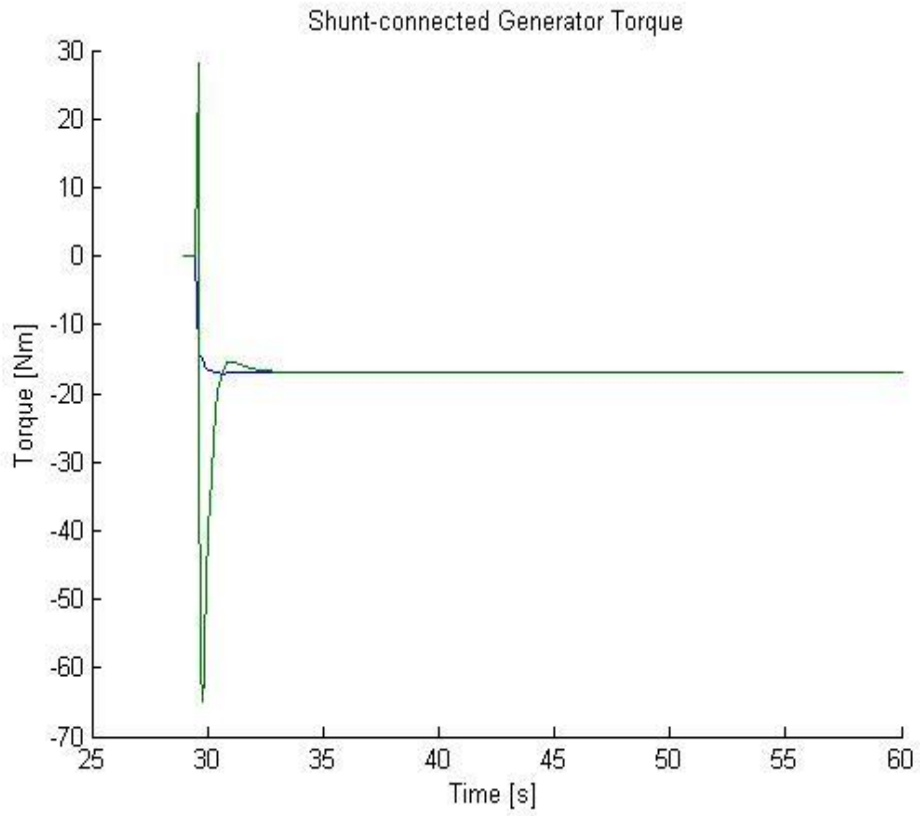

Figure A-11 Generator Torque (Landing)

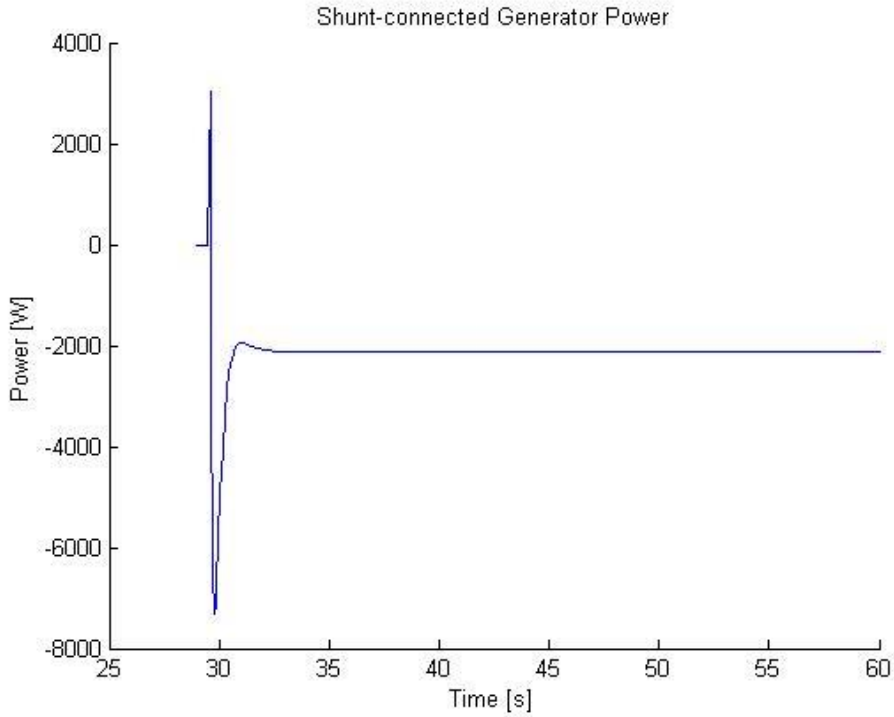

Figure A-12 Generator Power (Landing)

Appendix B Actuation System Results

B.1 Aerodynamic Analysis

B.1.1 Aerodynamic analysis in hover (BET approximations)

1. Untwisted Blade

Results on the left hand side are for the Bell 206L-4. Results on the right hand side correspond to the MBB Bo105.

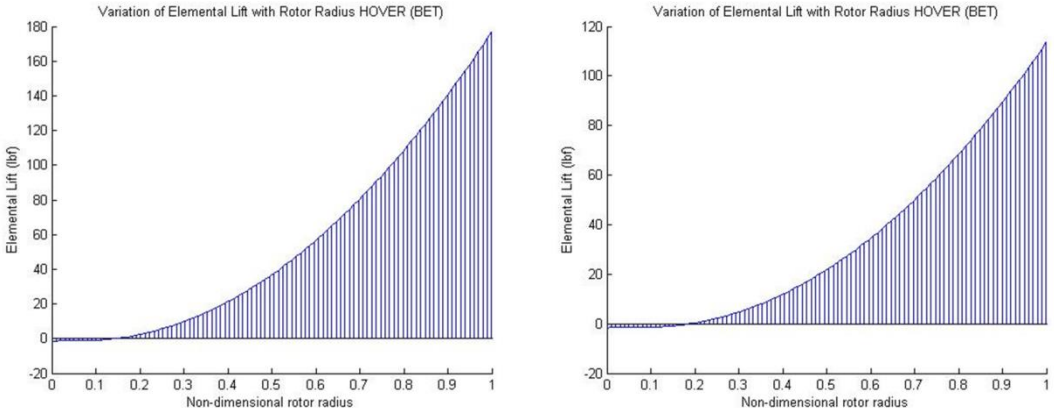

Figure B-1 Incremental lift

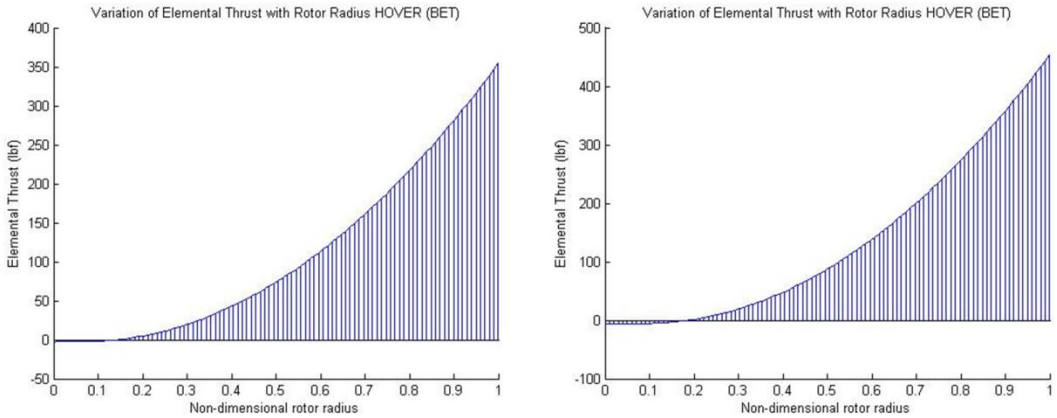

Figure B-2 Incremental thrust

2. Linearly twisted blade

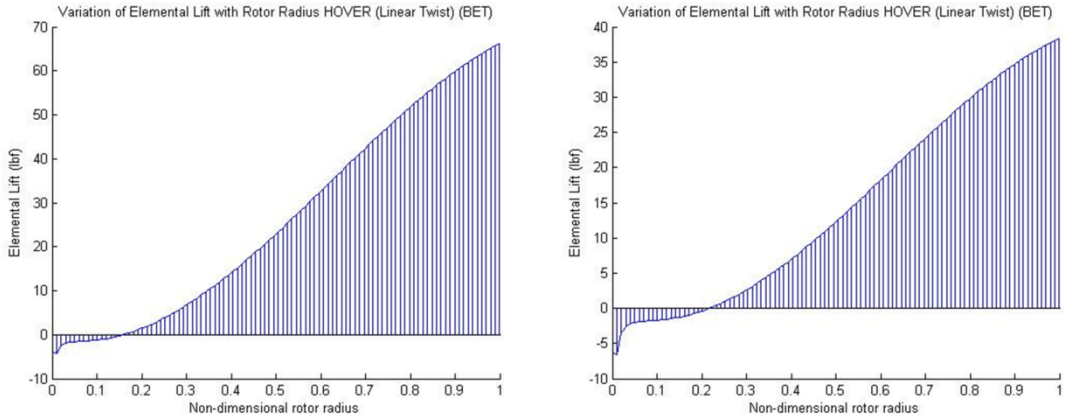

Figure B-3 Incremental lift

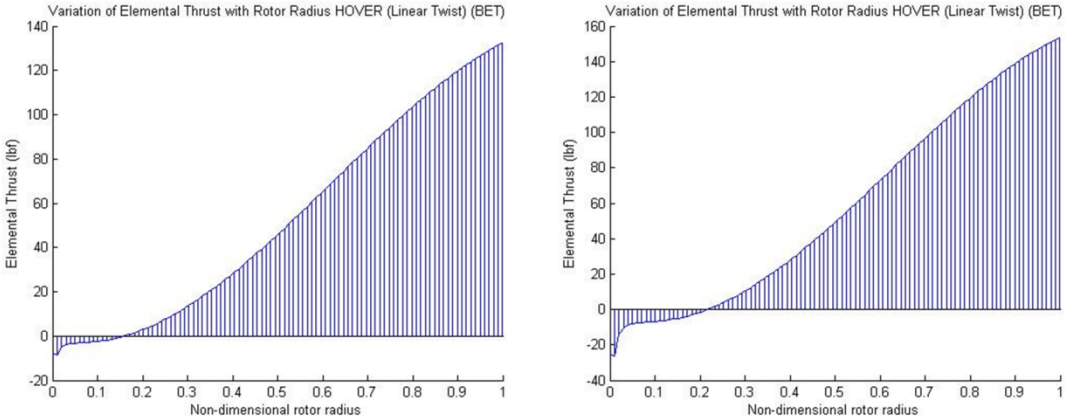

Figure B-4 Incremental Thrust

1. Tip loss factor and Blade root

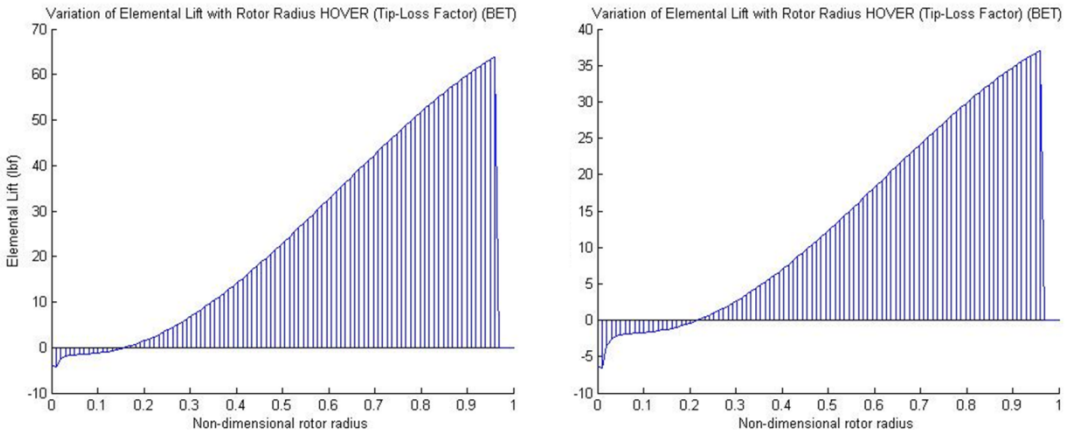

Figure B-5 Incremental lift

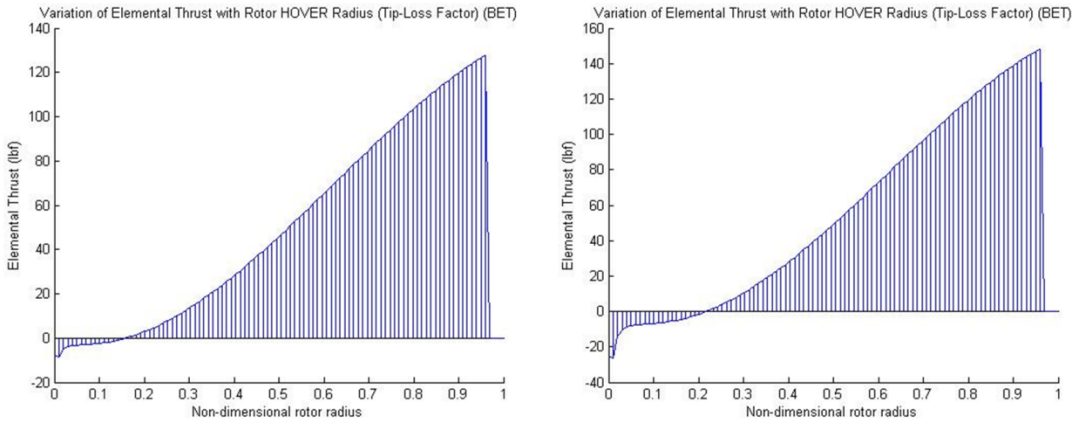

Figure B-6 Incremental Thrust

B.1.2 Swashplate Analysis

Bell 206L-4

Table B-1 Bell 206L-4 swashplate analysis in Hover

1. HOVER												
Collective pitch theta 0.2617 [rad]												
Axis	azimuth 0 [rad]			azimuth 1.5708 [rad]			azimuth 3.1416 [rad]			azimuth 4.7124 [rad]		
	rp [ft]	Cpl [ft]	rh [ft]	rp [ft]	Cpl [ft]	rh [ft]	rp [ft]	Cpl [ft]	rh [ft]	rp [ft]	Cpl [ft]	rh [ft]
E1	0.550	-0.019	0.531	0.000	0.010	-0.290	-0.550	0.019	-0.531	0.000	-0.010	0.290
E2	0.000	-0.010	0.290	0.550	-0.019	0.531	0.000	0.010	-0.290	-0.550	0.019	-0.531
E3	0.000	2.209	0.162	0.000	2.209	0.162	0.000	2.209	0.162	0.000	2.209	0.162
magnitude	0.550	2.209	0.627	0.550	2.209	0.627	0.550	2.209	0.627	0.550	2.209	0.627
Cyclic pitch 0 [rad]												
Axis	azimuth 0 [rad]			azimuth 1.5708 [rad]			azimuth 3.1416 [rad]			azimuth 4.7124 [rad]		
	rp [ft]	Cpl [ft]	rh [ft]	rp [ft]	Cpl [ft]	rh [ft]	rp [ft]	Cpl [ft]	rh [ft]	rp [ft]	Cpl [ft]	rh [ft]
E1	0.550	0.000	0.550	0.000	0.000	-0.300	-0.550	0.000	-0.550	0.000	0.000	0.300
E2	0.000	0.000	0.300	0.550	0.000	0.550	0.000	0.000	-0.300	-0.550	0.000	-0.550
E3	0.000	2.209	0.000	0.000	2.209	0.000	0.000	2.209	0.000	0.000	2.209	0.000
magnitude	0.550	2.209	0.627	0.550	2.209	0.627	0.550	2.209	0.627	0.550	2.209	0.627
swashplate angle [rad]	0.000			0.000			0.000			0.000		
PITCH LINK FORCE RESULT												
Pitch link force [lbf]	2269.000			2269.000			2269.000			2269.000		

Table B-2 Bell 206L-4 swashplate analysis in Climb

CLIMB												
Collective pitch 0.2741 [rad]												
Axis	azimuth 0 [rad]			azimuth 1.5708 [rad]			azimuth 3.1416 [rad]			azimuth 4.7124 [rad]		
	rp [ft]	Cpl [ft]	rh [ft]	rp [ft]	Cpl [ft]	rh [ft]	rp [ft]	Cpl [ft]	rh [ft]	rp [ft]	Cpl [ft]	rh [ft]
E1	0.550	-0.021	0.530	0.000	0.011	-0.289	-0.550	0.021	-0.530	0.000	-0.011	0.289
E2	0.000	-0.011	0.289	0.550	-0.021	0.530	0.000	0.011	-0.289	-0.550	0.021	-0.530
E3	0.000	2.209	0.170	0.000	2.209	0.170	0.000	2.209	0.170	0.000	2.209	0.170
magnitude	0.550	2.209	0.627	0.550	2.209	0.627	0.550	2.209	0.627	0.550	2.209	0.627
Cyclic pitch 0 [rad]												
Axis	azimuth 0 [rad]			azimuth 1.5708 [rad]			azimuth 3.1416 [rad]			azimuth 4.7124 [rad]		
	rp [ft]	Cpl [ft]	rh [ft]	rp [ft]	Cpl [ft]	rh [ft]	rp [ft]	Cpl [ft]	rh [ft]	rp [ft]	Cpl [ft]	rh [ft]
E1	0.550	0.000	0.550	0.000	0.000	-0.300	-0.550	0.000	-0.550	0.000	0.000	0.300
E2	0.000	0.000	0.300	0.550	0.000	0.550	0.000	0.000	-0.300	-0.550	0.000	-0.550
E3	0.000	2.209	0.000	0.000	2.209	0.000	0.000	2.209	0.000	0.000	2.209	0.000
magnitude	0.550	2.209	0.627	0.550	2.209	0.627	0.550	2.209	0.627	0.550	2.209	0.627
swashplate angle [rad]	0.000			0.000			0.000			0.000		
PITCH LINK FORCE RESULT												
Pitch link force [lbf]	2385.300			2385.300			2385.300			2385.300		

Table B-3 Bell 206L-4 Swashplate analysis in forward flight

FORWARD FLIGHT												
Collective pitch 0.2204 [rad]												
Axis	azimuth 0 [rad]			azimuth 1.5708 [rad]			azimuth 3.1416 [rad]			azimuth 4.7124 [rad]		
	rp [ft]	Cpl [ft]	rh [ft]	rp [ft]	Cpl [ft]	rh [ft]	rp [ft]	Cpl [ft]	rh [ft]	rp [ft]	Cpl [ft]	rh [ft]
E1	0.550	-0.013	0.537	0.000	0.007	-0.293	-0.550	0.013	-0.537	0.000	-0.007	0.293
E2	0.000	-0.007	0.293	0.550	-0.013	0.537	0.000	0.007	-0.293	-0.550	0.013	-0.537
E3	0.000	2.209	0.137	0.000	2.209	0.137	0.000	2.209	0.137	0.000	2.209	0.137
magnitude	0.550	2.209	0.627	0.550	2.209	0.627	0.550	2.209	0.627	0.550	2.209	0.627
Cyclic pitch 0 [rad]												
Axis	azimuth 0 [rad]			azimuth 1.5708 [rad]			azimuth 3.1416 [rad]			azimuth 4.7124 [rad]		
	rp [ft]	Cpl [ft]	rh [ft]	rp [ft]	Cpl [ft]	rh [ft]	rp [ft]	Cpl [ft]	rh [ft]	rp [ft]	Cpl [ft]	rh [ft]
E1	0.550	0.000	0.550	0.000	0.000	-0.300	-0.550	0.000	-0.550	0.000	0.000	0.300
E2	0.000	0.000	0.300	0.550	0.000	0.550	0.000	0.000	-0.300	-0.550	0.000	-0.550
E3	0.000	2.209	0.000	0.000	2.209	0.000	0.000	2.209	0.000	0.000	2.209	0.000
magnitude	0.550	2.209	0.627	0.550	2.209	0.627	0.550	2.209	0.627	0.550	2.209	0.627
swashplate angle [rad]	0.000			0.000			0.000			0.000		
PITCH LINK FORCE RESULT												
Pitch link force [lbf]	1859.500			1859.500			1859.500			1859.500		

MBB Bo105

Table B-4 Mbb Bo105 swashplate analysis in Hover

HOVER												
Collective pitch theta 15 [rad]												
Axis	azimuth 0 [rad]			azimuth 1.5708 [rad]			azimuth 3.1416 [rad]			azimuth 4.7124 [rad]		
	rp [ft]	Cpl [ft]	rh [ft]	rp [ft]	Cpl [ft]	rh [ft]	rp [ft]	Cpl [ft]	rh [ft]	rp [ft]	Cpl [ft]	rh [ft]
E1	-0.096	-0.061	-0.157	0.096	0.047	-0.209	0.096	0.061	0.157	-0.096	-0.047	0.209
E2	-0.096	-0.047	0.209	-0.096	-0.061	-0.157	0.096	0.047	-0.209	0.096	0.061	0.157
E3	0.000	0.271	0.070	0.000	0.271	0.070	0.000	0.271	0.070	0.000	0.271	0.070
magnitude	0.135	0.282	0.271	0.135	0.282	0.271	0.135	0.282	0.271	0.135	0.282	0.271
Cyclic pitch 0 [rad]												
Axis	azimuth 0 [rad]			azimuth 1.5708 [rad]			azimuth 3.1416 [rad]			azimuth 4.7124 [rad]		
	rp [ft]	Cpl [ft]	rh [ft]	rp [ft]	Cpl [ft]	rh [ft]	rp [ft]	Cpl [ft]	rh [ft]	rp [ft]	Cpl [ft]	rh [ft]
E1	-0.096	-0.067	-0.163	0.096	0.040	-0.217	0.096	0.067	0.163	-0.096	-0.040	0.217
E2	-0.096	-0.040	0.217	-0.096	-0.067	-0.163	0.096	0.040	-0.217	0.096	0.067	0.163
E3	0.000	0.271	0.000	0.000	0.271	0.000	0.000	0.271	0.000	0.000	0.271	0.000
magnitude	0.135	0.282	0.271	0.135	0.282	0.271	0.135	0.282	0.271	0.135	0.282	0.271
swashplate angle [rad]	0.000			0.000			0.000			0.000		
PITCH LINK FORCE RESULT												
Pitch link force [lbf]	2133.400			2133.400			2133.400			2133.400		

Table B-5 Mbb Bo105 swashplate analysis in Climb

CLIMB												
Collective pitch 15.7103 [rad]												
Axis	azimuth 0 [rad]			azimuth 1.5708 [rad]			azimuth 3.1416 [rad]			azimuth 4.7124 [rad]		
	rp [ft]	Cpl [ft]	rh [ft]	rp [ft]	Cpl [ft]	rh [ft]	rp [ft]	Cpl [ft]	rh [ft]	rp [ft]	Cpl [ft]	rh [ft]
E1	-0.096	-0.061	-0.156	0.096	0.048	-0.208	0.096	0.061	0.156	-0.096	-0.048	0.208
E2	-0.096	-0.048	0.208	-0.096	-0.061	-0.156	0.096	0.048	-0.208	0.096	0.061	0.156
E3	0.000	0.271	0.075	0.000	0.271	0.075	0.000	0.271	0.075	0.000	0.271	0.075
magnitude	0.135	0.282	0.271	0.135	0.282	0.271	0.135	0.282	0.271	0.135	0.282	0.271
Cyclic pitch 0 [rad]												
Axis	azimuth 0 [rad]			azimuth 1.5708 [rad]			azimuth 3.1416 [rad]			azimuth 4.7124 [rad]		
	rp [ft]	Cpl [ft]	rh [ft]	rp [ft]	Cpl [ft]	rh [ft]	rp [ft]	Cpl [ft]	rh [ft]	rp [ft]	Cpl [ft]	rh [ft]
E1	-0.096	-0.067	-0.163	0.096	0.040	-0.217	0.096	0.067	0.163	-0.096	-0.040	0.217
E2	-0.096	-0.040	0.217	-0.096	-0.067	-0.163	0.096	0.040	-0.217	0.096	0.067	0.163
E3	0.000	0.271	0.000	0.000	0.271	0.000	0.000	0.271	0.000	0.000	0.271	0.000
magnitude	0.135	0.282	0.271	0.135	0.282	0.271	0.135	0.282	0.271	0.135	0.282	0.271
swashplate angle [rad]	0.000			0.000			0.000			0.000		
PITCH LINK FORCE RESULT												
Pitch link force [lbf]	2345.400			2345.400			2345.400			2345.400		

Table B-6 Mbb Bo105 Swashplate analysis in forward flight

FORWARD FLIGHT												
Collective pitch 12.63 [rad]												
Axis	azimuth 0 [rad]			azimuth 1.5708 [rad]			azimuth 3.1416 [rad]			azimuth 4.7124 [rad]		
	rp [ft]	Cpl [ft]	rh [ft]	rp [ft]	Cpl [ft]	rh [ft]	rp [ft]	Cpl [ft]	rh [ft]	rp [ft]	Cpl [ft]	rh [ft]
E1	-0.096	-0.063	-0.159	-0.096	0.045	-0.212	-0.096	0.063	0.159	-0.096	-0.045	0.212
E2	-0.096	-0.045	0.212	-0.096	-0.063	-0.159	-0.096	0.045	-0.212	-0.096	0.063	0.159
E3	0.000	0.271	0.057	0.000	0.271	0.057	0.000	0.271	0.057	0.000	0.271	0.057
magnitude	0.550	2.209	0.627	0.550	2.209	0.627	0.550	2.209	0.627	0.550	2.209	0.627
Cyclic pitch 0 [rad]												
Axis	azimuth 0 [rad]			azimuth 1.5708 [rad]			azimuth 3.1416 [rad]			azimuth 4.7124 [rad]		
	rp [ft]	Cpl [ft]	rh [ft]	rp [ft]	Cpl [ft]	rh [ft]	rp [ft]	Cpl [ft]	rh [ft]	rp [ft]	Cpl [ft]	rh [ft]
E1	-0.096	-0.067	-0.163	0.096	0.040	-0.217	0.096	0.067	0.163	-0.096	-0.040	0.217
E2	-0.096	-0.040	0.217	-0.096	-0.067	-0.163	0.096	0.040	-0.217	0.096	0.067	0.163
E3	0.000	0.271	0.000	0.000	0.271	0.000	0.000	0.271	0.000	0.000	0.271	0.000
magnitude	0.135	0.282	0.271	0.135	0.282	0.271	0.135	0.282	0.271	0.135	0.282	0.271
swashplate angle [rad]	0.000			0.000			0.000			0.000		
PITCH LINK FORCE RESULT												
Pitch link force [lbf]	1580.400			1580.400			1580.400			1580.400		

B.2 Actuator forces algorithm

```
clear all
clc
%Helicopter Parameters
w=4338.7;% helicopter weight [lb]
R=18.50;% main rotor radius [ft]
nb=2;% number of rotor blades
rav=41.26;% rotor angular velocity [rad/s]

%Atmospheric Parameters
Altitude=5;% [m] altitude 5 for hover 100 for climb 200 forward flight
Isadev=0;% Isa deviation

%Blade Parameters
cla=6.113;% blade lift curve slope [1/rad]
cd0=0.017;% zero lift drag coefficient
Cm0=0.03;% zero lift moment coefficient
Ib=170.893;% mass moment of inertia of the blade about flap hinge
slug-ft^2
Ifb=0.9780;% blade angular moment of inertia about the feathering axis
[lb-ft^2]
```

```
kr=715.91;% ft-lb/rad
c=1;% blade chord [ft]
thetatw=-0.14;% blade twist rate [rad]
TL=1-(c/(2*R)); % Tip-Loss factor 0.95<=TL<=0.98
BR=0.25;%Blade root non-dimensional position
d=0*c;% distance from flexural axis to aerodynamic center [ft]

%Flight Parameters
FLIGHTSEGMENT=4;
t0=15;% for hover 15 for climb 15.7103 forward flight 12.63 or 11.75
t1c=0;
t1s=0;
a=1.45*pi/180;%0.0698;% rotor disc angle of attack [rad]
AirSpeed=36.01;% flight velocity [m/s]
Vc=0;% climb velocity (used in hover=0) [ft/s];
vcc=4.6101;% climb velocity [m/s] max 6.7 [m/s]
Vcc=vcc*3.28;% climb velocity [ft/s]

rho=((((1-((0.0065/288.16)*Altitude))^5.2561)/((288.16-...
    (Altitude*0.0065)+Isadev)/288.16))*1.225)*0.001940;% slug/ft3
r=(0:0.010101:1);% nondimensional radial position 100 parts
y=r*R;% dimensional radial position
f=2*pi/4;% for blade position
psi=(0:f:2*pi); % blade Azimuth Angles
dr=R*0.010101;
A=pi*R^2;% rotor area [ft^2]
s=(nb*c)/(pi*R); % Rotor solidity
Ut=rav*y;% In-Plane velocity component[ft/s]
bts=Ut(1,100);% Blade Tip Speed =rav*R [ft/s]
IFb=(1:100);
IFb(1:100)=Ifb/100;% blade section angular moment of inertia about the
feathering axis [slug-ft^2]
%SWASHPLATE KINEMATICS%%%%%%%%%%%%%%
%%%%%%%%INITIAL COORDINATES%%%%%%%%%%%%
rp1=[0 0.55 0]';% swashplate center-swashplate pitch link connection
distance [ft]
Rp1=norm(rp1);
rp2=[-0.55 0 0]';
Rp2=norm(rp2);
rp3=[0 -0.55 0]';
Rp3=norm(rp3);
rp4=[0.55 0 0]';
Rp4=norm(rp4);
cpl1=[0 0 2.209]';% pitch link distance [ft]
Cpl1=norm(cpl1);
cpl2=[0 0 2.209]';
Cpl2=norm(cpl2);
cpl3=[0 0 2.209]';
Cpl3=norm(cpl3);
cpl4=[0 0 2.209]';
Cpl4=norm(cpl4);
rh1=[-0.3 0.55 0]';% blade pitch horn center to pitch link horn
connection [ft]
Rh1=norm(rh1);
rh2=[-0.55 -0.3 0]';
Rh2=norm(rh2);
rh3=[0.3 -0.55 0]';
Rh3=norm(rh3);
```

```
rh4=[0.55 0.3 0]';
Rh4=norm(rh4);
rb1=rp1+cpl1-rh1;
Rb1=norm(rb1);
rb2=rp2+cpl2-rh2;
Rb2=norm(rb2);
rb3=rp3+cpl3-rh3;
Rb3=norm(rb3);
rb4=rp4+cpl4-rh4;
Rb4=norm(rb4);
k1=rb1+rh1-rp1;
K1=norm(k1);
k2=rb2+rh2-rp2;
K2=norm(k2);
k3=rb3+rh3-rp3;
K3=norm(k3);
k4=rb4+rh4-rp4;
K4=norm(k4);
%%%%%AFTER APPLYING THE ROTATION MATRIX rh11=rh21=rh31=rh41
alphar1=asin(rh1(1)/Rh1);
alphar2=asin(rh2(1)/Rh2);
alphar3=asin(rh3(1)/Rh3);
alphar4=asin(rh4(1)/Rh4);
betar1=-alphar1;
betar2=pi+alphar2;
betar3=pi+alphar3;
betar4=-alphar4;
Rz1=[cos(betar1) sin(betar1) 0;-sin(betar1) cos(betar1) 0;0 0 1];
Rz2=[cos(betar2) sin(betar2) 0;-sin(betar2) cos(betar2) 0;0 0 1];
Rz3=[cos(betar3) sin(betar3) 0;-sin(betar3) cos(betar3) 0;0 0 1];
Rz4=[cos(betar4) sin(betar4) 0;-sin(betar4) cos(betar4) 0;0 0 1];
rh11=Rz1*rh1;
rh21=Rz2*rh2;
rh31=Rz3*rh3;
rh41=Rz4*rh4;
Rz11=[cos(-betar1) sin(-betar1) 0;-sin(-betar1) cos(-betar1) 0;0 0 1];
Rz21=[cos(-betar2) sin(-betar2) 0;-sin(-betar2) cos(-betar2) 0;0 0 1];
Rz31=[cos(-betar3) sin(-betar3) 0;-sin(-betar3) cos(-betar3) 0;0 0 1];
Rz41=[cos(-betar4) sin(-betar4) 0;-sin(-betar4) cos(-betar4) 0;0 0 1];
%%cyclic input
psi1=psi(1,2);%azimuthual position of blade 1
psi2=psi(1,3);%azimuthual position of blade 2
psi3=psi(1,4);%azimuthual position of blade 3
psi4=psi(1,5);

Ra1=[sin(psi2) -cos(psi2) 0;cos(psi2) sin(psi2) 0;0 0 1];
Ra2=[sin(psi3) -cos(psi3) 0;cos(psi3) sin(psi3) 0;0 0 1];
Ra3=[sin(psi4) -cos(psi4) 0;cos(psi4) sin(psi4) 0;0 0 1];
Ra4=[sin(psi1) -cos(psi1) 0;cos(psi1) sin(psi1) 0;0 0 1];

rb1a=Ra1*rb1;
rb2a=Ra2*rb2;
rb3a=Ra3*rb3;
rb4a=Ra4*rb4;

theta0=t0*pi/180;% blade collective pitch [rad]
theta1c=t1c*pi/180;% blade lateral cyclic pitch [rad]
theta1s=t1s*pi/180;% blade longitudinal cyclic pitch [rad]
```

```
Ln=(rho*cla*c*R^4)/Ib; % Lock number
dM=0.5.*rho.*(Ut.^2).*c^2.*Cm0.*dr; % Blade section moment
M=sum(dM);
Th=w;% thrust in hover [lb]
Cthm=Th/(rho*A*(rav*R)^2);% thrust coefficient in hover
syms x
if FLIGHTSEGMENT==4
    %%%%%%%%%%%%%%%%%%%%%%%%%%MOMENTUM THEORY%%%%%%%%%%%%%%%%%%%
    %%%%%HOVER%%%%%%%%%
    theta0h=theta0;
    thetatwh=theta0h+(r*thetatw);
    theta1ch=theta1c;
    theta1sh=theta1s;
    t1ch=theta1ch*cos(psi);
    t1sh=theta1sh*sin(psi);
    vihm=-(Vc/2)+sqrt((Vc/2)^2+(Th/(2*rho*A)));% induced velocity
[ft/s]
    vhm=vihm;% induced velocity in hover [ft/s]
    Phm=(Th*vihm)/550;% power [hp]
    Phm=(Th*vihm)/737;% power [Kw]
    DL=Th/A;% disk loading
    PL=Th/Phm;% power loading
    lambdahm=sqrt(Cthm/2);%vihm/(rav*R)% induced inflow ratio
    Cphm=Cthm*lambdahm;%~Cthm^(3/2)/sqrt(2)~
(Th*vihm)/(rho*A*(rav*R)^3)

    dCthmj=4*lambdahm^2.*r*0.01;
    Cthmj=sum(dCthmj);

    %%%%%%%%%%%%%%%%%%%%%%%%%%BLADE ELEMENT THEORY%%%%%%%%%%%%%%%%
    %%%%%%%%%%%%%%%HOVER%%%%%%%%%%%%%%%%%%
    %%%%%no simplification assumptions
    Uph=(Vc+vihm);% Out-of-Plane velocity component [ft/s]
    Uh_1=sqrt(Uph.^2+Ut.^2);%total velocity [ft/s]
    phi_1= (atan2(Uph,Ut));% relative inflow angle [rad]
    alpha_1= theta0h-phi_1;% effective angle of attack [rad]
    dLhbet_1=(1./2).*rho.*Uh_1.^2.*c.*cla.*alpha_1*dr;% elemental lift
[lbf]
    Lhbet_1=sum(dLhbet_1);% lift [lbf]
    dCthbet_1=(nb*dLhbet_1)/(rho*A*(rav*R)^2);
    Cthbet_1=sum(dCthbet_1);
    Thbet_1=Cthbet_1*(rho*A*(rav*R)^2);
    lambdahbet_1=Uph/(rav*R);

    dCthbet_11=(1/2)*s*cla.*alpha_1.*r.^2.*0.010101;
    Cthbet_11=sum(dCthbet_11);
    Thbet_11=Cthbet_11*(rho*A*(rav*R)^2);
    lambdahbet_11=phi_1.*r;
            %%%%%simplification
            Uh_2=Ut;
            phi_2=Uph./Ut;
            phi_2(1,1)=phi_2(1,2);
            alpha_2=theta0h-phi_2;
            dLhbet_2=(1./2).*rho.*Uh_2.^2.*c.*cla.*alpha_2*dr;
            Lhbet_2=sum(dLhbet_2);% lift [lbf]
            dCthbet_2=(nb*dLhbet_2)/(rho*A*(rav*R)^2);
```

```
            Cthbet_2=sum(dCthbet_2);
            Thbet_2=Cthbet_2*(rho*A*(rav*R)^2);
            lambdahbet_2=phi_2.*r;
        %%%%%%integrating constant theta0
        Inhbet_1=int((theta0h*x^2-lambdahbet_1*x),x,0,1);
        Cthbet_int1=(1/2)*s*cla*double(Inhbet_1);
        Thbet_int1=Cthbet_int1*(rho*A*(rav*R)^2);

        %%%%integral solved
        Cth_21=(1/2)*s*cla*((theta0h/3)-(lambdahbet_1/2));
        Thbet_21=Cth_21*(rho*A*(rav*R)^2);

    %%%%%%%%%linearly twisted blade, uniform inflow
    alpha_3=thetatwh-phi_2;
    dLhbet_3=(1./2).*rho.*Uh_1.^2.*c.*cla.*alpha_3*dr;% elemental lift
[lbf]
    Lhbet_3=sum(dLhbet_3);% lift [lbf]
    dCthbet_3=(nb*dLhbet_3)/(rho*A*(rav*R)^2);
    Cthbet_3=sum(dCthbet_3);
    Thbet_3=Cthbet_3*(rho*A*(rav*R)^2);

    %%%%%%%integrating
    Inhbet_2=int(((theta0h+(x*thetatw))*x^2-lambdahbet_1*x),x,0,1);
    Cthbet_int2=(1/2)*s*cla*double(Inhbet_2);
    Thbet_int2=Cthbet_int2*(rho*A*(rav*R)^2);

    Cthbet_31=(1/2)*s*cla*((theta0h/3)+(thetatw/4)-(lambdahbet_1/2));
    Thbet_31=Cthbet_31*(rho*A*(rav*R)^2);

    Inhbet_3=int(((thetatwh(1,75)+((x-0.75)*thetatw))*x^2-
lambdahbet_1*x),x,0,1);
    Cthbet_int3=(1/2)*s*cla*double(Inhbet_3);
    Thbet_int3=Cthbet_int3*(rho*A*(rav*R)^2);

    Cthbet_32=(1/2)*s*cla*((thetatwh(1,75)/3)-(lambdahbet_1/2));
    Thbet_32=Cthbet_32*(rho*A*(rav*R)^2);

    %%%%%%%%%tip loss factor, linearly twisted blade, uniform inflow
    dLhbet_4=dLhbet_3;
    dLhbet_4(1,((round(TL*100)/100)*100):end)=0;
    Lhbet_4=sum(dLhbet_4);% lift [lbf]
    dCthbet_4=(nb*dLhbet_4)/(rho*A*(rav*R)^2);
    Cthbet_4=sum(dCthbet_4);
    Thbet_4=Cthbet_4*(rho*A*(rav*R)^2);

    %%%%%%%integrating
    Inhbet_4=int(((theta0h+(x*thetatw))*x^2-lambdahbet_1*x),x,0,TL);
    Cthbet_int4=(1/2)*s*cla*double(Inhbet_4);
    Thbet_int4=Cthbet_int4*(rho*A*(rav*R)^2);
            %%%%%%%%%%from jhonson pg60
    Cthbet_41=(1/2)*s*cla*((theta0h*(TL^3/3))+(thetatw*(TL^4/4))-
(lambdahbet_1*(TL^2/2)));
    Thbet_41=Cthbet_41*(rho*A*(rav*R)^2);

    %%%%%%%%root cutout
    dLhbet_5=dLhbet_4;
    dLhbet_5(1,1:25)=0;
```

```
    Lhbet_5=sum(dLhbet_5);% lift [lbf]
    dCthbet_5=(nb*dLhbet_5)/(rho*A*(rav*R)^2);
    Cthbet_5=sum(dCthbet_5);
    Thbet_5=Cthbet_5*(rho*A*(rav*R)^2);

    %%%%%%%integrating
    Inhbet_5=int(((theta0h+(x*thetatw))*x^2-lambdahbet_1*x),x,BR,TL);
    Cthbet_int5=(1/2)*s*cla*double(Inhbet_5);
    Thbet_int5=Cthbet_int5*(rho*A*(rav*R)^2);


    dDh=(1./2).*rho.*Ut.^2.*c.*cd0*dr;% elemental drag [lbf]
    Dh=sum(dDh);% drag [lbf]
    dCthj=(s*cla/(2*(rav^2)*(R^3)))*((theta0h.*Ut.^2)-(Ut.*Uph))*dr;
    Cthj=sum(dCthj);
    dCthj1=s*cla/2*((theta0h.*r.^2)-(Uph/bts).*r)*0.0101;
    Cthj1=sum(dCthj1);

%     %%%%%%%%linearly twisted blade
    lambdaihj=(s*cla/16)*((sqrt(1+((64/(3*s*cla))*thetatwh(1,75)))-
1));
%     %vihj=lambdaihj*rav*R;

    Cth1j=(s*cla/2)*((thetatwh(1,75)/3)-((Uph/bts)/2));
 error=100-((Thrusthoverbet1/Thbet1)*100);% error in %

thrusthoverbet1=(1/2)*rho*nb*c*cla*rav^2*R^3*((1/3)*((theta0h)+((3/4)*
thetatw))-(lambda/2));
    error1=100-((thrusthoverbet1/Thbet1)*100);% error in %
    dPh1=((dLh1.*phi)+(dDh)).*Ut;
    Ph1=nb*(sum(dPh1))/550;
    PH1=((Thbet1*(Uph))+((1/8)*rho*nb*c*R^4*rav^3*cd0))/550;
    %%%%%%%%BLADE ROOT AND TIP LOSS FACTOR%%%%%%%%%%%%%
    error2=100-((Thrusthoverbet2/Thbet2)*100);% error in %
    error3=100-((thrusthoverbet2/Thbet2)*100);% error in %
    diPh2=(dLh2.*(vihm./Ut)).*Ut;
    diPh2(1,1)=0;
    iPh2=nb*sum(diPh2)/550;
    duPh2=(dLh2.*(Vc./Ut)).*Ut;
    duPh2(1,1)=0;
    uPh2=nb*sum(duPh2)/550;
    dpPh2=(dDh.*Ut);
    pPh2=nb*sum(dpPh2)/550;
    dPh2=((dLh2.*phi)+(dDh)).*Ut;
    Ph2=nb*(sum(dPh2))/550;%[hp]
    PH2=((Thbet2*(Uph))+((1/8)*rho*nb*c*R^4*rav^3*cd0))/550;
    %%%%%%%%%%BLADE ELEMENT MOMENTUM THEORY
    %%%%%%%%HOVER%%%%%%%%%%%%%%
    vihbemt_vt=-
(cla*s/16)+sqrt((cla*s/16)^2+((cla*s/8)*((y/R).*thetatwh)));
    vihbemt_vt(1,((round(TL*100)/100)*100):end)=0;
    vihbemt_vt(1,1:25,1)=0;
    vihbemt=vihbemt_vt.*bts;
    Uphbemt=(Vc+vihbemt);
    Vhbemt=sqrt(Uphbemt.^2+Ut.^2);
    phihbemt= atan2(Uphbemt,Ut);
    phihbemt(1,1)=0;
    alphahbemt= thetatwh-phihbemt;
```

```
    dLhbemt=(1./2).*rho.*Vhbemt.^2.*c.*cla.*alphahbemt*dr;
    dLhbemt(1,((round(TL*100)/100)*100):end)=0;
    dLhbemt(1,1:25,1)=0;
    Lhbemt=sum(dLhbemt);
    dCthbemt=(nb*dLhbemt)/(rho*A*bts^2);
    Cthbemt_1=sum(dCthbemt);
    Thbemt_1=Cthbemt_1*(rho*A*bts^2);


    %%%%%%%integrating
    Inhbemt_1=int((theta0h*x^2)+(((thetatw/R)*x^3))-
(((Vc+vihbemt(1,75))/rav)*x),x,y(1,25),y(1,97));
    Thbemt_int1=(1/2)*rho*cla*nb*c*rav^2*double(Inhbemt_1);
    Cthbemt_int1=Thbemt_int1/(rho*A*bts^2);
    %%%%integral solved

Thbemt_11=(1/2)*rho*nb*c*cla*rav^2*R^3*((1/3)*((theta0h)+((3/4)*thetat
w))-(vihbemt_vt(1,75)/2));
    Cthbemt_11=Thbemt_11/(rho*A*bts^2);
    error4=100-((Thrusthoverbemt/Thbemt)*100);


    error5=100-((thrusthoverbemt/Thbemt)*100);
    %%%%%%%%%%Cyclic inputs%%%%%%%%%%
    for i=1:100
        for j=1:5
            thetah(i,j)=(thetatwh(i))+(t1ch(j))+(t1sh(j));
        end
    end
    alphahcbemt1= thetah(:,2)'-phihbemt;%[rad] effective angle of
attack blade1
    alphahcbemt2= thetah(:,3)'-phihbemt;%[rad] effective angle of
attack blade2
    alphahcbemt3= thetah(:,4)'-phihbemt;%[rad] effective angle of
attack blade3
    alphahcbemt4= thetah(:,5)'-phihbemt;%[rad] effective angle of
attack blade4
    dLhcbemt1=(1./2).*rho.*Ut.^2.*c.*cla.*alphahcbemt1*dr;%[lbf]
elemental lift blade1
    dLhcbemt2=(1./2).*rho.*Ut.^2.*c.*cla.*alphahcbemt2*dr;%[lbf]
elemental lift blade2
    dLhcbemt3=(1./2).*rho.*Ut.^2.*c.*cla.*alphahcbemt3*dr;%[lbf]
elemental lift blade3
    dLhcbemt4=(1./2).*rho.*Ut.^2.*c.*cla.*alphahcbemt4*dr;%[lbf]
elemental lift blade4
    dLhcbemt1(1,((round(TL*100)/100)*100):end)=0;
    dLhcbemt2(1,((round(TL*100)/100)*100):end)=0;
    dLhcbemt3(1,((round(TL*100)/100)*100):end)=0;
    dLhcbemt4(1,((round(TL*100)/100)*100):end)=0;
    dLhcbemt1(1,1:25,1)=0;
    dLhcbemt2(1,1:25,1)=0;
    dLhcbemt3(1,1:25,1)=0;
    dLhcbemt4(1,1:25,1)=0;
    Lh1cbemt=sum(dLhcbemt1);%[lbf]
    Lh2cbemt=sum(dLhcbemt2);%[lbf]
    Lh3cbemt=sum(dLhcbemt3);%[lbf]
    Lh4cbemt=sum(dLhcbemt4);%[lbf]
    if nb==4
```

```
dCthcbemt=(dLhcbemt1+dLhcbemt2+dLhcbemt3+dLhcbemt4)/(rho*A*bts^2);
    elseif nb==2
        dCthcbemt=(dLhcbemt1+dLhcbemt3)/(rho*A*bts^2);
    end

    Cthcbemt=sum(dCthcbemt);
    Thbemtc=Cthcbemt*(rho*A*bts^2);
    %%%%SWASHPLATE KINEMATICS%%%%%%%%%%
    %%%%COLLECTIVE INPUT%%%%%%%%%%
    rh22=[0 Rh2*cos(theta0h) Rh2*sin(theta0h)]';
    rh12=rh22;
    rh32=rh22;
    rh42=rh22;
    rhcol1=Rz11*rh12;
    Rhcol1=norm(rhcol1);
    rhcol2=Rz21*rh22;
    Rhcol2=norm(rhcol2);
    rhcol3=Rz31*rh32;
    Rhcol3=norm(rhcol3);
    rhcol4=Rz41*rh42;
    Rhcol4=norm(rhcol4);
    %%%TO VALIDATE RESULTS, Rhcol1,2,3,4=Rh1,2,3,4 (equal magnitudes)
    kcol1=rb1+rhcol1-rp1;
    kcol2=rb2+rhcol2-rp2;
    kcol3=rb3+rhcol3-rp3;
    kcol4=rb4+rhcol4-rp4;
    zcol1=kcol1(3)-sqrt(Cpl1^2-(kcol1(1))^2-(kcol1(2))^2);
    Zcol1=[0 0 zcol1]';
    zcol2=kcol2(3)-sqrt(Cpl2^2-(kcol2(1))^2-(kcol2(2))^2);
    Zcol2=[0 0 zcol2]';
    zcol3=kcol3(3)-sqrt(Cpl3^2-(kcol3(1))^2-(kcol3(2))^2);
    Zcol3=[0 0 zcol3]';
    zcol4=kcol4(3)-sqrt(Cpl4^2-(kcol4(1))^2-(kcol4(2))^2);
    Zcol4=[0 0 zcol4]';
    Cpl1_2=kcol1(1)^2+kcol1(2)^2+(kcol1(3)-zcol1)^2;
    Cpl2_2=kcol2(1)^2+kcol2(2)^2+(kcol2(3)-zcol2)^2;
    Cpl3_2=kcol3(1)^2+kcol3(2)^2+(kcol3(3)-zcol3)^2;
    Cpl4_2=kcol4(1)^2+kcol4(2)^2+(kcol4(3)-zcol4)^2;
    cplcol1=[kcol1(1,1) kcol1(2,1) (kcol1(3,1)-zcol1)]';
    cplcol2=[kcol2(1,1) kcol2(2,1) (kcol2(3,1)-zcol2)]';
    cplcol3=[kcol3(1,1) kcol3(2,1) (kcol3(3,1)-zcol3)]';
    cplcol4=[kcol4(1,1) kcol4(2,1) (kcol4(3,1)-zcol4)]';
    %%%%CYCLIC INPUT%%%%%%%%%%
    theta1c1s1h=t1ch(1,2)+t1sh(1,2);
    theta1c1s2h=t1ch(1,3)+t1sh(1,3);
    theta1c1s3h=t1ch(1,4)+t1sh(1,4);
    theta1c1s4h=t1ch(1,5)+t1sh(1,5);
    rhcyc1=[0 Rh1*cos(theta1c1s1h) Rh1*sin(theta1c1s1h)]';
    rhcyc2=[0 Rh2*cos(theta1c1s2h) Rh2*sin(theta1c1s2h)]';
    rhcyc3=[0 Rh3*cos(theta1c1s3h) Rh3*sin(theta1c1s3h)]';
    rhcyc4=[0 Rh4*cos(theta1c1s4h) Rh4*sin(theta1c1s4h)]';
    rh1cyc=Rz11*rhcyc1;
    rh2cyc=Rz21*rhcyc2;
    rh3cyc=Rz31*rhcyc3;
    rh4cyc=Rz41*rhcyc4;
    rh1cyca=Ra1*rh1cyc;
    rh2cyca=Ra2*rh2cyc;
    rh3cyca=Ra3*rh3cyc;
```

```
    rh4cyca=Ra4*rh4cyc;
    kcyc1=rb1a+rh1cyca;
    kcyc2=rb2a+rh2cyca;
    kcyc3=rb3a+rh3cyca;
    kcyc4=rb4a+rh4cyca;
    A1=((kcyc1(1)^2+kcyc1(2)^2+kcyc1(3)^2+Rp1^2-
Cpl1_2)/(2*Rp1))+kcyc1(1);
    A2=((kcyc2(1)^2+kcyc2(2)^2+kcyc2(3)^2+Rp2^2-
Cpl2_2)/(2*Rp2))+kcyc2(1);
    A3=((kcyc3(1)^2+kcyc3(2)^2+kcyc3(3)^2+Rp3^2-
Cpl3_2)/(2*Rp3))+kcyc3(1);
    A4=((kcyc4(1)^2+kcyc4(2)^2+kcyc4(3)^2+Rp4^2-
Cpl4_2)/(2*Rp4))+kcyc4(1);
    B1=((kcyc1(1)^2+kcyc1(2)^2+kcyc1(3)^2+Rp1^2-Cpl1_2)/(2*Rp1))-
kcyc1(1);
    B2=((kcyc2(1)^2+kcyc2(2)^2+kcyc2(3)^2+Rp2^2-Cpl2_2)/(2*Rp2))-
kcyc2(1);
    B3=((kcyc3(1)^2+kcyc3(2)^2+kcyc3(3)^2+Rp3^2-Cpl3_2)/(2*Rp3))-
kcyc3(1);
    B4=((kcyc4(1)^2+kcyc4(2)^2+kcyc4(3)^2+Rp4^2-Cpl4_2)/(2*Rp4))-
kcyc4(1);
    n1=2*atan((kcyc1(3)-sqrt(kcyc1(3)^2-(A1*B1)))/A1);
    n2=2*atan((kcyc2(3)-sqrt(kcyc2(3)^2-(A2*B2)))/A2);
    n3=2*atan((kcyc3(3)-sqrt(kcyc3(3)^2-(A3*B3)))/A3);
    n4=2*atan((kcyc4(3)-sqrt(kcyc4(3)^2-(A4*B4)))/A4);
    rp1cyc=[Rp1*cos(n1) 0 Rp1*sin(n1)]';
    rp2cyc=[Rp2*cos(n2) 0 Rp2*sin(n2)]';
    rp3cyc=[Rp3*cos(n3) 0 Rp3*sin(n3)]';
    rp4cyc=[Rp4*cos(n4) 0 Rp4*sin(n4)]';
    cpl1cyca=rb1a+rh1cyca-rp1cyc;
    cpl1cyc=Ra1\cpl1cyca;
    cpl2cyca=rb2a+rh2cyca-rp2cyc;
    cpl2cyc=Ra2\cpl2cyca;
    cpl3cyca=rb3a+rh3cyca-rp3cyc;
    cpl3cyc=Ra3\cpl3cyca;
    cpl4cyca=rb4a+rh4cyca-rp4cyc;
    cpl4cyc=Ra4\cpl4cyca;
    Cpl1cyc=norm(rb1a+rh1cyca-rp1cyc);
    Cpl2cyc=norm(rb2a+rh2cyca-rp2cyc);
    Cpl3cyc=norm(rb3a+rh3cyca-rp3cyc);
    Cpl4cyc=norm(rb4a+rh4cyca-rp4cyc);
    Cpl1cyc_2=(kcyc1(1)-rp1cyc(1))^2+kcyc1(2)^2+(kcyc1(3)-
rp1cyc(3))^2;
    Cpl2cyc_2=(kcyc2(1)-rp2cyc(1))^2+kcyc2(2)^2+(kcyc2(3)-
rp2cyc(3))^2;
    Cpl3cyc_2=(kcyc3(1)-rp3cyc(1))^2+kcyc3(2)^2+(kcyc3(3)-
rp3cyc(3))^2;
    Cpl4cyc_2=(kcyc4(1)-rp4cyc(1))^2+kcyc4(2)^2+(kcyc4(3)-
rp4cyc(3))^2;
    ra1=Ra1\rp1cyc;
    ra2=Ra2\rp2cyc;
    ra3=Ra3\rp3cyc;
    ra4=Ra4\rp4cyc;
    %%%% SWASHPLATE DYNAMICS %%%%%
    MAh1=M+(-Lh1cbemt*d);%ft-lbf
    MAh2=M+(-Lh2cbemt*d);
    MAh3=M+(-Lh3cbemt*d);
    MAh4=M+(-Lh4cbemt*d);
    d2tdpsih= -t1ch-t1sh;
```

```
I1h=sum(IFb'.*rav.^2.*(d2tdpsih(1,2)+thetah(:,2)));%%sum(IFb.*rav.^2.*
thetatwh)
    I2h=sum(IFb'.*rav.^2.*(d2tdpsih(1,3)+thetah(:,3)));
    I3h=sum(IFb'.*rav.^2.*(d2tdpsih(1,4)+thetah(:,4)));
    I4h=sum(IFb'.*rav.^2.*(d2tdpsih(1,5)+thetah(:,5)));
    KR1h=thetah(1,2)*kr;
    KR2h=thetah(1,3)*kr;
    KR3h=thetah(1,4)*kr;
    KR4h=thetah(1,5)*kr;
    Ucpl1h=(cplcol1+cpl1cyc-cpl1)/Cpl1;
    Ucpl2h=(cplcol2+cpl2cyc-cpl2)/Cpl2;
    Ucpl3h=(cplcol3+cpl3cyc-cpl3)/Cpl3;
    Ucpl4h=(cplcol4+cpl4cyc-cpl4)/Cpl4;
    UFpl1h=Ucpl1h;
    UFpl2h=Ucpl2h;
    UFpl3h=Ucpl3h;
    UFpl4h=Ucpl4h;
    thetah1_2=cos(thetah(1,2));
    thetah1_3=cos((pi/2)-thetah(1,2));
    thetah1_1=real(sqrt(1-(thetah1_2)^2-(thetah1_3)^2));
    Uthetah1=[thetah1_1 thetah1_2 thetah1_3]';
    thetah2_1=-cos(thetah(1,3));
    thetah2_3=cos((pi/2)-thetah(1,3));
    thetah2_2=real(sqrt(1-(thetah2_1)^2-(thetah2_3)^2));
    Uthetah2=[thetah2_1 thetah2_2 thetah2_3]';
    thetah3_2=-cos(thetah(1,4));
    thetah3_3=cos((pi/2)-thetah(1,4));
    thetah3_1=real(sqrt(1-(thetah3_2)^2-(thetah3_3)^2));
    Uthetah3=[thetah3_1 thetah3_2 thetah3_3]';
    thetah4_1=cos(thetah(1,5));
    thetah4_3=cos((pi/2)-thetah(1,5));
    thetah4_2=real(sqrt(1-(thetah4_1)^2-(thetah4_3)^2));
    Uthetah4=[thetah4_1 thetah4_2 thetah4_3]';
    tp1=dot(Uthetah1,cross((rhcol1+rh1cyc-rh1),UFpl1h));
    tp2=dot(Uthetah2,cross((rhcol2+rh2cyc-rh2),UFpl2h));
    tp3=dot(Uthetah3,cross((rhcol3+rh3cyc-rh3),UFpl3h));
    tp4=dot(Uthetah4,cross((rhcol4+rh4cyc-rh4),UFpl4h));
    FPL1=((MAh4+I4h+KR4h)/tp4)*4.448;
    FPL2=((MAh1+I1h+KR1h)/tp1)*4.448;
    FPL3=((MAh2+I2h+KR2h)/tp2)*4.448;
    rpa1=theta0h+theta1c1s4h;
    rpa2=theta0h+theta1c1s1h;
    rpa3=theta0h+theta1c1s2h;
    aeromoment1=MAh4;
    aeromoment2=MAh1;
    aeromoment3=MAh2;
    inertia1=I4h;
    inertia2=I1h;
    inertia3=I2h;
    kr1=KR4h;
    kr2=KR1h;
    kr3=KR2h;
elseif FLIGHTSEGMENT==2
    theta0c=theta0;
    thetatwc=theta0c+(r*thetatw);
    theta1cc=theta1c;
    theta1sc=theta1s;
    t1cc=theta1cc*cos(psi);
```

```
    t1sc=theta1sc*sin(psi);
    %%%%%%%%%%%%%%%%%%%%%%%%%%%%MOMENTUM THEORY%%%%%%%%%%%%%%%%%%%%
    %%%%%CLIMB%%%%%%%%%
    vicm=-(Vcc./2)+sqrt((Vcc./2).^2+(Th./(2.*rho.*A)));
    lambdacm=Vcc/(rav*R);
    lambdaicm=(lambdacm/2)+sqrt((lambdacm/2)^2+(Cthm/2));
    uPcm=Th*Vcc/737;% power [Kw];
    iPcm=(Th*vicm/737);
    Pcm=(Th*(Vcc+vicm))/737;
    %%%%%%%%%%BLADE ELEMENT MOMENTUM THEORY
    %%%%%%%CLIMB%%%%%%%%%%%%%

    vicbemt=-((1/2).*(Vcc+((cla.*nb.*c.*rav)/(8.*pi))))+((1/2).*...
        sqrt((Vcc+((cla.*nb.*c.*rav)/(8*pi)))^2-(((cla*nb*c*rav)/...
        (2*pi)).*(Vcc-(rav.*y.*thetatwc)))));
    vicbemt(1,((round(TL*100)/100)*100):end)=0;
    vicbemt(1,1:25,1)=0;
    vicbemt_vt=vicbemt/bts;
    Upcbemt=(Vcc+vicbemt);
    Vcbemt=sqrt(Upcbemt.^2+Ut.^2);
    phicbemt= (atan2(Upcbemt,Ut));
    alphacbemt= thetatwc-phicbemt;
    dLcbemt_1=(1./2).*rho.*Vcbemt.^2.*c.*cla.*alphacbemt*dr;
    dLcbemt_1(1,((round(TL*100)/100)*100):end)=0;
    dLcbemt_1(1,1:25,1)=0;
    Lcbemt_1=sum(dLcbemt_1);
    dCtcbemt_1=(nb*dLcbemt_1)/(rho*A*bts^2);
    Ctcbemt_1=sum(dCtcbemt_1);
    Tcbemt_1=Ctcbemt_1*(rho*A*bts^2);

        %%%%%%%integrating
    Incbemt_1=int((theta0c*x^2)+(((thetatw/R)*x^3))-
(((Vcc+vicbemt(1,75))/rav)*x),x,y(1,25),y(1,97));
    Tcbemt_int1=(1/2)*rho*cla*nb*c*rav^2*double(Incbemt_1);
    %%%%integral solved

Tcbemt_11=(1/2)*rho*nb*c*cla*bts^2*R*((1/3)*((theta0c)+((3/4)*thetatw)
)-((Upcbemt(1,75)/bts)/2));

    error6=100-((Thrustclimbbemt/Tcbemt)*100);% error in %


    error7=100-((thrustclimbbemt/Tcbemt)*100);% error in %
    %%%jonhson%%%%%
    lambdaicbemtj= sqrt(((s*cla/16)-(Vcc/(rav*R))/2)^2+((s*cla/8)*...
        theta0c.*r))-((s*cla/16)-(Vcc/(rav*R))/2);
    %%%%%%%%%%Cyclic inputs%%%%%%%%%%
    for i=1:100
        for j=1:5
            thetac(i,j)=(thetatwc(i))+(t1cc(j))+(t1sc(j));
        end
    end
    alphaccbemt1= thetac(:,2)'-phicbemt;%[rad] effective angle of
attack blade1
    alphaccbemt2= thetac(:,3)'-phicbemt;%[rad] effective angle of
attack blade2
    alphaccbemt3= thetac(:,4)'-phicbemt;%[rad] effective angle of
attack blade3
```

```
    alphaccbemt4= thetac(:,5)'-phicbemt;%[rad] effective angle of
attack blade4
    dLccbemt1=(1./2).*rho.*Ut.^2.*c.*cla.*alphaccbemt1*dr;%[lbf]
elemental lift blade1
    dLccbemt2=(1./2).*rho.*Ut.^2.*c.*cla.*alphaccbemt2*dr;%[lbf]
elemental lift blade2
    dLccbemt3=(1./2).*rho.*Ut.^2.*c.*cla.*alphaccbemt3*dr;%[lbf]
elemental lift blade3
    dLccbemt4=(1./2).*rho.*Ut.^2.*c.*cla.*alphaccbemt4*dr;%[lbf]
elemental lift blade4
    dLccbemt1(1,((round(TL*100)/100)*100):end)=0;
    dLccbemt2(1,((round(TL*100)/100)*100):end)=0;
    dLccbemt3(1,((round(TL*100)/100)*100):end)=0;
    dLccbemt4(1,((round(TL*100)/100)*100):end)=0;
    dLccbemt1(1,1:25,1)=0;
    dLccbemt2(1,1:25,1)=0;
    dLccbemt3(1,1:25,1)=0;
    dLccbemt4(1,1:25,1)=0;
    Lc1cbemt=sum(dLccbemt1);
    Lc2cbemt=sum(dLccbemt2);
    Lc3cbemt=sum(dLccbemt3);
    Lc4cbemt=sum(dLccbemt4);
    if nb==4

dCtccbemt=(dLccbemt1+dLccbemt2+dLccbemt3+dLccbemt4)/(rho*A*bts^2);
    elseif nb==2
        dCtccbemt=(dLccbemt1+dLccbemt3)/(rho*A*bts^2);
    end
    Ctccbemt=sum(dCtccbemt);
    Tcbemtc=Ctccbemt*(rho*A*bts^2);
    %%%%%%%%%%%%%%BLADE ELEMENT THEORY CLIMB%%%%%%%%%%%%%%%%%%%%%%%%
    Upcbet=(Vcc+vicbemt);
    Vcbet=sqrt(Upcbet.^2+Ut.^2);
    phicbet= (atan2(Upcbet,Ut));
    alphacbet= thetatwc-phicbet;
    dLcbet=(1./2).*rho.*Vcbet.^2.*c.*cla.*alphacbet*dr;
    dLcbet(1,((round(TL*100)/100)*100):end)=0;
    dLcbet(1,1:25,1)=0;
    Lcbet=sum(dLcbet);
    dCtcbet=(nb*dLcbet)/(rho*A*bts^2);
    Ctcbet=sum(dCtcbet);
    Tcbet=Ctcbet*(rho*A*bts^2);
    %%%%SWASHPLATE KINEMATICS%%%%%%%%%%
    %%%%COLLECTIVE INPUT%%%%%%%%%%
    rh22c=[0 Rh2*cos(theta0c) Rh2*sin(theta0c)]';
    rh12c=rh22c;
    rh32c=rh22c;
    rh42c=rh22c;
    rhcol1c=Rz11*rh12c;
    rhcol2c=Rz21*rh22c;
    rhcol3c=Rz31*rh32c;
    rhcol4c=Rz41*rh42c;
    kcol1c=rb1+rhcol1c-rp1;
    kcol2c=rb2+rhcol2c-rp2;
    kcol3c=rb3+rhcol3c-rp3;
    kcol4c=rb4+rhcol4c-rp4;
    zcol1c=kcol1c(3)-sqrt(Cpl1^2-(kcol1c(1))^2-(kcol1c(2))^2);
    Zcol1c=[0 0 zcol1c]';
    zcol2c=kcol2c(3)-sqrt(Cpl2^2-(kcol2c(1))^2-(kcol2c(2))^2);
```

```
    Zcol2c=[0 0 zcol2c]';
    zcol3c=kcol3c(3)-sqrt(Cpl3^2-(kcol3c(1))^2-(kcol3c(2))^2);
    Zcol3c=[0 0 zcol3c]';
    zcol4c=kcol4c(3)-sqrt(Cpl4^2-(kcol4c(1))^2-(kcol4c(2))^2);
    Zcol4c=[0 0 zcol4c]';
    cplcol1c=[kcol1c(1,1) kcol1c(2,1) (kcol1c(3,1)-zcol1c)]';
    cplcol2c=[kcol2c(1,1) kcol2c(2,1) (kcol2c(3,1)-zcol2c)]';
    cplcol3c=[kcol3c(1,1) kcol3c(2,1) (kcol3c(3,1)-zcol3c)]';
    cplcol4c=[kcol4c(1,1) kcol4c(2,1) (kcol4c(3,1)-zcol4c)]';
    %%%%CYCLIC INPUT%%%%%%%%%%
    theta1c1s1c=t1cc(1,2)+t1sc(1,2);
    theta1c1s2c=t1cc(1,3)+t1sc(1,3);
    theta1c1s3c=t1cc(1,4)+t1sc(1,4);
    theta1c1s4c=t1cc(1,5)+t1sc(1,5);
    rhcyc1c=[0 Rh1*cos(theta1c1s1c) Rh1*sin(theta1c1s1c)]';
    rhcyc2c=[0 Rh2*cos(theta1c1s2c) Rh2*sin(theta1c1s2c)]';
    rhcyc3c=[0 Rh3*cos(theta1c1s3c) Rh3*sin(theta1c1s3c)]';
    rhcyc4c=[0 Rh4*cos(theta1c1s4c) Rh4*sin(theta1c1s4c)]';
    rh1cycc=Rz11*rhcyc1c;
    rh2cycc=Rz21*rhcyc2c;
    rh3cycc=Rz31*rhcyc3c;
    rh4cycc=Rz41*rhcyc4c;
    rh1cycac=Ra1*rh1cycc;
    rh2cycac=Ra2*rh2cycc;
    rh3cycac=Ra3*rh3cycc;
    rh4cycac=Ra4*rh4cycc;
    kcyc1c=rb1a+rh1cycac;
    kcyc2c=rb2a+rh2cycac;
    kcyc3c=rb3a+rh3cycac;
    kcyc4c=rb4a+rh4cycac;
    A1c=((kcyc1c(1)^2+kcyc1c(2)^2+kcyc1c(3)^2+Rp1^2-
Cpl1^2)/(2*Rp1))+kcyc1c(1);
    A2c=((kcyc2c(1)^2+kcyc2c(2)^2+kcyc2c(3)^2+Rp2^2-
Cpl2^2)/(2*Rp2))+kcyc2c(1);
    A3c=((kcyc3c(1)^2+kcyc3c(2)^2+kcyc3c(3)^2+Rp3^2-
Cpl3^2)/(2*Rp3))+kcyc3c(1);
    A4c=((kcyc4c(1)^2+kcyc4c(2)^2+kcyc4c(3)^2+Rp4^2-
Cpl4^2)/(2*Rp4))+kcyc4c(1);
    B1c=((kcyc1c(1)^2+kcyc1c(2)^2+kcyc1c(3)^2+Rp1^2-Cpl1^2)/(2*Rp1))-
kcyc1c(1);
    B2c=((kcyc2c(1)^2+kcyc2c(2)^2+kcyc2c(3)^2+Rp2^2-Cpl2^2)/(2*Rp2))-
kcyc2c(1);
    B3c=((kcyc3c(1)^2+kcyc3c(2)^2+kcyc3c(3)^2+Rp3^2-Cpl3^2)/(2*Rp3))-
kcyc3c(1);
    B4c=((kcyc4c(1)^2+kcyc4c(2)^2+kcyc4c(3)^2+Rp4^2-Cpl4^2)/(2*Rp4))-
kcyc4c(1);
    n1c=2*atan((kcyc1c(3)-sqrt(kcyc1c(3)^2-(A1c*B1c)))/A1c);
    n2c=2*atan((kcyc2c(3)-sqrt(kcyc2c(3)^2-(A2c*B2c)))/A2c);
    n3c=2*atan((kcyc3c(3)-sqrt(kcyc3c(3)^2-(A3c*B3c)))/A3c);
    n4c=2*atan((kcyc4c(3)-sqrt(kcyc4c(3)^2-(A4c*B4c)))/A4c);
    rp1cycc=[Rp1*cos(n1c) 0 Rp1*sin(n1c)]';
    rp2cycc=[Rp1*cos(n2c) 0 Rp2*sin(n2c)]';
    rp3cycc=[Rp1*cos(n3c) 0 Rp3*sin(n3c)]';
    rp4cycc=[Rp1*cos(n4c) 0 Rp4*sin(n4c)]';
    cpl1cycca=rb1a+rh1cycac-rp1cycc;
    cpl1cycc=Ra1\cpl1cycca;
    cpl2cycca=rb2a+rh2cycac-rp2cycc;
    cpl2cycc=Ra2\cpl2cycca;
    cpl3cycca=rb3a+rh3cycac-rp3cycc;
```

```
cpl3cycc=Ra3\cpl3cycca;
cpl4cycca=rb4a+rh4cycac-rp4cycc;
cpl4cycc=Ra4\cpl4cycca;
ra1c=Ra1\rp1cycc;
ra2c=Ra2\rp2cycc;
ra3c=Ra3\rp3cycc;
ra4c=Ra4\rp4cycc;
%%%% SWASHPLATE DYNAMICS %%%%%
MAc1=M+(-Lc1cbemt*d);
MAc2=M+(-Lc2cbemt*d);
MAc3=M+(-Lc3cbemt*d);
MAc4=M+(-Lc4cbemt*d);
d2tdpsic= -t1cc-t1sc;
I1c=sum(IFb'.*rav.^2.*(d2tdpsic(1,2)+thetac(:,2)));
I2c=sum(IFb'.*rav.^2.*(d2tdpsic(1,3)+thetac(:,3)));
I3c=sum(IFb'.*rav.^2.*(d2tdpsic(1,4)+thetac(:,4)));
I4c=sum(IFb'.*rav.^2.*(d2tdpsic(1,5)+thetac(:,5)));
KR1c=thetac(1,2)*kr;
KR2c=thetac(1,3)*kr;
KR3c=thetac(1,4)*kr;
KR4c=thetac(1,5)*kr;
Ucpl1c=(cplcol1c+cpl1cycc-cpl1)/Cpl1;
Ucpl2c=(cplcol2c+cpl2cycc-cpl2)/Cpl2;
Ucpl3c=(cplcol3c+cpl3cycc-cpl3)/Cpl3;
Ucpl4c=(cplcol4c+cpl4cycc-cpl4)/Cpl4;
UFpl1c=Ucpl1c;
UFpl2c=Ucpl2c;
UFpl3c=Ucpl3c;
UFpl4c=Ucpl4c;
thetac1_2=cos(thetac(1,2));
thetac1_3=cos((pi/2)-thetac(1,2));
thetac1_1=real(sqrt(1-(thetac1_2)^2-(thetac1_3)^2));
Uthetac1=[thetac1_1 thetac1_2 thetac1_3]';
thetac2_1=-cos(thetac(1,3));
thetac2_3=cos((pi/2)-thetac(1,3));
thetac2_2=real(sqrt(1-(thetac2_1)^2-(thetac2_3)^2));
Uthetac2=[thetac2_1 thetac2_2 thetac2_3]';
thetac3_2=-cos(thetac(1,4));
thetac3_3=cos((pi/2)-thetac(1,4));
thetac3_1=real(sqrt(1-(thetac3_2)^2-(thetac3_3)^2));
Uthetac3=[thetac3_1 thetac3_2 thetac3_3]';
thetac4_1=cos(thetac(1,5));
thetac4_3=cos((pi/2)-thetac(1,5));
thetac4_2=real(sqrt(1-(thetac4_1)^2-(thetac4_3)^2));
Uthetac4=[thetac4_1 thetac4_2 thetac4_3]';
tp1c=dot(Uthetac1,cross((rhcol1c+rh1cycc-rh1),UFpl1c));
tp2c=dot(Uthetac2,cross((rhcol2c+rh2cycc-rh2),UFpl2c));
tp3c=dot(Uthetac3,cross((rhcol3c+rh3cycc-rh3),UFpl3c));
tp4c=dot(Uthetac4,cross((rhcol4c+rh4cycc-rh4),UFpl4c));
FPL1=((MAc4+I4c+KR4c)/tp4c)*4.448;
FPL2=((MAc1+I1c+KR1c)/tp1c)*4.448;
FPL3=((MAc2+I2c+KR2c)/tp2c)*4.448;
rpa1=theta0c+theta1c1s1c;
rpa2=theta0c+theta1c1s2c;
rpa3=theta0c+theta1c1s3c;
aeromoment1=MAc4;
aeromoment2=MAc1;
aeromoment3=MAc2;
inertia1=I4c;
```

```
    inertia2=I1c;
    inertia3=I2c;
    kr1=KR4c;
    kr2=KR1c;
    kr3=KR2c;

elseif FLIGHTSEGMENT==3
    vf=AirSpeed*3.28;
    theta0f=theta0;
    thetaf=theta0f+(r*thetatw);
    theta1cf=theta1c;
    theta1sf=theta1s;
    t1cf=theta1cf*cos(psi);
    t1sf=theta1sf*sin(psi);
    %%%%%%%%%%%%%%%%%%%%FORWARD FLIGHT%%%%%%%%%%%%%%%%%%%%
    ar=(vf*cos(a))/(rav*R);
    %%%%%%%MOMENTUM THEORY
    %%%from momentum theory
    lambdah=sqrt(Cthm/2); %Inflow Ratio in Hover using Ct in hover
    %%%%%%%from cooke low speed approximation
    vif=sqrt(-
(((vf/(lambdah*bts))^2)/2)+sqrt((((vf/(lambdah*bts))^4)/4)+1))*(lambda
h*bts);
    %%%%from leishman inflow ratio calculation
    lambdaf=lambdah;% first value for iteration
    lambdafn=((ar*tan(a)))+(Cthm/(2*sqrt(ar^2+lambdaf^2)));
    errorf=abs((lambdafn-lambdaf)/lambdafn);
    while errorf > 0.0005
        lambdaf=lambdafn;
        lambdafn=((ar*tan(a)))+(Cthm/(2*sqrt(ar^2+lambdaf^2)));
        errorf=abs((lambdafn-lambdaf)/lambdafn);
    end
    lambdaf=lambdafn;
    errorf;
    lambdaif=Cthm/(2*sqrt(ar^2+lambdaf^2));
    Lambdaif=lambdaf-(ar*tan(a));

Tf=2*rho*A*(lambdaif*bts)*sqrt((vf*cos(a))^2+((vf*sin(a))+(lambdaif*bt
s))^2);% thrust [lb]

    Tf_1=(lambdaf-
(ar*tan(a)))*(2*sqrt((ar^2)+(lambdaf^2)))*(rho*A*bts^2);


    %%%from leishman pg 68 vertical equilibrium
    Tff=w/cos(a);
    Ctff=Tff/(rho*A*(rav*R)^2);
    lambdafn=((ar*tan(a)))+(Ctff/(2*sqrt(ar^2+lambdaf^2)));
    errorf=abs((lambdafn-lambdaf)/lambdafn);
    while errorf > 0.0005
        lambdaf=lambdafn;
        lambdafn=((ar*tan(a)))+(Ctff/(2*sqrt(ar^2+lambdaf^2)));
        errorf=abs((lambdafn-lambdaf)/lambdafn);
    end
    lambdaf=lambdafn;
    errorf;
    lambdaif=Ctff/(2*sqrt(ar^2+lambdaf^2));
    Lambdaif=lambdaf-(ar*tan(a));
```

```
Tf=2*rho*A*(lambdaif*bts)*sqrt((vf*cos(a))^2+((vf*sin(a))+(lambdaif*bt
s))^2);% thrust [lb]


    %%%from carlos models
    lambdafn=((ar*tan(a)))+(Cthm/(2*sqrt(ar^2+lambdaf^2)));
    errorf=abs((lambdafn-lambdaf)/lambdafn);
    while errorf > 0.0005
        lambdaf=lambdafn;
        lambdafn=((ar*tan(a)))+(Cthm/(2*sqrt(ar^2+lambdaf^2)));
        errorf=abs((lambdafn-lambdaf)/lambdafn);
    end
    lambdaf=lambdafn;
    errorf;
    lambdaif=Cthm/(2*sqrt(ar^2+lambdaf^2));
    Lambdaif=lambdaf-(ar*tan(a));
    Tf=2*rho*A*(lambdaf*bts)^2;% thrust [lb]


    for i=1:100
        for j=1:5
            Tr(i,j)=thetaf(i)+t1cf(j)+t1sf(j);
        end
    end
    B0=Ln*(((theta0f/8)*(1+ar^2))+((thetatw/10)*(1+(ar^2*(5/6))))+...
        (theta1sf.*(ar/6))-(lambdaf/6));
    B1c=-theta1sf+(((-8/3)*ar)*(theta0f-(lambdaf*3/4)+...
        (ar*theta1sf.*3/4)+(thetatw*3/4)))/(1+(0.5*ar^2));
    B1s=theta1cf+(((-4/3)*ar.*B0)/(1+(0.5*ar^2)));
    B_psi=B0+(B1c.*cos(psi))+(B1s.*sin(psi));
    dBdpsi=rav.*((B1s.*cos(psi))-(B1c.*sin(psi)));
    g=(ar.*rav.*R.*sin(psi));
    for i=1:100
        for j=1:5
            UT(i,j)=(rav*y(i))+g(j);
        end
    end
    h=ar.*rav.*R.*B_psi.*cos(psi);
    for i=1:100
        for j=1:5
            UP(i,j)=((lambdaf).*rav.*R)+(y(i).*dBdpsi(j))+(h(j));
        end
    end
    dLF=0.5.*rho.*c.*cla.*((Tr.*UT.^2)-(UP.*UT)).*dr;
    dLF(round(TL*100):end,:)=0;
    dLF(1:25,:)=0;
    dLF1=dLF(:,2);
    LF1=sum (dLF1);
    dLF2=dLF(:,3);
    LF2=sum (dLF2);
    dLF3=dLF(:,4);
    LF3=sum (dLF3);
    dLF4=dLF(:,5);
    LF4=sum (dLF4);

    if nb==4
        dCtfcbemt=(dLF1+dLF2+dLF3+dLF4)/(rho*A*bts^2);
```

```
    elseif nb==2
        dCtfcbemt=(dLF1+dLF3)/(rho*A*bts^2);
    end

    Ctfcbemt=sum(dCtfcbemt);
    Tfbemtc=Ctfcbemt*(rho*A*bts^2);


CTMR=(s*cla/2)*((theta0f/3)*(1+((3/2)*ar^2))+((thetatw/4)*(1+ar^2))+((
ar/2)*theta1sf)-(lambdaf/2));
    %%%%FORWARD FLIGHT%%%%%%%%%%
    %%%%COLLECTIVE INPUT%%%%%%%%%%
    rh22f=[0 Rh2*cos(theta0f) Rh2*sin(theta0f)]';
    rh12f=rh22f;
    rh32f=rh22f;
    rh42f=rh22f;
    rhcol1f=Rz11*rh12f;
    rhcol2f=Rz21*rh22f;
    rhcol3f=Rz31*rh32f;
    rhcol4f=Rz41*rh42f;
    kcol1f=rb1+rhcol1f-rp1;
    kcol2f=rb2+rhcol2f-rp2;
    kcol3f=rb3+rhcol3f-rp3;
    kcol4f=rb4+rhcol4f-rp4;
    zcol1f=kcol1f(3)-sqrt(Cpl1^2-(kcol1f(1))^2-(kcol1f(2))^2);
    Zcol1f=[0 0 zcol1f]';
    zcol2f=kcol2f(3)-sqrt(Cpl2^2-(kcol2f(1))^2-(kcol2f(2))^2);
    Zcol2f=[0 0 zcol2f]';
    zcol3f=kcol3f(3)-sqrt(Cpl3^2-(kcol3f(1))^2-(kcol3f(2))^2);
    Zcol3f=[0 0 zcol3f]';
    zcol4f=kcol4f(3)-sqrt(Cpl4^2-(kcol4f(1))^2-(kcol4f(2))^2);
    Zcol4f=[0 0 zcol4f]';
    cplcol1f=[kcol1f(1,1) kcol1f(2,1) (kcol1f(3,1)-zcol1f)]';
    cplcol2f=[kcol2f(1,1) kcol2f(2,1) (kcol2f(3,1)-zcol2f)]';
    cplcol3f=[kcol3f(1,1) kcol3f(2,1) (kcol3f(3,1)-zcol3f)]';
    cplcol4f=[kcol4f(1,1) kcol4f(2,1) (kcol4f(3,1)-zcol4f)]';
    %%%%CYCLIC INPUT%%%%%%%%%%
    theta1c1s1f=t1cf(1,2)+t1sf(1,2);
    theta1c1s2f=t1cf(1,3)+t1sf(1,3);
    theta1c1s3f=t1cf(1,4)+t1sf(1,4);
    theta1c1s4f=t1cf(1,5)+t1sf(1,5);
    rhcyc1f=[0 Rh1*cos(theta1c1s1f) Rh1*sin(theta1c1s1f)]';
    rhcyc2f=[0 Rh2*cos(theta1c1s2f) Rh2*sin(theta1c1s2f)]';
    rhcyc3f=[0 Rh3*cos(theta1c1s3f) Rh3*sin(theta1c1s3f)]';
    rhcyc4f=[0 Rh4*cos(theta1c1s4f) Rh4*sin(theta1c1s4f)]';
    rh1cycf=Rz11*rhcyc1f;
    rh2cycf=Rz21*rhcyc2f;
    rh3cycf=Rz31*rhcyc3f;
    rh4cycf=Rz41*rhcyc4f;
    rh1cycaf=Ra1*rh1cycf;
    rh2cycaf=Ra2*rh2cycf;
    rh3cycaf=Ra3*rh3cycf;
    rh4cycaf=Ra4*rh4cycf;
    kcyc1f=rb1a+rh1cycaf;
    kcyc2f=rb2a+rh2cycaf;
    kcyc3f=rb3a+rh3cycaf;
    kcyc4f=rb4a+rh4cycaf;
```

```
    A1f=((kcyc1f(1)^2+kcyc1f(2)^2+kcyc1f(3)^2+Rp1^2-
Cpl1^2)/(2*Rp1))+kcyc1f(1);
    A2f=((kcyc2f(1)^2+kcyc2f(2)^2+kcyc2f(3)^2+Rp2^2-
Cpl2^2)/(2*Rp2))+kcyc2f(1);
    A3f=((kcyc3f(1)^2+kcyc3f(2)^2+kcyc3f(3)^2+Rp3^2-
Cpl3^2)/(2*Rp3))+kcyc3f(1);
    A4f=((kcyc4f(1)^2+kcyc4f(2)^2+kcyc4f(3)^2+Rp4^2-
Cpl4^2)/(2*Rp4))+kcyc4f(1);
    B1f=((kcyc1f(1)^2+kcyc1f(2)^2+kcyc1f(3)^2+Rp1^2-Cpl1^2)/(2*Rp1))-
kcyc1f(1);
    B2f=((kcyc2f(1)^2+kcyc2f(2)^2+kcyc2f(3)^2+Rp2^2-Cpl2^2)/(2*Rp2))-
kcyc2f(1);
    B3f=((kcyc3f(1)^2+kcyc3f(2)^2+kcyc3f(3)^2+Rp3^2-Cpl3^2)/(2*Rp3))-
kcyc3f(1);
    B4f=((kcyc4f(1)^2+kcyc4f(2)^2+kcyc4f(3)^2+Rp4^2-Cpl4^2)/(2*Rp4))-
kcyc4f(1);
    n1f=2*atan((kcyc1f(3)-sqrt(kcyc1f(3)^2-(A1f*B1f)))/A1f);
    n2f=2*atan((kcyc2f(3)-sqrt(kcyc2f(3)^2-(A2f*B2f)))/A2f);
    n3f=2*atan((kcyc3f(3)-sqrt(kcyc3f(3)^2-(A3f*B3f)))/A3f);
    n4f=2*atan((kcyc4f(3)-sqrt(kcyc4f(3)^2-(A4f*B4f)))/A4f);
    rp1cycf=[Rp1*cos(n1f) 0 Rp1*sin(n1f)]';
    rp2cycf=[Rp1*cos(n2f) 0 Rp2*sin(n2f)]';
    rp3cycf=[Rp1*cos(n3f) 0 Rp3*sin(n3f)]';
    rp4cycf=[Rp1*cos(n4f) 0 Rp4*sin(n4f)]';
    cpl1cycfa=rb1a+rh1cycaf-rp1cycf;
    cpl1cycf=Ra1\cpl1cycfa;
    cpl2cycfa=rb2a+rh2cycaf-rp2cycf;
    cpl2cycf=Ra2\cpl2cycfa;
    cpl3cycfa=rb3a+rh3cycaf-rp3cycf;
    cpl3cycf=Ra3\cpl3cycfa;
    cpl4cycfa=rb4a+rh4cycaf-rp4cycf;
    cpl4cycf=Ra4\cpl4cycfa;
    ra1f=Ra1\rp1cycf;
    ra2f=Ra2\rp2cycf;
    ra3f=Ra3\rp3cycf;
    ra4f=Ra4\rp4cycf;
    %%%% SWASHPLATE DYNAMICS %%%%%
    MAf1=M+(-LF1*d);
    MAf2=M+(-LF2*d);
    MAf3=M+(-LF3*d);
    MAf4=M+(-LF4*d);
    d2tdpsif= -t1cf-t1sf;
    I1f=sum(IFb'.*rav.^2.*(d2tdpsif(1,2)+Tr(:,2)));
    I2f=sum(IFb'.*rav.^2.*(d2tdpsif(1,3)+Tr(:,3)));
    I3f=sum(IFb'.*rav.^2.*(d2tdpsif(1,4)+Tr(:,4)));
    I4f=sum(IFb'.*rav.^2.*(d2tdpsif(1,5)+Tr(:,5)));
    KR1f=Tr(1,2)*kr;
    KR2f=Tr(1,3)*kr;
    KR3f=Tr(1,4)*kr;
    KR4f=Tr(1,5)*kr;
    Ucpl1f=(cplcol1f+cpl1cycf-cpl1)/Cpl1;
    Ucpl2f=(cplcol2f+cpl2cycf-cpl2)/Cpl2;
    Ucpl3f=(cplcol3f+cpl3cycf-cpl3)/Cpl3;
    Ucpl4f=(cplcol4f+cpl4cycf-cpl4)/Cpl4;
    UFpl1f=Ucpl1f;
    UFpl2f=Ucpl2f;
    UFpl3f=Ucpl3f;
    UFpl4f=Ucpl4f;
    thetaf1_2=cos(Tr(1,2));
```

```
    thetaf1_3=cos((pi/2)-Tr(1,2));
    thetaf1_1=real(sqrt(1-(thetaf1_2)^2-(thetaf1_3)^2));
    Uthetaf1=[thetaf1_1 thetaf1_2 thetaf1_3]';
    thetaf2_1=-cos(Tr(1,3));
    thetaf2_3=cos((pi/2)-Tr(1,3));
    thetaf2_2=real(sqrt(1-(thetaf2_1)^2-(thetaf2_3)^2));
    Uthetaf2=[thetaf2_1 thetaf2_2 thetaf2_3]';
    thetaf3_2=-cos(Tr(1,4));
    thetaf3_3=cos((pi/2)-Tr(1,4));
    thetaf3_1=real(sqrt(1-(thetaf3_2)^2-(thetaf3_3)^2));
    Uthetaf3=[thetaf3_1 thetaf3_2 thetaf3_3]';
    thetaf4_1=cos(Tr(1,5));
    thetaf4_3=cos((pi/2)-Tr(1,5));
    thetaf4_2=real(sqrt(1-(thetaf4_1)^2-(thetaf4_3)^2));
    Uthetaf4=[thetaf4_1 thetaf4_2 thetaf4_3]';
    tp1f=dot(Uthetaf1,cross((rhcol1f+rh1cycf-rh1),UFpl1f));
    tp2f=dot(Uthetaf2,cross((rhcol2f+rh2cycf-rh2),UFpl2f));
    tp3f=dot(Uthetaf3,cross((rhcol3f+rh3cycf-rh3),UFpl3f));
    tp4f=dot(Uthetaf4,cross((rhcol4f+rh4cycf-rh4),UFpl4f));
    FPL1=((MAf4+I4f+KR4f)/tp4f)*4.448;
    FPL2=((MAf1+I1f+KR1f)/tp1f)*4.448;
    FPL3=((MAf2+I2f+KR2f)/tp2f)*4.448;
    rpa1=theta0f+theta1c1s4f;
    rpa2=theta0f+theta1c1s1f;
    rpa3=theta0f+theta1c1s2f;
    aeromoment1=MAf4;
    aeromoment2=MAf1;
    aeromoment3=MAf1;
    inertia1=I4f;
    inertia2=I1f;
    inertia3=I2f;
    kr1=KR4f;
    kr2=KR1f;
    kr3=KR2f;
elseif FLIGHTSEGMENT==1
    FPL1=0*4.448;
    FPL2=0*4.448;
    FPL3=0*4.448;
    rpa1=0;
    rpa2=0;
    rpa3=0;
    aeromoment1=0;
    aeromoment2=0;
    aeromoment3=0;
    inertia1=0;
    inertia2=0;
    inertia3=0;
    kr1=0;
    kr2=0;
    kr3=0;
elseif FLIGHTSEGMENT==5
    FPL1=0*4.448;
    FPL2=0*4.448;
    FPL3=0*4.448;
    rpa1=0;
    rpa2=0;
    rpa3=0;
    aeromoment1=0;
    aeromoment2=0;
```

```
    aeromoment3=0;
    inertia1=0;
    inertia2=0;
    inertia3=0;
    kr1=0;
    kr2=0;
    kr3=0;
end
fpl1=FPL1;
fpl2=FPL2;
fpl3=FPL3;
RPA1=rpa1;
RPA2=rpa2;
RPA3=rpa3;
AEROMOMENT1=aeromoment1;
AEROMOMENT2=aeromoment2;
AEROMOMENT3=aeromoment3;
INERTIA1=inertia1;
INERTIA2=inertia2;
INERTIA3=inertia3;
KR1=kr1;
KR2=kr2;
KR3=kr3;
%%%%%%%%%%%%%%%%%%%%%%RESULTS%%%%%%%%%%%%%%%%%%%%%%
fprintf(1,'HELICOPTER DATA:\n\n\t');
fprintf('Helicopter Weight %0.3f [lbf]\n\t', w);
fprintf('Rotor Angular Velocity %0.3f [rad/s]\n\t', rav)
fprintf('Rotor Radius %0.3f [ft]\n\t', R);
fprintf('Blade Chord %0.3f [ft]\n\t', c);
fprintf('Main Rotor Linear Twist angle %0.3f [rad]\n\t', thetatw);
fprintf('Tip-Loss Factor %0.5f \n\t', TL);
fprintf('Blade Root (non-dimensional position) %0.5f \n\t', 0.25);
fprintf('Blade Lift Curve Slope %0.3f [1/rad]\n\t', cla)
fprintf('Blade Zero Lift-Drag Coefficient %0.3f \n\t', cd0)
fprintf('Moment Coefficient %0.3f \n\t', Cm0)
fprintf('Rotor Solidity %0.3f \n\t', s);
fprintf('Mass Moment Of Inertia Flap Hinge %0.3f [slug-ft^2]\n\t', Ib)
fprintf('Angular Moment Of Inertia Feathering axis %0.3f [slug-
ft^2]\n\t', Ifb)
fprintf('Spring Constant for the Blade Root %0.3f [ft-lb/rad]\n\t',
kr)
fprintf('Aerodynamic Center to Flexural Axis Distance %0.3f [ft]\n\n',
d);

if FLIGHTSEGMENT==4
    fprintf(1,'HOVER INPUTS:\n\n\t');
    fprintf('Main Rotor Collective pitch %0.3f [rad]\n\t', theta0h);
    fprintf('Main Rotor Lateral cyclic pitch %0.3f [rad]\n\t',
theta1ch);
    fprintf('Main Rotor Longitudinal cyclic pitch %0.3f [rad]\n\n',
theta1sh);

    fprintf(1,'HOVER RESULTS:\n\n');
    fprintf(1,'MOMENTUM THEORY:\n\n\t');
    fprintf('Induced Velocity %0.5f [ft/s]\n\t', vhm);
    fprintf('Thrust %0.3f [lbf]\n\t', Th);
    fprintf('Thrust Coefficient %0.3f \n\t', Cthm);
    fprintf('Induced Inflow Ratio %0.5f \n\t', lambdahm);
```

```
    fprintf('Disk Loading %0.5f [lb/ft^2]\n\n', DL)
    fprintf(1,'BLADE ELEMENT THEORY:\n\n\t');
    fprintf('Out-of-Plane Velocity Component Up %0.5f [ft/s]\n\t',
Uph);
    fprintf('Blade Tip Speed %0.5f [ft/s]\n\t', bts)
    fprintf('Total Velocity %0.5f [ft/s]\n\t', Uh_1(1,100));
    fprintf('Lift %0.5f [lbf]\n\t', Lhbet_1);
    fprintf('Thrust Coefficient %0.5f \n\t', Cthbet_1,Cthbet_11,...
        Cthbet_2,Cthbet_int1,Cth_21);
    fprintf('Thrust %0.5f [lbf]\n\t', Thbet_1);
    fprintf('Lift Linear Twist %0.5f [lbf]\n\t', Lhbet_3);
    fprintf('Thrust Coefficient Linear Twist %0.5f \n\t', Cthbet_3,...
        Cthbet_int2,Cthbet_31,Cthbet_int3,Cthbet_32)
    fprintf('Thrust Linear Twist %0.5f [lbf]\n\t', Thbet_3);
    fprintf('Lift Tip-Loss Factor %0.5f [lbf]\n\t', Lhbet_4);
    fprintf('Thrust Coefficient Tip-Loss Factor %0.5f \n\t',...
        Cthbet_4,Cthbet_int4,Cthbet_41);
    fprintf('Thrust Tip-Loss Factor %0.5f [lbf]\n\t', Thbet_4);
    fprintf('Lift root cutout %0.5f [lbf]\n\t', Lhbet_5);
    fprintf('Thrust Coefficient root cutout %0.5f \n\t', Cthbet_5,...
        Cthbet_int5);
    fprintf('Thrust root cutout %0.5f [lbf]\n\t', Thbet_5);
    fprintf(1,'BLADE ELEMENT MOMENTUM THEORY:\n\n\t');
    fprintf('Lift %0.5f [lbf]\n\t', Lhbemt);
    fprintf('Thrust Coefficient %0.5f \n\t',
Cthbemt_1,Cthbemt_int1,Cthbemt_11);
    fprintf('Thrust %0.5f [lbf]\n\t', Thbemt_1);
    fprintf('Lift Blade 1 Cyclic %0.5f [lbf]\n\t', Lh1cbemt);
    fprintf('Lift Blade 2 Cyclic %0.5f [lbf]\n\t', Lh2cbemt);
    fprintf('Lift Blade 3 Cyclic %0.5f [lbf]\n\t', Lh3cbemt);
    fprintf('Lift Blade 4 Cyclic %0.5f [lbf]\n\t', Lh4cbemt);
    fprintf('Thrust Coefficient Cyclic %0.5f \n\t', Cthcbemt);
    fprintf('Thrust Cyclic %0.5f [lbf]\n\n', Thbemtc);
    fprintf('Blade 1 Pitch Link Force %0.5f [lbf]\n', FPL1);
    fprintf('Blade 2 Pitch Link Force %0.5f [lbf]\n', FPL2);
    fprintf('Blade 3 Pitch Link Force %0.5f [lbf]\n\n', FPL3);


    figure;
    hold on
    stem (r,dLhbet_1,'Marker','none');
    plot(r,dLhbet_1)
    hold off
    figure(1)
    xlabel('Non-dimensional rotor radius');
    ylabel('Elemental Lift (lbf)');
    title ('Variation of Elemental Lift with Rotor Radius HOVER
(BET)');

    figure;
    hold on
    stem (r,(nb*dLhbet_1),'Marker','none');
    plot(r,(nb*dLhbet_1))
    hold off
    figure(2)
    xlabel('Non-dimensional rotor radius');
    ylabel('Elemental Thrust (lbf)');
```

```
    title ('Variation of Elemental Thrust with Rotor Radius HOVER
(BET)');

    figure;
    hold on
    stem (r,dLhbet_3,'Marker','none');
    plot(r,dLhbet_3)
    hold off
    figure(3)
    xlabel('Non-dimensional rotor radius');
    ylabel('Elemental Lift (lbf)');
    title ('Variation of Elemental Lift with Rotor Radius HOVER
(Linear Twist) (BET)');

    figure;
    hold on
    stem (r,(nb*dLhbet_3),'Marker','none');
    plot(r,(nb*dLhbet_3))
    hold off
    figure(4)
    xlabel('Non-dimensional rotor radius');
    ylabel('Elemental Thrust (lbf)');
    title ('Variation of Elemental Thrust with Rotor Radius HOVER
(Linear Twist) (BET)');

    figure;
    hold on
    stem (r,dLhbet_4,'Marker','none');
    plot(r,(dLhbet_4))
    hold off
    figure(5)
    xlabel('Non-dimensional rotor radius');
    ylabel('Elemental Lift (lbf)');
    title ('Variation of Elemental Lift with Rotor Radius HOVER (Tip-
Loss Factor) (BET)');

    figure;
    hold on
    stem (r,(nb*dLhbet_4),'Marker','none');
    plot(r,(nb*dLhbet_4))
    hold off
    figure(6)
    xlabel('Non-dimensional rotor radius');
    ylabel('Elemental Thrust (lbf)');
    title ('Variation of Elemental Thrust with Rotor HOVER Radius
(Tip-Loss Factor) (BET)');

    figure;
    hold on
    stem (r,dLhbet_5,'Marker','none');
    plot(r,(dLhbet_5))
    hold off
    figure(7)
    xlabel('Non-dimensional rotor radius');
    ylabel('Elemental Lift (lbf)');
    title ('Variation of Elemental Lift with Rotor Radius HOVER (Blade
Root) (BET)');
```

```
    figure;
    hold on
    stem (r,(nb*dLhbet_5),'Marker','none');
    plot(r,(nb*dLhbet_5))
    hold off
    figure(8)
    xlabel('Non-dimensional rotor radius');
    ylabel('Elemental Thrust (lbf)');
    title ('Variation of Elemental Thrust with Rotor HOVER Radius
(Blade Root) (BET)');

    figure;
    hold on
    stem (r,dLhbemt,'Marker','none');
    plot(r,(dLhbemt))
    hold off
    figure(9)
    xlabel('Non-dimensional rotor radius');
    ylabel('Elemental Lift (lbf)');
    title ('Variation of Elemental Lift with Rotor Radius HOVER
(BEMT)');

    figure;
    hold on
    stem (r,(nb*dLhbemt),'Marker','none');
    plot(r,(nb*dLhbemt))
    hold off
    figure(10)
    xlabel('Non-dimensional rotor radius');
    ylabel('Elemental Thrust (lbf)');
    title ('Variation of Elemental Thrust with Rotor Radius HOVER
(BEMT)');

    figure;
    hold on
    stem (r,dLhcbemt1,'Marker','none');
    plot(r,(dLhcbemt1))
    hold off
    figure(11)
    xlabel('Non-dimensional rotor radius');
    ylabel('Elemental Lift (lbf)');
    title ('Variation of Elemental Lift with Rotor Radius HOVER Blade
1(BEMT)');

    figure;
    hold on
    stem (r,dLhcbemt2,'Marker','none');
    plot(r,(dLhcbemt2))
    hold off
    figure(12)
    xlabel('Non-dimensional rotor radius');
    ylabel('Elemental Lift (lbf)');
    title ('Variation of Elemental Lift with Rotor Radius HOVER Blade
2(BEMT)');

    figure;
    hold on
    stem (r,dLhcbemt3,'Marker','none');
```

```
    plot(r,(dLhcbemt3))
    hold off
    figure(13)
    xlabel('Non-dimensional rotor radius');
    ylabel('Elemental Lift (lbf)');
    title ('Variation of Elemental Lift with Rotor Radius HOVER Blade
3(BEMT)');

    figure;
    hold on
    stem (r,dLhcbemt4,'Marker','none');
    plot(r,(dLhcbemt4))
    hold off
    figure(14)
    xlabel('Non-dimensional rotor radius');
    ylabel('Elemental Lift (lbf)');
    title ('Variation of Elemental Lift with Rotor Radius HOVER Blade
4(BEMT)');

    figure;
    hold on
    stem (r,(dLhcbemt1+dLhcbemt3),'Marker','none');
    plot(r,(dLhcbemt1+dLhcbemt3))
    hold off
    figure(15)
    xlabel('Non-dimensional rotor radius');
    ylabel('Elemental Thrust (lbf)');
    title ('Variation of Elemental Thrust with Rotor Radius HOVER
(Cyclic) (BEMT)');



elseif FLIGHTSEGMENT==2
    fprintf(1,'CLIMB INPUTS:\n\n\t');
    fprintf('Main Rotor Collective pitch %0.3f [rad]\n\t', theta0c);
    fprintf('Main Rotor Lateral cyclic pitch %0.3f [rad]\n\t',
theta1cc);
    fprintf('Main Rotor Longitudinal cyclic pitch %0.3f [rad]\n\n',
theta1sc);

    fprintf(1,'CLIMB RESULTS:\n\n');
    fprintf(1,'MOMENTUM THEORY:\n\n\t');
    fprintf('Induced velocity in climb %0.5f [ft/s]\n\t', vicm);
    fprintf('Inflow Ratio %0.5f \n\t', lambdacm);
    fprintf('Induced Inflow Ratio %0.5f \n\n', lambdaicm);

    fprintf(1,'BLADE ELEMENT MOMENTUM THEORY:\n\n\t');
    fprintf('Lift %0.5f [lbf]\n\t', Lcbemt_1);
    fprintf('Thrust Coefficient %0.5f [lbf]\n\t', Ctcbemt_1);
    fprintf('Thrust %0.5f [lbf]\n\t', Tcbemt_1);
    fprintf('Lift Blade 1 Cyclic %0.5f [lbf]\n\t', Lc1cbemt);
    fprintf('Lift Blade 2 Cyclic %0.5f [lbf]\n\t', Lc2cbemt);
    fprintf('Lift Blade 3 Cyclic %0.5f [lbf]\n\t', Lc3cbemt);
    fprintf('Lift Blade 4 Cyclic %0.5f [lbf]\n\t', Lc4cbemt);
    fprintf('Thrust Coefficient %0.5f [lbf]\n\t', Ctccbemt);
    fprintf('Thrust %0.5f [lbf]\n\n', Tcbemtc);
    fprintf('Blade 1 Pitch Link Force %0.5f [lbf]\n', FPL1);
```

```
    fprintf('Blade 2 Pitch Link Force %0.5f [lbf]\n', FPL2);
    fprintf('Blade 3 Pitch Link Force %0.5f [lbf]\n\n', FPL3);

    figure;
    hold on
    stem (r,dLcbemt_1,'Marker','none');
    plot(r,(dLcbemt_1))
    hold off
    figure(1)
    xlabel('Non-dimensional rotor radius');
    ylabel('Elemental Lift (lbf)');
    title ('Variation of Elemental Lift with Rotor Radius
CLIMB(BEMT)');

    figure;
    hold on
    stem (r,(dLcbemt_1*nb),'Marker','none');
    plot(r,(dLcbemt_1*nb))
    hold off
    figure(2)
    xlabel('Non-dimensional rotor radius');
    ylabel('Elemental Thrust (lbf)');
    title ('Variation of Elemental Thrust with Rotor Radius
CLIMB(BEMT)');

    figure;
    hold on
    stem (r,dLccbemt1,'Marker','none');
    plot(r,(dLccbemt1))
    hold off
    figure(3)
    xlabel('Non-dimensional rotor radius');
    ylabel('Elemental Lift (lbf)');
    title ('Variation of Elemental Lift with Rotor Radius Blade 1
CLIMB(BEMT)');

    figure;
    hold on
    stem (r,dLccbemt2,'Marker','none');
    plot(r,(dLccbemt2))
    hold off
    figure(4)
    xlabel('Non-dimensional rotor radius');
    ylabel('Elemental Lift (lbf)');
    title ('Variation of Elemental Lift with Rotor Radius Blade 2
CLIMB(BEMT)');

    figure;
    hold on
    stem (r,dLccbemt3,'Marker','none');
    plot(r,(dLccbemt3))
    hold off
    figure(5)
    xlabel('Non-dimensional rotor radius');
    ylabel('Elemental Lift (lbf)');
    title ('Variation of Elemental Lift with Rotor Radius Blade 3
CLIMB(BEMT)');
```

```
    figure;
    hold on
    stem (r,dLccbemt4,'Marker','none');
    plot(r,(dLccbemt4))
    hold off
    figure(6)
    xlabel('Non-dimensional rotor radius');
    ylabel('Elemental Lift (lbf)');
    title ('Variation of Elemental Lift with Rotor Radius Blade 4
CLIMB(BEMT)');

    figure;
    hold on
    stem (r,dLccbemt1+dLccbemt3,'Marker','none');
    plot(r,(dLccbemt1+dLccbemt3))
    hold off
    figure(7)
    xlabel('Non-dimensional rotor radius');
    ylabel('Elemental Thrust (lbf)');
    title ('Variation of Elemental Thrust with Rotor Radius
CLIMB(BEMT)');

elseif FLIGHTSEGMENT==3
    fprintf(1,'FORWARD FLIGHT INPUTS:\n\n\t');
    fprintf('Main Rotor Collective Pitch %0.6f [rad]\n\t', theta0f);
    fprintf('Main Rotor Lateral Cyclic Pitch %0.6f [rad]\n\t',
theta1cf);
    fprintf('Main Rotor Longitudinal Cyclic Pitch %0.6f [rad]\n\n',
theta1sf);

    fprintf(1,'FORWARD FLIGHT RESULTS:\n\n\t');
    fprintf('Advance Ratio %0.5f \n\t', ar);
    fprintf('Inflow Ratio %0.5f \n\t', lambdaf);
    fprintf('Induced Inflow Ratio %0.5f \n\t', lambdaif);
    fprintf('Lock Number %0.5f \n\t', Ln);
    fprintf('Lift Blade 1 %0.5f [lbf]\n\t', LF1);
    fprintf('Lift Blade 2 %0.5f [lbf]\n\t', LF2);
    fprintf('Lift Blade 3 %0.5f [lbf]\n\t', LF3);
    fprintf('Lift Blade 4 %0.5f [lbf]\n\n', LF4);
    fprintf('Blade 1 Pitch Link Force %0.5f [lbf]\n', FPL1);
    fprintf('Blade 2 Pitch Link Force %0.5f [lbf]\n', FPL2);
    fprintf('Blade 3 Pitch Link Force %0.5f [lbf]\n\n', FPL3);

    figure;
    hold on
    stem (r,dLF1,'Marker','none');
    plot(r,(dLF1))
    hold off
    figure(1)
    xlabel('Non-dimensional rotor radius');
    ylabel('Elemental Lift (lbf)');
    title ('Variation of Elemental Lift with Rotor Radius Blade 1
FORWARD FLIGHT');

    figure;
    hold on
    stem (r,dLF2,'Marker','none');
    plot(r,(dLF2))
```

```
    hold off
    figure(2)
    xlabel('Non-dimensional rotor radius');
    ylabel('Elemental Lift (lbf)');
    title ('Variation of Elemental Lift with Rotor Radius Blade 2
FORWARD FLIGHT');

    figure;
    hold on
    stem (r,dLF3,'Marker','none');
    plot(r,(dLF3))
    hold off
    figure(3)
    xlabel('Non-dimensional rotor radius');
    ylabel('Elemental Lift (lbf)');
    title ('Variation of Elemental Lift with Rotor Radius Blade 3
FORWARD FLIGHT');

    figure;
    hold on
    stem (r,dLF4,'Marker','none');
    plot(r,(dLF4))
    hold off
    figure(4)
    xlabel('Non-dimensional rotor radius');
    ylabel('Elemental Lift (lbf)');
    title ('Variation of Elemental Lift with Rotor Radius Blade 4
FORWARD FLIGHT');

    figure;
    hold on
    stem (r,dLF1+dLF3,'Marker','none');
    plot(r,(dLF1+dLF3))
    hold off
    figure(5)
    xlabel('Non-dimensional rotor radius');
    ylabel('Elemental Thrust (lbf)');
    title ('Variation of Elemental Thrust with Rotor Radius FORWARD
FLIGHT');
end
```

Appendix C RMEM-HPM integration results

C.1 GROUND CONDITION

Table C-1 Parametric analysis results for Ground

GROUND										
ISA conditions (ISA Deviation) [°c]							20			
throttle position							60%			
no RMEM	time	1	2	3	4	5	6	7	8	9
	fuel burn [kg]	1.46	2.93	4.39	5.85	7.32	8.78	10.24	11.71	13.17
	Power requirement [kw]	103.9	103.9	103.9	103.9	103.9	103.9	103.9	103.9	103.9
	helicopter weight [kg]	1813	1811	1810	1808	1807	1805	1804	1802	1801
RMEMVA2	fuel burn [kg]	1.47	2.94	4.41	5.88	7.34	8.81	10.28	11.75	13.22
	helicopter weight [kg]	1813	1811	1810	1808	1807	1805	1804	1802	1801
	AS Power required [kw]	0.00	0.00	0.00	0.00	0.00	0.00	0.00	0.00	0.00
	ES Power required [kw]	0.59	0.59	0.59	0.59	0.59	0.59	0.59	0.59	0.59
	FS Power required [kw]	0.09	0.09	0.09	0.09	0.09	0.09	0.09	0.09	0.09
	IPS Power required [kw]	0.00	0.00	0.00	0.00	0.00	0.00	0.00	0.00	0.00
	ECS Power required [kw]	0.33	0.33	0.33	0.33	0.33	0.33	0.33	0.33	0.33
RMEM fuel burn increase [kg]		0.01	0.01	0.02	0.02	0.03	0.03	0.04	0.04	0.05
%		0.41	0.38	0.39	0.38	0.37	0.38	0.39	0.34	0.38

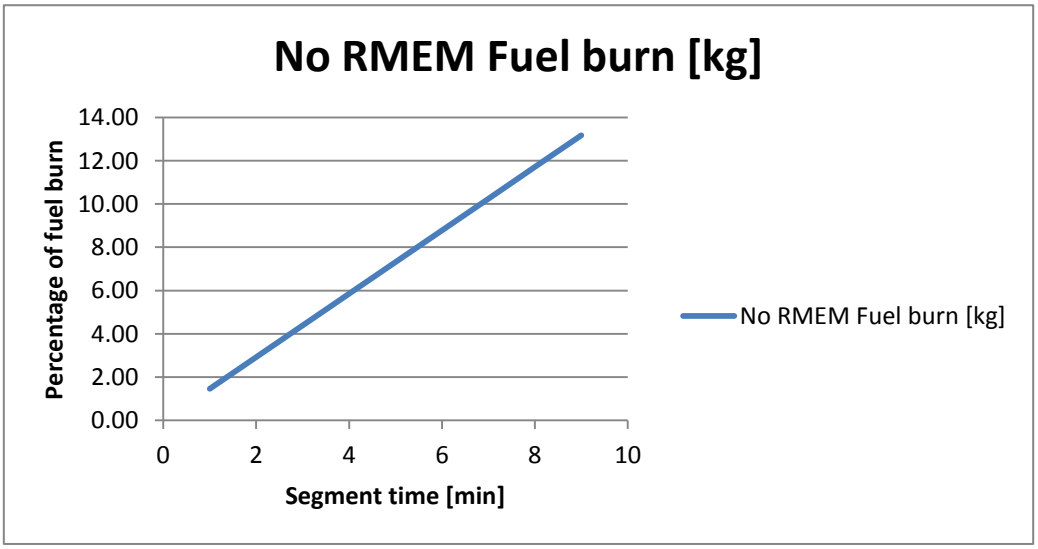

Figure C-1 no RMEM fuel burn Ground

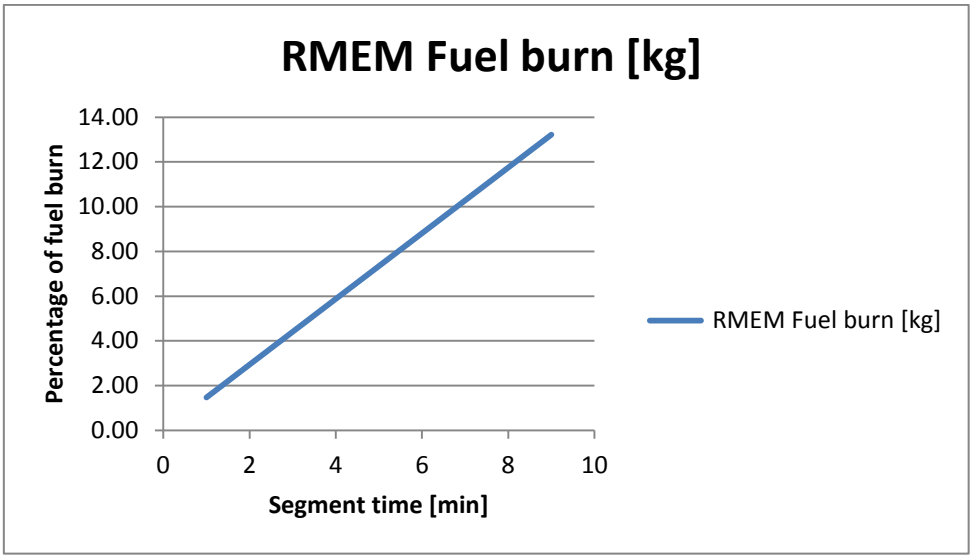

Figure C-2 RMEM fuel burn Ground

C.2 HOVER CONDITION

Table C-2 Parametric analysis results for Hover

HOVER										
ISA conditions (ISA Deviation) [°c]							20			
initial weight [kg]							1806.684			
	time [min]						5			
	skid height [m]	1	2	3	4	5	6	7	8	9
no RMEM	fuel burn [kg]	6.30	7.97	9.15	9.85	10.26	10.53	10.70	10.81	10.90
	induced inflow ratio	0.04	0.04	0.04	0.04	0.04	0.04	0.04	0.04	0.04
	Ct	0.00	0.00	0.00	0.00	0.00	0.00	0.00	0.00	0.00
	helicopter weight [kg]	1800	1799	1798	1797	1796	1796	1796	1796	1796
	ISA conditions (ISA Deviation) [°c]						20			
	initial weight						1806.657			
	time						5			
	skid height [m]	1	2	3	4	5	6	7	8	9
	theta [deg]	14.56	14.56	14.56	14.56	14.56	14.56	14.56	14.56	14.56
	fuel burn ESH [kg]	6.420	8.089	9.266	9.965	10.380	10.640	10.810	10.930	11.010
	fuel burn EM [kg]	6.398	8.066	9.243	9.943	10.360	10.620	10.790	10.910	10.990
	fuel burn EH [kg]	6.407	8.076	9.252	9.952	10.370	10.630	10.800	10.920	11.000
RMEMVA 2	induced inflow ratio	0.038	0.038	0.038	0.038	0.038	0.038	0.038	0.038	0.038
	Ct	0.003	0.003	0.003	0.003	0.003	0.003	0.003	0.003	0.003
	helicopter weight [kg]	1800	1799	1797	1797	1796	1796	1796	1796	1796
	AS ESH Power required [kw]	1.57	1.57	1.57	1.57	1.57	1.57	1.57	1.57	1.57
	AS EM Power required [kw]	0.78	0.78	0.78	0.78	0.78	0.78	0.78	0.78	0.78
	AS EH Power required [kw]	1.11	1.11	1.11	1.11	1.11	1.11	1.11	1.11	1.11
	ES Power required [kw]	2.17	2.17	2.17	2.17	2.17	2.17	2.17	2.17	2.17
	FS Power required [kw]	0.09	0.09	0.09	0.09	0.09	0.09	0.09	0.09	0.09
	IPS Power required [kw]	0.00	0.00	0.00	0.00	0.00	0.00	0.00	0.00	0.00
	ECS Power required [kw]	0.33	0.33	0.33	0.33	0.33	0.33	0.33	0.33	0.33
fuel burn increase ESH [kg]		0.12	0.12	0.12	0.12	0.12	0.11	0.11	0.12	0.11
%		1.87	1.48	1.30	1.20	1.17	1.04	1.03	1.11	1.01
fuel burn increase EM [kg]		0.10	0.10	0.10	0.10	0.10	0.09	0.09	0.10	0.09
%		1.52	1.19	1.05	0.97	0.97	0.85	0.84	0.93	0.83
fuel burn increase EH [kg]		0.11	0.11	0.11	0.11	0.11	0.10	0.10	0.11	0.10
%		1.67	1.32	1.15	1.07	1.07	0.95	0.93	1.02	0.92

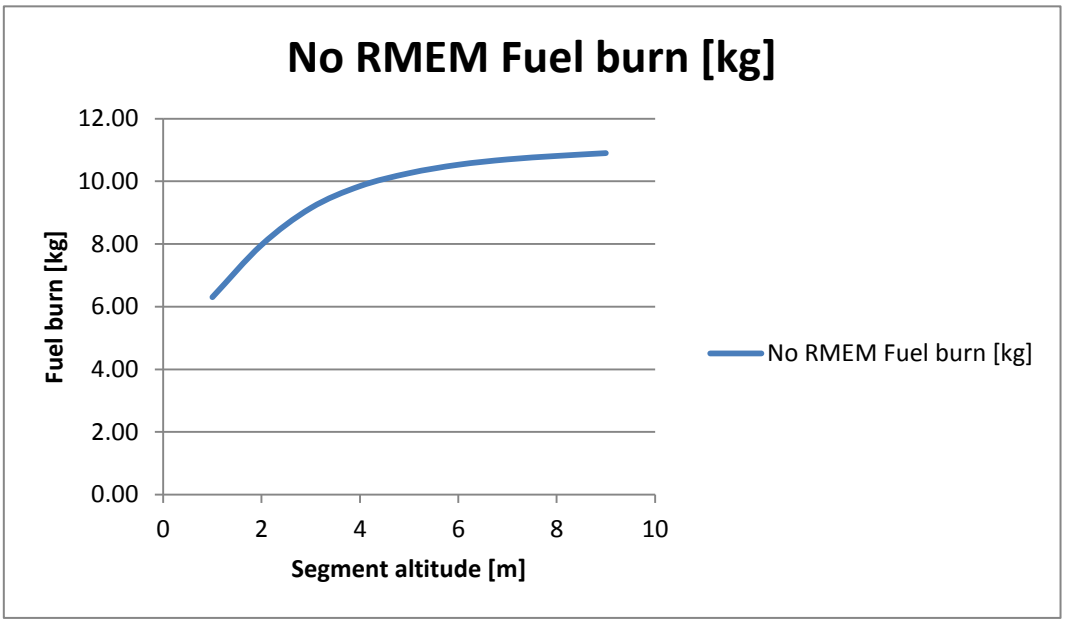

Figure C-3 no RMEM fuel burn Hover

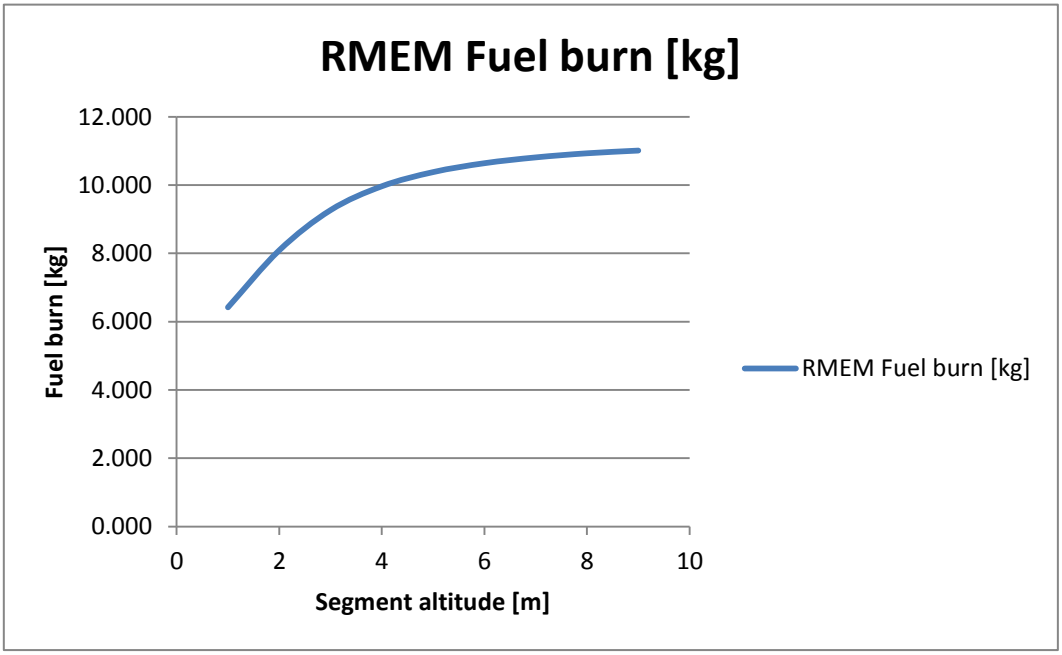

Figure C-4 RMEM fuel burn Hover

C.3 CLIMB CONDITION

Table C-3 Parametric analysis results for Climb

CLIMB										
ISA conditions (ISA Deviation) [°c]							20			
initial weight [kg]							1796.424			
no RMEM	initial altitude [m]	5	5	5	5	5	5	5	5	5
	final altitude [m]	1000	1000	1000	1000	1000	1000	1000	1000	1000
	forward speed [knots]	30	35	40	50	55	60	70	80	90
	fuel burn [kg]	16.74	14.93	13.89	13.08	13.09	13.33	14.62	17.56	24.65
	helicopter weight [kg]	1780	1781	1783	1783	1783	1783	1782	1779	1772
	average rate of climb [m/s]	4.492	5.04	5.418	5.757	5.753	5.646	5.148	4.282	3.045
	ISA conditions (ISA Deviation) [°c]							20		
	initial weight [kg]							1796.277		
	initial altitude [m]	5	5	5	5	5	5	5	5	5
	final altitude [m]	1000	1000	1000	1000	1000	1000	1000	1000	1000
	forward speed [knots]	30	35	40	50	55	60	70	80	90
	theta	12.93	12.73	12.59	12.41	12.37	12.36	12.39	12.51	12.69
	fuel burn ESH [kg]	16.92	15.09	14.04	13.22	13.23	13.48	14.78	17.75	24.91
	fuel burn EM [kg]	16.88	15.06	14.01	13.19	13.20	13.45	14.74	17.71	24.86
RMEMVA2	fuel burn EH [kg]	16.90	15.07	14.02	13.20	13.21	13.46	14.75	17.72	24.87
	helicopter weight [kg]	1779	1781	1782	1783	1783	1783	1782	1779	1771
	average rate of climb [m/s]	4.49	5.04	5.42	5.76	5.75	5.65	5.15	4.28	3.05
	AS ESH Power required [kw]	1.59	1.59	1.60	1.60	1.60	1.60	1.60	1.60	1.59
	AS EM Power required [kw]	0.70	0.69	0.68	0.67	0.67	0.67	0.67	0.68	0.69
	AS EH Power required [kw]	0.99	0.98	0.97	0.96	0.95	0.95	0.96	0.96	0.98
	ES Power required [kw]	2.34	2.34	2.34	2.34	2.34	2.34	2.34	2.34	2.34
	FS Power required [kw]	0.09	0.09	0.09	0.09	0.09	0.09	0.09	0.09	0.09
	IPS Power required [kw]	0	0	0	0	0	0	0	0	0
	ECS Power required [kw]	0.33	0.33	0.33	0.33	0.33	0.33	0.33	0.33	0.33
fuel burn increase ESH [kg]		0.18	0.16	0.15	0.14	0.14	0.15	0.16	0.19	0.26
%		1.08	1.07	1.08	1.07	1.07	1.13	1.09	1.08	1.05
fuel burn increase EM [kg]		0.14	0.13	0.12	0.11	0.11	0.12	0.12	0.15	0.21
%		0.84	0.87	0.86	0.84	0.84	0.90	0.82	0.85	0.85
fuel burn increase EH [kg]		0.16	0.14	0.13	0.12	0.12	0.13	0.13	0.16	0.22
%		0.96	0.94	0.94	0.92	0.92	0.98	0.89	0.91	0.89

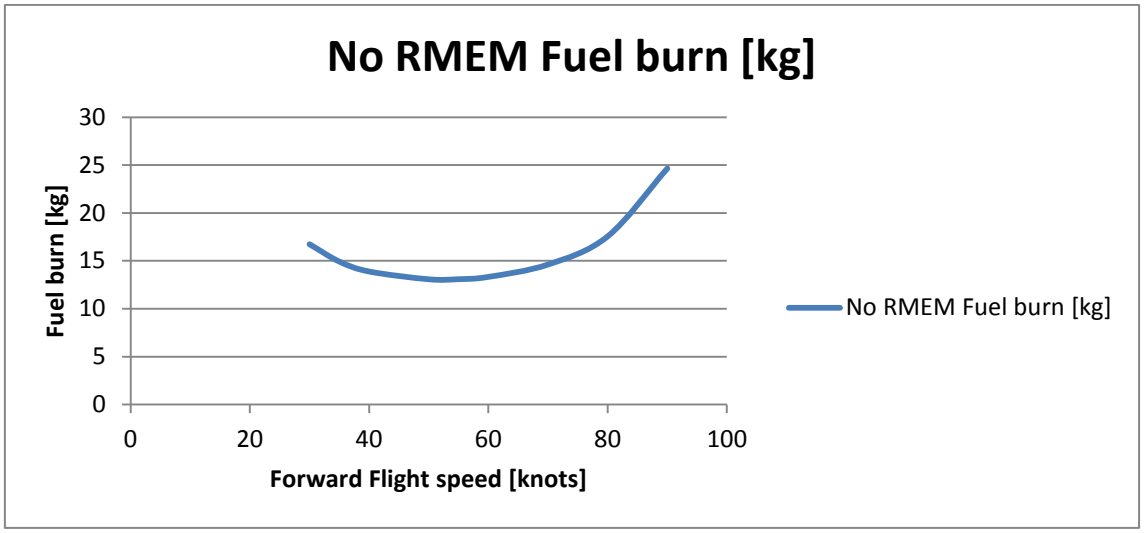

Figure C-5 no RMEM fuel burn Climb

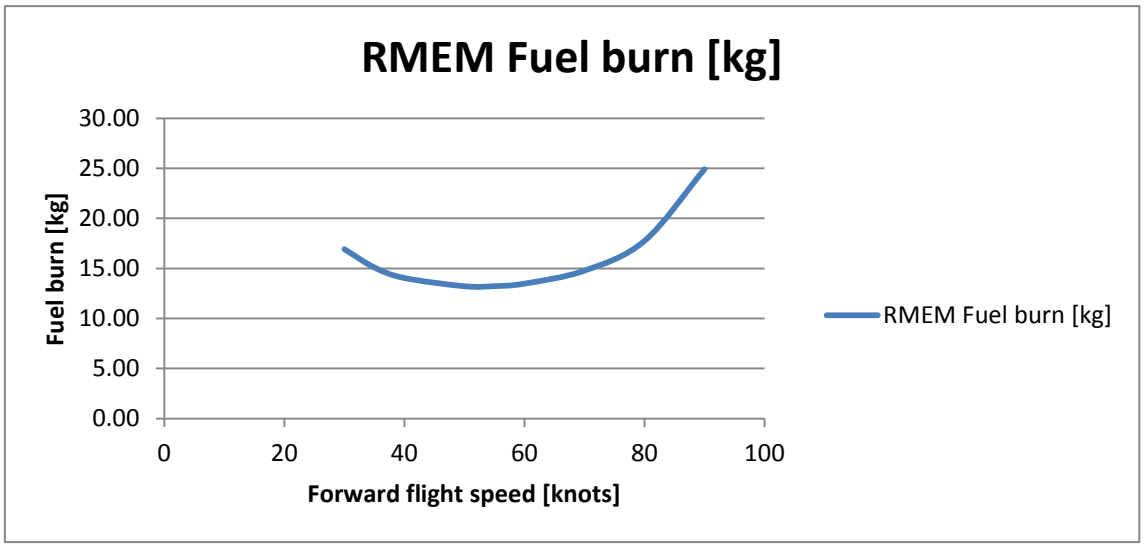

Figure C-6 RMEM fuel burn Climb

C.4 FORWARD FLIGHT CONDITION

Table C-4 Parametric analysis results for Forward flight

FORWARD FLIGHT										
ISA conditions (ISA Deviation) [°c]						20				
initial weight [kg]						1783.094				
no RMEM	initial altitude					1000				
	forward speed [knots]	30	35	40	50	60	70	80	90	100
	fuel burn [kg]	159.1	131.6	112.1	87.28	73.06	64.68	59.88	57.48	56.81
	helicopter weight [kg]	1624	1651	1671	1696	1710	1718	1723	1726	1726
RMEMVA2	ISA conditions (ISA Deviation) [°c]						20			
	initial weight						1782.797			
	altitude [m]					1000				
	forward speed [knots]	30.00	35.00	40.00	50.00	60.00	70.00	80.00	90.00	100.00
	theta	13.58	13.37	13.21	13.01	12.94	12.96	13.05	13.22	13.46
	fuel burn ESH [kg]	161.40	133.70	113.90	88.74	74.28	65.73	60.80	58.30	57.55
	fuel burn EM [kg]	161.00	133.20	113.60	88.44	74.03	65.52	60.61	58.14	57.40
	fuel burn EH [kg]	161.10	133.40	113.70	88.54	74.11	65.58	60.68	58.19	57.45
	helicopter weight [kg]	1621	1649	1669	1694	1709	1717	1722	1724	1725
	AS ESH Power required [kw]	1.59	1.59	1.59	1.59	1.59	1.59	1.59	1.59	1.59
	AS EM Power required [kw]	0.72	0.71	0.70	0.69	0.69	0.69	0.69	0.70	0.71
	AS EH Power required [kw]	1.02	1.01	0.99	0.98	0.98	0.98	0.98	1.00	1.01
	ES Power required [kw]	2.38	2.38	2.38	2.38	2.38	2.38	2.38	2.38	2.38
	FS Power required [kw]	0.09	0.09	0.09	0.09	0.09	0.09	0.09	0.09	0.09
	IPS Power required [kw]	0.00	0.00	0.00	0.00	0.00	0.00	0.00	0.00	0.00
	ECS Power required [kw]	0.32	0.32	0.32	0.32	0.32	0.32	0.32	0.32	0.32
fuel burn increase ESH [kg]		2.3	2.1	1.8	1.46	1.22	1.05	0.92	0.82	0.74
%		1.45	1.60	1.61	1.67	1.67	1.62	1.54	1.43	1.30
fuel burn increase EM [kg]		1.90	1.60	1.50	1.16	0.97	0.84	0.73	0.66	0.59
%		1.19	1.22	1.34	1.33	1.33	1.30	1.22	1.15	1.04
fuel burn increase EH [kg]		2.00	1.80	1.60	1.26	1.05	0.90	0.80	0.71	0.64
%		1.26	1.37	1.43	1.44	1.44	1.39	1.34	1.24	1.13

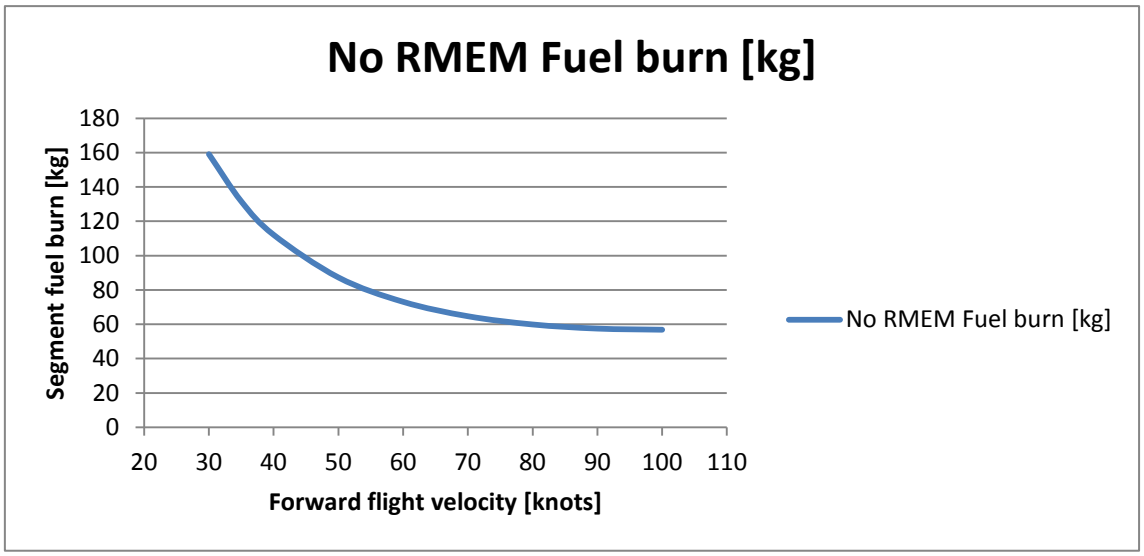

Figure C-7 no RMEM fuel burn Forward flight

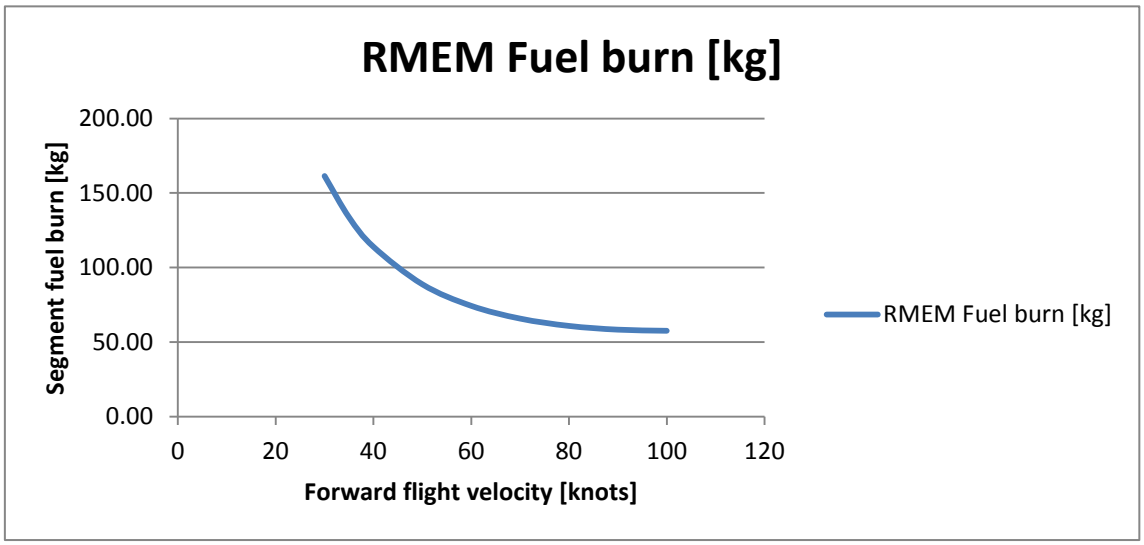

Figure C-8 RMEM fuel burn Forward flight